Groundwater Flow Dynamics and Hydro-geochemical Processes in Coastal Aquifers of the Mekong Delta, Vietnam

January 2020

TRAN DANG AN

Groundwater Flow Dynamics and Hydro-geochemical Processes in Coastal Aquifers of the Mekong Delta, Vietnam

A Dissertation Submitted to

the Graduate School of Life and Environmental Sciences,

the University of Tsukuba

in Partial Fulfillment of the Requirements

for the Degree of Doctor of Philosophy in Environmental Studies

(Doctoral Program in Sustainable Environmental Studies)

TRAN DANG AN

Abstract

Groundwater is a crucial freshwater resource for global drinking, industries, and irrigation development. It becomes more important in coastal regions where groundwater is a primary source for a rapidly growing population, intensive agricultural and industrial development. However, groundwater resources in these regions are highly vulnerable to overexploitation, seawater intrusion, climate change, and sea-level rise. Seawater intrusion is among the most severe water-related issues affecting millions of people and destroying agricultural systems and ecosystems. Similarly, the Vietnamese Mekong Delta (VMD) is experiencing such a problem, and its impacts are considered more severe under climate change. Therefore, the study aims to investigate the groundwater flow dynamics, hydrogeochemical characteristics, origin of groundwater and groundwater salinization processes in the coastal aquifers of the VMD.

To obtain the objectives, the integrated methodologies were employed. Firstly, field surveys were conducted in dry and rainy seasons between 2017 and 2018 to measure physicochemical parameters (groundwater level, pH, T^{o}C, EC, ORP and DO) and collect a total of 278 groundwater and 79 river and canal water samples. Secondly, water samples were analyzed to obtain chemical composition (Na^{+}, K^{+}, Ca^{2+}, Mg^{2+}, SiO_2, HCO_3^{-}, SO_4^{-}, and NO_3^{-}) and stable isotopes ($\delta^{18}O$, $\delta^{2}H$). Thirdly, all obtained data were analyzed using the statistical and graphical analysis to understand the characteristics of groundwater in the study area. Eventually, groundwater modelling and machine learning algorithms were employed to predict groundwater salinization processes and to assess its controlling factors.

The major findings from this study include the main parts as below:

(i) Groundwater flow dynamics

In the coastal lowland area of the Mekong Delta, shallow groundwater flow (water level and flow direction) shows highly seasonal variation while that of deep groundwater changes sensitively under impacts of groundwater exploitation with significant groundwater level depletion (0.85 m/year) in dense pumping locations and tidal fluctuation along the coast. Notably, vertical groundwater flow also occurs intensively in depression areas leading to an increase of salinity in deeper aquifers.

(i) Hydrogeochemical characteristics and origin of groundwater

Groundwater in the study area has different water types such as Na-Cl, Na-Mg-Ca-HCO3, Na-Mg-Ca-HCO3-SO4 and Na-HCO3-Cl. Groundwater showed a spatial heterogeneity in isotopic and chemical composition, reflecting different recharge sources and different magnitudes of mixing with brackish water. Shallow groundwater might originate from local rainfall with less evaporative losses, and experience seawater intrusion due to the rapid sea-level rise during the late Holocene age. In contrast, deep groundwater might originate from regional rainfall in high elevation areas and/or evaporated surface water sources in the last glacial period with fewer influences of mixing with brackish water.

(ii) Hydrogeochemical processes

The main hydro-geochemical processes which control groundwater quality in the Mekong Delta are included: (i) seawater intrusion in shallow aquifers and freshening process in deep aquifers, (ii) carbonate-silicate weathering and minerals dissolution have occurred in both shallow and deep aquifers (iii) leaking saline from upper layers to lower layers occurs naturally, and it is worse due to characteristics of discontinuous impermeable layers and significant groundwater level depletion in the deeper aquifers.

(iii) Groundwater salinization processes in coastal aquifers

The results of groundwater flow dynamics, hydro-geochemistry and stable isotopes showed that groundwater salinization in a coastal area of the MD was caused by various processes, including paleo-saline water trapped in sediment/rock, halite dissolution, and leaking saline from upper layers to lower layers. However, the problem of groundwater salinization is further exacerbated in recent years due to excessive groundwater exploitation with an increase of hydraulic connection between saline and fresh aquifers.

End member mixing analysis shows that both groundwaters shallow and deep groundwater were recharged dominantly by rainfall with an average ratio of 59% and 56%, respectively. Evaporation has a strong influence on deep groundwater, which contributed to 41% of deep groundwater. In contrast, brackish water has a substantial impact on the shallow aquifer, providing to 15% for shallow groundwater compared to only 5% for deep groundwater.

The prediction results of groundwater salinization based on three state-of-art machine learning models showed that high salinity affected-areas extends from coastal inlet to the central city with a length of 40 km and width of 20 km. The highest affected-areas were

predicted in the areas close to the massive groundwater exploitation, the hydraulic connection between upper and lower layers, and paleo-saline sources. In practice, therefore, the groundwater exploitation in the areas close to paleo-saline sources with substantial extraction rate and significant groundwater level depletion need to be limited.

The projection of groundwater exploitation and regional groundwater levels fluctuation in different scenarios indicates that continuing increase of pumping capacity together with decreasing groundwater levels in surrounding areas may cause significant groundwater level depletion, especially in central and coastal cities. Meanwhile, reducing groundwater pumping capacity in combination with stopping regional groundwater level depletion will help groundwater levels in the study area recovery remarkably.

These findings could provide insights into the groundwater flow system, hydrogeochemical characteristics and seawater intrusion processes in coastal aquifers of the Mekong Delta. It may also help water authorities and policymakers in Vietnam and other countries to propose appropriate policies and regulations on sustainable water resources use and management under pressure of human activities and unpredictable impacts of climate change and sea-level rise in coastal lowland regions around the world.

Keywords: Groundwater flow system, hydrogeochemistry, stable isotopes, seawater intrusion, aquifer interconnection, groundwater modelling, coastal aquifers, Mekong Delta.

Acknowledgements

First of all, I would like to express my sincere thanks to my supervisor, Prof. Dr Maki Tsujimura for his excellent guidance and great support during my study in Japan. Without his guidance, I will not be able to get my dream of completing my higher education in Japan. A special thanks to Prof. Dr Michiaki Sugita, Prof. Dr Jun Asanuma, and Prof. Dr Tsutomu Yamanaka for their helpful and valuable comments on my research.

I am incredibly grateful to MEXT (Ministry of Education, Culture, Sports, Science, and Technology), Japanese Government for financial support to pursue my PhD degree at the Graduate School of Life and Environment Sciences, University of Tsukuba, Japan.

Special thanks to all my colleagues at Thuyloi University and my friends in Soc Trang province, Vietnam, for their great support during field works. Thanks to Prof. Dr Vo Le Phu, Prof. Dr Bui Tien Dieu, Dr Dang Duc Thanh, Dr Pham Tien Dat, Mr Nguyen Le Duy, and Mr Nguyen Van Tam for very efficiency in research collaboration. Thank you to all my friends, especially Nguyen Duc Chinh and Phan Cao Duong for all the good times and support.

Furthermore, I would like to thank Tsujimura Lab members for their great supports during field surveys and water samples analysis. Thanks to Nagaosa-san and Imaizumi-san for the encouragement and teaching me the Japanese Language while in Japan.

To my family: my wife – Pham Thi Duy Hoa, my sons -Tran Hoang Nhat and Tran Tuan Kiet, who are always with me, love and encourage me to complete my study. Last but not least, special thanks to parents and young brother for their great help taking care of our sons when myself and my wife were not at home. From the bottom of my heart, I would love to say thank all of my family members, without your love and encouragement I could not achieve my PhD degree. I love you all and highly appreciate your support and help.

Table of Contents

Abbreviations

DWRPIS	Division for Water Resources Planning and Investigation for the South of Vietnam
EC	Electrical Conductivity
EMMA	End Member Mixing Analysis
GMWL	Global Meteoric Water Line
GWL	Groundwater Level
LMWL	Local Meteoric Water Line
MD	Mekong Delta
m.a.m.s.l	Meter above mean sea level
SGW	Shallow aquifer (Depth < 40 m)
DGW	Deep groundwater (Depth > 40 m)

List of Tables

List of Figures

List of Papers

Peer-reviewed Publications

1. **Tran Dang An**, Tsujimura M, Vo LP, Nguyen VT, Kambuku D, Dang TD. *Hydrogeochemical characteristics of a multi-layered coastal aquifer system in the Mekong Delta, Vietnam*. Environmental Geochemistry and Health (2019). https://doi.org/10.1007/s10653-019-00400-9.
2. **Tran Dang An,** Maki Tsujimura, Vo Le Phu, Nguyen Van Tam, and Nguyen Le Duy. "Stable Isotopes Characteristics of Water Resources in the Coastal Areas of the Vietnamese Mekong Delta". Journal of Isotopes in Environmental and Health Studies (2019). https://doi.org/10.1080/10256016.2019.1673746.
3. **Tran Dang An**, Tsujimura M, Phu VL, Ha DT, Hai NV. *Isotopic and Hydrogeochemical Signatures in Evaluating Groundwater Quality in the Coastal Area of the Mekong Delta, Vietnam*. In: Tien Bui D, Ngoc Do A, Bui H-B, Hoang N-D, editors. *Advances and Applications in Geospatial Technologies and Earth Resources: Proceedings of the International Conference on Geo-Spatial Technologies and Earth Resources 2017*. Springer International Publishing, Cham, 2018, pp. 293-314.

Conference proceeding

1. **Tran Dang An,** Maki Tsujimura, Vo Le Phu, Trieu Anh Ngoc, and Nguyen Van Tam. Evaluation of groundwater salinization processes in the coastal area of the Vietnamese Mekong Delta, IAH 2018 Congress, Daejeon, Korea.
2. **Tran Dang An**, Maki Tsujimura, Vo Le Phu, Trieu Anh Ngoc, Doan Thu Ha and Nguyen Van ai. Characteristics of seawater intrusion in a coastal region of the Vietnamese Mekong Delta. Proceedings of the International Symposium on Lowland Technology (ISLT 2018), Sep 2018.

Currently submitted papers:

1. **Tran Dang An,** Maki Tsujimura, Tien Dat Pham, Nguyen Van Tam, Dieu Tien Bui, Thanh Duc Dang, Trieu Anh Ngoc, Vo Le Phu, Doan Thu Ha. "*Spatial Prediction of Groundwater Salinity in Coastal Aquifers of the Mekong River Delta (Vietnam) using artificial intelligence*". (**Submitted to Journal of Hydrology 2nd Oct. 2019**).

CHAPTER 1 INTRODUCTION

1.1. Global groundwater resources

Water covers over 75% of the planet's surface; however, available freshwater is very limited directly to human use, accounting for less than 1.0 % of the total freshwater resources on the Earth (Trenberth, Smith, Qian, Dai, & Fasullo, 2007). Moreover, freshwater distributes unevenly from local to regional scales, and it has a wide variety in different seasons depending on natural cycles of freezing and thawing and fluctuations in precipitation, water runoff patterns and evapotranspiration processes (UN-Water, 2010b). Therefore, it is not easy for humans to access freshwater throughout the world. More seriously, global water resources are in crisis due to rapid population growth, fast urbanization, and severe impacts of climate change (IPCC, 2007). Many parts of the world are facing physical and economic freshwater scarcity which has negative influences on sustainable socio-economic development and ecosystem services. The global freshwater shortage occurs mainly because of the rapid increase of water demand, unstainable water management in combination with unpredictable impacts of climate change and sea level rise (Arnell, 2004; Vörösmarty, Green, Salisbury, & Lammers, 2000).

Among freshwater resources, groundwater is the largest accessible source of freshwater and plays a vital role in satisfying the primary water demand for humanity and ecosystems (Cuthbert et al., 2019; de Graaf et al., 2017; Evaristo & McDonnell, 2017). Groundwater has been widely used to many purposes in long history because of good quality, high yield, and less vulnerable to quality degradation and droughts compared to other available water resources on our planet. It serves as a primary source for many purposes such as drinking water, irrigation and industrial activities from arid, semi-arid to tropical regions around the world. For example, groundwater provides about 40% of the global water consumption in irrigation (Siebert et al., 2010), and approximately 50% of the world’s current potable water depend on groundwater resources (Giordano, 2009). It also becomes an indispensable water resource in many regions, especially in arid and semi-arid areas where frequently face water scarcity due to limited annual rainfall. In these regions, groundwater is the primary buffers against drought for both individual requirements and crop production, as shown in Figure 1 (Dalin, Wada, Kastner, & Puma, 2017a). In the United States, groundwater provides more than 65% of the total water demand for irrigation,

livestock, and 26% of domestic water use (Maupin, 2014). In the Asian and Pacific regions, groundwater provides more than 32% of the total water demand for human consumptions, and more than 80% irrigated water requirements (UN-Water, 2010a). In China, groundwater accounts for 45% total amount of water supply and 67% of total irrigated water (Udimal, Jincai, Ayamba, & Mensah Owusu, 2017). More noticeably, India is the largest groundwater consumer in the world where uses about 230-250 cubic kilometer per year accounting for 25% of the global groundwater use and more than the total amount of groundwater consumption in China and the United States (Giordano, 2009). Although more than 89% groundwater in India is extracted for irrigation system, it is also crucial freshwater source for human consumption providing approximately 50% of urban water demand and 85% of rural domestic water requirements (Bank, 2010). Even in tropical and sub-tropical regions with abundant surface water, groundwater is often an essential source of drinking water because groundwater has good quality and easy to use, especially in the areas where lack the water supply system. More specifically, groundwater in many coastal regions is primary freshwater source for both human activities and irrigation development because surface water has been increasingly polluted and severely intruded by seawater (Velis, Conti, & Biermann, 2017).

Despite crucial role of groundwater for both human development and ecosystems, groundwater resources in many regions across the world have been deteriorated (Cloquet, Carignan, Libourel, Sterckeman, & Perdrix, 2006; Ducci, Della Morte, Mottola, Onorati, & Pugliano, 2019; Zeidan, 2017; Zhai et al., 2017). For example, severe groundwater contamination(Stuckey, Schaefer, Kocar, Benner, & Fendorf, 2016) and severe seawater intrusion (Tiwari, Pisciotta, & De Maio, 2019b; Zanetti, Zegada-Lizarazu, Lambertini, & Monti, 2019) in many coastal regions and poses significant challenges to sustainable groundwater management in the context of extensive groundwater exploitation and sea-level rise.

The current situation in combination with unpredictable impacts of climate change and sea-level rise will pose extreme challenges to sustainable groundwater use and management in many parts of the world, especially in coastal lowland regions (Ferguson & Gleeson, 2012a). Therefore, understanding groundwater flow dynamics and hydrogeochemical processes under influences of natural variation and human activities as well relationship between groundwater and surface water within watersheds is needed (Llamas, Custodio, Coleto, Huerga, & Cortina, 2001; Takizawa, 2008).

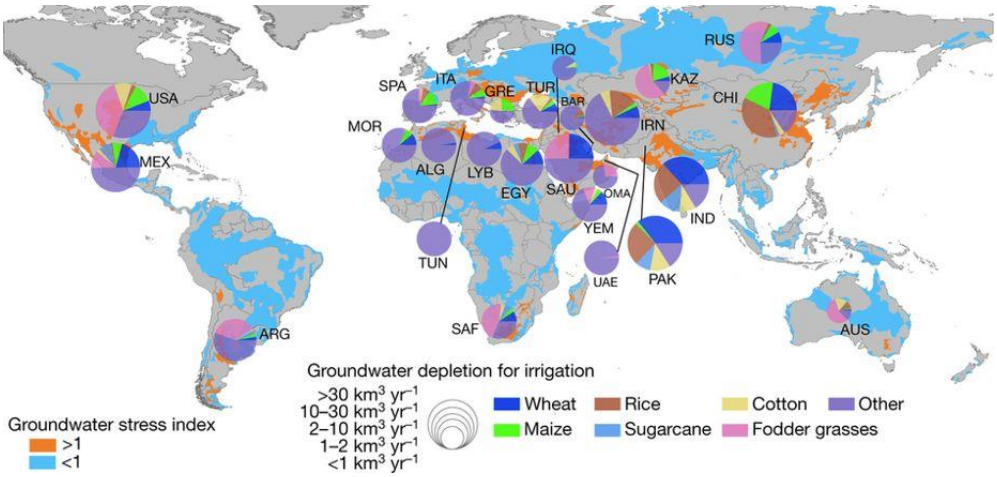

Figure 1-1: Crop-specific contribution to groundwater depletion worldwide in 2010 (Dalin et al., 2017a))

1.2. Groundwater in coastal lowland regions

The coastal region is a home of more than 2 billion people living around 200 km from the coast to inland around the world (Creel, 2003), thanks to secure access to the transportation system. These regions depend significantly on groundwater resources for drinking, industrial and agricultural development. However, groundwater resource is often very limited to human use and irrigation due to high salinity. Moreover, over-groundwater exploitation often leads to significant groundwater level depletion, groundwater contamination, and especially seawater intrusion given the prospects of climate change and sea-level rise (Ferguson & Gleeson, 2012a).

Nowadays, seawater intrusion (SWI) has become a global issue (Abu Al Naeem et al., 2019). SWI is a process of moving the salt source into the fresh aquifer system due to natural processes and human activities. SWI causes high salinity concentration in groundwater resources, exceeding water quality standard for drinking (chloride < 0.25 g/L) and irrigation purposes (TDS < 2 g/L). This situation poses a significant challenge to sustainable water use and management in many coastal regions across the world (Alfarrah & Walraevens, 2018). In particular, water containing high salinity not only strikes directly to crops and ecosystem (H. E. R. et al., 2015; Williams, 2009) but also potential threats to human health (A. Khan, Ireson, & Kovats, 2011; A. E. Khan et al., 2014; Talukder et al., 2017). High salinity in irrigation groundwater also causes land degradation via interconnection between saltwater and soil layers, resulting in the difficult recovery of agricultural lands in affected areas (Arslan & Demir, 2013). Therefore, understanding of groundwater salinization is a key to

prevent undesirable effects on agriculture activities and freshwater supply systems in many coastal regions in the world.

High salinity concentration in coastal groundwater is due to different seawater intrusion processes such as direct seawater intrusion into fresh aquifers (D. Han & M. J. Currell, 2018; A. Russak, Yechieli, Herut, Lazar, & Sivan, 2015), up coning by upward flow in the confining aquifers (Reilly & Goodman, 1987; Vincent & Violette, 2017), leaking saline from upper to lower layers (Cary et al., 2015; Gasda, Bachu, & Celia, 2004), and past marine transgressions (Hung Van, Van Geer, Bui Tran, Dubelaar, & Oude Essink, 2019; Larsen et al., 2017a). Over the past several decades, groundwater salinization has been reported in different magnitudes from regional to global scales (D. Han & M. J. Currell, 2018; Kanagaraj, Elango, Sridhar, & Gowrisankar, 2018). Most of the coastal aquifers in China, for example, has experienced seawater intrusion, resulting in rapid expanding saline-affected areas since 2003 (L. Shi & Jiao, 2014). Although the Chinese government has made the great effort to solve seawater intrusion problem SWI is still a severe issue due to tremendous increase of groundwater exploitation for the enormous amount of water consumption along the coast (D. Han & M. J. Currell, 2018). In the United States, the earliest report on SWI in all coastal aquifers has been conducted by Todd (1960). Afterwards, seawater intrusion has intensively reported by Konikow et al. (Konikow & Reilly, 1999) and Barlow et al. (Barlow & Reichard, 2010). Similarly, seawater intrusion has become a severe issue in coastal regions of India (Datta, Vennalakanti, & Dhar, 2009; Kanagaraj et al., 2018). In Africa, groundwater salinization was also observed in many coastal regions (Steyl & Dennis, 2010) such as in the Nile Delta (Nofal, Amer, El-Didy, & Fekry, 2015), in coastal areas of Libya (Sadeg & Karahanoðlu, 2001), Morocco (Haddout, Igouzal, & Maslouhi, 2017; Himi et al., 2017), and Tunisia (Ayed, Jmal, Sahal, Saidi, & Bouri, 2018; N. Trabelsi, Triki, Hentati, & Zairi, 2016; Zghibi, Tarhouni, & Zouhri, 2013). Additionally, seawater intrusion has been well documented in many coastal regions in Europe (Alfarrah & Walraevens, 2018). In recently, seawater intrusion increases the risks of water shortage and threat to national and global food security under impacts of climate change and sea-level rise (Ferguson & Gleeson, 2012a; Parizi, Hosseini, Ataie-Ashtiani, & Simmons, 2019). Although seawater intrusion in coastal region has been studied intensively for last several decades (Badaruddin, Werner, & Morgan, 2017), the processes of moving saline water into fresh aquifers largely depend on specific geo-environmental conditions and human activities. Moreover, groundwater salinization becomes a severe issue in the coastal lowland regions

where have experienced both historical geological formation processes and natural variation as well as human intervention (Fleckenstein, Krause, Hannah, & Boano, 2010). Therefore, understanding of groundwater salinization processes in these regions is a crucial task to sustainable groundwater resources use and management practices.

1.3. Literature review on groundwater flow system and hydrogeochemical processes

1.3.1. Global coastal aquifers

The coastal aquifer system is a transitional station in global water cycle between inland and ocean. Therefore, any human activities and natural variation will directly or indirectly influence the aquifer system and cause a change of groundwater flow dynamics and geochemistry (Figure 2).

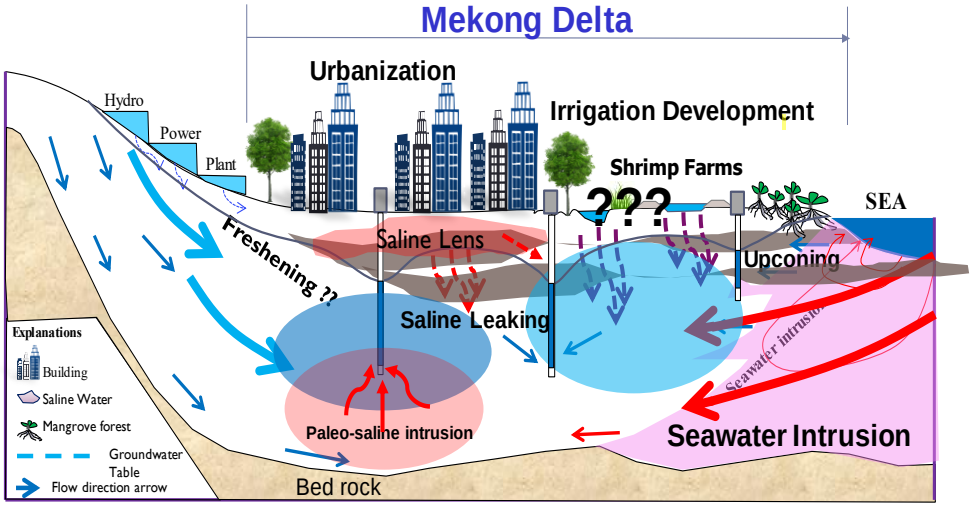

Figure 2-2: Conceptual model of the groundwater flow system from inland to the ocean.

Groundwater often originates from recharge areas to coastal regions, and groundwater flow system is regulated by many geo-environmental influencing factors (e.g., topography, geological and lithological conditions, recharge mechanism, tidal regime, and hydraulic gradients). The changes in hydraulic gradients play a crucial role in regulating groundwater flow dynamics in coastal regions where have a flat topography with relatively low elevation.

Many coastal lowland plains have experienced saltwater inundation during the past transgression processes, and saltwater intends to move downward due to difference of solute concentration between upper and lower layers. This process, however, is intensified rapidly due to significant groundwater level depletion and land subsidence. Besides, specific

characteristics of coastal lowland aquifers (e.g., discontinuous aquitards, saline groundwater trapped in sediment and clay layers) may cause serious groundwater salinization. Additionally, excessive groundwater pumping practices causes significant groundwater level depletion and reinforces seawater intrusion into fresh coastal aquifers (Erban, Gorelick, Zebker, & Fendorf, 2013; Samantara, Padhi, Sowmya, Kumaran, & Satpathy, 2017; Winkel, Berg, Amini, Hug, & Annette Johnson, 2008b). Climate change and sea-level rise are also likely increasing seawater intrusion in both surface and subsurface water system. This fact poses significant challenges to sustainable water resources management and ensuring water security to coastal regions worldwide (Ferguson & Gleeson, 2012a; Masciopinto & Liso, 2016; W. Shi et al., 2018).

Because of the critical role in the sustainable water supply to socio-economic development, numerous studies conducted to investigate groundwater flow system in coastal regions during the last several decades. These studies found out the main characteristics of groundwater in the coastal area. Firstly, groundwater originated from rainwater and mixed with seawater in coastal areas (Befus, Darhower, Liefert, & Shuman, 2019; Howcroft, Cartwright, Fifield, & Cendón, 2017; Huizer, Radermacher, de Vries, Oude Essink, & Bierkens, 2018). Secondly, the interrelation between groundwater and surface water also occurred as a result of hydraulic connectivity, discontinuous layer and groundwater level depletion (Hillel et al., 2019; Lucía, Romina, Eleonora, Esteban, & Héctor, 2019). Thirdly, groundwater geochemistry was controlled by water-rock interaction, seawater intrusion, and especially groundwater contamination (Gopinath, Srinivasamoorthy, Saravanan, & Prakash, 2019; Mahmoodzadeh & Karamouz, 2019); and groundwater in coastal areas are highly vulnerable to seawater intrusion and contamination.

For last several decades, many approaches have been applied to understand groundwater flow system such as conventional methods (e.g., field survey and monitoring, water chemistry and physical models) and innovative techniques (environmental tracers, numerical modelling, remote sensing and applied machine learning). Recently, the integration of conventional methods and innovative technologies has been widely used to provide a better understanding of the groundwater flow system in coastal regions. However, hydrological processes and geo-environmental influencing factors on groundwater flow dynamics and geochemical evolution are very complex, depending on specific natural conditions and human activities. Additionally, the origin of fresh and groundwater of coastal multi-layers in the lowland environment is also not fully understood. These issues pose a

significant challenge to sustainable groundwater management in coastal lowland regions across the world, especially in the context of intensive socio-economic development and global climate change.

1.3.2. Groundwater in the Vietnamese Mekong Delta

The Vietnamese Mekong Delta (VMD) is one of the most vulnerable regions to climate change and sea-level rise (Shrestha, Bach, & Pandey, 2016). In recent years, inappropriate water resources use, and management in the Mekong River Basin have resulted in water-related issues especially seawater intrusion and water contamination in the downstream regions including the VMD (Hecht, Lacombe, Arias, Dang, & Piman, 2019). Additionally, rapid population growth, fast urbanization, and intensive agricultural development in combination with unpredictable impacts of climate change and sea-level rise are also exacerbated groundwater depletion and water quality degradation which put high pressure on sustainable socio-economic development in the VMD. Groundwater is a primary water source for drinking, industrial and agricultural, especially in coastal areas of the VMD.

As having an essential role in sustainable socio-economic development in the VMD, groundwater resources have been studied since the 1970s. In their studies, Eugene D. Michael (Michael, 1971) and Anderson, H. R. (H. R. Anderson, 1978) provided the fundamental understanding of hydrogeological characteristics and groundwater flow system in the whole of Mekong Delta including Vietnam and Cambodia. In the next several decades, many studies focused on groundwater salinization assessment (Ho et al., 1991), groundwater modelling (Boehmer, 2000) and groundwater degradation, especially arsenic contamination in groundwater (Erban et al., 2013; Y. Huang et al., 2016; Yuheng Wang et al., 2018; Winkel et al., 2008b), recharge processes and groundwater-surface water interrelation (Duy et al., 2019; Kazama, Hagiwara, Ranjan, & Sawamoto, 2007) and groundwater geochemistry (An, Tsujimura, Le Phu, Kawachi, & Ha, 2014b; H. T. Hoang & Bäumle, 2018). Moreover, groundwater-related issues are threating to the VMD such as land subsidence (Minderhoud et al., 2017) and arsenic-related health problems (Berg et al., 2007; Merola, Hien, Quyen, & Vengosh, 2015; Shinkai, Truc, Sumi, Canh, & Kumagai, 2007). Recently, groundwater level depletion and seawater intrusion have become a severe issue in the Delta, mainly because of excessive groundwater exploitation and inappropriate groundwater management (Ha, Dieperink, Dang Tri, Otter, & Hoekstra, 2018). Seawater intrusion does put not only widespread threats to surface water resources and ecosystem in coastal areas of the VMD

(Trung & Tri, 2014) but also increase the high risk to water users including residents, animals, fishes, and crops. However, insights into groundwater salinization processes, aquifer interchange, the origin of saltwater, and influencing factors on geochemical evolution have been very limited due to data sparsity. Therefore, insights into tempo-spatial variation in the groundwater flow system and hydrogeochemical evolution are needed to ensure safe water supply system in a coastal area of the VMD – representative tropical regions.

1.4. Objectives of the study

The general aim of the present study to understand the spatial variability and temporal dynamics of groundwater flow, hydrogeochemical characteristics, groundwater salinization and its influencing factors. This research aims to address the knowledge gaps associated with groundwater flow dynamics and hydrogeochemical processes in coastal multi-layers in lowland regions under impacts of natural variation and human activities. To study groundwater flow dynamics and geochemical evolution in a coastal area of the VMD, the research was divided into four parts: Groundwater flow dynamics (Part I), Hydrogeochemical and stable isotopic characteristics and influencing factors (Part II), Groundwater salinization prediction and its controlling factors (Part III), and Synthesis and discussion, summary and conclusions (Part IV). The specific research questions of this PhD thesis have been addressed in the different chapters and are formulated as follows:

Part I: Groundwater flow dynamics in coastal aquifers

- What are the nature and spatial variability of groundwater flow and how does groundwater flow direction change under influences of pumping and tidal regime (chapter 4)?

Part II: Hydrogeochemical and stable isotopic characteristics and influencing factors

- What are geochemical characteristics and evolutions in coastal multi-aquifers, and which are the main influencing factors on groundwater quality in the study area? (Chapter 5)
- What are the isotopic characteristics of groundwater and surface water in the study area? How evaporation and seawater intrusion influences on groundwater quality? (Chapter 6)

Part III: Groundwater salinization and its controlling factors

- What are geochemical characteristics and evolutions in coastal multi-aquifers, and which are the main influencing factors on groundwater quality in the study area? (Chapter 7 and Chapter 8).

Part IV: General discussion, Conclusions and perspectives

- Chapter 9 discusses on main findings and compares with previous studies.
- Chapter 10 gives conclusions and perspectives.

Accordingly, key objectives can be listed as follows:

- To investigate characteristics of groundwater flow dynamics (groundwater level variation and flow direction) in coastal multi-aquifers under impacts of excessive groundwater exploitation and tidal regime.
- To examine groundwater origin and to estimate contribution ratio of each potential recharge sources to shallow and deep groundwater.
- To identify hydrogeochemical characteristics, especially minerals dissolution/precipitation, fresh-seawater mixing processes, and its influencing factors.

1.5. Thesis outline

Following the introduction, the structure of the thesis is as follows:

Chapter 1 is a brief introduction to this study. It describes the research background from three aspects: global groundwater status and groundwater in coastal lowland regions; literature review on groundwater flow system; and hydrogeochemical processes in coastal areas and the Vietnamese Mekong Delta. It also introduces the research objectives and structures of this PhD-Thesis.

Chapter 2 describes the study area, including geography, topography, geology, meteorology, hydrology and hydrogeology. Moreover, water use and other factors that affect water resources in these areas introduced in this chapter.

Chapter 3 presents the approaches and methodologies which were used in this study to obtain the objectives. Integrated approaches were applied in the present study, including

annual field surveys, on-site monitoring and measurement, water chemistry and isotopic analysis, multivariate statistical data analysis and groundwater modelling.

Chapter 4 investigates groundwater levels changes under the impacts of groundwater exploitation and tidal regimes.

Chapter 5 characterizes groundwater geochemistry and hydrogeochemical processes that control groundwater quality. This chapter also discusses groundwater salinization and nitrate contamination in the study area (mainly based on paper one published in the **Journal of Environmental Geochemistry and Health**, **SCIE IF 3.25 Q1**).

Chapter 6 studies isotopic characteristics of groundwater and surface water quantify influences of evaporation and seawater intrusion and investigate the origin of groundwater and surface water in the study area (mainly based on paper two published on **Journal of Isotopes and Environmental Health Studies**, **SCIE IF 1.367 Q2**).

Chapter 7 exams the main controlling factors of groundwater salinization. It also predicts chloride concentration and evaluates groundwater salinization risk in the study area (mainly based on paper three submitted to **Journal of Hydrology and, SCI IF 4.40 Q1**).

Chapter 8 predicts the influences of groundwater exploitation on salinization in the study area based on future groundwater use scenarios (paper four preparing to submit to the **Journal of Hydrological Processes, SCI IF 3.19 Q1)**.

Chapter 9 present general discussion on hydrogeochemical processes, seawater intrusion, the origin of groundwater and groundwater flow systems

Chapter 10 Summarizes the main findings, conclusions and perspectives.

CHAPTER 2 STUDY AREA

The study was carried out in a coastal area of the MD, Vietnam which could represent coastal tropical climate Asian monsoon regions. The geography, topography, geology, meteorology, hydrology and hydrogeology are described in this chapter. Besides, water use and other factors that affect water resources in these areas also introduced.

2.1. Location of Soc Trang Province

Soc Trang province is located in the lowest parts of the Mekong River Basin (MRB). It covers an area of 3,223.30 km^2, approximately 0.7 % and 5.9 % of Vietnam and the Mekong Delta, respectively with an average population of 1.621 million people in 2019 (General Office for Population and Family Planning). The study area consists of ten districts and one city of Soc Trang province, including Ke Sach, Chau Thanh, My Tu, Nga Nam, Thanh Tri, My Xuyen, Cu Lao Dung, Long Phu, Vinh Chau and Tran De districts and Soc Trang city, in which the Soc Trang city is the political - economic-social center of the province. Soc Trang administrative boundaries are contiguous with four provinces in the Mekong Delta: to the northwest is Hau Giang province; the northeast part connects with Vinh Long and Tra Vinh through the Hau river; the western part links to Bac Lieu province, and the southeast part connects directly to East Sea (Figure 2-1).

2.2. Natural conditions

2.2.1. Topography and geology

In the study area – Soc Trang province, the topography is relatively low and flat, which has an elevation ranging from 0.20 to 2.0 m above mean sea level (see Figure 2.2). The entire province of Soc Trang is located in the south of the Hau River estuary, and its topographical variability ranges from 0.2 to 2 m above mean sea level with an average high infield from 0.5 to 1.0 m. The elevation decreases from the Hau river to central inland while along with the coastal areas and Quang Lo channel, topography reflects lower land with hillocks on riparian land and Sea. Low-lying regions located in the southwestern part including My Tu, Chau Thanh, Thanh Tri, Nga Nam, and My Xuyen districts where frequently experience flooding in the rainy season. High terrain distributes along Hau River and along the coast including Vinh Chau town, Tran De, Long Phu, and Cu Lao Dung districts with average elevation ranging from 1.2 to 2.5 m. The highest area located in the sand dunes areas along the coastal line and the Hau River. In general, because of having low terrain dense canal and

river system connecting to the East Sea, the study area may be highly vulnerable to saltwater intrusion, especially in the dry season.

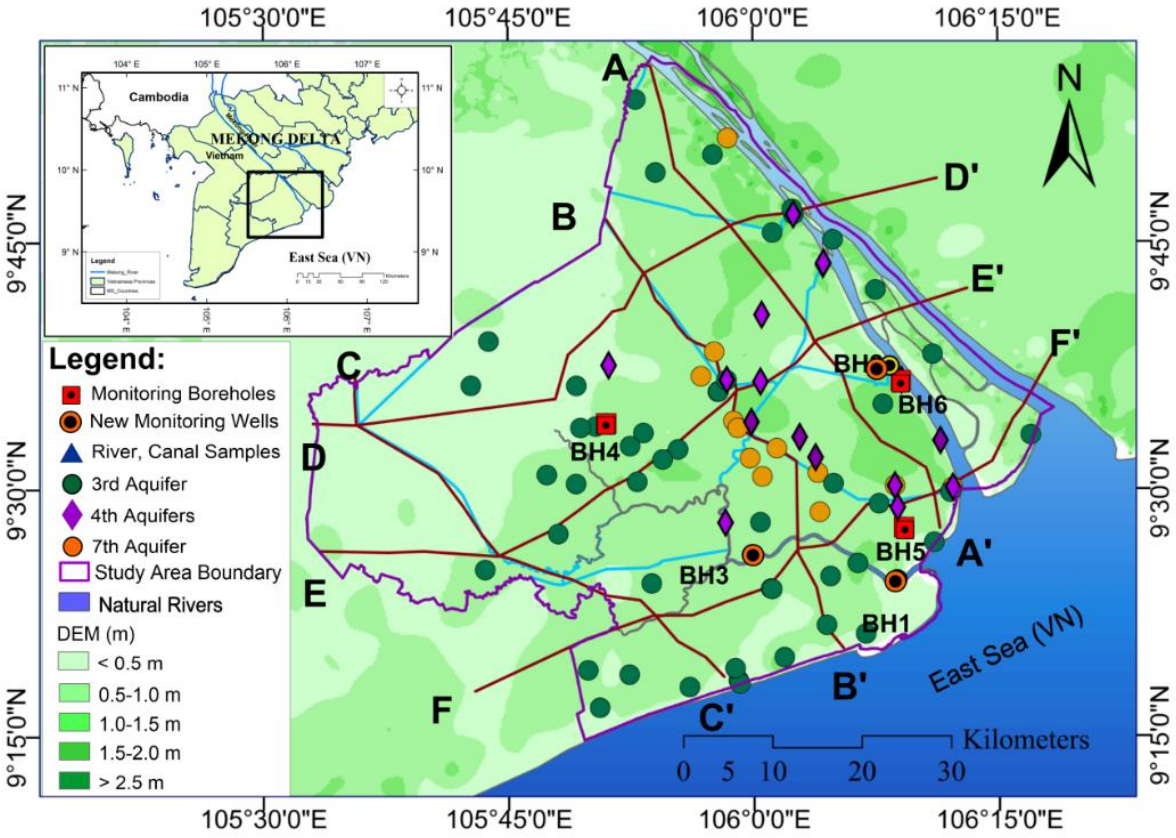

Figure 2- 1: Location and topography map of the study area – Soc Trang province in the Mekong Delta, Vietnam

2.2.2. Meteorology

In the study area, the climate consists of two tropical monsoon seasons (the dry and rainy season). The Southwest monsoon dominates in the rainy season, starting from May until October. This season accounts for 90% of total annual rainfall with high humidity (over 80%). The Northeast monsoon dominates in the dry season starting from November until April the following year, bringing dry air with hardly any precipitation (10% of the annual rainfall), and lower humidity. The averagely yearly rainfall ranges from 1660 to 2230 mm (Figure 2.2), and the temperature varies little and is 26-28°C (Figure 2.3). The relative humidity is highest from August to October (84-89%) and lowest in February to March (65-75%) as shown in Fig.2.4. The main wind flow directions are included the West, Southwest, Northeast, and Southeast depending on the dominance of the northeast monsoon and southwest monsoon. The wind flow direction is strongly influenced by the southwest

monsoon in the rainy season and the northeast monsoon in the dry season with an average wind speed of 1.77 m /s. Although Soc Trang province locates in a low frequency of tropical cyclone in the South East Asian region, the area has experienced two strong storm surges in 1952 and 1997 causing a massive number of deaths and destroying properties and infrastructure system (Takagi, Anh, & Danh Thao, 2017).

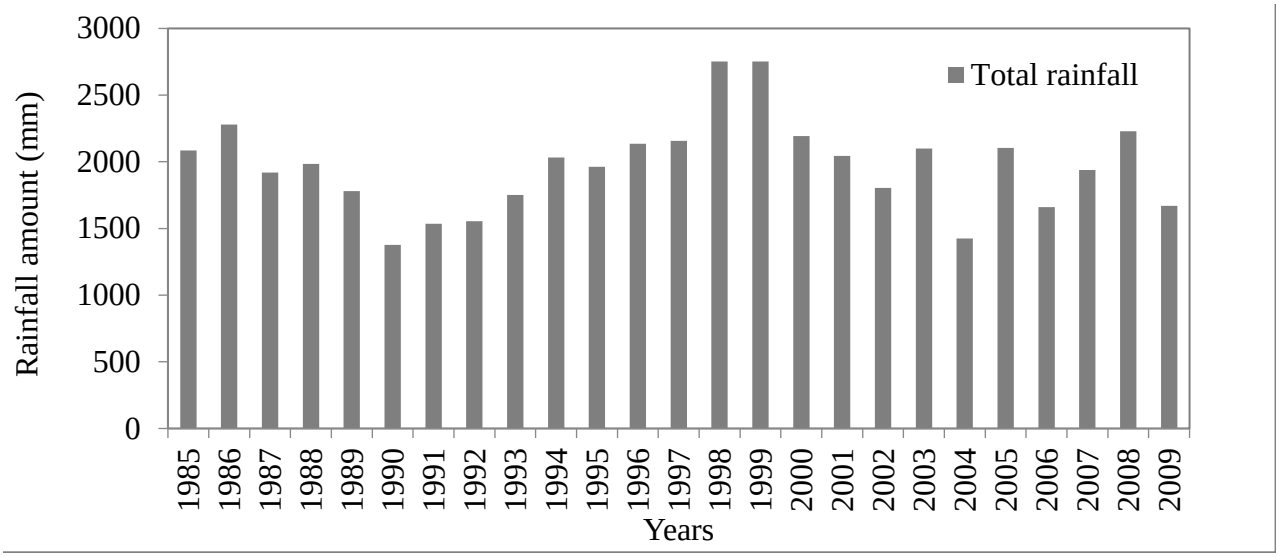

Figure 2- 2: Annual rainfall (mm) between 1985 and 2009 in Soc Trang Province, South Vietnam. (Source: DONRE, Soc Trang, 2013)

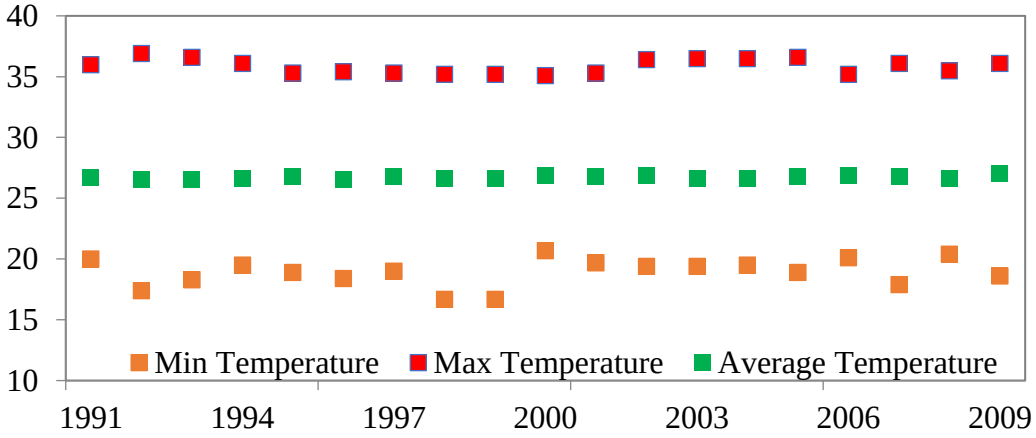

Figure 2- 3: The temperature in Soc Trang Province, South Vietnam

(Source: DONRE, Soc Trang, 2013)

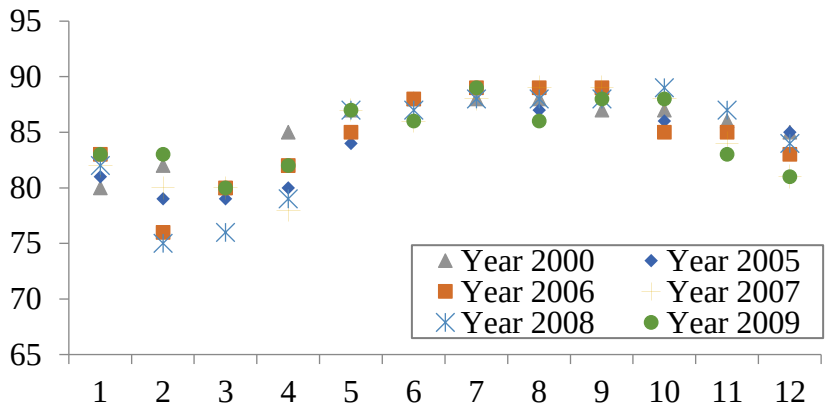

Figure 2- 4: Monthly Humidity distribution between 2000 and 2009 in Soc Trang Province, South Vietnam. (Source: DONRE, Soc Trang, 2013).

2.2.3. Hydrology

In Soc Trang province, rivers and canals have well connected with the river system in the MD and have a strong influence of upstream discharge and tidal fluctuation (Dang, Cochrane, Arias, Van, & de Vries, 2016). The annual release of the entire the Mekong River Basin into the MD distributes unevenly throughout the main tributaries (Figure 2-5). Moreover, yearly discharge into the Delta changes remarkably between the dry season with the maximum release of 2,100 m^3/s in April (low-flow season) and the rainy season with the maximum discharge of 40,000 m^3/s in September (high-flow season).

Soc Trang is one of the transit station between water from inland to the sea where water resources are mainly discharged through Dinh An and Tran De estuaries with capacity of 649 and 273 m3/s, comprising 11.5% and 27.4 % of the total water discharge into the Vietnamese Mekong Delta, respectively (Anh Duc Nguyen, Savenije, Pham, & Tang, 2008). According to Wolanski and Nhan, the Mekong River transports enormous amounts of sediments to coastal waters, discharging approximately 160 million tons annually, with the suspended sediment mainly comprising fine silt, but includes clay as well. However, the hydrological system in the Mekong Delta has changed unpredictably due to hydropower plants development. This situation causes seawater intrusion into the MD, especially in coastal areas (see Figure 2-6 and Figure 2-7).

Along with the coastal areas of Soc Trang province, river water levels and flow are most affected by many complex factors, mainly because of tide regime and inflow from upstream of the Mekong River. The tide is semi-diurnal with two daily peaks and two

bottoms. The highest peak is 158 cm (on October 13th), the lowest height was 123 cm (on May 8th) while the bottom is -24 cm (May 11th) and the smallest bottom reach to -221 cm (June 27th), the average tidal amplitude from 194-220 cm (Figure 2-8). River and canal water sources are the results of a mixture of onsite rainfall, seawater and water from upstream of the Mekong River. In estuary areas, surrounding Dinh An and Tran De estuaries, the relatively strong wave during the rainy season affect more than four miles away. Field nautical seasonal and coastal currents dominate water flow in the Dinh An estuary river - flows from the southwest are mainly (about 54 %) in the dry season and to the northeast (about 44, 6 %) in the rainy season. The surface water system is seriously influenced seawater intrusion in the dry season while in the rainy season in some parts of Soc Trang, 40 to 60 km from the coast, river water can be used for irrigated agriculture.

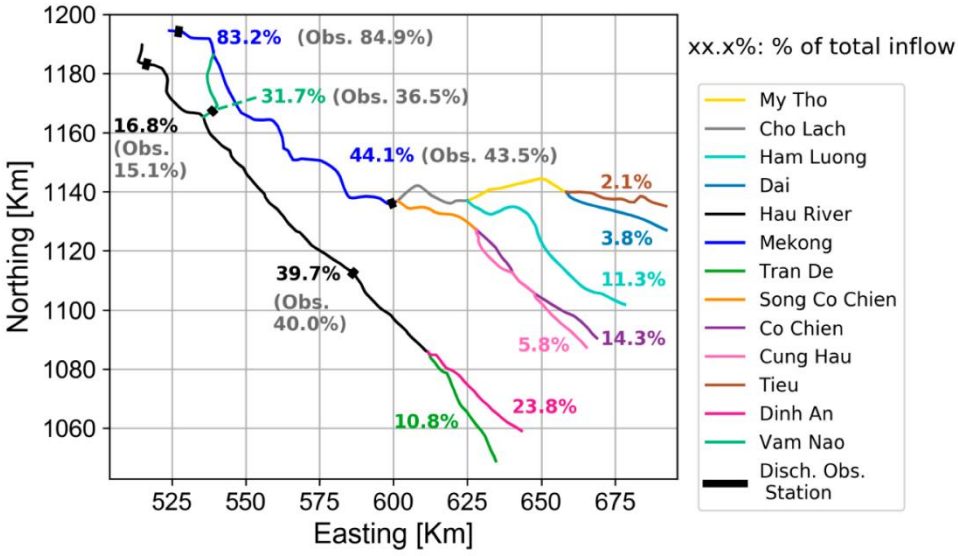

Figure 2- 5: Distribution of observed and predicted discharge flow ratio in the main tributaries of the Mekong River in the Vietnamese Mekong Delta (Eslami et al., 2019).

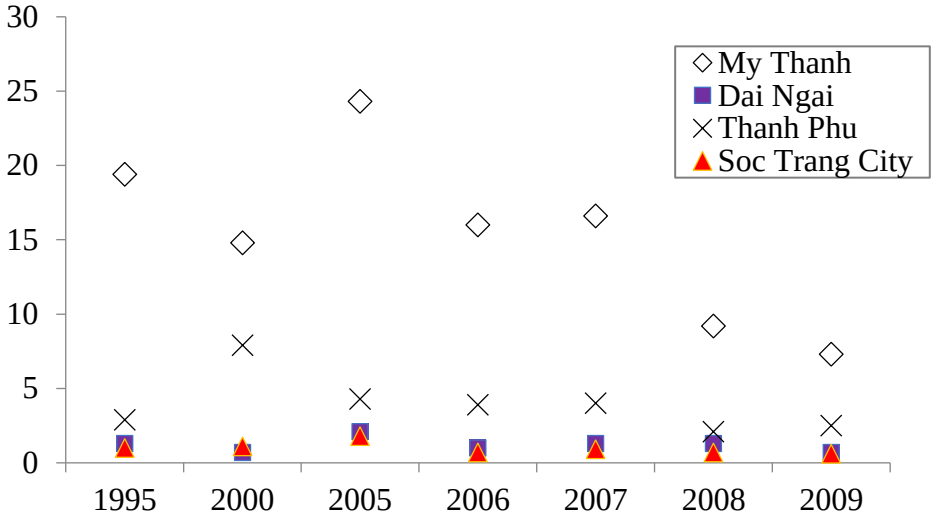

Figure 2- 6: Salinity distribution in 1991- 2009 in the meteorological station along Hau River (Source: DONRE, Soc Trang province, 2013)

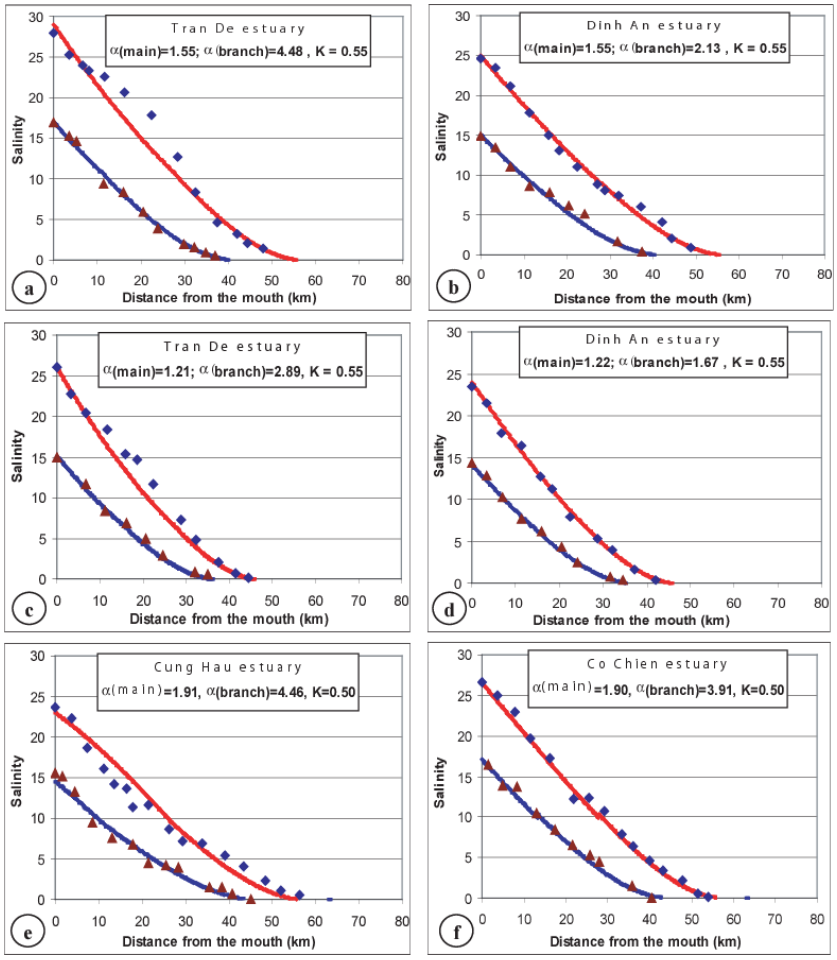

Figure 2- 7: The distribution of salinity concentration in the Mekong River.

(A. D. Nguyen & Savenije, 2006)

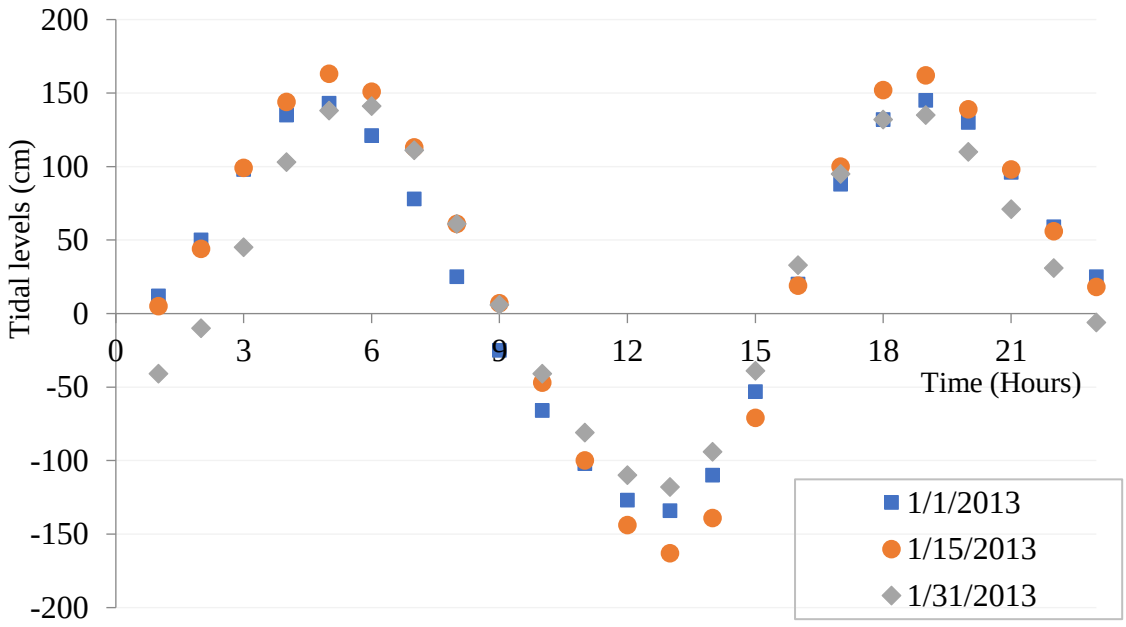

Figure 2- 8: Tidal regime in three periods of January 2013 in My Thanh station, Soc Trang province, Vietnam (Source: DONRE, Soc Trang province, 2013)

2.3.4. Hydrogeology

The aquifer system of the Mekong Delta was formed by the glacial-eustatic sea-level change and the ongoing tectonic subsidence of the Mekong Basin, therefore, its hydrogeology is somewhat complicated. To understand the hydro-geological characteristic of Soc Trang province, we should consider the formation process of hydro-geology in the MD. The delta was formed by sediment deposition approximately 6,000 years ago (V. L. Nguyen, Ta, & Tateishi, 1998; Wagner, Tran, & Renaud, 2010). Based on management perspectives, the aquifer system in the MD consists of five geological units: Holocene (qh);) Upper-Middle Pleistocene (qp2-3; Lower Pleistocene (qp1); Pliocene (m4); and Upper Miocene (m3). Figure 2-9 shows the hydrogeological cross-sections of the Mekong Delta, showing the vertical distribution of these water-bearing layers concerning the surface in the MD. The yellow layers described aquifers from Holocene (qh) to Upper Miocene aquifer (m3) which are capable of storage and flow among porous media. Whereas, the remaining layers represent largely impermeable units, such as clay and silt, that impede the flow of water between aquifers.

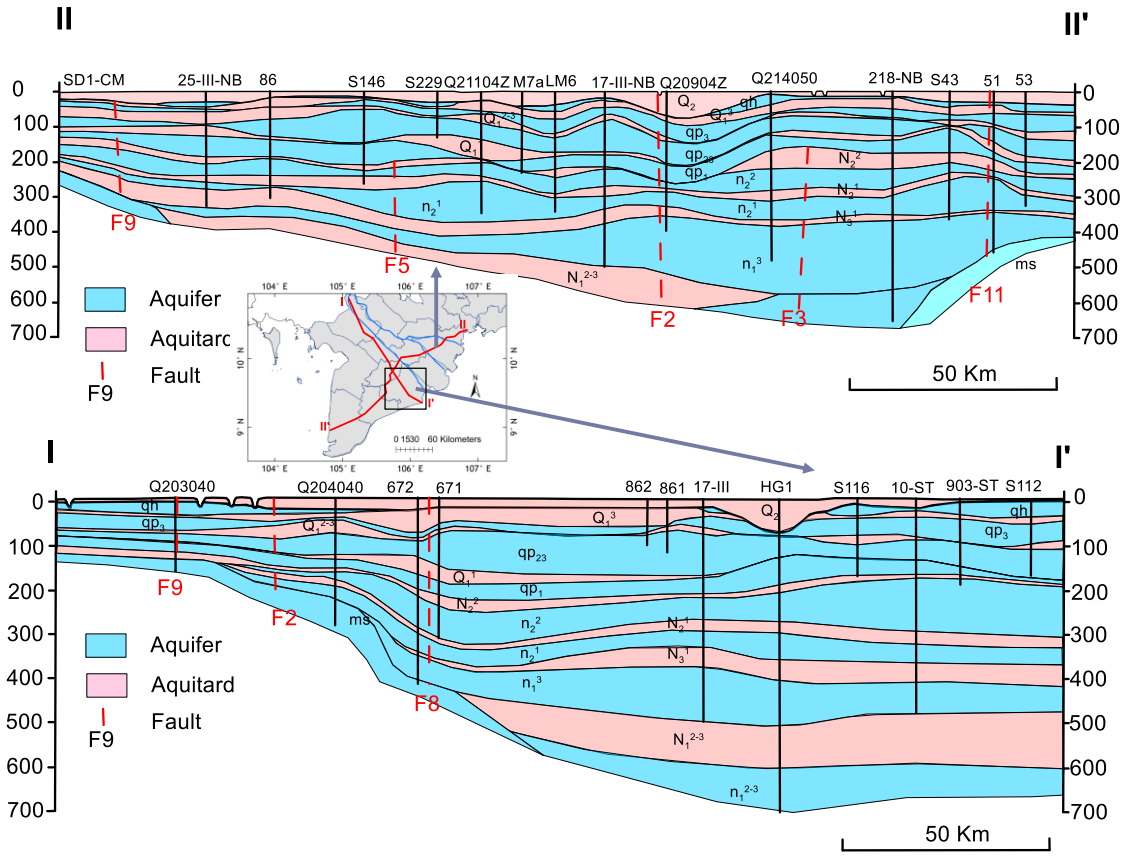

Figure 2- 9: Cross-section of the Mekong Delta roughly following the path of the Bassac River (Source: DWRPIS, 2010)

Aquifer system in the Soc Trang province is a part of the Mekong Delta system, which was formed by the processes of sediment deposition under impacts of river-sea interactions (Wagner, Tran, & Renaud, 2012). The aquifer system includes seven subdivision units, namely Holocene (qh), Upper Pleistocene (qp_3), Upper-Middle Pleistocene (qp_{23}), Lower Pleistocene (qp_1), Middle Pliocene (n_{22}), Lower Pliocene (n_{21}) and Upper Miocene (n_{13}) aquifer layers. Each hydrogeological unit has the upper and lower layer with different lithological characteristics. The top layer consists of silt, clay or mixed silt clay with low water yield (Wagner et al., 2012). In contrast, the lower part is relatively permeable, consisting of fine to coarse sand, gravel, and pebbles which water yield varies widely ranging from 0.03 L/s to 17.62 L/s as shown in the geological and hydrogeological units in Table 2-1. For the last several decades, pumping capacity from the qp_{23} and qp_1 aquifer has increased

rapidly because of high yield (17.6 L/s) and good quality. Meanwhile, groundwater extraction capacity from other aquifers is small due to low yields and high salinity (An, Tsujimura, Phu, Ha, & Hai, 2018). Table 2-1 showed the characteristics of aquifers and aquitards in the study.

Table 2- 1: Geological and hydrogeological units showing the classification of aquifers in Soc Trang province, Southern Vietnam.

Age	Subseries	Geological unit	Aquifers	Hydrogeological unit	Aver. depth below the surface (m)	Aver. layer thickness(m)	Yield (L/s)	Drawdown S (m)	Discharge rate (L/s.m)
Holocene	Upper	$mQ_{II}^{3}lm$	qh_3	Aquitard 1	9	18	N/A	N/A	N/A
	Middle/Lower	am,mQ_{II}^{2-3}/ am,mQ_{II}^{1-2}	qh_{2-3}/ qh_1	Aquifer 1	27	6.5	0.03	1.03	0.025
Pleistocene	Upper	$mQ_I^{3}lm$		Aquitard 2	50.39	22	N/A	N/A	N/A
		$amQ_I^{3}lm$	qp_3	Aquifer 2	53	20.5	0.53	2.57	0.195
	Middle	$mQ_I^{2-3}lt$		Aquitard 3	77	39	N/A	N/A	N/A
		$amQ_I^{2-3}lt$	qp_{2-3}	Aquifer 3	82.63	49.75	14.57	10.53	2.063
	Lower	$Q_I^{1}bm$		Aquitard 4	145.29	39	N/A	N/A	N/A
		$amQ_I^{1}bm$	qp_1	Aquifer 4	149	40.29	17.62	8.48	2.726
Pliocene	Upper/Middle	N_2^{3}/ $N_2^{2}nc$		Aquitard 5	201.4	44	N/A	N/A	N/A
		$amN_2^{2}nc$	n_2^{2}	Aquifer 5	212	96.22	2.63	30.95	0.086
	Lower	$N_2^{1}ct$		Aquitard 6	271	38	N/A	N/A	N/A
		$amN_2^{1}ct$	n_2^{1}	Aquifer 6	320.15	65.38	7.02	20.8s3	0.361
Miocene	Upper	$N_1^{3}ph$		Aquitard 7	332	41	N/A	N/A	N/A
		$amN_1^{3}ph$	n_1^{3}	Aquifer 7	403.72	59	10.7	11.2	1.827

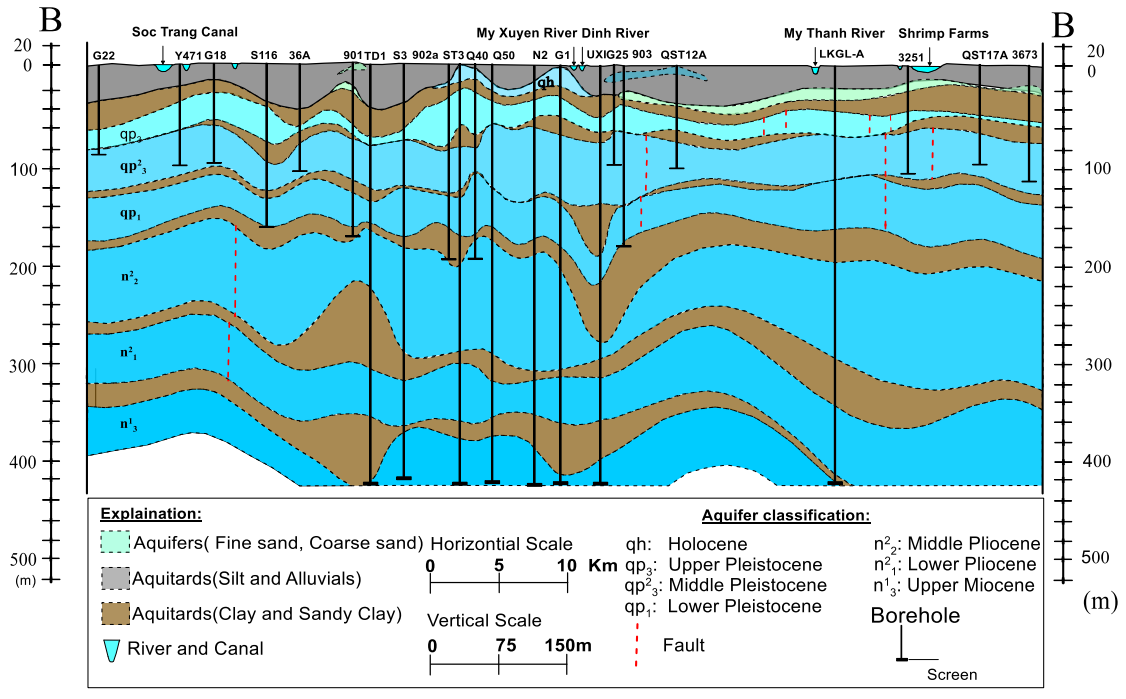

Figure 2- 10: Hydrogeological cross-section B-B' from NW to SE

(Source: DONRE, Soc Trang province, 2013)

2.3.4. Soil properties and land use

In the coastal area of the VMD, soil comprises silts and alluvial clays that are formed by the sediment transportation and deposition processes of the Mekong River. Therefore, land in this province has high fertility and is suitable for the development of rice cultivation, short-term industrial crops like sugarcane, soybeans, corn, and vegetables, such as onions, garlic and fruit trees such as grapefruit, mango and durian. Currently, agricultural land occupies 84.03% of Soc Trang province (33,160 ha) and forested land account 4.40% as shown in Figure 2-12. Additionally, salt and acid sulfate soil make up 0.97 % of total areas. Although in Soc Trang province there are various types of soil types, they can be divided into four main groups: group sandy, alluvial soils, soil salinity and others. Currently, the province is facing soil acidity and soil salinisation due to lowering groundwater levels and seawater intrusion.

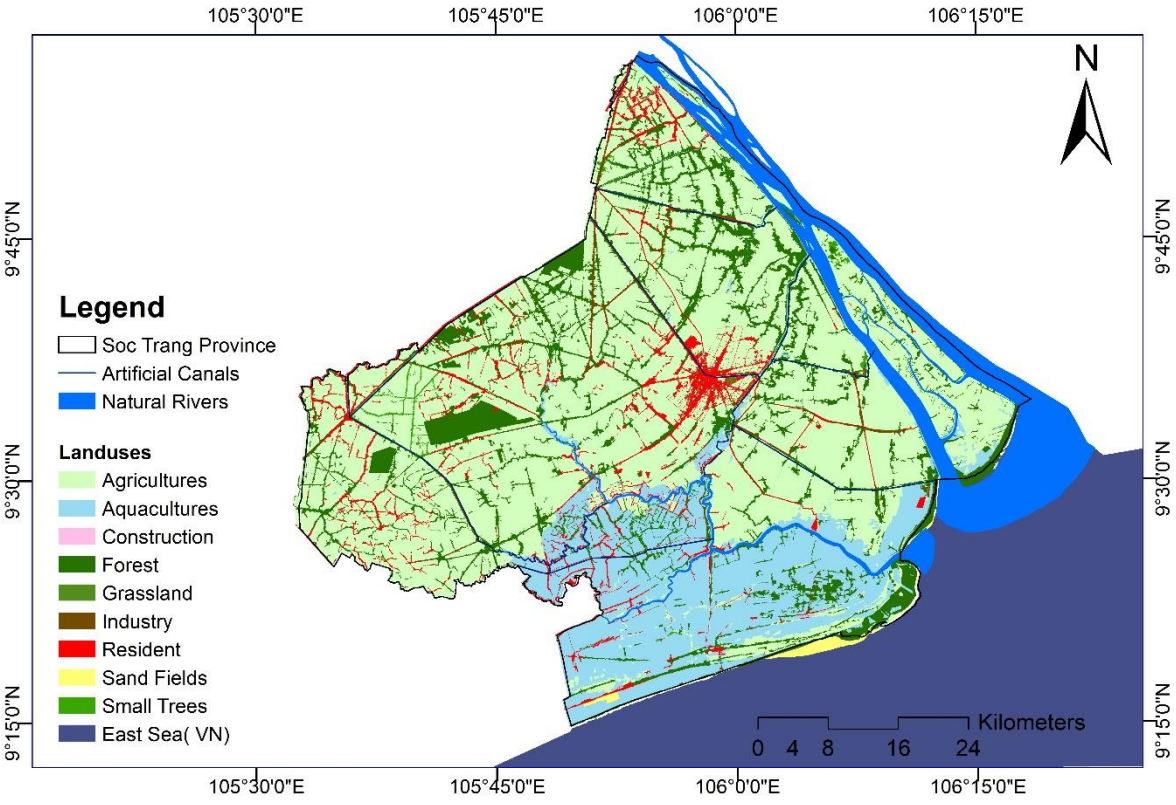

Figure 2- 11: Land use /land cover in the study area in 2013.

(Source: DONRE, Soc Trang province, 2013)

2.3. Groundwater use and current issues

Groundwater is a primary water resource in Mekong Delta, providing freshwater demand for around 2.0 million m^3/day for domestic, industrial and agricultural development (Bui Tran Vuong, 2016). For example, most of rural and urban water supply in the Mekong Delta depends on groundwater because it has a good quality, high yield, low treatment cost and simple operation and maintenance. Groundwater is extracted through different types of wells such as dug wells in Holocene aquifer, private tube wells, and industrial well with high capacity in Water Supply Company, Center for Rural Water Supply and Sanitation and private companies. Due to rapid population growth, fast urbanisation and intensive agricultural development, the groundwater use in the Mekong Delta have increased from 0.5 million m3/day in the 1990s to around 2.0 million m3/day in the 2010s (Minderhoud et al., 2017). This situation caused many groundwater-related problems such as arsenic contamination (Huyen et al., 2019), seawater intrusion (D. A. Tran et al., 2019) and land subsidence (Minderhoud et al., 2017). Although the Mekong Delta has seven aquifers, most of the groundwater derives from the Pleistocene aquifers (qp_3, qp_{23} and qp_1) which account for 60 % of the wells of the delta.

As a coastal area – Soc Trang province faces severe water shortage annually, especially in the dry season when surface water has very high salinity due to seawater intrusion. Groundwater, therefore, plays a crucial role in socio-economic development in this province, it provides fresh water supply not only to drinking and industrial development but also to the irrigation system. Currently, groundwater was extracted from 79,117 tube wells, and 804 dug wells with a total volume of approximately 245,000 m^3/day with 183,000 m^3/day from small private wells and 62,000 m^3/day of production wells from Soc Trang water supply company, Center for Rural Water Supply and Sanitation. Similar to many coastal regions in Vietnam and other countries in the world, groundwater in Soc Trang province has been deteriorated mainly because of over groundwater exploitation and unstainable groundwater management. The groundwater depletion may be exacerbated by negative impacts of climate change, and seawater levels rise (Shrestha et al., 2016). How to ensure residents in coastal areas can access adequate water remains a big challenge for water policymakers, researchers and managers. Therefore, understanding of groundwater flow dynamics and geochemical evolution under the influences of both human activities and natural changes is necessary.

CHAPTER 3 MATERIALS AND METHODS

3.1. Groundwater monitoring and field investigation

3.1.1. Groundwater level monitoring

In the present study, auto groundwater level and electrical conductivity (EC) measurements were installed in two boreholes in the coastal area and the main river (Figure 3-1). The groundwater level and EC values were measured in an hour interval. Also, groundwater levels at the national and provincial groundwater monitoring system, production wells from Soc Trang Water Supply Company and Center for Rural Water Supply and Sanitation as well as household wells were directly measured during field surveys in the dry and rainy season between 2017 and 2018.

3.1.2. In-situ measurement and sampling collection

A total of 278 groundwater and 79 surface water samples were collected between 2017 and 2018 in Soc Trang province (Figure 3.1). All water samples were taken into 100 ml plastic bottles then shipped to Japan for chemical and stable isotopes analysis at the University of Tsukuba.

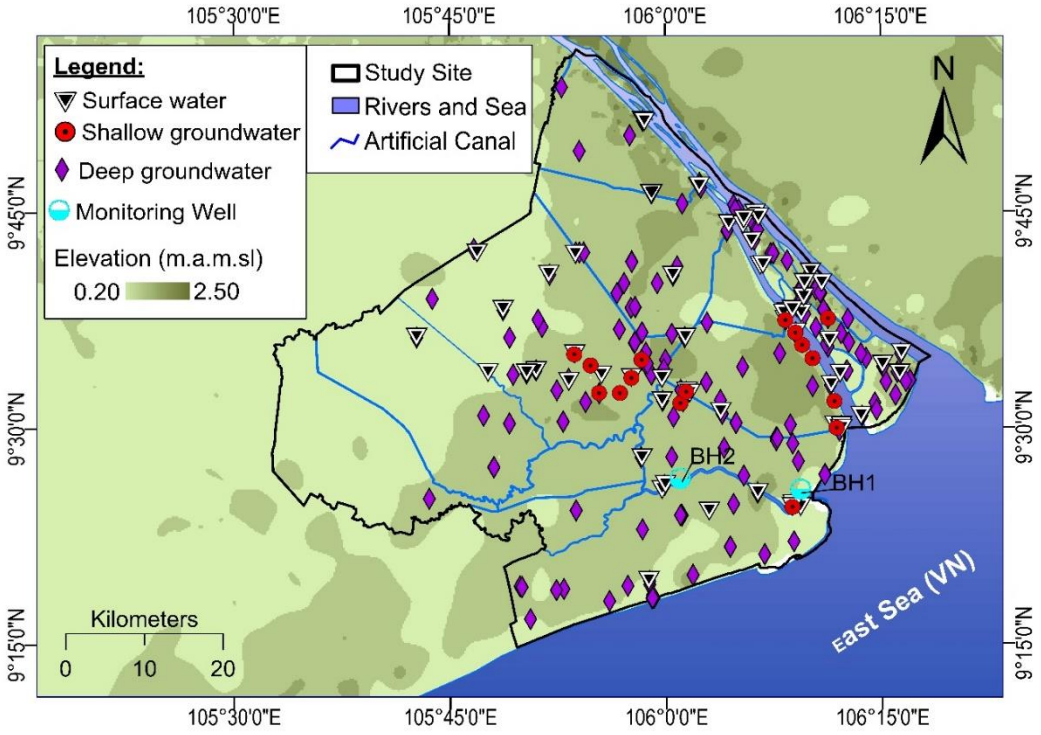

Figure 3- 1: Sampling locations in the study area (Soc Trang province).

The groundwater samples derived from private wells in households, municipal groundwater treatment plants and monitoring boreholes while surface water samples were collected from rivers and canal system. On-site measurement was conducted to obtained physical parameters such as temperature (T^{o}C), pH, dissolved oxygen (DO), and electrical conductivity (EC) using HANNA portable instruments.

3.2. Methodology

3.2.1. Chemical and stable isotopes analysis

For chemical and stable isotopes analysis, all water samples were filtered with a 0.02 µm cellulose ester filter. The bicarbonate (HCO_3^-) was deduced by using the titration method with sulphuric acid (0.05 M H_2SO_4). Major anions (Cl^-, SO_4^{2-}, and NO_3^-) were analysed using ion liquid chromatography (Shimadzu Co. Ltd., HIC-SP/VP Super) at the Hydrological sciences laboratory in the University of Tsukuba. The major cations (Na^+, K^+, Ca^{2+} and Mg^{2+}) were analysed using inductively coupled plasma optical emission spectrometer (ICP-OES, PERKIN ELMER, Optima 7300) at the Center of Chemical Analysis, University of Tsukuba, Japan. The analysis of stable isotopes ($\delta^{18}O$, $\delta^{2}H$) of water samples was done by a PICARRO L2120-I water analyser utilising the cavity ring-down spectroscopy technology. The results of isotopic measurements were calibrated to the international standards of Vienna Standard (V-SMOW). The stable isotopes of oxygen and hydrogen are presented in the delta notation ($\delta^{18}O$, $\delta^{2}H$) in per mil (‰) as follows:

$$\delta_{sample} = \left(\frac{R_{sample} - R_{standard}}{R_{standard}} \right) \times 1000 \qquad (3.1)$$

Where R is the ratio of the heavy to light isotopes, R = $^{2}H/^{1}H$ for hydrogen and $^{18}O/^{16}O$ for oxygen (Richards et al., 2018). The analysis precision is ± 0.1‰ for $\delta^{18}O$ and ±1‰ for $\delta^{2}H$. The deuterium excess (herein *d*-excess) values of water samples were estimated using the relation defined by Dansgaard (1964):

$$d = \delta^2H - 8 \times \delta^{18}O \qquad (3.2)$$

3.2.2. Hydro-geochemical Evaluation Methods

Seawater intrusion processes in coastal aquifers are very complex in space and time. Therefore, the multi-analysis approaches were used to investigate the status of salinisation and freshening processes. The method includes several steps, as follow:

- **Step 1**: Statistical analysis of hydrogeochemical parameters was employed to understand tempo-spatial distribution salinity in water bodies.
- **Step 2:** Ion deviations (Δ_{mi}) were estimated based on the theory of fresh-seawater mixing to quantify the extent of chemical reactions occurring during seawater intrusion and freshening aquifers(C. Appelo, Postma, D, 2005; Appelo, 1994).
- **Step 3:** End member mixing analysis was also employed to estimate the contribution ratio of each potential member to end member (D. J. R., Oude, J., & J., 2013).

a. Fresh-seawater mixing analysis

It was assumed that Cl^- is a conservative tracer and mainly originates from seawater. Therefore, the fraction of seawater (f_{sea}) in the water sample can be obtained from chloride concentrations of saltwater and freshwater as follows (Appelo, 1994):

$$f_{sea} = \frac{m_{Cl^-,sample} - m_{Cl^-,fresh}}{m_{Cl^-,sea} - m_{Cl^-,fresh}} \qquad (3.3)$$

Where, $m_{Cl^-,sample}$, $m_{Cl^-,fresh}$ and $m_{Cl^-,sea}$ are the concentration of Cl^- in the water sample, freshwater and seawater, all are expressed in mmol/L. In the coastal delta, fresh groundwater contains mainly Ca^{2+} and HCO_3^- which are added due to minerals dissolution process. Therefore, the appearance of all other ions in the water sample may attribute to seawater admixture. In this case, $mi_{fresh} = 0$ for all components except Ca^{2+} and HCO_3^- (Alfarrah & Walraevens, 2018) and seawater fraction ratio in the Eq.3.3 become:

$$f_{sea} = \frac{m_{Cl^-,sample}}{m_{Cl^-,sea}} = \frac{m_{Cl^-,sample}}{566} \qquad (3.4)$$

The concentration of ion i (mi) in the mixed fresh-seawater was calculated using the mass fraction of seawater (f_{sea}) followed the Eq.3.4 as below:

$$mi_{mix} = f_{sea} \times mi_{sea} + (1 - f_{sea}) mi_{fresh} \qquad (3.5)$$

Where mi_{mix} is a concentration of an ion i in mmol/L of expected mixed fresh-seawater, and subscripts mix, sea, and fresh indicate the conservative mixture, and end members seawater and freshwater, respectively. Any change in concentration $mi_{reaction}$ (Δ_{mi}) because of reactions without mixing then becomes:

$$\Delta_{mi} = mi_{sample} - mi_{mix} \qquad (3.6)$$

Where mi_{sample} is the measured concentration in the sample in mmol/L. The deviation of chemical composition from a fresh-seawater mixture represents chemical reactions, occurring due to seawater intrusion. A positive value means that the ion has been added to the water sample, e.g., due to desorption from the exchange complex while a negative value may indicate the absorption processes.

b. End members mixing analysis (EMMA)

The present study employs the simplified mixing model, namely End Member Mixing Analysis (EMMA) to estimate the contribution ratio of potential water sources to surface water and groundwater. The EMMA is a popular hydro-geochemical mixing model, and it has been widely used in hydrogeology study to identify and qualify the contribution ratios of different water sources to surface water and groundwater (Barthold et al., 2011; Hooper, Christophersen, & Peters, 1990; James & Roulet, 2006; Pelizardi, Bea, Carrera, & Vives, 2017). It uses the dominant chemical compositions of potential end members within the watershed to determine the ratios (percentage) of each original parent's water contributing to a final member (Gracz, Moffett, Siegel, & Glaser, 2015; Sakakibara, Tsujimura, Song, & Zhang, 2017). The mixing model, therefore, is based on the four assumptions including (i) surface water/groundwater is a final mixture of different water sources, (ii) the mixing

process follows linear and hydrodynamic mechanism, (iii) the mixed compositions are conservative tracers, and (iv) the source solutions are dominant concentrations (Barthold et al., 2011). However, the hydrological processes in the watershed vary in time and space. Therefore, the selection of end members should consider carefully before applying EMMA approach (Barthold et al., 2011; Pelizardi et al., 2017). In the coastal estuarial region, water sources generally originated from various sources such as rainfall, surface water, seawater and groundwater in different aquifers. To simplify involved contributors, we assume that surface water originated from rain, upstream surface water and seawater while groundwater derived from rain and seawater. The estimation of contribution ratio for each end members to surface water and groundwater based on following the equations:

For surface water:

$$f_R + f_{UPW} + f_{SW} = 1 \quad (3.7)$$

$$f_R \times \delta_R + f_{UPW} \times \delta_{UPW} + f_{SW} \times \delta_{SW} = \delta_S \quad (3.8)$$

$$f_R \times Cl_R + f_{UPW} \times Cl_{UPW} + f_{SW} \times Cl_{SW} = Cl_S \quad (3.9)$$

For groundwater:

$$f_R + f_{SW} = 1 \quad (3.10)$$

$$f_R \times Cl_R + f_{SW} \times Cl_{SW} = Cl_G \quad (3.11)$$

Where, f- Contribution ratio of each end member to final mixtures (f_R – the local ratio of rainfall, f_{SW} – the ratio of seawater, and f_{UPW} – the ratio of upstream freshwater. Notation of δ, Cl is the stable isotope of oxygen-18 ($\delta^{18}O$ ‰) and chloride (mg/L), considering as the conservative tracers. End members were chose including R- rainwater ($\delta^{18}O$ = -9.29 ‰, Cl = 0.99 mg/L), SW- seawater ($\delta^{18}O$ = -0.82 ‰, Cl = 16020.59 mg/L) which were collected during field survey in 2017, and UPW- average upstream fresh surface water ($\delta^{18}O$ = -7.20 ‰, Cl = 6.75 mg/L) in Dong Thap province approximately 150 km without effect of seawater intrusion.

3.2.3. Quantification influences of evaporation and seawater intrusion on stable isotopes

Evaporation and seawater intrusion are the major processes causing changes in stable isotopes of surface water and groundwater in coastal areas. Fresh-seawater mixing is a common phenomenon in many coastal regions worldwide. Groundwater and surface water samples in a coastal area can be found as the mixtures of freshwater and seawater (Figure 3-2). The stable isotope compositions of $\delta^{18}O$ or $\delta^{2}H$ in groundwater and surface water before mixing with seawater, δ_{bm}, can be estimated as follows [63]:

$$\delta_{bm} = [\ \delta_m \times (C_{sw} - C_{fw}) - \delta_{sw} \times (C_m - C_{fw})] \ / \ (C_{sw} C_m) \qquad (3.10)$$

Where δ_m and δ_{sw} are the $\delta^{18}O$ or $\delta^{2}H$ (‰) values of a measured sample and seawater, C_{fw} is the Cl^- concentration of freshwater (rainwater in this study), C_{sw} is the Cl^- concentration of seawater, C_m is the measured Cl^- concentration (mg L^{-1}) in water samples.

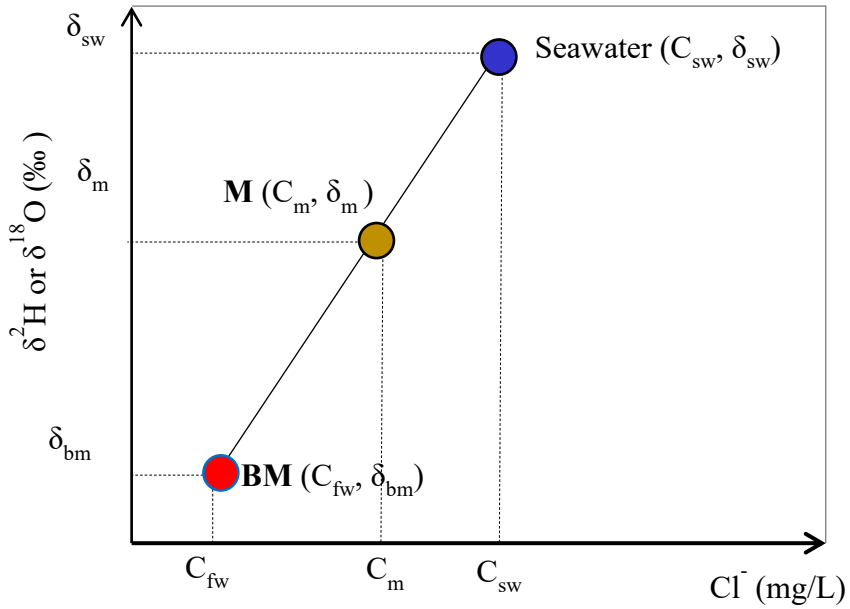

Figure 3- 2: The conceptual diagram explaining the correction scheme for isotopic changes due to seawater intrusion.

In this study, the Cl^- concentration of the freshwater end-member is 1.0 mg L^{-1} (based on the average Cl^- concentration of rainwater samples collected in the rainy seasons of 2017 and 2018). The Cl^- concentration of the seawater end-member is selected as 23,000 mg L^{-1}

(Tsutomu et al., 2011). Figure 3 shows the changes in stable isotope compositions in water due to evaporation and seawater mixing. In more detail, the two processes are (1) changes in stable isotope compositions from the source of water R ($\delta^{18}O_o$, $\delta^{2}H_o$) to evaporated water BM ($\delta^{18}O_{bm}$, $\delta^{2}H_{bm}$) and (2) mixing of evaporated water BM with seawater to form M ($\delta^{18}O_m$, $\delta^{2}H_m$) at sampling points. To derive the original isotopic composition of water R ($\delta^{18}O_o$, $\delta^{2}H_o$), after calculating evaporated water BM, Equations (4) and (5) can be solved to obtain the stable isotope composition from the source R as shown in Figure 3 (Phillips, Peeters, Tansey, & Davis, 1986; Tsutomu et al., 2011). This is because R is the intersection point of the local meteoric water line for the Mekong Delta (purple line, Figure 3) and the evaporation line that passes through BM ($\delta^{18}O_{bm}$, $\delta^{2}H_{bm}$) (red line, Figure 3-3).

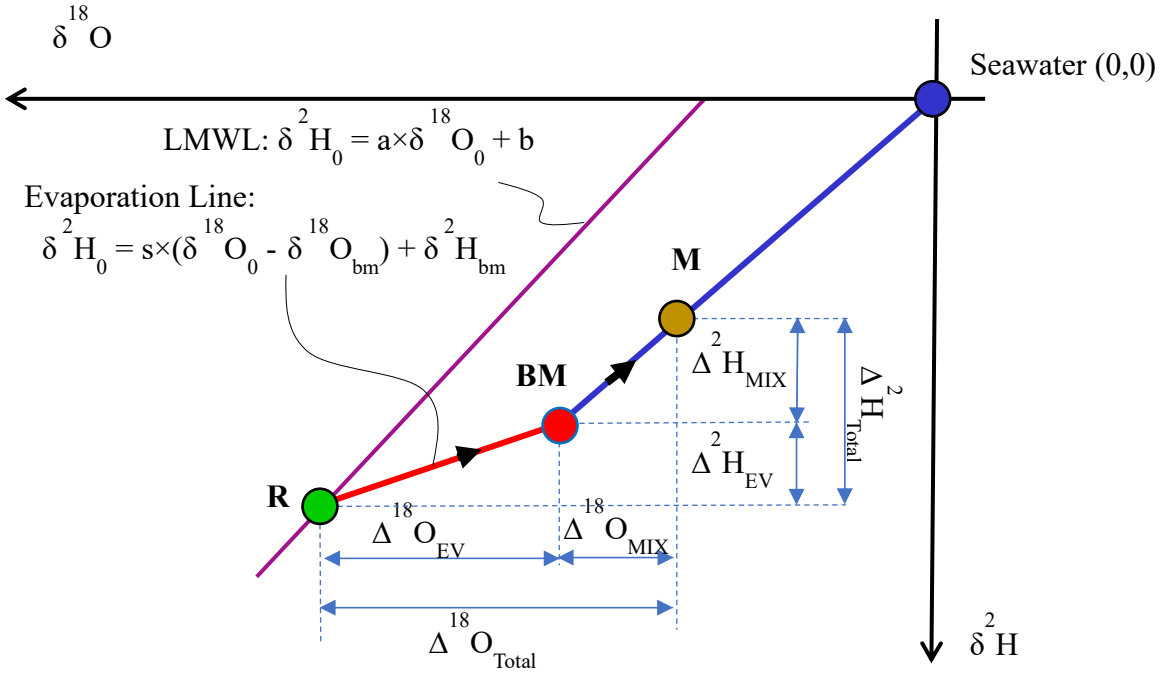

Figure 3- 3: Conceptual diagram explaining the isotopic change due to evaporation effects and seawater mixing. The green point R ($\delta^{18}O_o$, $\delta^{2}H_o$) represents the source of a water sample without evaporation effects and seawater mixing, which is considered as a fresh-end member. The red point BM ($\delta^{18}O_{bm}$, $\delta^{2}H_{bm}$) denotes the evaporated water before mixing with seawater. The orange point M ($\delta^{18}O_m$, $\delta^{2}H_m$) is the measured sample at the sampling point.

The blue point Seawater (0,0) is the standard seawater as the seawater-end member (adapted from Yamanaka et al., 2011).

$$\delta^2H_o = \left(\delta^2H_{bm} - s \times \delta^{18}O_{bm} - s \times b/a\right) / \left(1 - s/a\right) \quad (3.11)$$

$$\delta^{18}O_o = \left(\delta^2H_o - b\right)/a \quad (3.12)$$

Where is the slope of the evaporation line, a =7.56 and b =7.26 are the slope and intercept of local meteoric water lines (LWML: $\delta^2H = 7.56 \times \delta^{18}O + 7.26$) in the Mekong Delta, respectively (N. Le Duy, Heidbüchel, Meyer, Merz, & Apel, 2018). The slope of the evaporation line (denoted as s) was estimated based on the average relative humidity (h) and temperature (T) in the study area. The average surface air temperature of 26.8 ºC and the average relative humidity of 0.80 (based on data series from 2000 to 2016) were used to estimate the slope of evaporation following the Eq. 3.13 below (P. Huang & Wang, 2017):

$$s = \frac{24.844(10^6/(T+273)^2) - 76.248(10^3/(T+273)) + 52.612 + 12.5(1-h)}{1.137(10^6/(T+273)^2) - 0.4156(10^3/(T+273)) - 2.0667 + 14.2(1-h)} \quad (3.13)$$

Accordingly, the slope of the evaporation line (s) is 6.41, which is similar to the slope of the regression line for surface water in the dry season (6.45).

Subsequently, the changes in stable isotope compositions caused by evaporation processes and seawater intrusion could be estimated following equations:

For $\delta^{18}O$:

$$\Delta^{18}O_{total} = \delta^{18}O_m - \delta^{18}O_o \quad (3.14)$$

$$\Delta^{18}O_{MIX} = \delta^{18}O_m - \delta^{18}O_{bm} \quad (3.15)$$

$$\Delta^{18}O_{EV} = \delta^{18}O_{bm} - \delta^{18}O_{o} \quad (3.16)$$

For $\delta^{2}H$:

$$\Delta^{2}H_{total} = \delta^{2}H_{m} - \delta^{2}H_{o} \quad (3.17)$$

$$\Delta^{2}H_{MIX} = \delta^{2}H_{m} - \delta^{2}H_{bm} \quad (3.18)$$

$$\Delta^{2}H_{EV} = \delta^{2}H_{bm} - \delta^{2}H_{o} \quad (3.19)$$

Where $\Delta^{18}O_{total}$ and $\Delta^{2}H_{total}$ are the changes in $\delta^{18}O$ and $\delta^{2}H$ compositions caused by both evaporation and seawater intrusion, $\Delta^{18}O_{EV}$ and $\Delta^{2}H_{EV}$ are the changes in $\delta^{18}O$ and $\delta^{2}H$ of the source (R) caused by evaporation processes, $\Delta^{18}O_{MIX}$ and $\Delta^{2}H_{MIX}$ are the changes in $\delta^{18}O$ and $\delta^{2}H$ of the source (R) caused by seawater mixing. The contribution ratio of evaporation (F_{EV}) and seawater intrusion (F_{MIX}) that causes heavy isotope enrichment from sources can be estimated using the following equations:

For $\delta^{18}O$:

$$F^{18}O_{EV} = \Delta^{18}O_{EV} / \Delta^{18}O_{Total} \quad (3.20)$$

$$F^{18}O_{MIX} = \Delta^{18}O_{MIX} / \Delta^{18}O_{Total} \quad (3.21)$$

For $\delta^{2}H$:

$$F^{2}H_{EV} = \Delta^{2}H_{EV} / \Delta^{18}O_{Total} \quad (3.22)$$

$$F^{2}H_{MIX} = \Delta^{2}H_{MIX} / \Delta^{18}O_{Total} \quad (3.23)$$

The seawater/freshwater mixing ratio (f_{sw}) was estimated as to investigate influences of seawater intrusion on fresh groundwater in the study area as follows:

$$f_{sw} = Cl^-_{sample} / Cl^-_{seawater} \quad (3.24)$$

3.2.4. Vertical flow rate estimation

Vertical flow is a common process in the coastal aquifer system, which caused by different density between saline water in the upper layers and freshwater in lower layers. Also, the groundwater level depletion in lower layers compared with upper layers is also a driving force behind the movement of groundwater from shallow to deep aquifers. Based on two factors (different density and different hydraulic head between the upper and lower layers), the vertical flow rate can be estimated following equation 3.25 and 3.26. Hydraulically, an increase hydraulic gradient due to groundwater depletion coupled with high vertical hydraulic conductivity, think aquitard, and high-density gradients cause an increase of vertical flow rate as shown in the following equations (Q. Ma et al., 2015).

$$q_v = -\delta \times K_v \left[\frac{h_{up} - h_{low}}{\Delta L} + \varepsilon\left(\frac{C_{up} + C_{low}}{2}\right)\right] \quad (3.25)$$

$$\delta = \frac{\mu_0}{\mu} = 1 - \xi \times \varepsilon \quad (3.26)$$

Where: δ – the ratio of the dynamic viscosity of freshwater to seawater; K_v is a vertical hydraulic conductivity [m d^{-1}]; h_{up} and h_{low} denote the freshwater equivalent hydraulic heads at upper and lower layers [m], ΔL is the distance from upper to lower layers [m]; μ_0 and μ denote the dynamic viscosity [kg m^{-1} d^{-1}]; ξ is a constant; C_{up} is average observed salinity of pore water in upper aquifers [kg/m^3]; C_{low} is observed salinity of pore water in lower aquifers [kg/m^3], and ε is a constant. The similar findings were also found in other coastal aquifers in the world (Cary et al., 2015; Chatton et al., 2016a; Delsman et al., 2014a; Larsen et al., 2017c), which indicated strong influences of over groundwater exploitation on seawater intrusion in coastal aquifers (Han, Post, & Song, 2015; Yechieli et al., 2019; Yu & Michael, 2019). The vertical flow ratio combined with hydrogeochemical and stable isotopes could provide insight into aquifer interchanges and mixing processes between saline and fresh groundwater in the coastal area of the VMD.

3.2.5. Seawater intrusion prediction

In this study, we developed the state of art machine learning algorithms to predict groundwater salinity as represented by chloride concentration in each sampling locations. Besides, Aquaveo GMS 10.4.6 model was used to simulate groundwater flow system in the study area. The detail construction groundwater model was presented in Chapter 8.

CHAPTER 4 GROUNDWATER FLOW DYNAMICS

This chapter discusses changes in groundwater levels and groundwater flow direction under influences of pumping activities and tidal regime.

4.1. Characteristics of the groundwater flow system

The groundwater flow dynamics has an important role in groundwater evolution because it is a driving force of groundwater movement, solute transportation, and mixing processes along the groundwater flow path. The groundwater flow is controlled by the hydraulic head balance and lithological features of aquifers (Figure 4-1) as expressed by the Darcy equation below:

$$Q = \frac{K \times A(h_1 - h_2)}{L} = K\frac{dh}{dl} \times A = V \times A \quad (4.1)$$

Where:

V = K.J: Velocity of groundwater (L/T);

Q = Volume of water flow in L^3/T

K = Hydraulic conductivity in L/T

A = Cross-section area in L^2

J = dh/dl: hydraulic gradient

h1 = Hydraulic head at well 1 in L

h2 = Hydraulic head at well 2 in L

As described in the Eq.4-1, groundwater movement depends on hydraulic conductivity (K) and hydraulic gradient (J). Hydraulic conductivity (K) represents the characteristics of lithologic features, and it relatively stabilizes under natural conditions. However, the hydraulic gradient may change depending on groundwater pumping rate, especially in the lowland environment. In addition to this, the hydraulic gradient is regulated by recharged pattern and the tidal regime in coastal regions. Moreover, groundwater may be also dissolute and mix with different minerals in different environmental conditions, leading to changes in not only solutes but also stable isotopic composition. These signatures are good to determine groundwater flow path and the mixing process between groundwater and other water sources.

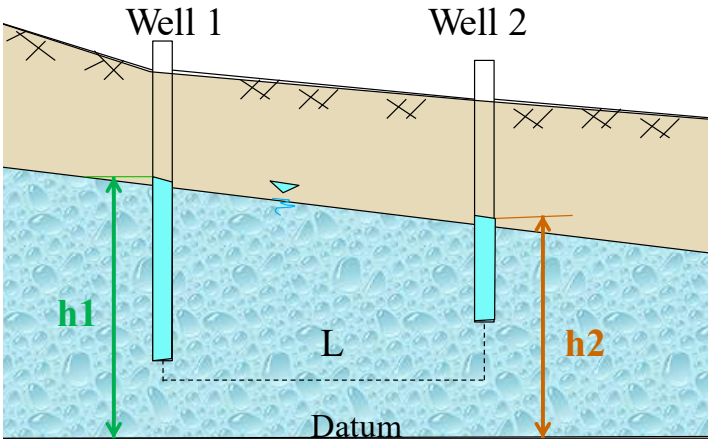

Figure 4- 1: Groundwater movement within aquifer flowing Darcy Law

In Soc Trang province, observation groundwater level between 2000 and 2016 showed a clear trend of groundwater level depletion with a depletion rate of 0.8/year, especially in the locations have high groundwater exploitation rate such as in central and coastal area (Figure 4-2). This situation may be attributed to groundwater exploitation with pumping capacity increase from around 3.0 million/month in 2000 to 8.0 million/month in 2016 (Figure 4-2).

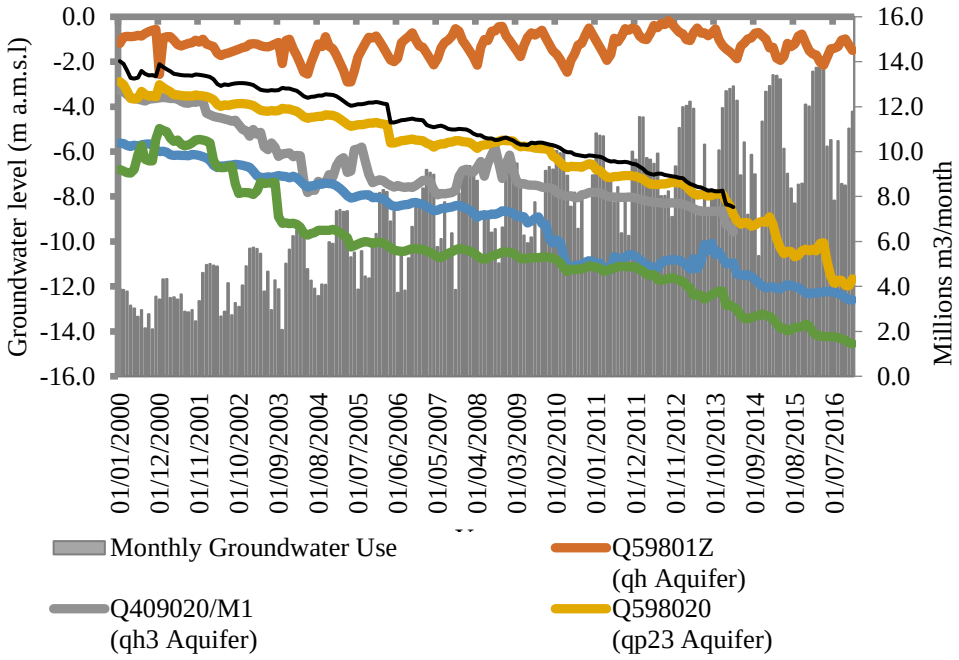

Figure 4- 2. Monthly observation groundwater levels and pumping capacity in the study area between 2000 and 2016

However, the groundwater level depletion trend showed a different magnitude between 2000 and 2016. In 2000, for example, groundwater levels were relatively high approximately -1.0 m a.m.s.l and the depression area were located in the southeast of the study area where groundwater level reached to a maximum peak of - 2.0 m a.m.s.l (Figure 4-3). However, from 2005 to 2016, the depression areas have expanded into many districts of the Soc Trang province with the maximum groundwater of -4.5 in 2005 (Figure 4-4), -7.0 in 2012 (Figure 4-5), and -12.5 m a.m.s.l in 2017 (Figure 4-6), extending toward the coastal areas and along the river before moving towards the centre of the study area. The seasonal variation in groundwater levels was also found in the study area that groundwater levels in the dry season were lower of 0.5 m than that of the rainy season. However, groundwater flow direction in the study did not show the evident change between dry season (Figure 4-6) and the rainy season (Figure 4-7) with the primary trend from surrounding areas to the central and coastal regions where have substantial groundwater exploitation activities.

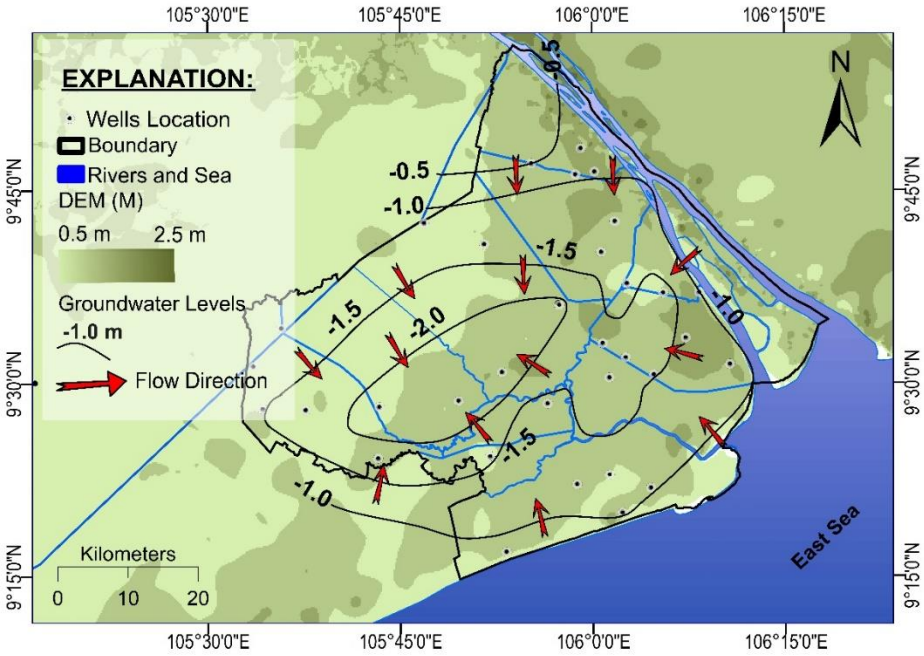

Figure 4- 3: Groundwater flow direction in middle Pleistocene aquifer (qp_{23}) in 2000, Soc Trang province, Vietnam

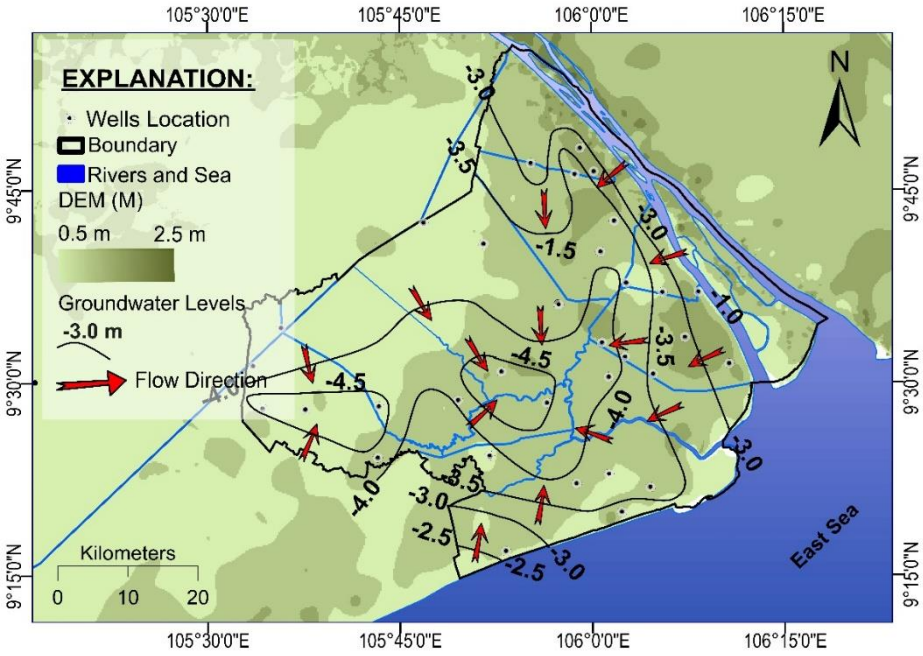

Figure 4- 4: Groundwater flow direction in middle Pleistocene aquifer (qp_{23}) in 2005, Soc Trang province, Vietnam

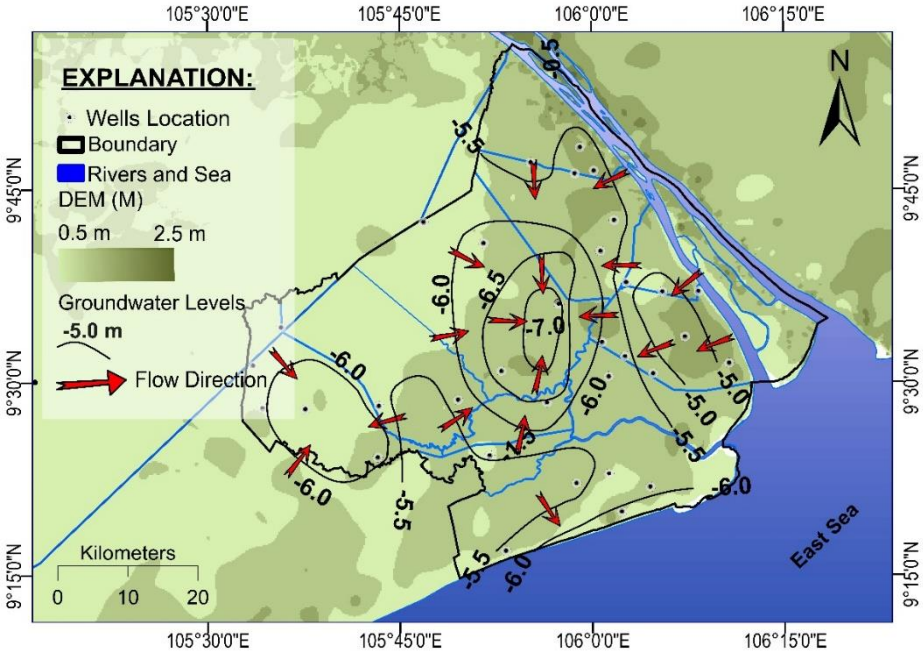

Figure 4- 5: Groundwater flow direction in middle Pleistocene aquifer (qp_{23}) in 2012, Soc Trang province, Vietnam

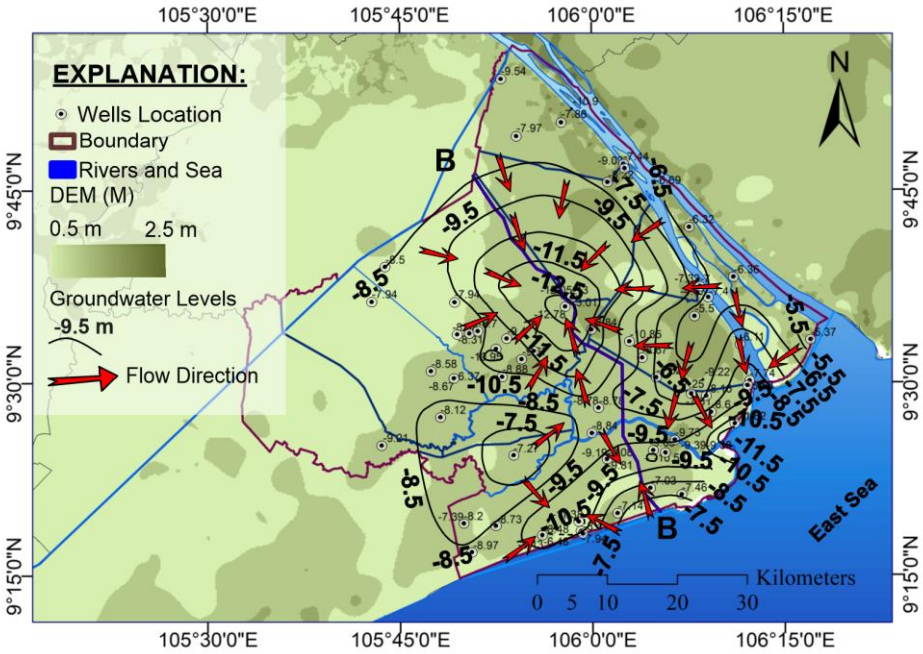

Figure 4- 6: Groundwater flow direction in middle Pleistocene aquifer (qp_{23}) in dry season 2017, Soc Trang province, Vietnam

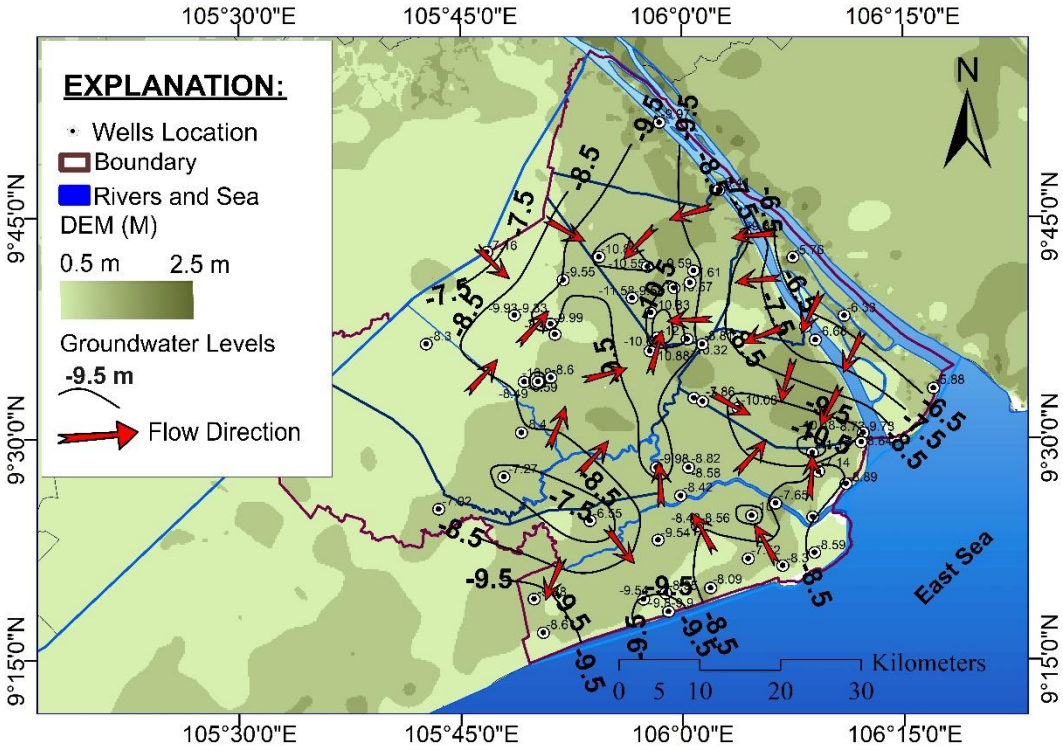

Figure 4- 7: Groundwater flow direction in middle Pleistocene aquifer (qp_{23}) in the rainy season (November 2017), Soc Trang province, Vietnam

4.2. Effects of the tide on groundwater sources

In this study, two monitoring wells were installed in the upper Pleistocene aquifer (Figure 4-8) to investigate the impact of tidal regime on groundwater flow dynamics.

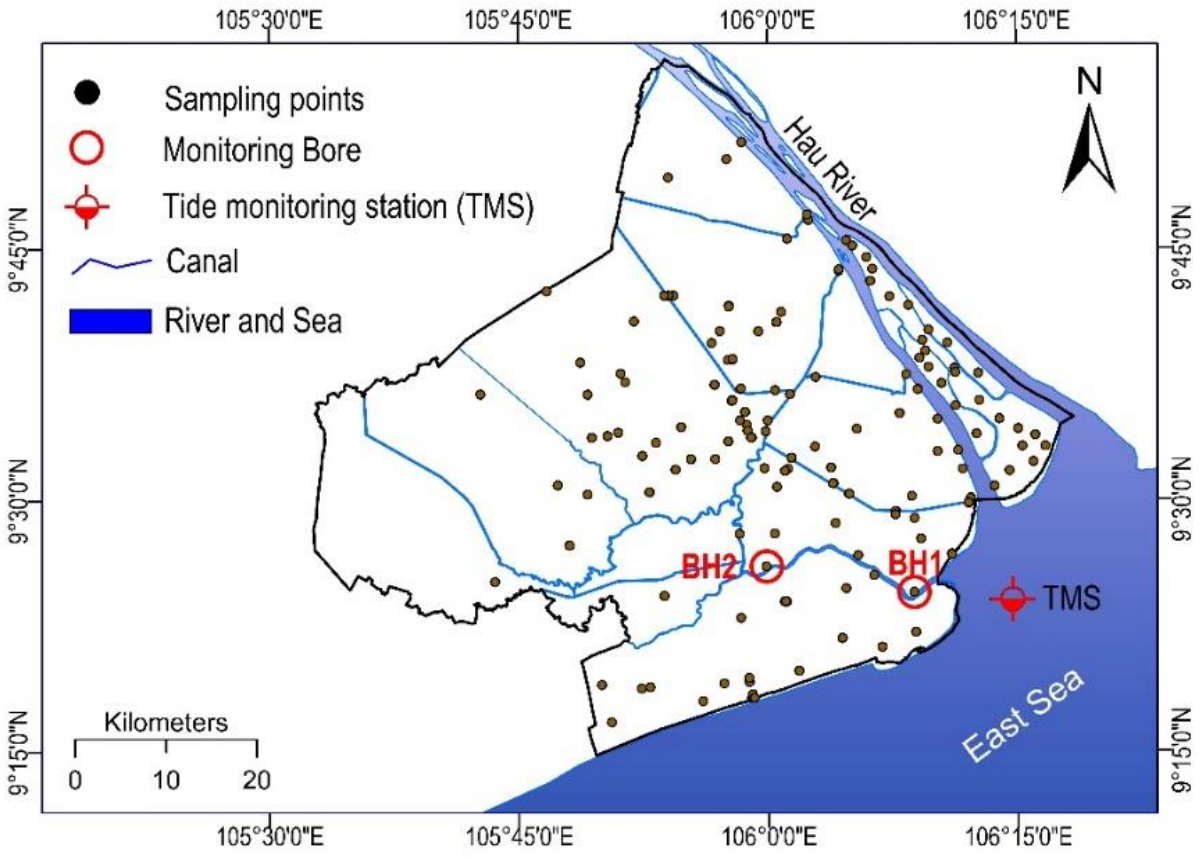

Figure 4- 8. Location of observation wells in the study area.

In these wells, the groundwater levels and electrical conductivity were installed and monitored hourly. Figure 4-9 showed influences of tidal fluctuation on groundwater levels in two wells with a fluctuation amplitude of 0.5 m while the groundwater level fluctuation has around four and a half hours' time lag compared to the tide.

Likewise, the observed groundwater levels in 2013 from provincial groundwater monitoring system showed that groundwater level fluctuation is very difference magnitudes, indicating different effects of the tidal regime, recharge and pumping rates on these areas (Figure 4-10). The most substantial tidal impact on groundwater level was observed in the monitoring well ST4 (Figure 4-11), with daily fluctuation amplitude of approximately 0.90 m. Similarly, the effect of the tidal regime on groundwater level fluctuation was also observed in the monitoring well ST3 (Figure 4-12), but the amplitudes are smaller than ST4.

The lowest tidal effect was in monitoring well ST11 with daily fluctuation amplitude of around 0.07 m.

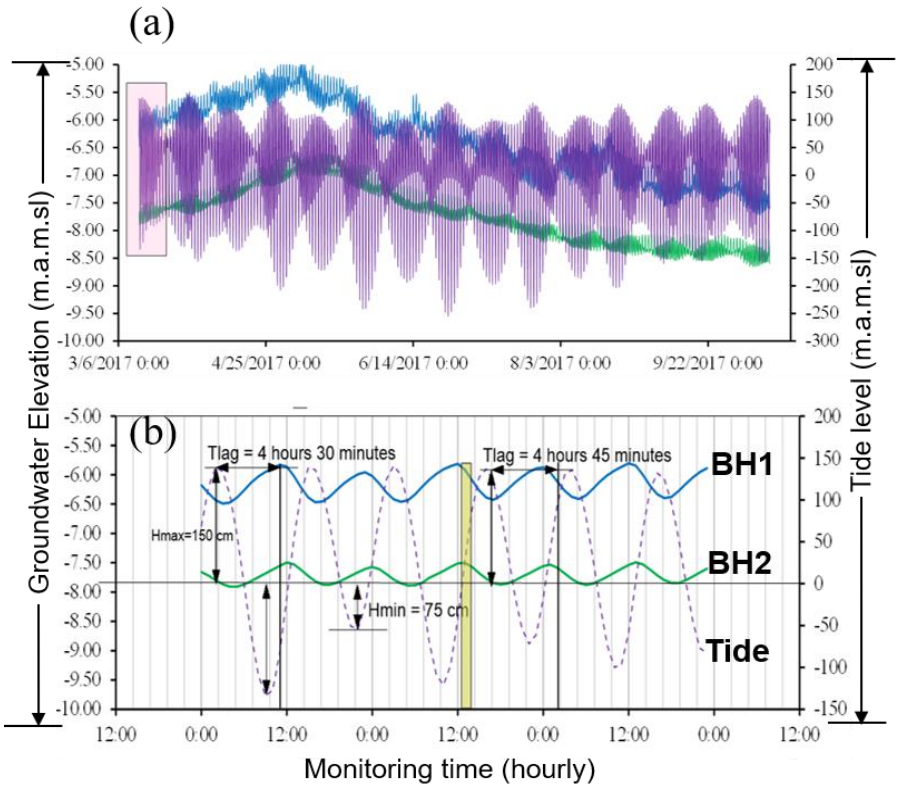

Figure 4- 9. Groundwater level fluctuation following tidal regime **a.** Long-time monitoring and **b.** Short-time monitoring.

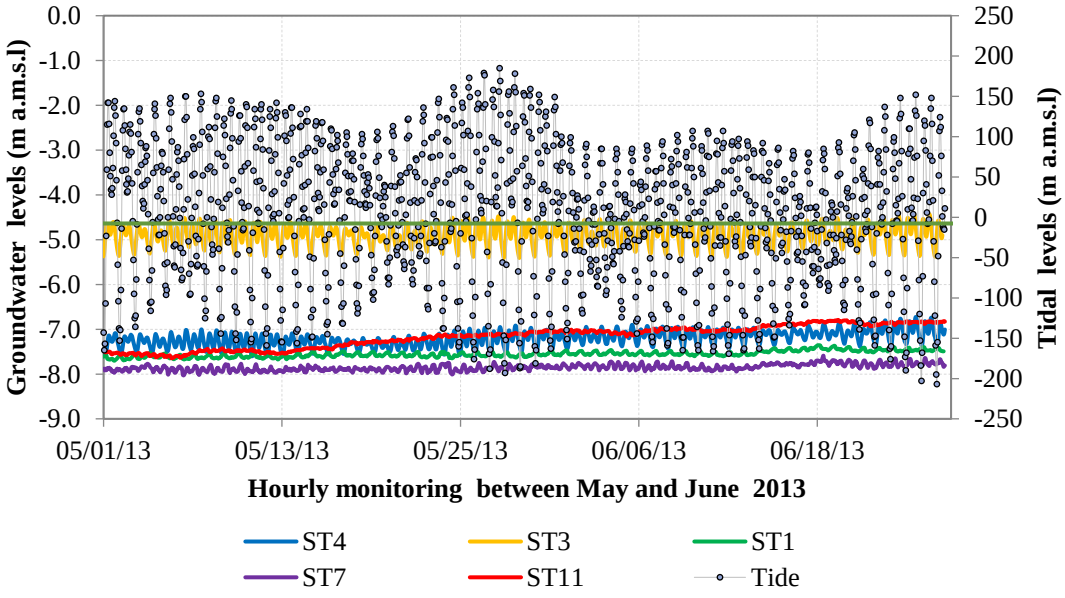

Figure 4- 10: Impacts of season water levels variation and tidal regime on groundwater at qp23 aquifer in Soc Trang province between May and June 2013

However, groundwater level fluctuations of ST3 and ST4 wells along the Hau River, have the time lags when compared to the tidal regime. Time lags in groundwater level from ST3 at the highest and lowest tidal peaks (Figure 4-13), were two and three hours, respectively with were much more than those of ST4 around one hour (Figure 4-14). The difference in amplitude may be due to the characteristics of aquifers and its distance to the sea.

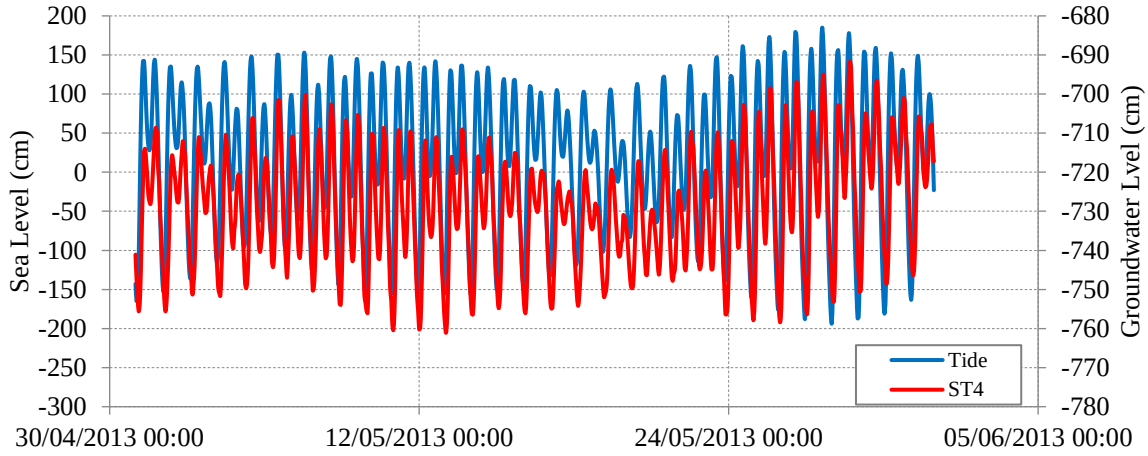

Figure 4- 11: Impacts of the tide on groundwater levels (ST4, qp23 aquifer)

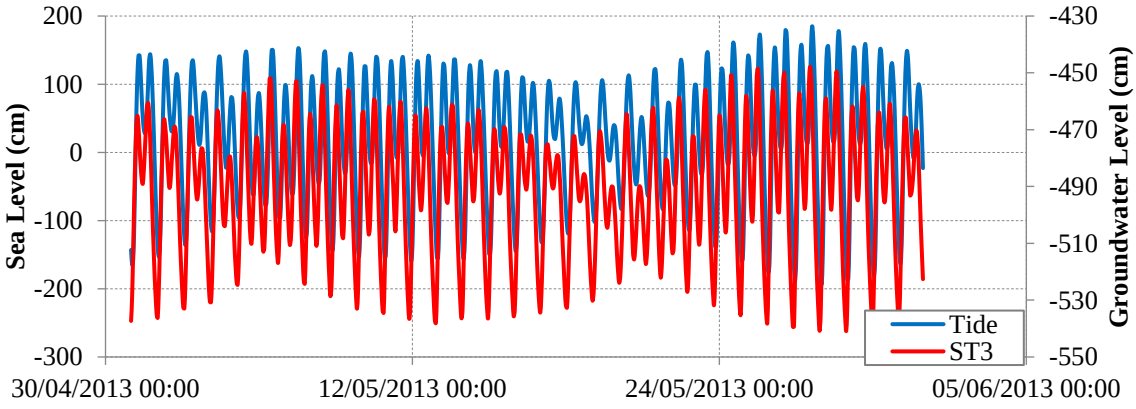

Figure 4- 12: Impacts of the tide on groundwater levels (ST3, qp23 aquifer)

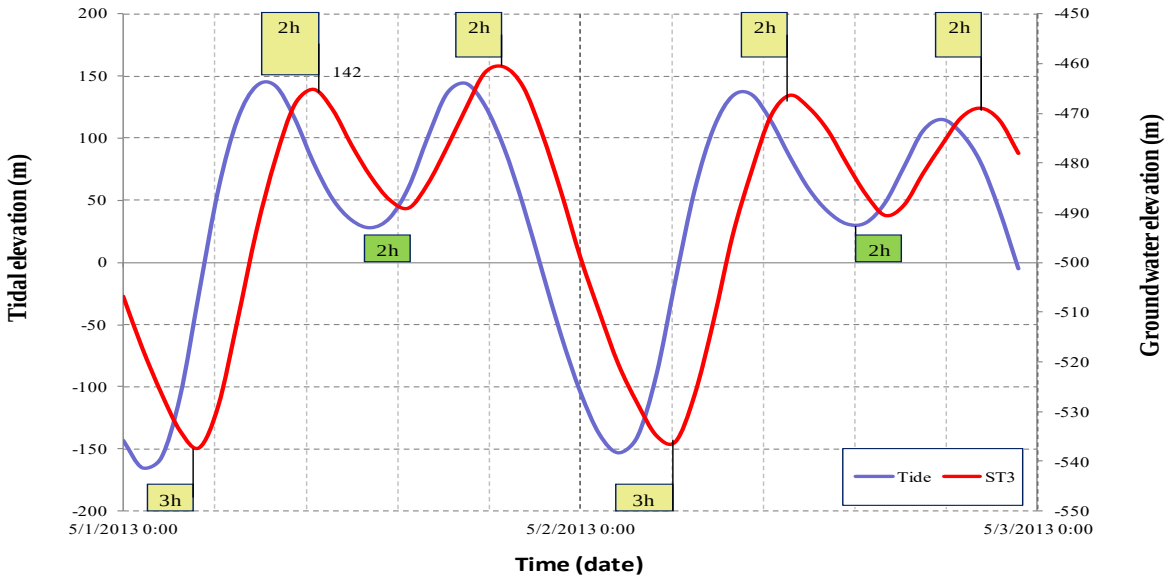

Figure 4- 13: Time lags between the tidal regime and groundwater levels from ST3

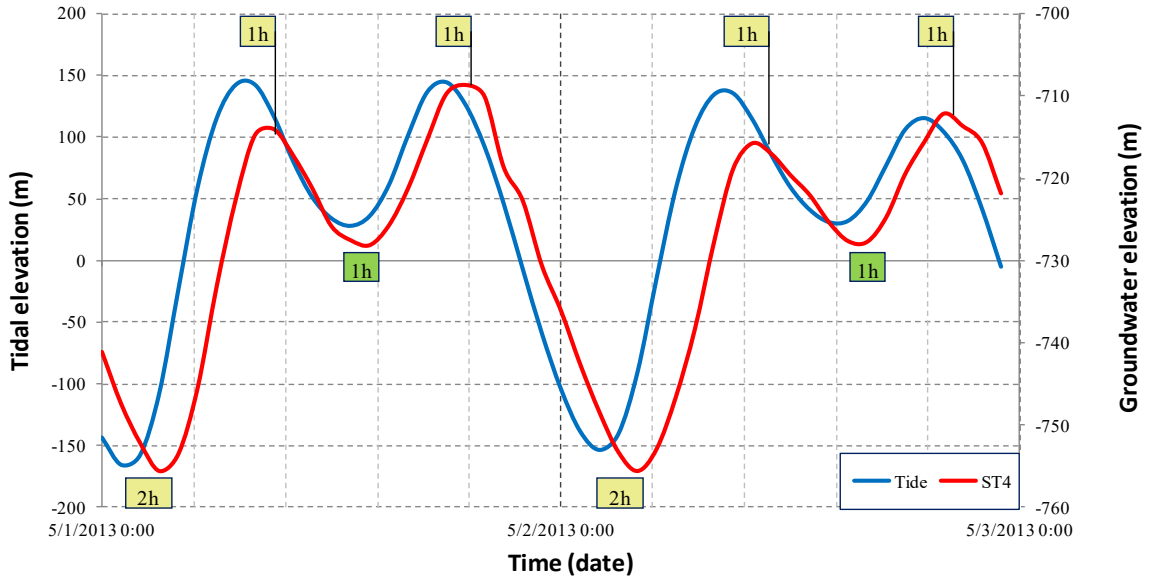

Figure 4- 14: Time lags between the tidal regime and groundwater levels from ST4

More notably, electrical conductivity (EC) showed slightly different between dry and rainy season 2017 with EC values increase from 8.5 mS/cm to 8.6 between March and September 2017. Similarly, EC values in the well ST7 showed seasonal variation increasing from 1.12 mS/cm to 1.18 mS/cm between April and June 2013 (Figure 4-15).

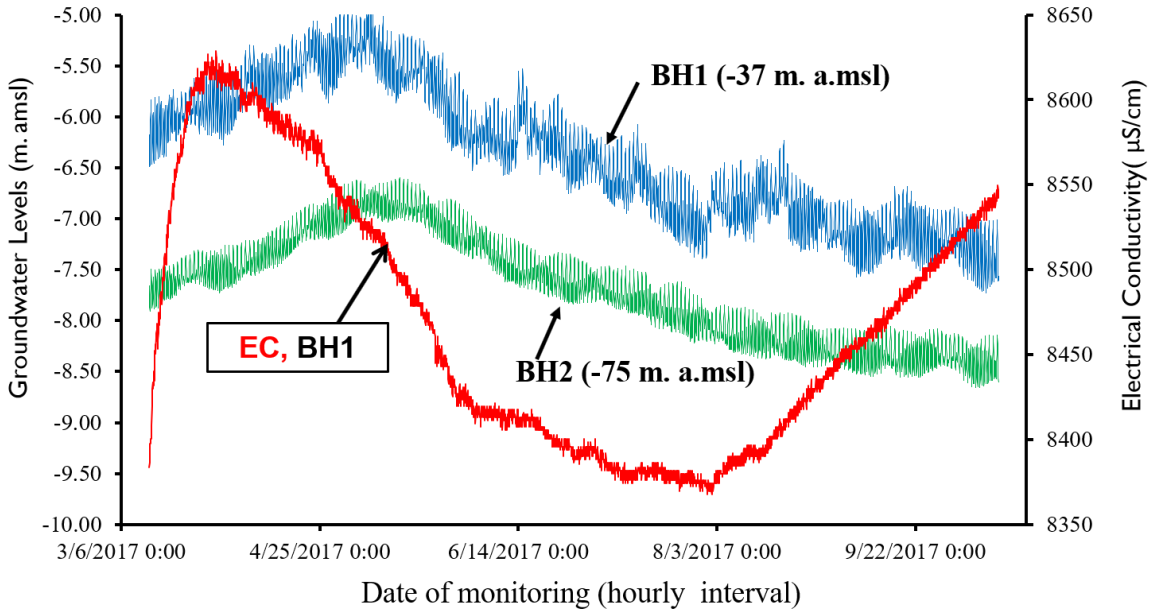

Figure 4- 15: Groundwater level fluctuation, tidal regime and electrical conductivity in Soc Trang province

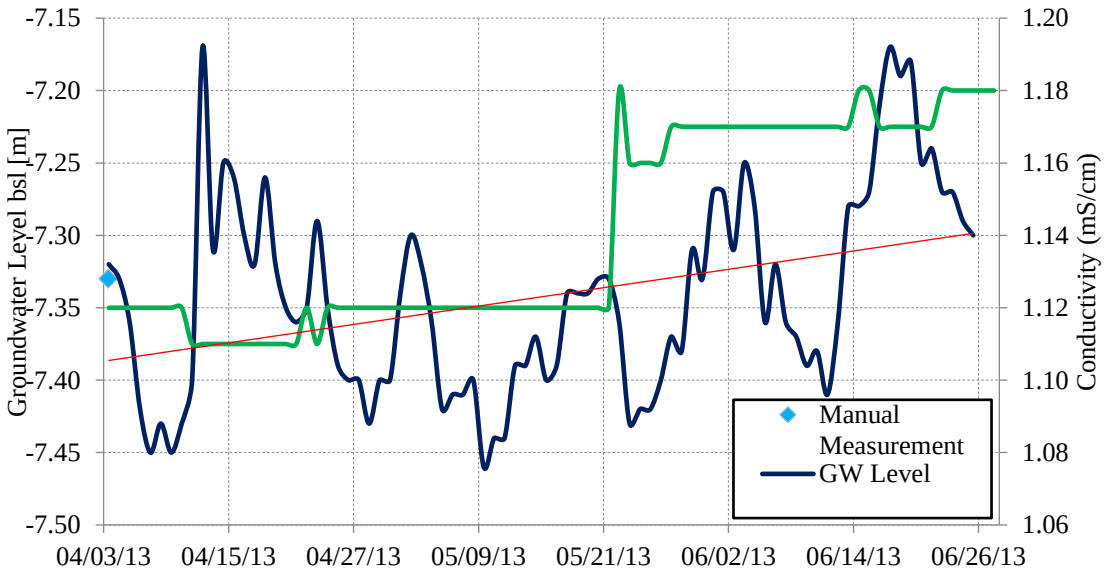

Figure 4- 16: The relationship between groundwater level and Electrical Conductivity in Monitoring Well ST7, Screen Depth 108 - 118 m (04/03/2013-06/26/2013)

CHAPTER 5 HYDROGEOCHEMICAL CHARACTERISTICS

Although groundwater plays a vital role in coastal regions, it is highly vulnerable due to natural variation and human activities, especially in coastal areas. In-depth understanding of groundwater geochemistry and its controlling factors is necessary for sustainable groundwater management. Chapter 5 presents new findings on the geochemical characteristics and its predominant factors under impacts of natural variation and human activities in the coastal aquifers of the MD, Vietnam. These findings were accepted for publication in Science Citation Index (SCI/SCIE) scientific journal entitled the Journal of Environmental Geochemistry and Health (Impact Factor 2018, IF =3.25), Springer Publisher. Also, a part of this chapter was shared during the International Conference on Geo-Spatial Technologies and Earth Resources GTER September 2017: Advances and Applications in Geospatial Technologies and Earth Resources.

5.1. Introduction

Groundwater is a crucial freshwater source of water for domestic, agricultural and industrial uses. Groundwater plays a vital role in socio-economic development (Gleeson, Befus, Jasechko, Luijendijk, & Cardenas, 2016; Jia et al., 2019). In recent years, groundwater sources in many areas are being threatened by various stresses (Dalin, Wada, Kastner, & Puma, 2017b; Ferguson & Gleeson, 2012a; D. Han & M. J. Currell, 2018). For example, in agricultural areas, excessive groundwater abstraction for irrigation has led to groundwater depletion (Dalin et al., 2017b; D. Han & M. J. Currell, 2018) and groundwater contamination (Abu-alnaeem, Yusoff, Ng, Alias, & Raksmey, 2018). In many coastal lowland regions, groundwater resources are being at risk of overexploitation and contamination (Bodrud-Doza et al., 2019; Nejatijahromi et al., 2019) due to rapid urbanization and intensive agricultural practices (Sheikhy Narany, Sefie, & Aris, 2018),. Also, groundwater in coastal areas is highly vulnerable to seawater intrusion due to sea-level rise (Ferguson & Gleeson, 2012a; D. Han & M. J. Currell, 2018). Therefore, developing a sustainable groundwater resource management for coastal areas is a crucial task, and understanding the hydrogeochemical characteristics of groundwater along with their controlling factors is a prerequisite (Isa, Aris, & Sulaiman, 2012).

Various studies on the hydrogeochemical processes of groundwater in coastal aquifers and their controlling factors have been conducted (Abboud, 2018; Abu Al Naeem et al., 2019; Argamasilla, Barberá, & Andreo, 2017; Nogueira, Stigter, Zhou, Mussa, & Juizo, 2019; Selvakumar, Chandrasekar, & Kumar, 2017; Sracek, Geršl, Faimon, & Bábek, 2019; Ziadi, Hariga, & Tarhouni, 2019). These studies showed that multivariate statistical analyses of the hydrogeochemical, environmental tracer analyses and inverse geochemical modelling approaches could be used to interpret the hydrodynamics and hydrogeochemical processes in coastal aquifers. These approaches are especially useful for analyzing the effect of geo-environmental factors (e.g., geologic conditions, mineral dissolution, and seawater intrusion) and human activities on groundwater geochemistry in multi-layer coastal aquifers (Sefie et al., 2018; Sheikhy Narany et al., 2018).

The common relations between the hydrogeochemical characteristics of groundwater, geo-environmental factors and anthropogenic activities have been extensively investigated. For example, the dissolution of calcite, dolomite, gypsum, anhydrite, and halite, increases the total hardness of groundwater (Argamasilla et al., 2017; Selvakumar et al., 2017). Seawater/freshwater mixing and cation-exchange processes could increase salinity in groundwater (D. Han & M. J. Currell, 2018; Amos Russak & Sivan, 2010). Sea level rise and excessive groundwater pumping could accelerate the landward movement of saline water (Loáiciga, Pingel, & Garcia, 2012; Praveena & Aris, 2010). Finally, anthropogenic activities (e.g., agricultural practices and industrial activities) could increase nitrate and heavy metal concentrations in groundwater (Bodrud-Doza et al., 2019; Nejatijahromi et al., 2019).

Apart from the aforementioned common drivers of hydrogeochemical characteristics, there are region-specific drivers. For example, the local variation of hydrology regimes has a strong influence on cation exchanges and the precipitation/dissolution of minerals in coastal aquifers (Idris et al., 2016; Taweesin, Seeboonruang, & Saraphirom, 2018; Wood & Harrington, 2015). Also, site-specific geological and lithological conditions may control groundwater geochemistry (Argamasilla et al., 2017; D. Han & M. J. Currell, 2018; Isa et al., 2012). Furthermore, local recharge could alter groundwater chemistry (K. C. P. Santos & Barrios, 2017; Xiao, Wang, Deng, & Jin, 2019). The generalization relationship between the hydrogeochemical characteristics of groundwater, geo-environmental factors, and anthropogenic activities is a challenging task. Thus, a site-specific investigation should be carried out for different regions.

The Mekong Delta (MD) is a mainly agricultural region in Vietnam. The delta contributes about half of the national agriculture and aquaculture products (Clauss, Ottinger, Leinenkugel, & Kuenzer, 2018). The delta has been identified as one of the most vulnerable regions to climate change and sea-level rise (Shrestha et al., 2016). In this region, groundwater is the primary source of freshwater supply (Ha et al., 2018). In recent decades, groundwater levels in the region have declined dramatically due to over-exploitation (Minderhoud et al., 2017). The area is also facing various groundwater quality problems, e.g., arsenic contamination (Berg et al., 2007), pesticide pollution (Chau, Sebesvari, Amelung, & Renaud, 2015), and salinity intrusion (An et al., 2018; H. T. Hoang & Bäumle, 2018). As a consequence, the sustainable development of the region is being threatened (Ha et al., 2018).

Several studies have been conducted in the Mekong delta to understand the causes and effects of groundwater-related issues as well as its current groundwater quality and quantity status (An et al., 2014b; An et al., 2018; Berg et al., 2007; H. T. Hoang & Bäumle, 2018; Nam, Akira, Kazutoshi, Trung, & Ngan, 2019; Yuheng Wang et al., 2018). These studies are either restricted to the two topmost aquifers of the multi-layer aquifer system in the region or conducted with insufficient data for fully understanding the whole aquifer system. Also, there is a limited understanding of seawater intrusion processes into the coastal aquifer system and the influences of both natural and anthropogenic factors on hydrogeochemical processes in the region. Hydrogeochemical investigation in this region should consider the linkage between aquifers and effects of natural processes and human activities on groundwater quality.

This chapter aims present (i) the hydrogeochemical characteristics of groundwater in different aquifers, (ii) the effects of salinization and evaporation processes on groundwater geochemistry, and (iii) the main factors influencing on chemical evolution in groundwater in the Mekong Delta.

5.2.Study Area and Field investigation

5.2.1. Study area

The study area is located in the Soc Trang province, which is the coastal zone of the Mekong Delta, Vietnam (Figure 5-1). The study area has an area of about 3,312 km^2 and borders with the Bassac River (Hau River) to the Northwest, with the East Sea to the Southwest. In the study area, anthropogenic and natural activities have severely affected the

region's sustainable groundwater management. Soc Trang province is located in the tropical monsoon climate with two distinct seasons, the rainy season (May-October) and the dry season (November-April). The annual average rainfall and temperature in the study area are 1,772 mm and 27^0C, respectively. The study area experiences a substantial seasonal variation in precipitation and temperature: rainfall in the rainy season accounts for 85% of the annual rainfall. The rainy season has a lower temperature and a higher humidity compared to the dry season.

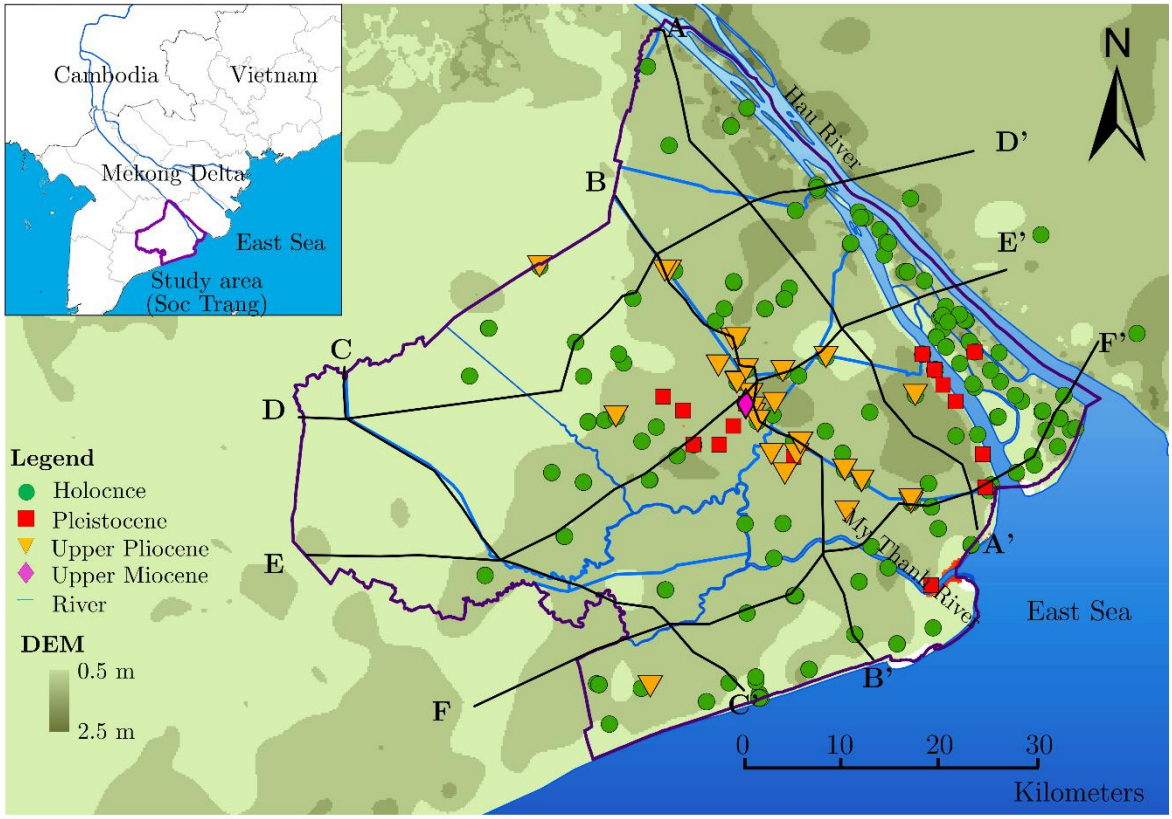

Figure 5-1: Location of the sampling points in the Mekong River Delta (Soc Trang, Vietnam).

The study area has a dense and complex river-canal network (Figure 5-1). The Hau River and My Thanh River are the main rivers in the study area, discharging water into the East Sea. The hydrological regime in the study area is strongly affected by the upstream flow regime of the Hau River and the tidal regime (Dang et al., 2016; Nhan, 2016; Truong, Nguyen, Ta, & Takemura, 2011). The underlying hydrogeological setting of the study area was formed during the late Tertiary and the Quaternary Periods. In the study area, there are seven aquifers (formed during different geologic periods) within a depth of about 450 m which are separated by aquitards (Figure 2-10).

5.2.2. Field investigation

In the study area, 286 groundwater samples were collected from production wells, private wells, and monitoring boreholes during 2013 and 2017, as shown in Figure 5-1 and Table 5-1. The groundwater samples were taken from the Holocene (qh), Upper Pleistocene (qp_3), Middle Pleistocene (qp_{23}), Lower Pleistocene (qp_1), Middle Pliocene (n_{22}), Lower Pliocene (n_{21}), and Miocene (n_{13}) aquifers. Most of the groundwater samples were taken from the qp_{23} and qp_1 aquifers because these aquifers have been intensively exploited (An et al., 2018). The physio-chemical parameters such as pH, dissolved oxygen (DO), electrical conductivity (EC), and oxidation-reduction potential (ORP) were measured directly during the sampling time using the HORIBA portable equipment.

Table 5- 1. Spatial and temporal sampling frequency

Aquifer	2013		2017	
	Dry season	Rainy season	Dry season	Rainy season
Holocene (qh)	2	-	-	7
Upper Pleistocene (qp_3)	4	-	4	4
Middle Pleistocene (qp_{23})	25	48	64	47
Lower Pleistocene (qp_1)	11	1	10	12
Middle Pliocene (n_{22})	1	-	-	-
Lower Pliocene (n_{21})	1	-	-	-
Upper Miocene (n_{13})	3	5	16	21
Total	47	54	94	91

"-"means no data

5.3.Methodology

5.3.1. Chemical Analysis Techniques

All groundwater samples were filtered with a 0.02 µcm cellulose ester filter before the chemical and stable isotope analyses. Dissolved anions such as chloride (Cl^-), sulfate (SO_4^{2-}), and nitrate (NO_3^-) were analyzed using an ion liquid chromatography (Shimadzu Co. Ltd., HIC-SP/VP Super). Bicarbonate (HCO_3^-) concentrations were measured using the titration method with sulphuric acid. Major cations such as sodium (Na^+), potassium (K^+), calcium (Ca^{2+}), and magnesium (Mg^{2+}) were analyzed using ICP-OES, PERKIN ELMER, and Optima 7300. The accuracy of the chemical analyses was evaluated by analyzing the milli-Q water samples and calibration curves as well as calculating ion balances (the error in ion balances should be below 5%). Stable isotopes of $\delta^{18}O$ and δ^2H were analyzed using the

PICARRO L2120-I water analyzer at the Hydrology and Water Environment Laboratory, University of Tsukuba, Japan. The errors of $\delta^{18}O$ and $\delta^{2}H$ are 0.10 ‰ and 0.50‰, respectively.

5.3.2. Graphical and Multivariate Statistical Analyses

Hydrogeochemical data were analyzed by using the Piper and Stiff diagrams (Piper, 1944; Stiff, 1951) in combination with bivariate plots (Yang2017, Carol2012) to identify groundwater geochemistry characteristics. Also, the principal component analysis (PCA) and hierarchical cluster analysis (HCA) methods were used to investigate the relationships between groundwater chemistry components (Piña, Donado, Blake, & Cramer, 2018; R. Trabelsi & Zouari, 2019). PCA transforms multidimensional data into fewer dimensions while preserving trends and patterns (Lever, Krzywinski, & Altman, 2017). The transformation functions of PCA are expressed as follows:

$$\left\{\begin{array}{l} x_1 = \alpha_{11}.f_1 + \alpha_{12}.f_2 + \ldots + \alpha_{1m}.f_m \\ x_2 = \alpha_{21}.f_1 + \alpha_{22}.f_2 + \ldots + \alpha_{2m}.f_m \\ \ldots. \\ x_n = \alpha_{n1}.f_1 + \alpha_{n2}.f_2 + \ldots + \alpha_{nm}.f_m \end{array}\right\} \qquad (5\text{-}1)$$

where x, α, f, n, and m refer to the component score, component loading, measured value, component number, and the number of measured variables, respectively.

HCA is a tool for clustering data having similar properties (Ziani, Boudoukha, Boumazbeur, Benaabidate, & Fehdi, 2016)and is frequently used for hydrogeochemical classification (Sracek et al., 2019). HCA consists of two different clustering techniques, agglomerative hierarchical clustering (AHC) and divisive hierarchical clustering (DHC).

In this study, PCA is used to identify the main components which characterize the hydrogeochemical characteristics of groundwater in the study area, while AHC is used to evaluate the relationship between physicochemical parameters in different aquifers quantitatively. The cluster analysis could also help to investigate hydrogeochemical characteristics relating to the geographical features of the study area. The physio-chemical data of groundwater in the study area have different scales and wide variances; therefore, the input data are first standardized using the following equation (Chekirbane et al., 2013; Iwamori et al., 2017):

$$Z_i = \frac{x_i - \mu_i}{\sigma} \qquad (5-2)$$

Where Z_i is the standardized value of x_i, μ and $\sigma$are the mean and standard deviation of x, respectively. Additionally, the Kaiser-Meyer-Olkin (KMO) and Bartlett's sphericity tests were used to assess the relationship between the correlation coefficients and partial correlation coefficients of the original variables (Kaiser, 1974). The KMO values range from 0 to 1, in which acceptable values should be higher than 0.50. The KMO values from 0.50 to 0.70 are "moderate", values between 0.70 and 0.80 are "good", and values higher than 0.80 are denoted as "great". The XLSTAT software package was used to conduct all mathematical and statistical computations. In this study, the KMO value of 0.78 was higher than 0.50, and in Bartlett's sphericity tests, the p-value of 0.0001 \textless 0.05 implies that the input parameters are suitable for PCA and AHC analyses.

5.3.4. Saturation Index

In this study, the saturation index (SI) of minerals is calculated as follows (C. a. P. Appelo, D. , 2005):

$$SI = log \frac{IAP}{K_s} \qquad (5-3)$$

Where IAP is the ion activity product of the mineral-water reaction, and K_s is the thermodynamic equilibrium. SI can be either a positive or a negative number: SI < 0 means subsaturation, SI > 0 means supersaturation, and SI = 0 means saturation. Practically, it should be noted that a mineral phase rarely stands at the equilibrium state (SI=0) due to the influences of complex natural conditions. Therefore, if the saturation index ranges between -0.50 and +0.50, the state is often assigned as a saturation condition. In this study, the WATEQ4F thermodynamic database of the PHREE QC model (Haase, Ebert, & Dethlefsen, 2016) was used to calculate the saturation index of primary minerals, e.g. calcite, dolomite, anhydrite, gypsum, and halite.

5.4. Results and Discussion

5.4.1. Physio-chemical characteristics

A statistical summary of the physio-chemical characteristics of all groundwater samples in the study area is shown in Table 2. The average groundwater temperature (31.10 ^{0}C) is above the average air temperature (27^{0}C). This result could be a result of geothermal activities in the study area, as described (Wagner et al., 2012). The measured pH values show

that groundwater is alkaline, and low pH values are observed in the rainy season due to the dilution of groundwater by rainwater.

Table 5- 2: Statistical summary of the main physiochemical compositions of groundwater

Parameters	Minimum	Mean	Maximum	Std. deviation	Drinking water*
T (^oC)	25.60	31.30	43.00	4.20	-
pH	6.12	7.32	9.33	0.49	7.50-8.50
DO	0.16	1.94	5.13	0.81	-
EC (µS/cm)	116.70	**1821.05**	**21200.00**	2577.00	750.00
Na^+ (mg/L)	16.88	**335.52**	**8535.80**	850.10	200.00
K^+(mg/L)	0.52	19.69	**278.81**	26.92	100.00
Ca^{2+}(mg/L)	0.11	52.19	**970.48**	112.01	75.00
Mg^{2+}(mg/L)	0.03	**51.58**	**1290.06**	115.60	30.00
SiO2(mg/L)	0.58	16.46	60.70	9.27	-
Cl^-(mg/L)	2.85	**489.89**	**16970.45**	1722.56	200.00
NO_3^-(mg/L)	0.11	10.73	**264.18**	32.65	45.00
$S0_4^{2-}$(mg/L)	0.02	127.08	**3239.46**	293.32	200.00
HCO_3^-(mg/L)	14.03	**332.69**	**779.23**	156.07	300.00

*WHO standard for drinking water (WWHO, 1984). Value exceeds the WHO standard for drinking water is in bold.

The variations of Na^+ and Cl^- concentrations were higher compared to other ions as shown by the standard deviations. The magnitude of seawater intrusion varies highly in space and time. The concentration of SiO_2 in groundwater is minor compared to others. While SiO_2 in groundwater is usually associated with the dissolution of silicate minerals in rocks (M. M. A. Khan & Umar, 2010), the low SiO_2 concentration could be either due to: (1) the presence of silicate minerals in rocks is very small or (2) the process of breaking down silicate minerals in rocks is prolonged due to the low velocity of groundwater flows (H. T. Hoang & Bäumle, 2018). Chemical data analyses show that most of the concentrations of major ions exceed the threshold limit values for drinking water (in terms of either mean or maximum values, Table 5-2).

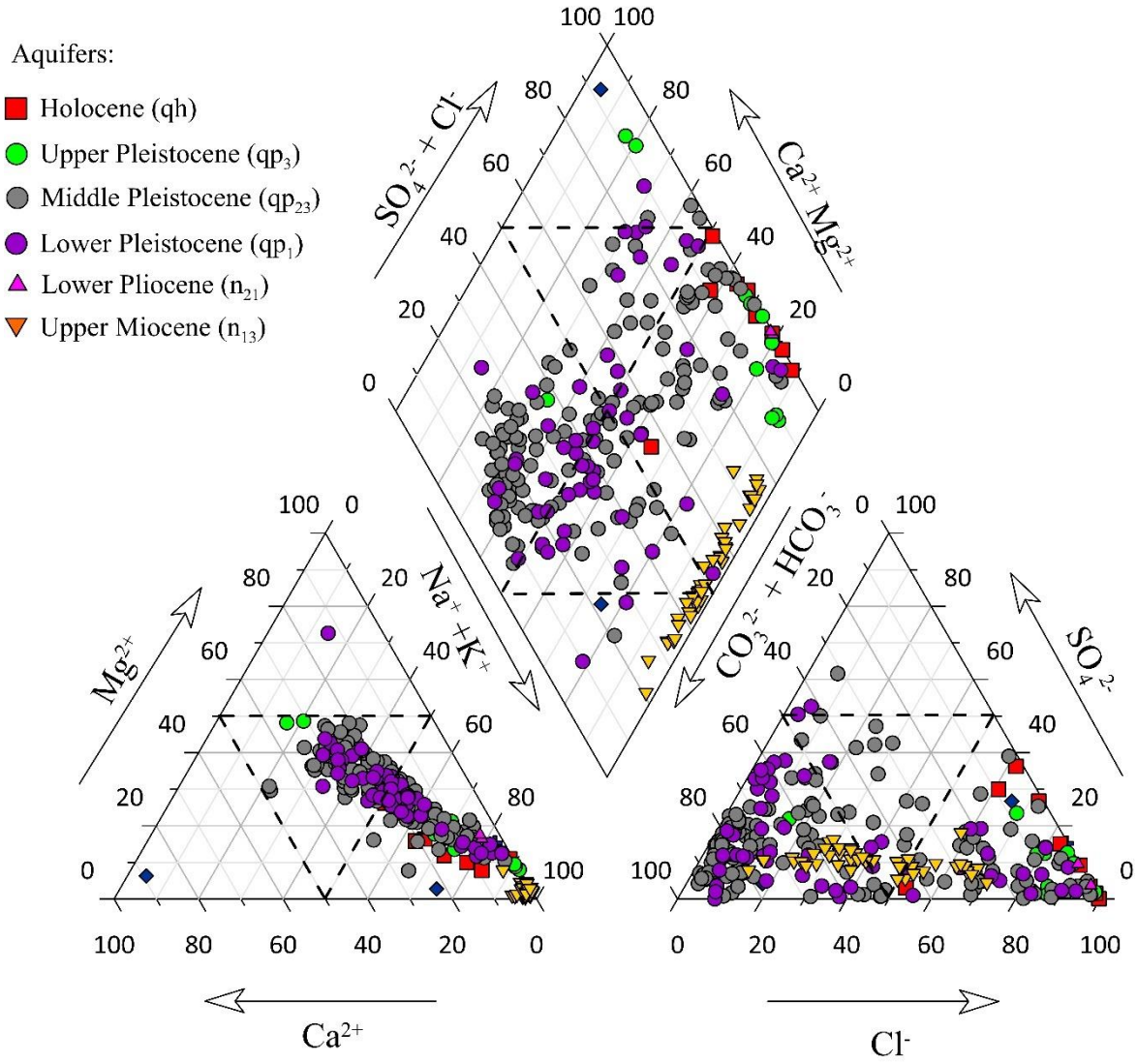

Figure 5- 2: Piper diagram of the water samples in the study area

Figure 5-2 is the graphical representation of groundwater chemistry in the study area. There is high spatial variability in the Na-Cl water type in all aquifers of the study area. Groundwater samples which contained the Na-Cl water type were mostly taken from the Holocene and upper Pleistocene aquifers. The existence of saline groundwater may suggest that different processes of seawater intrusion have been occurred in coastal aquifers of the Mekong Delta, primarily paleo- and modern seawater intrusion, which are common in lowland coastal aquifers (Amiri, Nakhaei, Lak, & Kholghi, 2016; Cary et al., 2015; J.-H. Kim, Kim, Thao, Batsaikhan, & Yun, 2017). Groundwater samples from the middle Pleistocene and lower Pleistocene aquifers which show wide variabilities in chemical compositions contain different water types, including Ca-HCO_3, Na-Cl, Ca-Na-HCO_3, and Ca-Mg-Cl. The various water facies in both Middle Pleistocene and Lower Pleistocene

indicate the different hydrogeochemical processes taking place in these aquifers. These processes may include the dissolution of several minerals (e.g., calcite, aragonite, dolomite, anhydrite, and gypsum), and ion exchanges (e.g., seawater intrusion and freshening aquifers). The similar distribution of groundwater samples in the Middle Pleistocene and Lower Pleistocene aquifers indicate that there could be a hydraulic connection between these aquifers, resulting in proper mixing of groundwater between these aquifers. Na-HCO_3 and Na-Cl-HCO_3 water types dominated in the Lower Pliocene and Upper Miocene aquifers. The formation of these groundwater types may originate from cation exchanges caused by water passing through sedimentary sequences containing clay layers before entering the igneous aquifers of the Mekong Delta.

5.4.2. Groundwater salinization

Seawater intrusion is threatening many coastal aquifers around the world (Tiwari, Pisciotta, & De Maio, 2019a). It could alter groundwater chemistry, resulting in high Cl^- concentrations. Once seawater immigrates into freshwater aquifers, it takes a long time to recover aquifer systems and may cost high prices for saline groundwater treatment. To have an appropriate saltwater remediation plan or to reduce the seawater intrusion, it is necessary to understand the processes of seawater intrusion into the coastal aquifer system. Many methods have been used to investigate seawater intrusions, such as hydro-geological observation, geophysics measurement, geochemical analysis, and isotopic techniques (Vengadesan & Lakshmanan, 2019). Generally, freshwater is dominated by calcium and bicarbonate, while seawater is dominated by Na^+, Cl^-, and Mg^{2+} (Mondal, Singh, Singh, & Saxena, 2010; Tiwari et al., 2019a). Therefore, the relationship among major ions such as Na^+, Ca^{2+}, Mg^{2+}, and Cl^- is a good indicator in identifying seawater intrusion (Kanagaraj et al., 2018).

In this study, the diagrams of Na^+/Cl^- vs. Cl^- (Figure 5-3a) and Mg^{2+}/Ca^{2+} vs. Cl^- (Figure 5-3b) show that groundwater samples from the Holocene (qh) and Upper Pleistocene (qp_3) aquifers were distributed along ratio lines (Na^+/Cl^- = 0.86 and Mg^{2+}/Ca^{2+} = 5.0), corresponding to an increase of Cl^- concentrations with the maximum Cl^- concentration of 16,970 mg/L. High salinity concentrations in groundwater were also found in many coastal aquifers around the world, such as in India (Mohanty & Rao, 2019), Mexico (Mahlknecht, Merchán, Rosner, Meixner, & Ledesma-Ruiz, 2017a), Palestine (Abu-alnaeem et al., 2018), France (Khaska et al., 2013b), China (Peng, He, Wang, Zhang, & Wang, 2018), and South

Korea (R.-H. Kim, Kim, Ryu, & Koh, 2018). This common situation may indicate the influences of rapid sea-level rise and seawater intrusion during the early Holocene period on coastal aquifers (Hung Van et al., 2019).

Groundwater samples have Na^+/Cl^- ratio < 0.86 may indicate the leaking saline from clay soil/sediment (Eq.5) and ion exchange processes due to leaking saline water from upper to lower layers as well as the paleo-saline water intrusion (Eq.6) into fresh aquifers due to excessive groundwater extraction. An increase in Na^+/Cl^- but having a decrease in the Cl^- concentration indicates the influence of silicate weathering processes on groundwater resources (Figure 5-3). The processes of increasing Na^+ and Cl^- concentrations could be expressed by the following equations (C. a. P. Appelo, D. , 2005):

Silicate weathering:

$$2NaAlSi_3O_8+2H_2CO_3+9H_2O \Rightarrow l2Si_2O_5(OH)_4+2Na^{++}+4H_4SiO_4+2HCO_3^- \quad (5\text{-}4)$$

Halite dissolution:

$$NaCl \Rightarrow Na^+ + Cl^- \quad (5\text{-}5)$$

Ion exchange processes:

$$Na^+ + 1/2Ca\text{-}X_2 \Leftrightarrow Na\text{-}X + 1/2Ca^{2+} \quad (5\text{-}6)$$

Although ionic ratios could be used to delineate the process of salinity accumulation in aquifers, saltwater in aquifers may originate from different sources (D. Han & M. J. Currell, 2018; R.-H. Kim et al., 2018). To investigate groundwater sources and the process of groundwater salinization, the scattered diagram of $\delta^{18}O$ vs Cl^- can be used (Nogueira et al., 2019). The majority of groundwater samples in the study area present an increase of Cl^- concentrations, ranging from 2.85 mg/L to 16,970.00 mg/L, while isotopic compositions ($\delta^{18}O$) vary from approximately -8.00‰ to - 4.00‰ (Figure 5-4). The wide variability in Cl^- concentrations of groundwater in combination with the low value of $\delta^{18}O$ indicating the leaching salinity from clay soil/sediment layers into fresh aquifers. This fact may be a result of an increase in hydraulic gradients due to significant declines in groundwater levels. Groundwater samples had low Cl^- concentrations and more enrichment of $\delta^{18}O$ but distributed above the rainfall-seawater mixing line, indicating the influence of evaporation processes. Also, most of the shallow and some of the deep groundwater samples distributed around the rainfall-seawater mixing line suggested that these samples may (1) originate from

meteoric water (2) and mix with seawater along groundwater flow paths. These processes were also observed in other coastal aquifers in Australia(Timms, Young, & Huth, 2012), France (Khaska et al., 2013b), Canada (Walter, Chesnaux, Cloutier, & Gaboury, 2017), and Malaysia (Sefie et al., 2018). These results implicate that evaporation processes and mixing with saltwater are common processes, influencing groundwater quality in worldwide coastal aquifers.

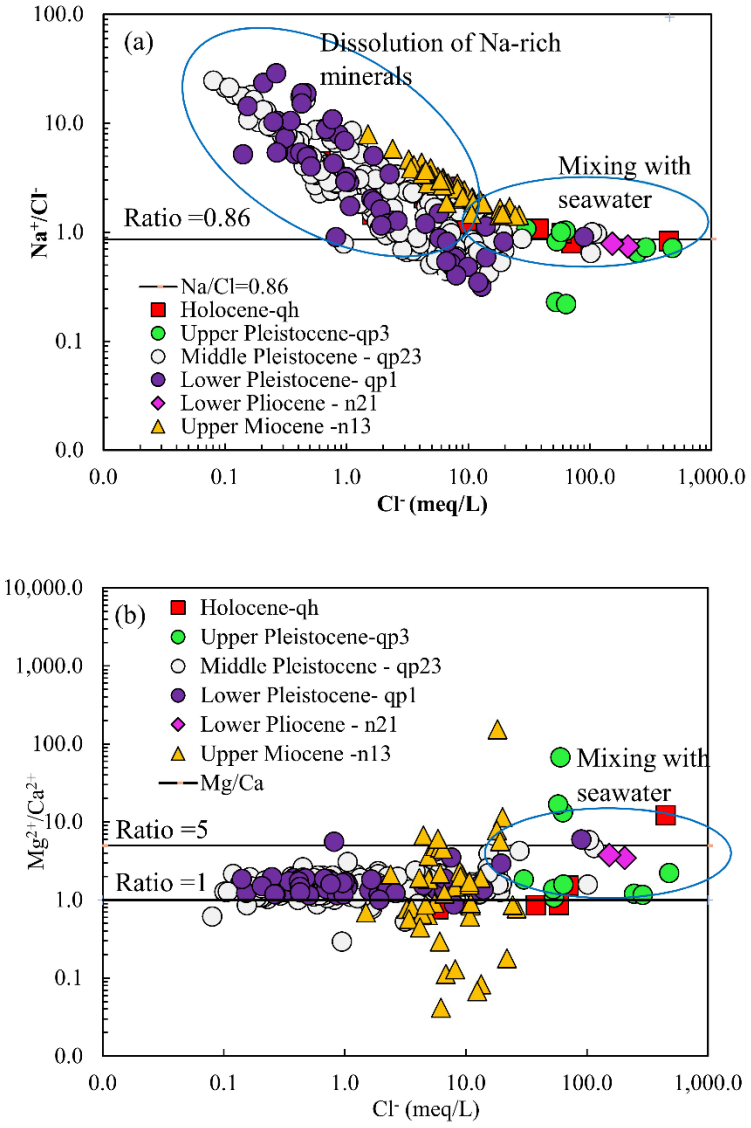

Figure 5- 3: Scattered plots. **a.** Cl versus Na/Cl, **b.** Cl versus Mg/Ca showing possible sources of salinity in groundwater.

5.4.3. Evaporation process

Evaporation is one of the most important hydrological processes which significantly influences the concentrations of all ions in groundwater (Skrzypek et al., 2015). This process occurs during the raindrop and recharge periods along groundwater flow paths due to groundwater level fluctuations (Gat & Tzur, 1967; Nogueira et al., 2019; Skrzypek et al., 2015). The influences of evaporation processes on water resources could be identified by the diagrams of $\delta^{18}O$ vs Cl^-, as mentioned previously. To depict these processes, deuterium excess (d-excess = $\delta^2H - 8*\delta^{18}O$ is a good indicator (Dansgaard, 1964; Tarki, Dassi, & Jedoui, 2012).

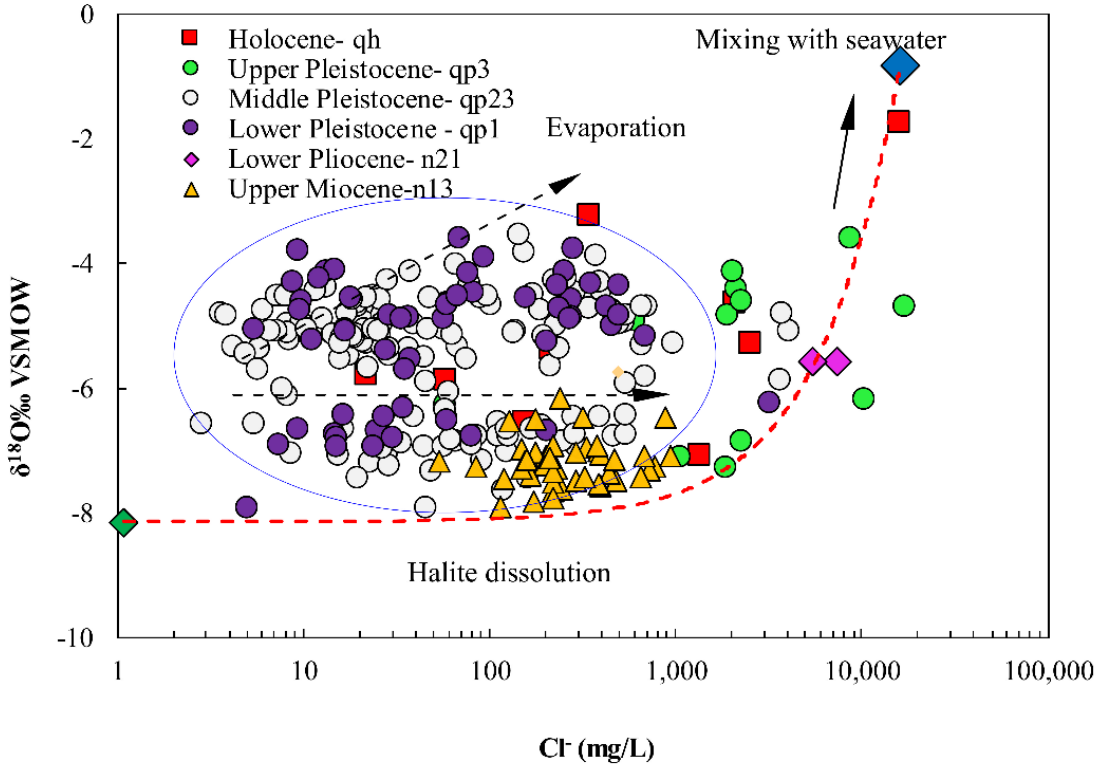

Figure 5- 4: The scattered diagram Cl versus $\delta^{18}O$ showing effects of groundwater salinization and evaporation on salinity and stable isotope ($\delta^{18}O$) concentration

Accordingly, if d-excess is higher than +10‰ of the average global rainfall, it indicates non-evaporation, while the reverse trend indicates an evaporation process (Cui, Tian, Biggs, & Wen, 2017; Tarki et al., 2012). In this study, the d-excess values of groundwater samples have a large variability, ranging from -12‰ to +20‰. More specifically, most of the d-excess values of groundwater samples in the study area were lower than the global d-excess = +10‰ (Figure 5-5), revealing that these groundwater samples might experience intense

evaporation during the recharge period and along groundwater flow paths. Moreover, the decrease of d-excesses does not relate to the increase of chloride concentrations in groundwater samples, indicating that evaporation may not play an essential role in accumulating salinity in the coastal superposed aquifers of the Mekong Delta. This finding is quite different compared to previous studies that showed the increases of salinity due to evaporation effects (D'Alessandro et al., 2017; Jankowski & Acworth, 1997). This result indicates that groundwater in the study area originates from open-surface water evaporation and predominantly experiences halite dissolution along groundwater flow paths with long resident times (H. T. Hoang & Bäumle, 2018).

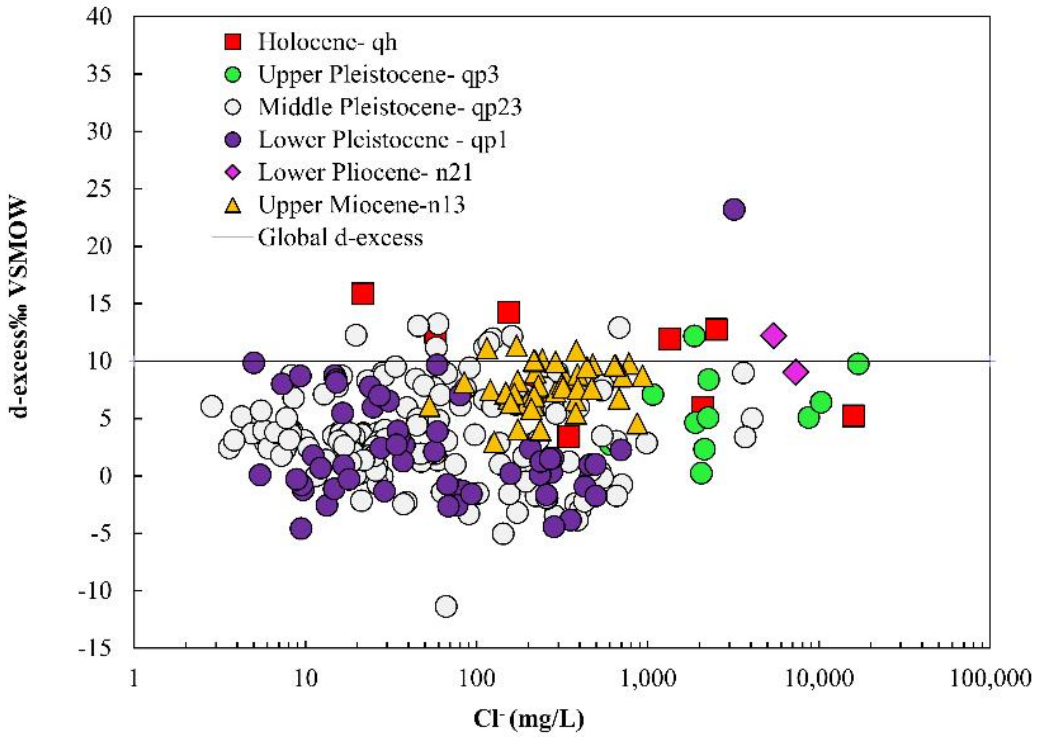

Figure 5- 5: The scattered diagram Cl versus d-excess showing effects of evaporation processes on different aquifers in the coastal area of the Mekong Delta.

5.4.4. Water-rock interaction

The saturation index was calculated to investigate geochemical evolution processes without collecting sediment/rock samples and analyzing the mineralogical characteristics (C. a. P. Appelo, D. , 2005). The results shows two distinct trends: (i) approximately 40% of total groundwater samples reached the near-equilibrium [-0.50; + 0.50] and saturation states with respect to aragonite ($CaCO_3$), calcite ($CaCO_3$), chalcedony (SiO_2), dolomite, and $CaMg(CO_3)_2$ (Figure 5-6), and (ii) remaining groundwater samples were unsaturated with

different magnitudes. The mineral phases such as aragonite, calcite, dolomite, and chalcedony are nearly-saturated to neutral in groundwater due to the combined effect of mineral dissolution, ion exchanges, and silicate weathering processes. These processes increase Ca^{2+}, Mg^{2+}, HCO_3, and SiO_2 concentrations in groundwater sources in the study area. The scatter diagram of (Mg^{2+}+ Ca^{2+}) versus (HCO_3^- + SO_4^{2-}) (Figure 5-7a) shows that (i) the reverse ion exchange and ion exchange and/or silicate weathering occurred in the Middle and Lower Pleistocene aquifers (qp_{23}) and qp_1), (ii) only the reverse ion exchange occurred in the upper Miocene aquifer (n_{13}), and (iii) the ion exchange and/or silicate weathering occurred in the Holocene, Upper Pleistocene, and Lower Pliocene aquifers (qh, qp_3, and n_{21}). The concentrations of (HCO_3^- + SO_4^{2-}) in the upper Miocene aquifer (n_{13}) varied in a narrow range while the variability in the Mg^{2+}/Ca^{2+} ratio indicates the source of magnesium from Mg-rich minerals (e.g. dolomite-CaMg(CO3); Figure 5-7b).

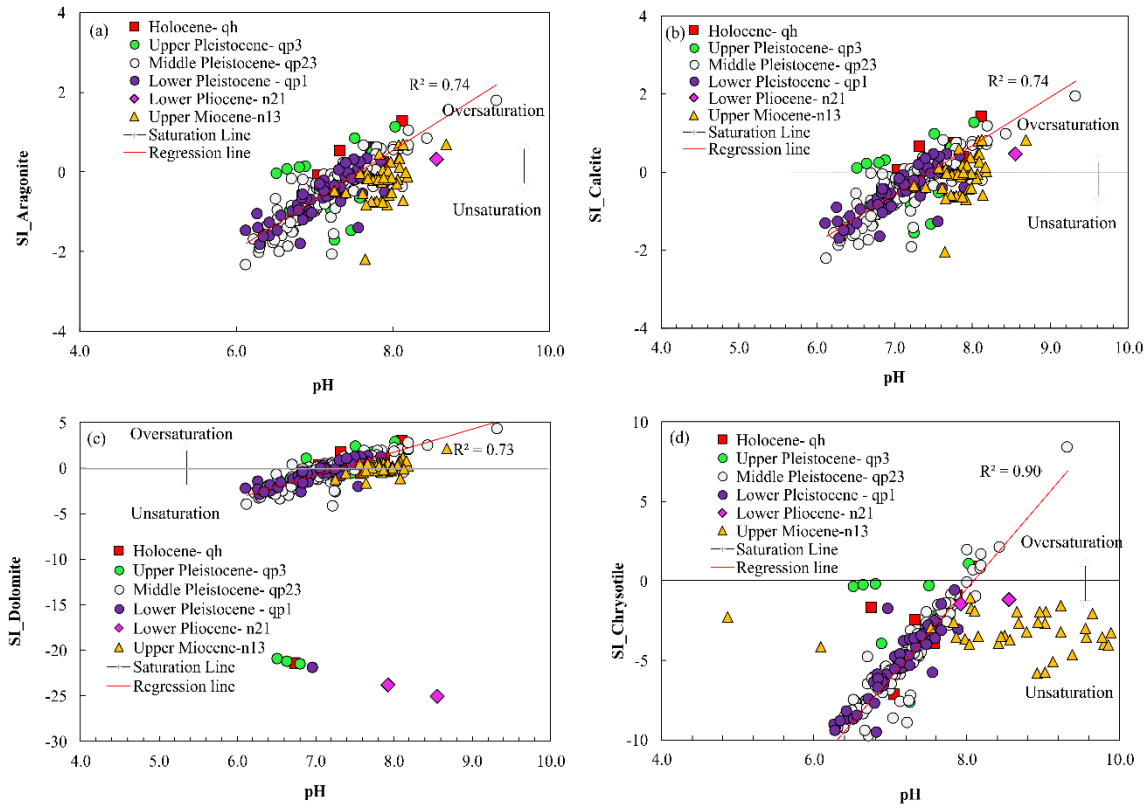

Figure 5- 6: Saturation indexes a. Aragonite, b. Calcite; c. Dolomite; d. Chrysotile with pH of groundwater

Groundwater samples in the study area show the unsaturated states of the halite (NaCl), anhydrite (CaSO4), and gypsum ($CaSO_4.2H_2O$) phases (Figure 5-8). This fact may indicate there is just a small amount of these minerals in aquifers and dissolution rates are low.

Furthermore, the high correlation between sulphate and the saturation index values of anhydrite (Figure 5-9a) and gypsum (Figure 5-9b) reveals that sulphate in groundwater may originate from the dissolution of these minerals.

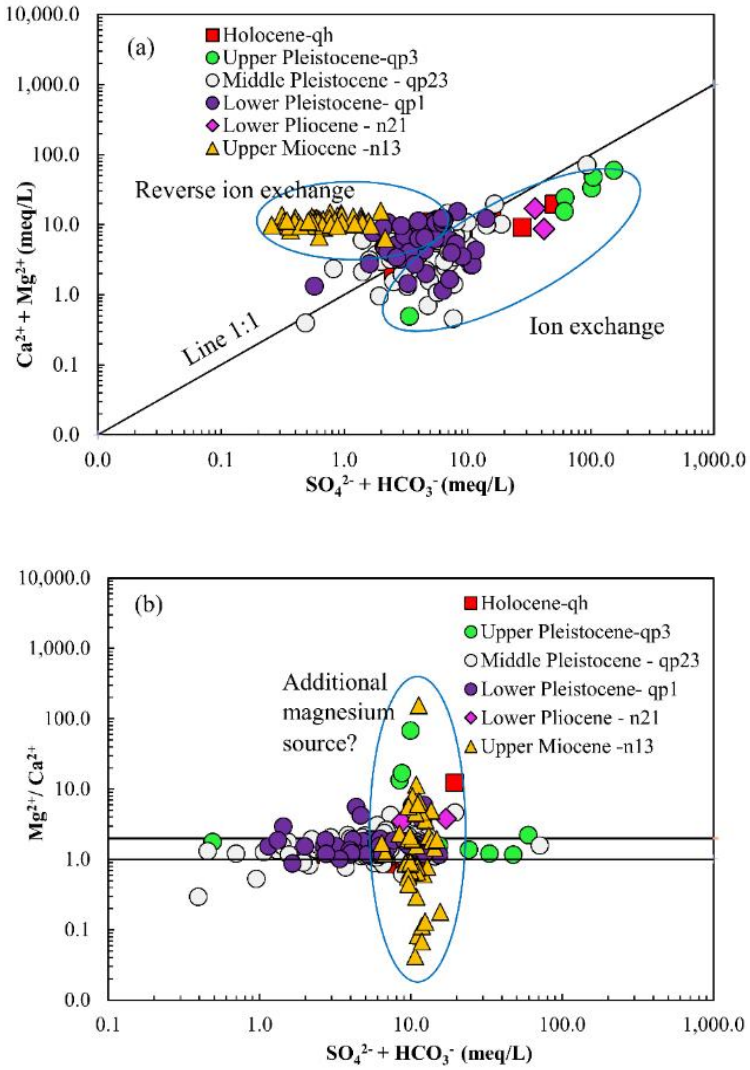

Figure 5- 7: Scattered plots: **a.**SO_4^{2-} + HCO_3^- versus Ca^{2+}/Mg^{2+} , **b.** SO_4^{2-} + HCO_3^- versus Ca^{2+} + Mg^{2+} identifying the potential sources of C Ca^{2+}, Mg^{2+} , SO_4^{2-} and HCO_3^- concentration in groundwater.

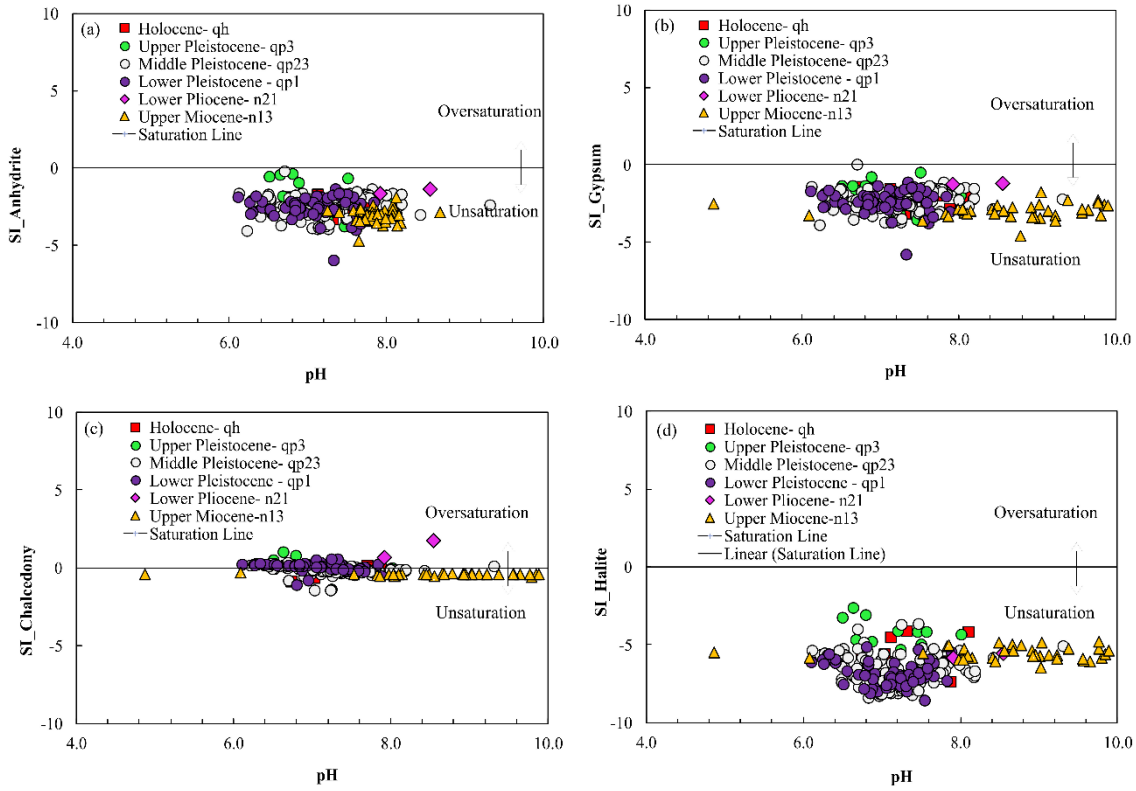

Figure 5- 8: Saturation indexes of **a.** Anhydrite, **b.** Gypsum, **c.** Chalcedony, and **d.** Halite with pH of groundwater.

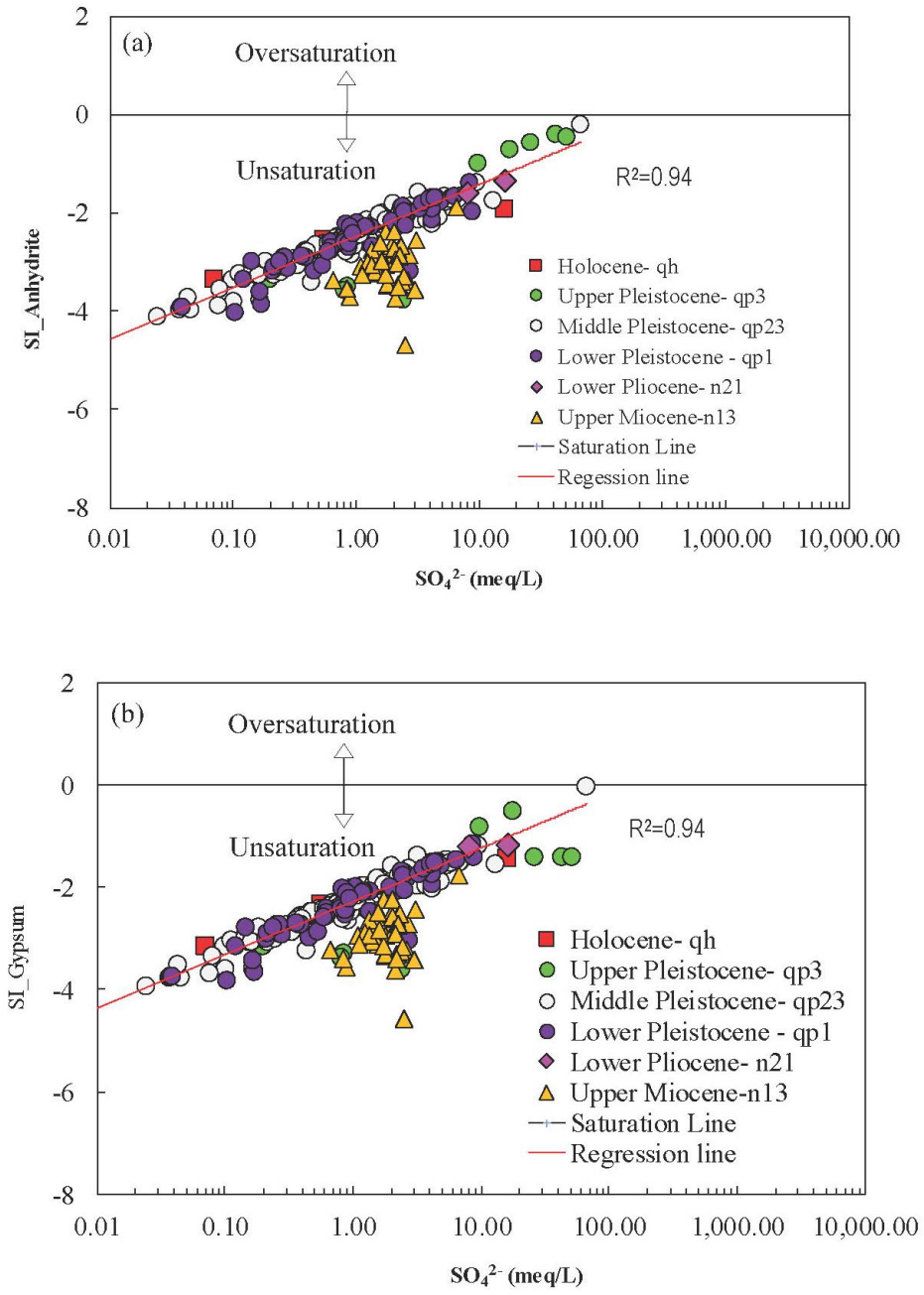

Figure 5- 9: Saturation indexes of (a) anhydrite and (b) gypsum concerning SO_2^{4-} concentration in groundwater.

The processes of anhydrite and gypsum dissolution are expressed in Eq. 5-7 and Eq. 5-8 as below.

Anhydrite dissolution:

$$CaSO_4 \Rightarrow Ca^{2+} + SO_4^{2-} \quad (5\text{-}7)$$

Gypsum dissolution:

$$CaSO4 \cdot 2H2O => Ca^{2+} + SO_4^{2-} + 2H_2O \quad (5\text{-}8)$$

The diagrams of Mg^{2+} vs SO_4^{2-} (Figure 5-10a) and Cl^- vs SO_4^{2-} (Figure 5-10b) show that some groundwater samples have relatively high Mg^{2+} and SO_4^{2-} concentrations. It suggests that Mg^{2+} and SO_4^{2-} in groundwater are originated from brackish connate water trapped in sediments with a low flushing rate of freshwater in these locations.

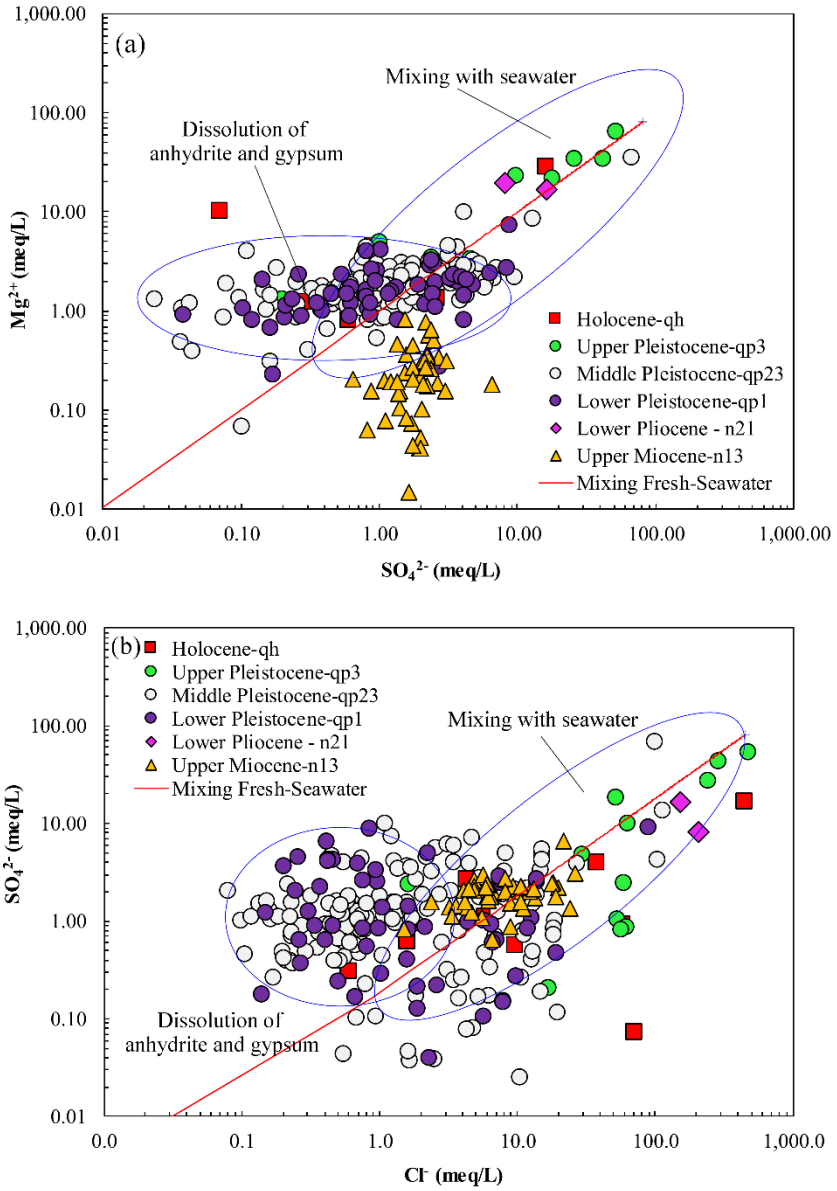

Figure 5- 10: Scattered plot of **a**. SO^{2-}_4 versus Mg^{2+} and **b.** Cl^- versusSO_4^{2-} showing the possible Mg^{2+} respect to groundwater salinization.

The dissolution and precipitation of minerals in coastal aquifers are influenced by mineral sources, pH, temperature, salinity, and flow rate (Blasco, Auqué, & Gimeno, 2019; Thom, Dipple, Power, & Harrison, 2013). The diagrams of pH vs the saturation indices of aragonite, calcite, dolomite, and chrysotile show strong correlations ($R^2 > 0.70$) (Figure 5-6). Groundwater tends to dissolve these minerals at pH < 7.0 while groundwater may reach the equilibrium state at pH = 8.0. This result suggests the potential influence of the pH condition on dissolution processes of such minerals.

Moreover, most of the groundwater samples from the Holocene, Upper Pleistocene, and Middle Pleistocene aquifers (qh, qp_3, and qp_{23}) have increased chloride concentrations respect to potassium (Figure 5-11), indicating the influence of salinity on the albitization process which releases potassium into groundwater (Blasco et al., 2019). The albitization process is shown in the Eq. 5-9 as below.

Albitization process:

$$KAlSi_3O_8(\text{K-filed}) + Na^+ \Rightarrow NaAlSi_3O_8(\text{alb}) + K^+ \qquad (5\text{-}9)$$

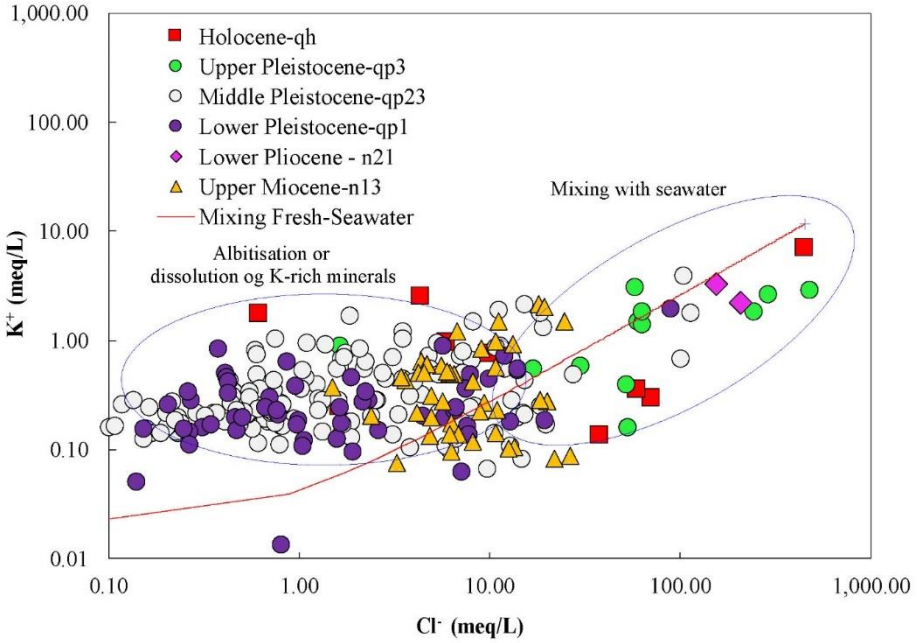

Figure 5- 11: Scattered plot of Cl^- vs. K^+ showing the potential source of K^+ in groundwater

Groundwater samples in the study area showed a weak correlation between the saturation index of anhydrite and chloride concentrations (Figure 12).

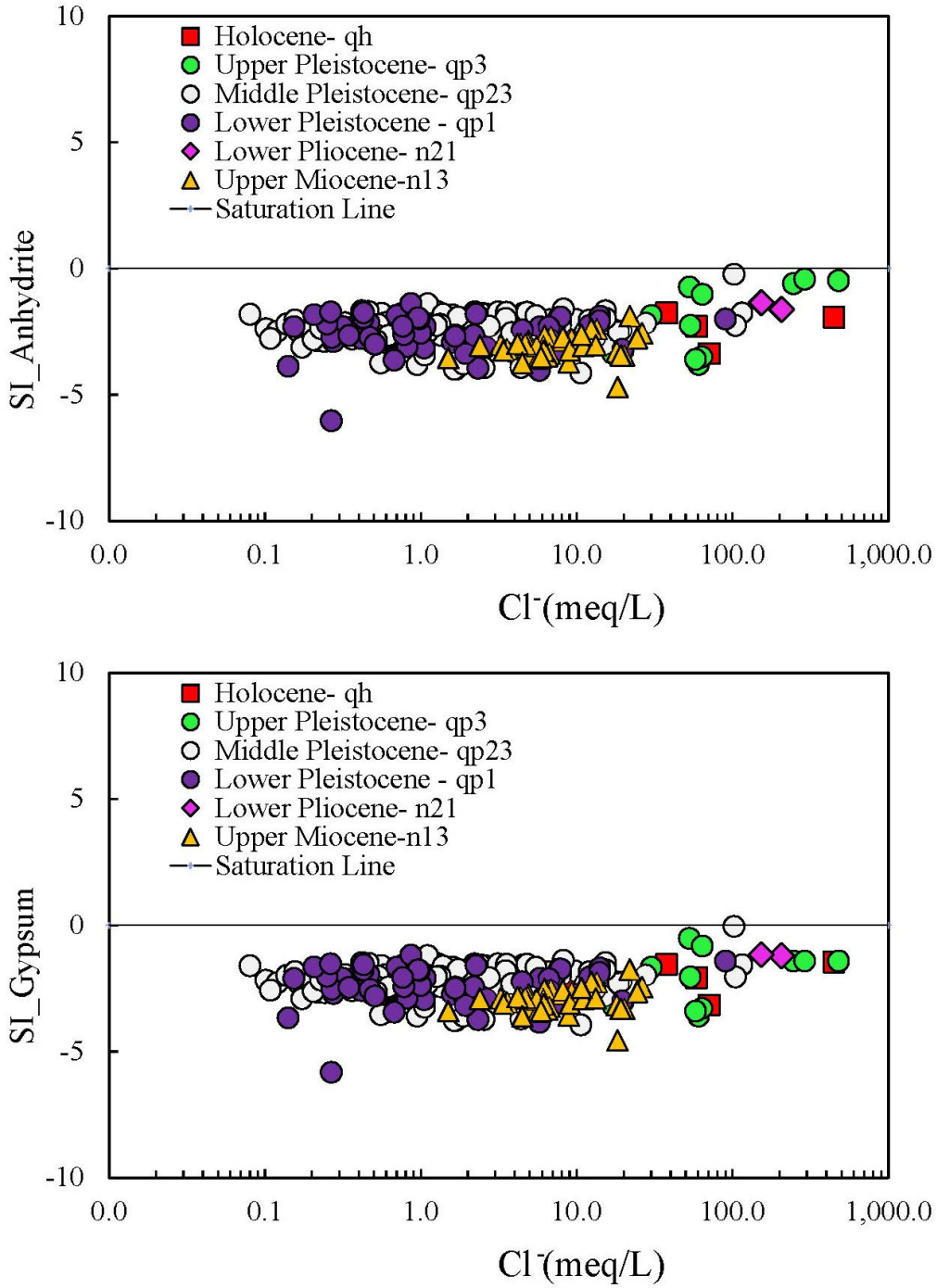

Figure 5- 12:Saturation index of anhydrite and gypsum concerning Cl^- concentration in groundwater.

Although previous studies showed that an increase of salinity in groundwater triggers the process of anhydrite dissolution, the result shows a reverse trend in which there is an unclear relationship between Cl^- and saturation indices of anhydrite. Groundwater flows also influence mineralization processes (Machel, 1999; G. Zhang, Lu, Wei, & Zhu, 2016). It is because the changes in groundwater flow rates influence the porosity and permeability in aquifers and mineral dissolution rates, leading to changes in the processes of mineral reactions. In general, the velocity of groundwater flows depends on many factors such as hydraulic gradients, lithological features and recharge rates. In a flat region like the Mekong Delta, an increase of hydraulic gradients due to groundwater level depletion may change the direction and velocity of groundwater flows. To investigate the effect of groundwater flow velocity on mineralization processes in the study area, the relationships between groundwater levels and saturation indices were employed. In the study area, the relationship between groundwater levels and saturation indices is insignificant (Figure 5-13).

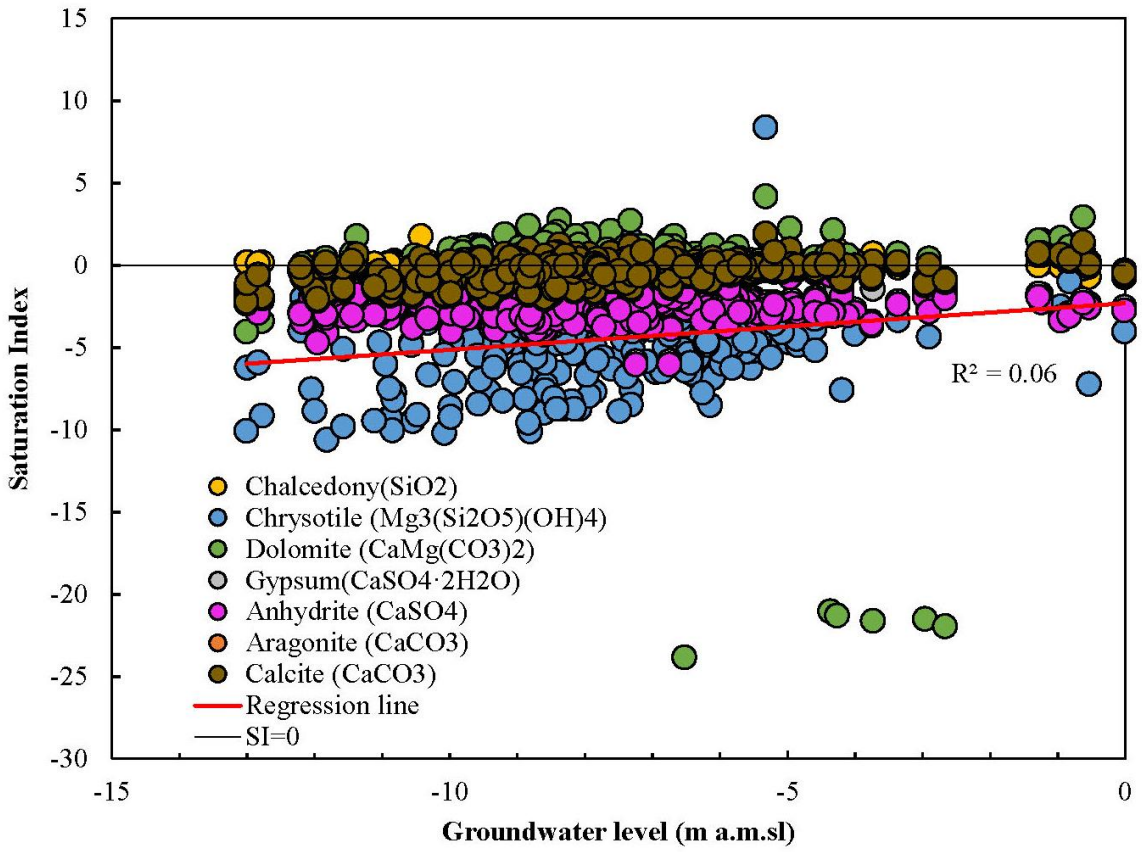

Figure 5- 13: Mineral saturation indexes concerning groundwater levels.

It means that the draw-down of groundwater levels in the present state (maximum -13 m.a.msl) has a minor influence on mineralization processes of groundwater. It also may be because the annual groundwater flow rate in the Mekong Delta aquifer system is still very low, approximately 3.60-7.60 m/year (H. T. Hoang & Bäumle, 2018) while the dissolution of minerals takes a much longer time. Similarly, groundwater temperature (27.50 – 43^{0}C) does not influence mineralization processes (Figure 5-14). The similar result was also found in other studies (Blasco et al., 2019; Schott, Bénézeth, Gautier, & Stefánsson, 2013).

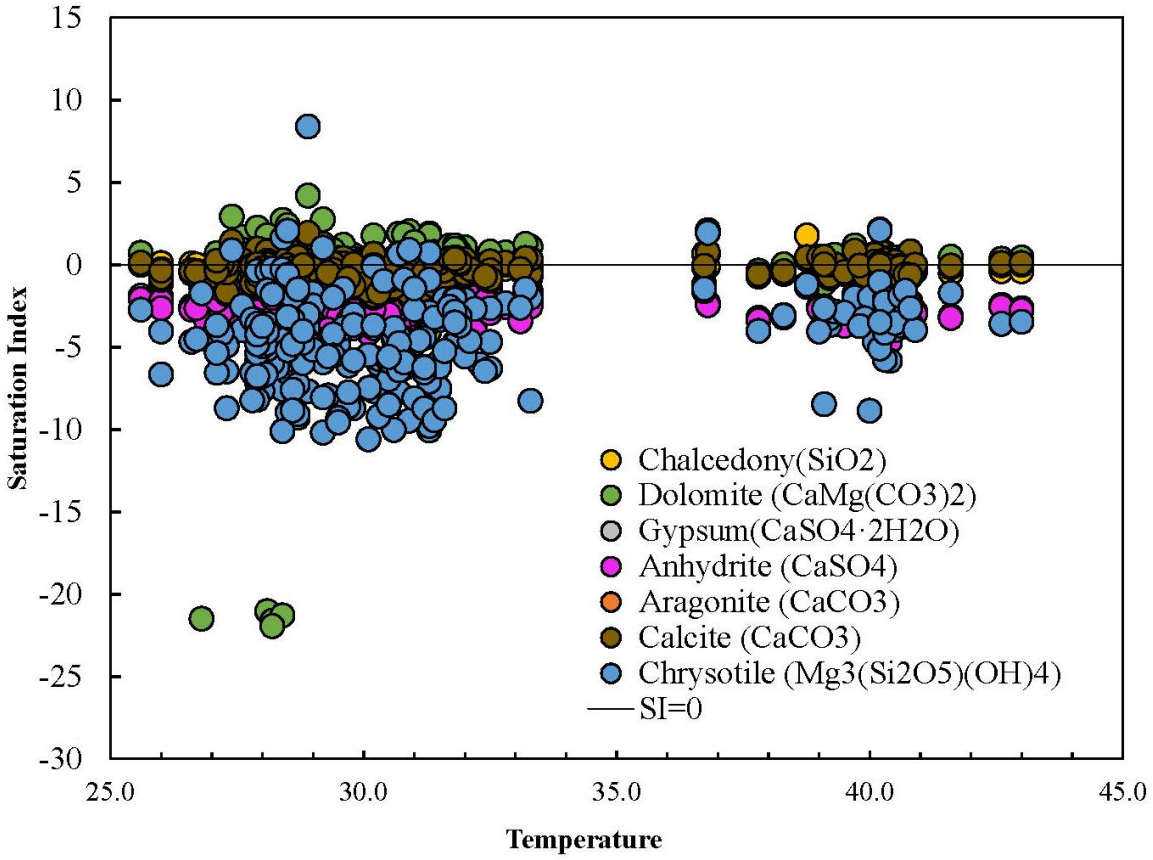

Figure 5- 14: Mineral saturation indexes concerning groundwater temperature

5.4.5. Nitrate contamination

Nitrate (NO_3^-) has become one of the most widely spreading contaminants in groundwater, causing severe health issues (Zhai et al., 2017). Naturally, the concentration of NO_3^- in groundwater is lower than 10 mg/L (Ameur, Hamzaoui–Azaza, & Gueddari, 2016; Batsaikhan, Lee, Nemer, & Woo, 2018). However, anthropogenic inputs may increase NO_3^- and cause severe health problems (Batsaikhan et al., 2018; Parra Suárez, Peiffer, & Gebauer, 2019). Although limited nitrate concentration in drinking water was below 50 mg/L (WHO), the concentration of 10-20 mg/L NO_3^- may influence human health (Ward et al., 2018). Since

NO_3^- in water is from various sources such as atmosphere deposition, soil organic matters, inorganic fertilizers, animal manure, and sewage (Ducci et al., 2019; Zuo et al., 2019) insights into the source of NO_3^- in groundwater could help to prevent groundwater pollution. To delineate nitrate sources in groundwater, one requires precise hydrogeological analyses with geo-environmental consideration (Mas-Pla & Menció, 2019). In this study, the NO_3^- concentration in each groundwater sample was spatially compared to its location in different land-use types, groundwater level, and the distance to surface water system to investigate the potential sources of nitrate.

The results showed that the concentrations of NO_3^- in groundwater samples vary widely among aquifers, ranging from 0.11 mg/L to 264.18 mg/L. For example, the average value of NO_3^- in shallow groundwater samples (Holocene and Upper Pleistocene) was 57.61 mg/L, much higher than 7.02 mg/L of NO_3^- in deep groundwater samples (Middle Pleistocene, Lower Pleistocene, Lower Pliocene, and Upper Miocene). Figure 5-15 shows that the majority of groundwater samples in the study area have low Cl^- and NO_3^- concentrations, indicating the minor effects of human activities on these wells. More seriously, more than 17% (49 samples) of the samples have NO_3^- higher than 10 mg/L, followed by 8.0 % (24 samples) and 3.0 % (9 samples) being higher than 20 mg/L and 50 mg/L, respectively.

The high NO_3^- concentrations in both the shallow and deep groundwater aquifers compared to approximately 10 mg/L of NO_3^- in natural groundwater were found in the urban and agricultural areas as well as in some locations close to rivers and canals (Figure 5-16). The result indicates the influences of human activities on nitrate concentrations in groundwater sources in the study area. Additionally, an increase of nitrate concentrations in aquifers may attribute to following reasons: (1) high nitrate in shallow groundwater aquifers might cause by nitrate infiltration from rice fields, polluted canals, and rivers, and fishery ponds, (2) high nitrate concentrations observed in deep aquifers maybe because of the leakage of nitrate sources through and along well casings due to significant groundwater level depletion in Soc Trang city. Likewise, high nitrate concentrations in groundwater were also found in many coastal aquifers such as in Tunisia (Ziadi et al., 2019), China (Peng et al., 2018), India (Rao, Vidyasagar, Surya Rao, & Bhanumurthy, 2017), Palestine (Abu Al Naeem et al., 2019), Mexico (Mahlknecht et al., 2017a), Malaysia (Sefie et al., 2018; Sheikhy Narany et al., 2018), and Indonesia (Taufiq, Effendi, Iskandar, Hosono, & Hutasoit, 2019). This situation indicates that nitrate pollution has become a common problem in many coastal aquifers in

the world, and suitable solutions should be taken to ensure groundwater quality for human uses.

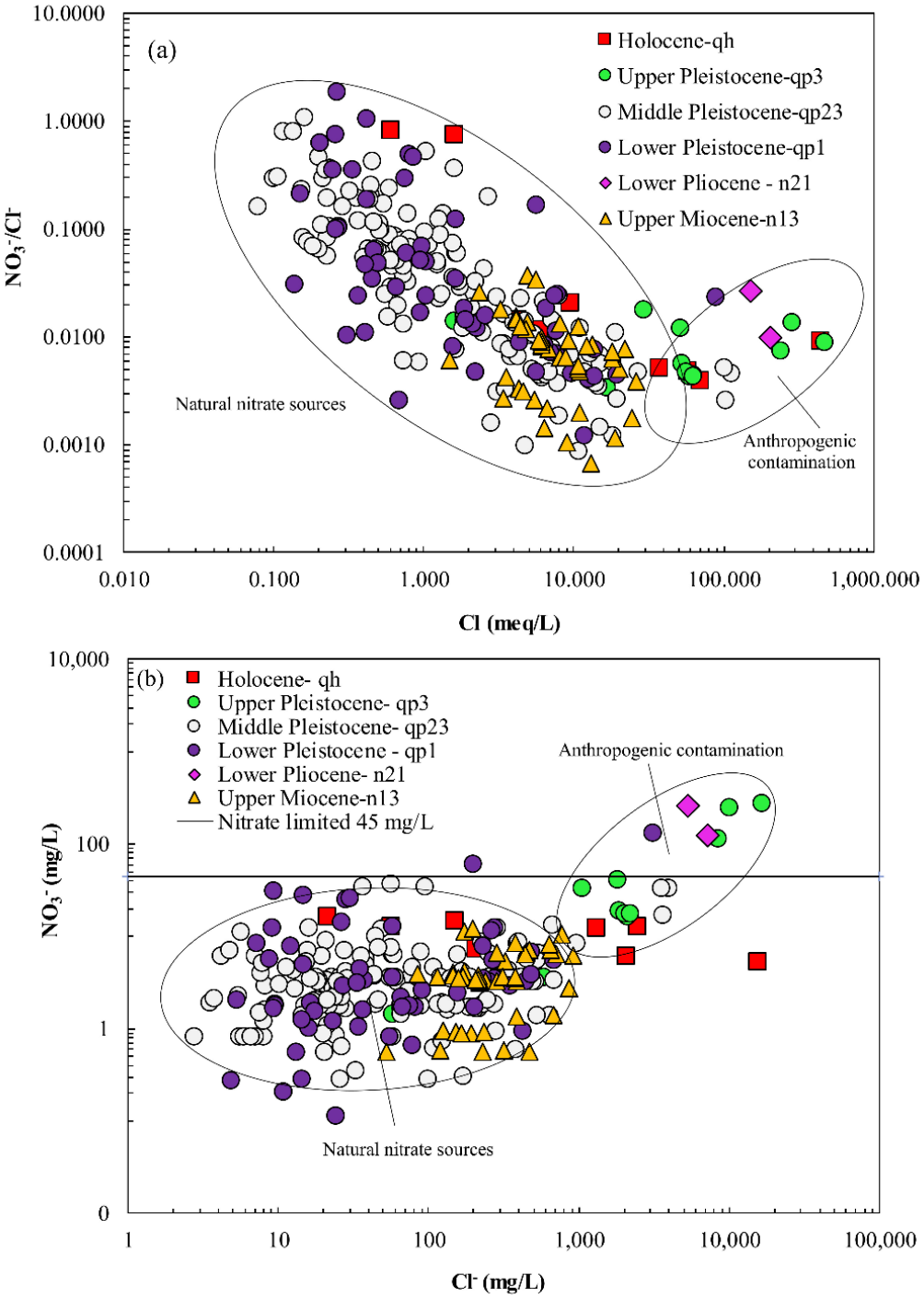

Figure 5- 15: Scattered plots. **a** Cl^- versus NO_3), **b** Cl^- versus NO_3^-/Cl^-) showing possible sources of nitrate in groundwater.

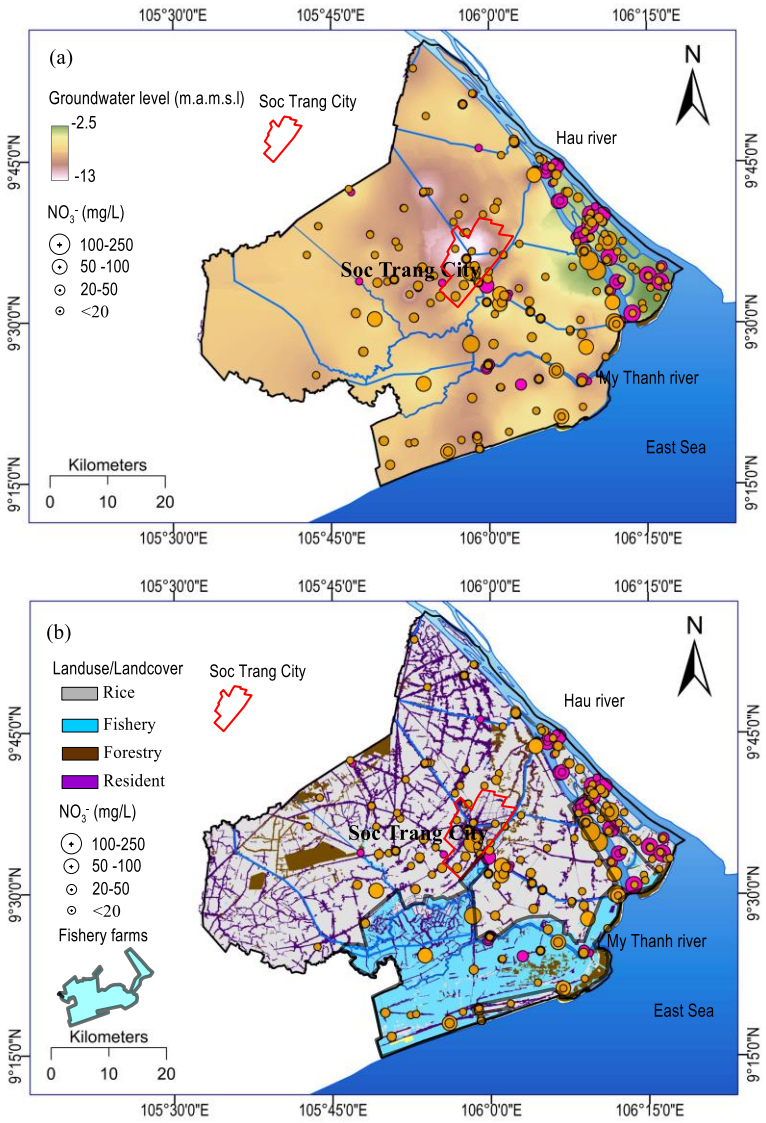

Figure 5- 16: Spatial distribution of NO_3^- concentration concerning (a) groundwater level depletion, (b) agricultural activities.

5.4.6. Multivariate Statistical Analysis

Table 5-2 shows four principal components (PCs) with eigenvalues greater than 1. These PCs explain 68.60% of the total variability of the original data. The first principle component (PC1) accounts for the most variance. PC1 consists of (Na^+, Cl^-, SO_4^{2-}, and HCO_3^-, EC, and TDS exhibited that the dissolution of halite (NaCl) and mixing with seawater were the main contributors to groundwater. The second principle component (PC2) has the high loading values of Ca^{2+} and Mg^{2+}; this PC2 represents the dissolution processes of calcite ($CaCO_3$) and dolomite ($CaMg(CO_3)_2$) contributing to Ca^{2+} and Mg^{2+} concentrations in groundwater samples. Four clusters (C1, C2, C3, and C4) obtained from the AHC analysis showed different groundwater characteristics (Figure 5-17).

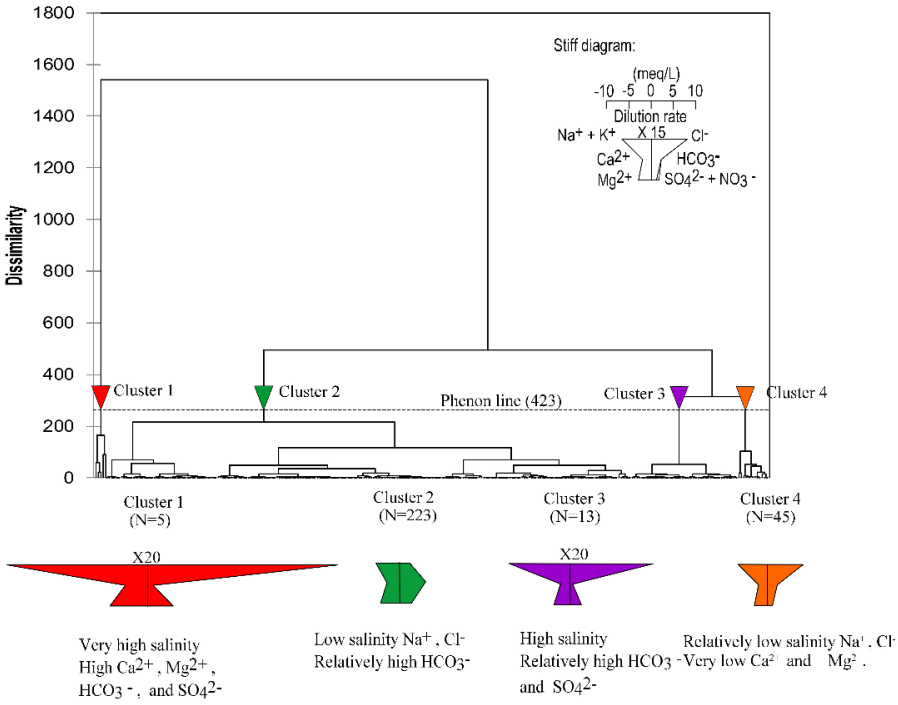

Figure 5- 17: Dendrogram of the agglomerative hierarchical clustering (AHC): when distance linkage (Dlink) is < 264 of Dmax (i.e., the position of the phenon line), the subset is divided into 4 Clusters (C1 to C4). b Log-scale spider diagram of major cation and anion concentrations for the 4 Clusters. Clusters 1 and 3 correspond to groundwater salinization where chloride ion dominates, and Cluster 2 occupies more than 80% of total groundwater samples with a wide variation in chloride, calcium, magnesium, and bicarbonate. Cluster 4 has relatively high salinity but low calcium and magnesium, concentration

The cluster C1 represents the saline hardness of groundwater (Na-Cl) with dominant compositions of $Cl^- > Na^+ > Mg^{2+} > Ca^{2+} > SO_4^{2-} > HCO_3^- > NO_3^- > K^+ > SiO_2$. This cluster represents groundwater samples from the Holocene and Upper Pleistocene aquifers, which have high chloride concentrations. In this cluster, high salinity concentrations in some wells far from the sea and saline rivers may reveal that saline sources may originate from leaching saline from soil/sediment due to significant groundwater depletion (Figure 5-8). Meanwhile, seawater intrusion or irrigation return flows may increase chloride concentrations in some wells close to the Hau River (Figure 5-18). The cluster C2 characterized fresh-hardness water with ion concentrations in the following order: $HCO_3^- > Mg^{2+} > Cl^- > Na^+ > Ca^{2+} > SO_4^{2-} > K^+ > SiO_2 > NO_3^-$. Groundwater samples in this cluster were spatially distributed throughout the whole area, indicating the cluster C2 dominated others in the study area. In the cluster C3, the concentrations of ions were in the order $Cl^- > Na^+ > HCO_3^- > Ca^{2+} > Mg^{2+}$

> K^+ > SO_4^{2-} > NO_3^-. Moreover, groundwater samples in the cluster C3 were distributed along the My Thanh River and in the central part of the study area. The cluster C3 was characterized by high Cl^-, Ca^{2+}, Mg^{2+}, and HCO_3^-, suggesting the processes of paleo-seawater intrusion and water-rock interaction. The cluster 4 was dominated by Na^+ > HCO_3^- > Cl^- > SO_4^{2-} > K^+ > Ca^{2+} > SiO_2 > Mg^{2+} > NO_3, which indicates the cation exchange processes occurring in rich Na-saturated marine clay/sediment. The cluster C4 also represented groundwater samples from the Upper Miocene aquifer (n13), which is also one of the major groundwater sources for municipal water supply systems.

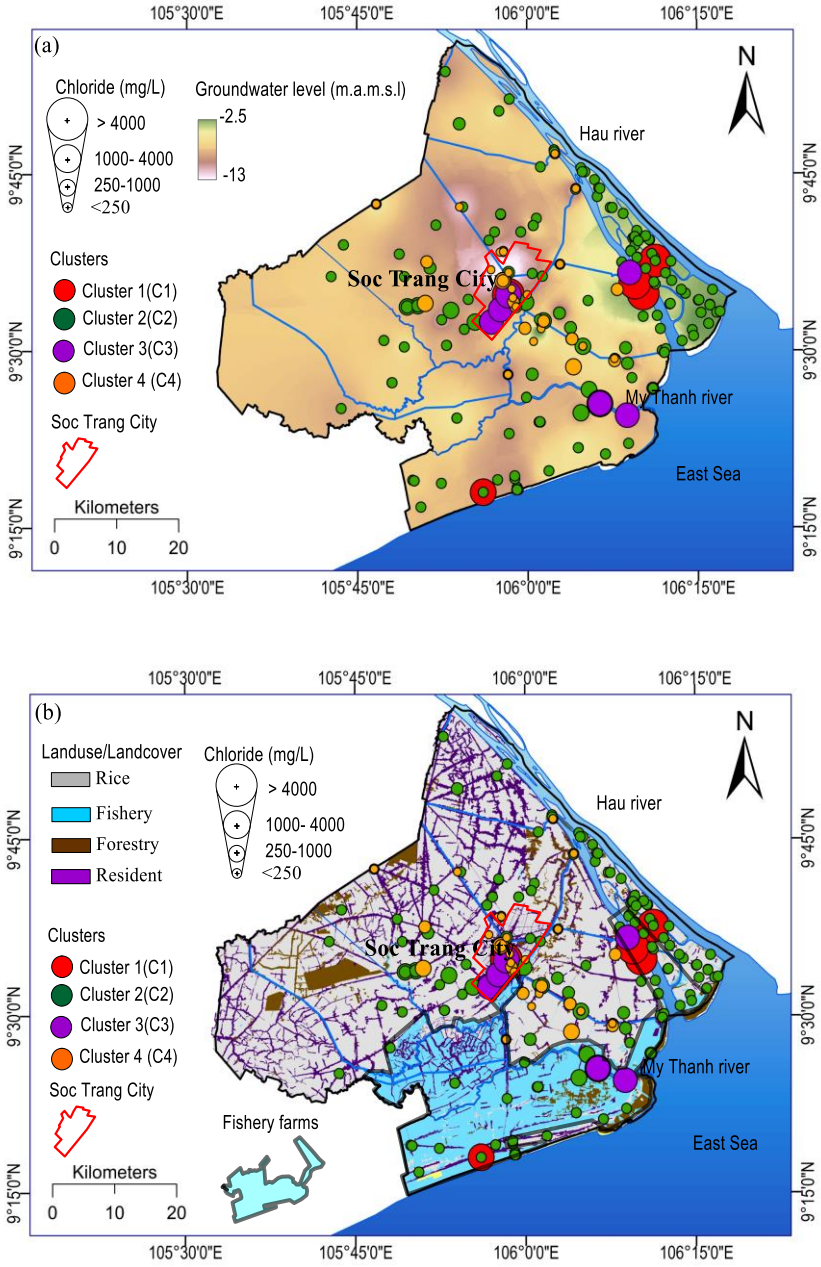

Figure 5- 18: Spatial distribution of Cl^- concentration in each group concerning agricultural development.

The representation of groundwater hydrogeochemical processes shows that groundwater in the superposed aquifers of the Mekong Delta has experienced complex interaction and feedback processes, including the effects of evaporation, mineral weathering and dissolution, and salinization. Based on the results of the PCA and HCA analyses, it was found that geochemical evolution in the coastal superposed aquifers of the Mekong Delta may follow four main trends (Figure 5-19). First, groundwater samples in C1 may become harder water (Na-Mg-Ca-SO_4-HCO_3) due to the dissolution of calcite and dolomite without the influences of groundwater salinization. Second, samples in C1 which have relatively high salinity may mix with paleo-saline water, modern seawater, or both under excessive groundwater exploitation. Third, some wells from C1 and C4, which have relatively high salinity, may increase calcium and magnesium concentrations as a result of calcite and dolomite dissolution. Finally, the majority of groundwater samples in C4 may increase salinity concentrations due to paleo-saline groundwater dissolution caused by the over-exploitation of groundwater resources. These processes may deteriorate groundwater quality in the coastal aquifers of the Mekong Delta in the context of unpredictable impacts of climate change and sea-level rise.

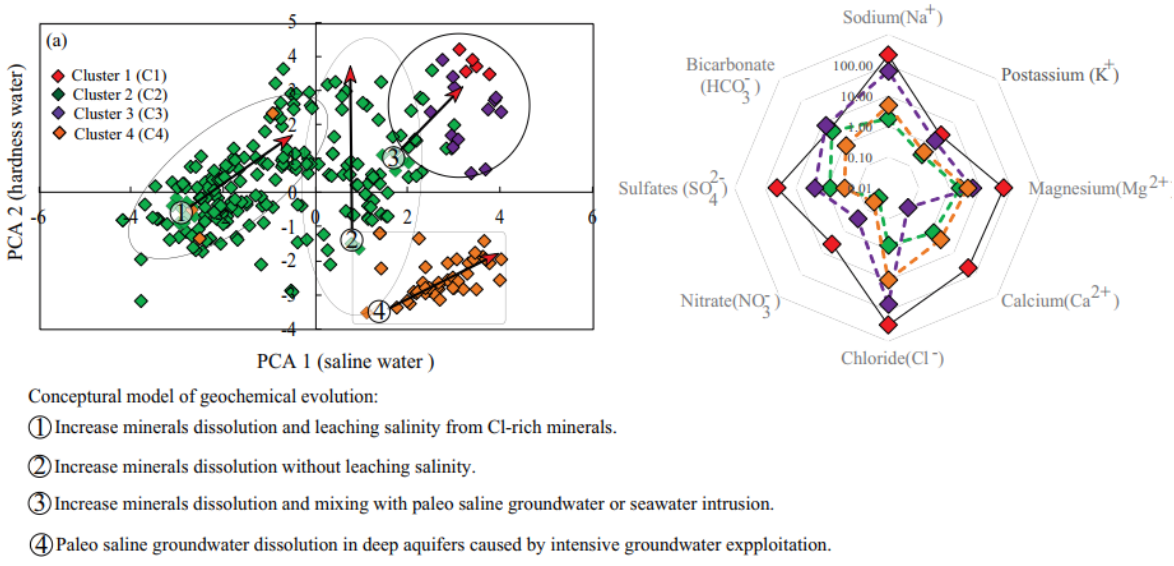

Conceptural model of geochemical evolution:

① Increase minerals dissolution and leaching salinity from Cl-rich minerals.

② Increase minerals dissolution without leaching salinity.

③ Increase minerals dissolution and mixing with paleo saline groundwater or seawater intrusion.

④ Paleo saline groundwater dissolution in deep aquifers caused by intensive groundwater expploitation.

Figure 5- 19: Conceptual model of groundwater geochemical evolution in a coastal area of the Mekong Delta

5.5. Conclusions

Groundwater chemical characteristics and its controlling factors in a coastal area of the Mekong Delta summarized as follows:

- Groundwater has significant spatial variability in the concentrations of ions dominated by HCO_3^-, Mg^{2+}, Cl^-, Na^+, Ca^{2+}, SO_4^{2-}, K^+, SiO_2, and NO_3^- in descending order. Since groundwater is the primary source of fresh water in the region, the high concentrations of Cl^- and Na^+, which exceed thresholds in the WHO guideline, may raise concerns about water quality and potential health problems. Also, the presences of other cations and anions are driven by complex geochemical evolutions, including silicate weathering, mineral dissolution concerning calcite, aragonite, dolomite, halite, chalcedony, and chrysotile.
- There is evidence of the heterogeneously distributed saline groundwater (Na-Cl) in different aquifers; therefore, the hydraulic disturbance may worsen the situation of saline intrusion. In the study area, seawater intrusion is caused by natural processes, including paleo-saline water trapped in sediment/rock, halite dissolution, and the leakages of saline from the upper layers to lower layers. However, the problem of seawater intrusion is further exacerbated in recent years due to excessive groundwater exploitation which increases the hydraulic connection between aquifer layers.
- It was found that pH has influenced the dissolution of calcite, aragonite, and dolomite chrysotile in groundwater while temperature, salinity and groundwater levels showed insignificant impacts.
- The high nitrate concentration in coastal aquifers of the study area may originate from (i) nitrate infiltration from rice fields, polluted canals, and rivers, and fishery ponds, (ii) leakage of nitrate sources through and along with well casings due to excessive groundwater exploitation in Soc Trang city.

The encroachment of seawater intrusion and nitrate contamination in the coastal region is a severe problem since many socio-economic activities are dependent on groundwater sources. Regarding this current situation, a long-term monitoring program for both shallow and deep groundwater sources is needed in the study area, especially in Soc Trang city and along the Hau River to the Tran De estuary. Strategies and solutions to reduce groundwater salinization and nitrate contamination are also required. Instead of just penalties in

environmental protection laws, immediate actions must be taken by water authorities. Possible solutions may consist of the following: (i) Setting up a proper groundwater monitoring system, so remediation actions could be proposed timely; (ii) Finding alternative freshwater resources for the water supply system in the Mekong Delta, combined with using and saving groundwater and reducing groundwater pumping; (iii) Attempting further studies on natural and artificial groundwater recharge to improve groundwater levels and prevent seawater intrusion.

CHAPTER 6 STABLE ISOTOPIC CHARACTERISTICS OF WATER RESOURCES IN COASTAL AREA OF THE MEKONG DELTA

Chapter 6 presents the main findings on the characteristics of stable isotopes and quantifying influences of evaporation and seawater intrusion processes on water resources in a coastal area of the Mekong Delta. These findings were accepted for publication in Science Citation Index (SCI/SCIE) scientific journal entitled the Journal of Isotopes in Environmental and Health Studies (Impact Factor 2018, IF =1.367).

6.1. Introduction

Coastal deltas provide shelters and livelihoods for approximately 40% of the world population (Barragán & de Andrés, 2015). However, many coastal regions are facing freshwater scarcity due to surface water pollution (Chau et al., 2015; Minh et al., 2007), groundwater contamination (Norrman et al., 2015; Pistocchi et al., 2017; Zhai et al., 2017), and seawater intrusion (Gemitzi, Stefanopoulos, Schmidt, & Richnow, 2014; Kumar, Jain, Yamanaka, Li, & Bhattacharya, 2018; Smajgl et al., 2015). Understanding the causes of these problems often requires long-term monitoring efforts which are usually costly. The stable oxygen and hydrogen isotope compositions ($\delta^{18}O$ and $\delta^{2}H$) can serve as a useful technique to track the origin of water and environmental changes because these isotopes undergo different fractionation during their transitional phases (e.g., evaporation, condensation, and sublimation) in the hydrologic cycle (Tian, Wang, Kaseke, & Bird, 2018). Therefore, stable isotopes have also been widely applied to investigate hydrological processes at local to regional scales (Bădăluță, Perșoiu, Ionita, Nagavciuc, & Bistricean, 2019; Conroy et al., 2017; Hoogewerff, Kemp, Leng, & Meier-Augenstein, 2019; Sánchez-Murillo & Birkel, 2016; Sprenger, Leistert, Gimbel, & Weiler, 2016).

In coastal regions, stable isotopes are especially useful for investigating the origin of water, recharge mechanisms, and evaporation and seawater/freshwater mixing processes

(Dublyansky, Klimchouk, Tokarev, Amelichev, & Spötl, 2019; González-Trinidad, Pacheco-Guerrero, Júnez-Ferreira, Bautista-Capetillo, & Hernández-Antonio, 2017; D. Han & M. J. Currell, 2018; Herrera et al., 2018; Okakita, Iwatake, Hirata, & Ueda, 2019; Seddique et al., 2019; Skrzypek et al., 2015; Sprenger, Tetzlaff, Tunaley, Dick, & Soulsby, 2017; Yeh, Lin, Lee, Hsu, & Wu, 2014). For instance, the seasonal variation of $\delta^{18}O$ and $\delta^{2}H$ isotopes in rainfall, surface water, and groundwater could be used to investigate the seasonal variation of groundwater recharge (González-Trinidad et al., 2017; Herrera et al., 2018; Okakita et al., 2019; Yeh et al., 2014). Stable isotopes have also been widely applied to estimate the evaporation ratio because evaporated water has a distinct stable isotopic composition compared to that of non-evaporated water (Skrzypek et al., 2015; Sprenger et al., 2017). Furthermore, an increase in both salinity and $\delta^{18}O$ in water bodies may denote the influences of seawater intrusion (D. Han & M. J. Currell, 2018; Seddique et al., 2019).

In the Mekong Delta, several studies have been conducted to investigate the characteristics of stable isotopes in precipitation (N. Le Duy et al., 2018), surface water (An et al., 2014b; Kabeya et al., 2008; K. C. Nguyen, Huynh, Le, Nguyen, & Tran, 2007), and groundwater (An et al., 2014b; An et al., 2018; Chau Tran Vinh et al., 2017; Ho et al., 1991; H. T. Hoang & Bäumle, 2018). For instance, Duy et al. (N. Le Duy et al., 2018) investigated the main factors controlling stable isotope variations of rainfall in the Mekong Delta (N. Le Duy et al., 2018). They found that (1) precipitation along the trajectories of the air mass movement is the most important climatic factor controlling stable isotope compositions in rainfall during the rainy season (May to October) and (2) the secondary fractionation processes controls isotopic compositions of rainfall in the dry season (November to April). Nguyen et al. (K. C. Nguyen et al., 2007) found that stable isotopes in the Mekong river have a seasonal variability with heavy isotope enrichment in the dry season compared to the rainy season. Furthermore, there is a spatial variability of stable isotope concentration in shallow

and deep aquifers due to influences of evaporation processes and seawater intrusion (An et al., 2014b; An et al., 2018; Ho et al., 1991; H. T. Hoang & Bäumle, 2018). These studies, however, did not investigate the origin of freshwater and saline water in the coastal aquifers of the Mekong Delta. In addition, insights into the influences of evaporation and seawater intrusion processes on changes in stable isotopes of surface water and groundwater are not well understood. Further applications of stable isotopes to investigate the origin of water, evaporation and seawater intrusion processes are essential for sustainable water resources management and environmental protection in coastal regions.

The objectives of this research are to (1) analyze the seasonal variation of the stable isotopes and salinity of surface water (section 3.1), (2) identify characteristics of stable isotopes and salinity in groundwater (section 3.2), (3) quantify the effects of evaporation and seawater intrusion on changes in stable isotope compositions (section 3.3), and (4) investigate the origin of groundwater in the coastal area of the Mekong Delta (section 3.4).

6.2. Materials and Methods

6.2.1. Study area

Soc Trang province, which is part of the Vietnamese Mekong Delta, has an area of approximately 3,312 km^2 (Figure 6-1a). The study area borders with the Vietnamese East Sea in the Southeast and with the Hau River in the Northeast. The southwest monsoon climate in the study area starts from May to October and the northeast monsoon climate from November to April. The average annual rainfall is about 1,875 mm, with 85% of the rainfall amount is in the rainy season. The mean yearly temperature is approximately 26.7°C. The mean relative humidity is about 85% in the dry season and 87% in the rainy season. The study area has a dense and complex river-canal system (Figure 6-1a).

Soc Trang province has a multi-layer aquifer system which was a result of long-term sediment transportation and deposition processes under impacts of river-sea interaction

processes (Figure 6-1b). The aquifer system of the study area could be divided into seven hydrogeological units: Holocene (qh), Upper Pleistocene (qp_3), Middle Pleistocene (qp_{23}), Lower Pleistocene (qp_1), Middle Pliocene (n_{22}), Lower Pliocene (n_{21}), and Upper Miocene (n_{13}) (Wagner et al., 2012). These aquifers consist of sedimentary deposits dominated by sands, fluvial, and gravels with various grain sizes while the aquitards consist of mud, silt, and clays. The detail description of hydrogeology in the study area was reported in detail elsewhere (H. T. Hoang & Bäumle, 2018; Hung Van et al., 2019).

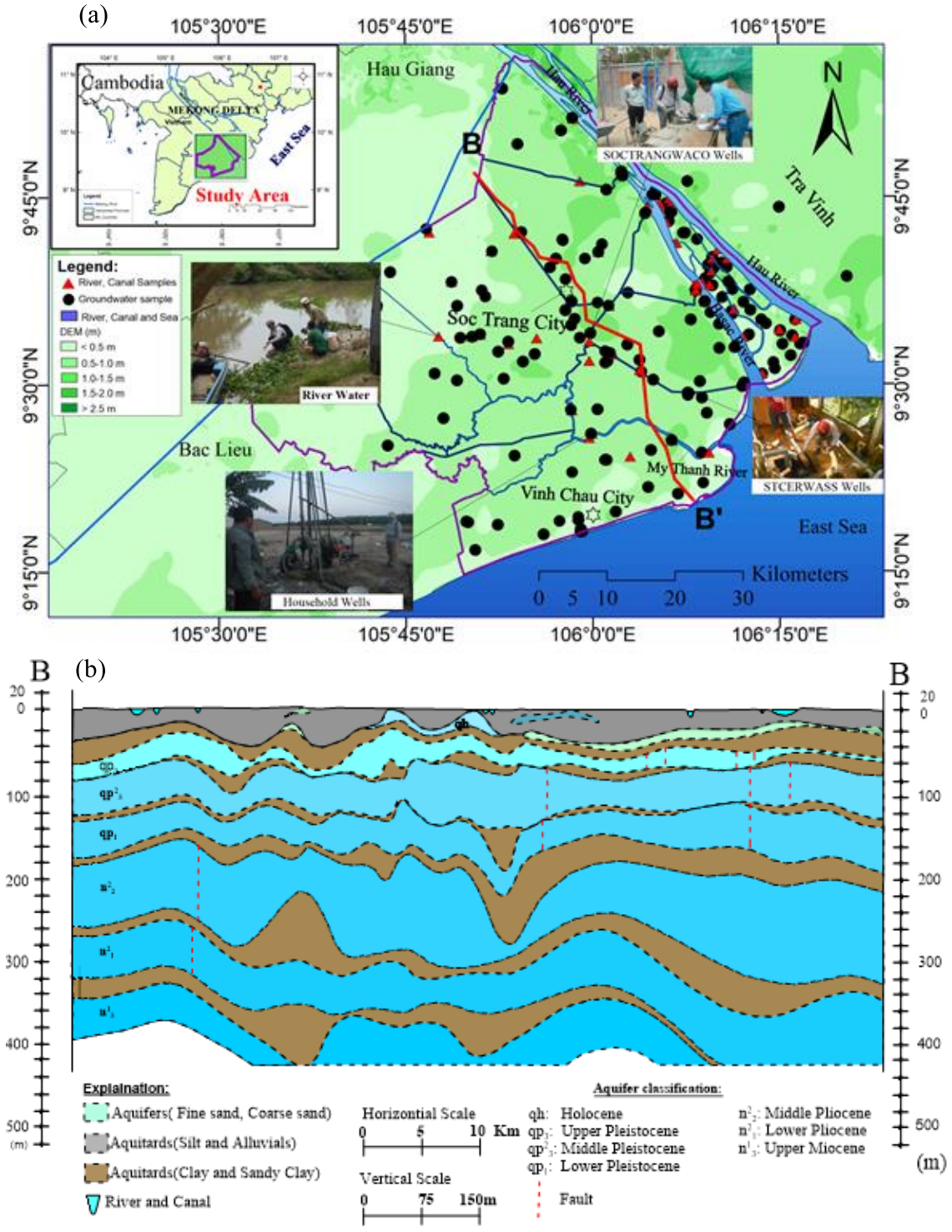

Figure 6- 1: Map of Soc Trang province (a) sampling locations and dense river-canal network system, (b) hydrogeological profile B-B'.

Hydrological regimes in the study area are influenced by the flow of the Mekong River, tidal regime, and operations of local hydraulic structures such as dykes and tidal barriers (Dang et al., 2016; Manh et al., 2015). In recent years, the impacts of seawater

intrusion on surface water in the study area are becoming more severe due to the reduction of river discharge, which is caused by the development of upstream reservoirs and irrigation activities (Pokhrel et al., 2018). Human activities in the region were also found to be one of the controlling factors affecting water quality (Chea, Grenouillet, & Lek, 2016; Whitehead et al., 2019). In such a complex water environment, understanding the characteristics of stable isotopes and influencing factors is pivotal of understanding surface and subsurface hydrological processes. This helps propose timely action to confront negative impacts.

6.2.2. Data collection and chemical analysis

In this study, 278 groundwater samples and 79 river water samples were collected in the dry season and rainy season between 2013 and 2017. The groundwater samples were collected from household wells and production wells from the Center for Rural Water Supply and Sanitation of Soc Trang (STCERWASS) and the Soc Trang Water Supply Company (SOCTRANGWACO). Surface water samples were collected from the river and canal system along the coast and up to 60 km inland during the dry and rainy seasons. For chemical and stable isotopes analysis, all water samples were filtered with a 0.02 µm cellulose ester. Chloride concentration in groundwater and surface water samples were analysed using an ion liquid chromatography (Shimadzu Co. Ltd., HIC-SP/VP Super). Stable isotopes ($\delta^{18}O$, $\delta^{2}H$) were analysed using a PICARRO L2120-I Analyzer system at the Tsujimura laboratory, University of Tsukuba, Japan. All isotopic measurements were calibrated according to the international standards of the Vienna Standard (V-SMOW). The stable isotope compositions of oxygen and hydrogen are presented in the delta notation ($\delta^{18}O$, $\delta^{2}H$) in per mil (‰) as follows:

$$\delta_{sample} = \left(\frac{R_{sample} - R_{standard}}{R_{standard}} \right) \times 1000 \qquad (6\text{-}1)$$

Where R is the ratio of the heavy to light isotopes, R = $^{2}H/^{1}H$ for hydrogen and $^{18}O/^{16}O$ for oxygen (Richards et al., 2018). The analysis precision is ± 0.1‰ for $\delta^{18}O$ and ±1‰ for $\delta^{2}H$. The deuterium excess (herein *d*-excess) values of water samples were estimated using the relation defined by Dansgaard (1964):

$$d = \delta^{2}H - 8 \times \delta^{18}O \qquad (6\text{-}2)$$

6.2.3. Quantifying effects of evaporation and mixing processes on isotopic enrichment

Evaporation and seawater intrusion have been recognized as the major processes causing changes in stable isotopes of water in coastal areas. Seawater/freshwater mixing is a common phenomenon in many coastal regions worldwide. Groundwater and surface water samples in a coastal area can found as the mixtures of freshwater and seawater (Figure 6-2). The stable isotope compositions of $\delta^{18}O$ or $\delta^{2}H$ in groundwater and surface water before mixing with seawater, δ_{bm}, can be estimated as follows [63]:

$$\delta_{bm} = [\ \delta_{m} \times (C_{sw} - C_{fw}) - \delta_{sw} \times (C_{m} - C_{fw})] \ / \ (C_{sw} - C_{m}\ ) \qquad (6\text{-}3)$$

where δ_{m} and δ_{sw} are the $\delta^{18}O$ or $\delta^{2}H$ (‰) values of a measured sample and seawater, C_{fw} is the Cl^{-} concentration of freshwater (rainwater in this study), C_{sw} is the Cl^{-} concentration of seawater, C_{m} is the measured Cl^{-} concentration (mg L^{-1}) in water samples.

In this study, the Cl^{-} concentration of the freshwater end-member is 1.0 mg L^{-1} (based on the average Cl^{-} concentration of rainwater samples collected in the rainy seasons of 2017 and 2018). The Cl^{-} concentration of the seawater end-member is selected as 23,000 mg L^{-1} (Tsutomu et al., 2011).

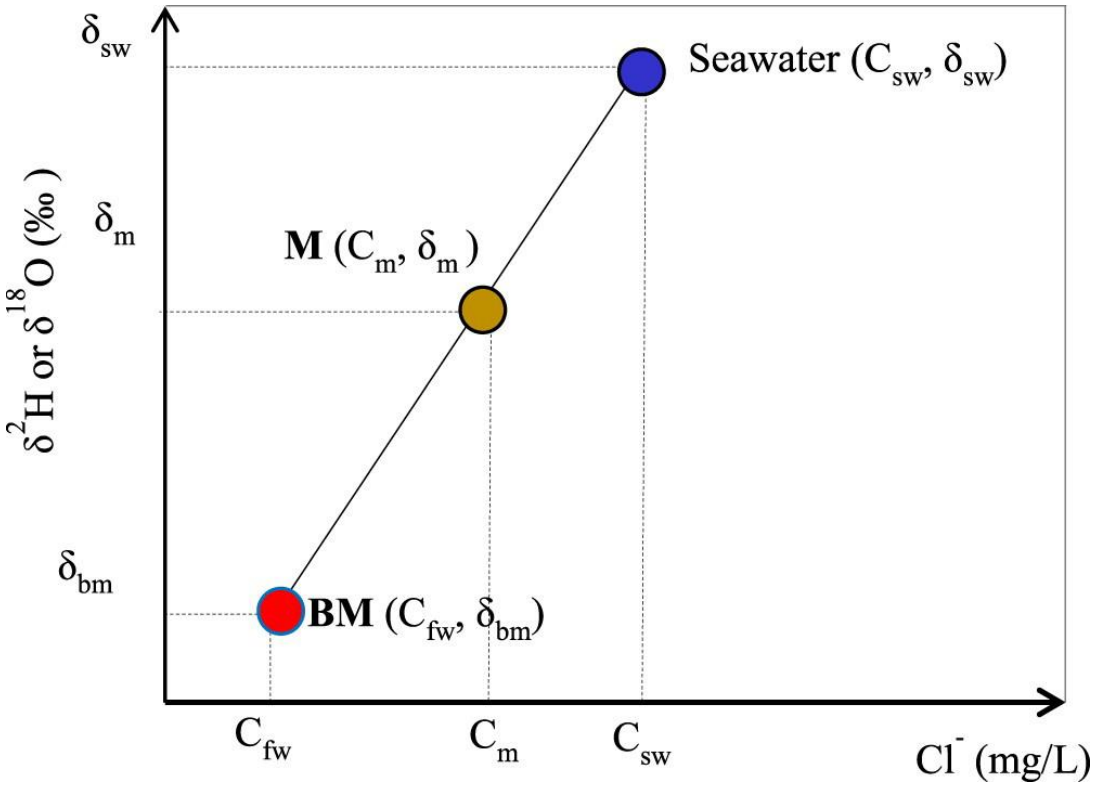

Figure 6- 2: The conceptual diagram explaining the correction scheme for isotopic changes due to seawater intrusion.

Figure 6-3 shows the changes in stable isotope compositions in water due to evaporation and seawater mixing. In more detail, the two processes are (1) changes in stable isotope compositions from the source of water R ($\delta^{18}O_o$, $\delta^{2}H_o$) to evaporated water BM ($\delta^{18}O_{bm}$, $\delta^{2}H_{bm}$) and (2) mixing of evaporated water BM with seawater to form M ($\delta^{18}O_m$, $\delta^{2}H_m$) at sampling points. To derive the original isotopic composition of water R ($\delta^{18}O_o$, $\delta^{2}H_o$), after calculating evaporated water BM, Equations (6-4) and (6-5) can be solved to obtain the stable isotope composition from the source R (Figure 6-3) (Phillips et al., 1986; Tsutomu et al., 2011). This is because R is the intersection point of the local meteoric water line for the Mekong Delta (purple line, Figure 6-3) and the evaporation line that passes through BM ($\delta^{18}O_{bm}$, $\delta^{2}H_{bm}$) (red line, Figure 6-3).

$$\delta^{2}H_o = (\delta^{2}H_{bm} - s \times \delta^{18}O_{bm} - s \times b/a)/ (1- s/a) \qquad (6\text{-}4)$$

$$\delta^{18}O_o = (\delta^{2}H_o - b)/a \qquad (6\text{-}5)$$

Where is the slope of the evaporation line, a =7.56 and b =7.26 are the slope and intercept of local meteoric water lines (LWML: $\delta^2H = 7.56 \times \delta^{18}O + 7.26$) in the Mekong Delta, respectively (N. Le Duy et al., 2018). The slope of the evaporation line (denoted as s) was estimated based on the average relative humidity (h) and temperature (T) in the study area. The average surface air temperature of 26.8 ºC and the average relative humidity of 0.80 (based on data series from 2000 to 2016) were used to estimate the slope of evaporation following the Eq. 6 below (P. Huang & Wang, 2017):

$$s = \frac{24.844(10^6/(T+273)^2) - 76.248(10^3/(T+273)) + 52.612 + 12.5(1-h)}{1.137(10^6/(T+273)^2) - 0.4156(10^3/(T+273)) - 2.0667 + 14.2(1-h)} \quad (6\text{-}6)$$

Accordingly, the slope of the evaporation line (s) is 6.41, which is similar to the slope of the regression line for surface water in the dry season (6.45).

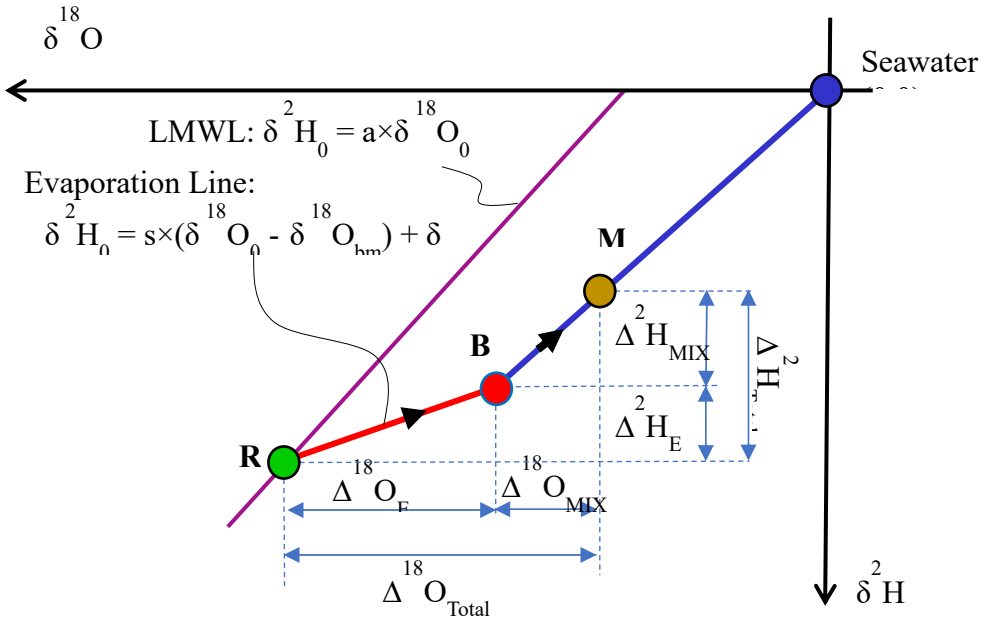

Figure 6- 3: Conceptual diagram explaining the isotopic change due to evaporation effects and seawater mixing. The green point R ($\delta^{18}O_o$, δ^2H_o) represents the source of a water sample without evaporation effects and seawater mixing, which is considered as a fresh-end member. The red point BM ($\delta^{18}O_{bm}$, δ^2H_{bm}) denotes the evaporated water before mixing with seawater. The orange point M ($\delta^{18}O_m$, δ^2H_m) is the measured sample at the sampling point. The blue

point Seawater (0,0) is the standard seawater as the seawater-end member (adapted from Yamanaka et al., 2011) [39].

Subsequently, the changes in stable isotope compositions caused by evaporation processes and seawater intrusion could be estimated following equations:

For $\delta^{18}O$:

$$\Delta^{18}O_{total} = \delta^{18}O_m - \delta^{18}O_o \quad (6\text{-}7)$$

$$\Delta^{18}O_{MIX} = \delta^{18}O_m - \delta^{18}O_{bm} \quad (6\text{-}8)$$

$$\Delta^{18}O_{EV} = \delta^{18}O_{bm} - \delta^{18}O_o \quad (6\text{-}9)$$

For $\delta^{2}H$:

$$\Delta^{2}H_{total} = \delta^{2}H_m - \delta^{2}H_o \quad (6\text{-}10)$$

$$\Delta^{2}H_{MIX} = \delta^{2}H_m - \delta^{2}H_{bm} \quad (6\text{-}11)$$

$$\Delta^{2}H_{EV} = \delta^{2}H_{bm} - \delta^{2}H_o \quad (6\text{-}12)$$

Where $\Delta^{18}O_{total}$ and $\Delta^{2}H_{total}$ are the changes in $\delta^{18}O$ and $\delta^{2}H$ compositions caused by both evaporation and seawater intrusion, $\Delta^{18}O_{EV}$ and $\Delta^{2}H_{EV}$ are the changes in $\delta^{18}O$ and $\delta^{2}H$ of the source (R) caused by evaporation processes, $\Delta^{18}O_{MIX}$ and $\Delta^{2}H_{MIX}$ are the changes in $\delta^{18}O$ and $\delta^{2}H$ of the source (R) caused by seawater mixing. The contribution ratio of evaporation (F_{EV}) and seawater intrusion (F_{MIX}) that causes heavy isotope enrichment from sources can be estimated using the following equations:

For $\delta^{18}O$:

$$F^{18}O_{EV} = \Delta^{18}O_{EV}/\Delta^{18}O_{Total} \quad (6\text{-}13)$$

$$F^{18}O_{MIX} = \Delta^{18}O_{MIX}/\Delta^{18}O_{Total} \quad (6\text{-}14)$$

For $\delta^{2}H$:

$$F^2H_{EV} = \Delta^2H_{EV}/\Delta^{18}O_{Total} \quad (6\text{-}15)$$

$$F^2H_{MIX} = \Delta^2H_{MIX}/\Delta^{18}O_{Total} \quad (6\text{-}16)$$

To investigate the relationship between changes in stable isotope compositions caused by seawater mixing and salinity concentrations in surface water and groundwater samples, the seawater/freshwater mixing ratio (f_{sw}) was estimated as followed:

$$f_{sw} = Cl^-_{sample}/ Cl^-_{seawater} \quad (6\text{-}17)$$

6.3. Results and Discussion

6.3.1. Characteristics of stable isotopes and d-excess of surface resources

The stable isotope compositions ($\delta^{18}O$ and δ^2H) and *d*-excess values of surface water samples in the study area varied largely, from -8.9 to -0.2 ‰ for $\delta^{18}O$, from -64 to -8 ‰ for δ^2H, and from -6 to 8 ‰ for *d*-excess (Table 6-1). All surface water samples in the dry season (Figure 4a) and the rainy season (Figure 4b) were located below the LMWL with a smaller slope (< slope of LMWL = 7.56). This indicates that these water samples were originated from rainfall. Surface water samples in both the dry and rainy seasons have *d*-excess values lower than that of the global precipitation (*d* = 10 ‰) indicated these surface water samples experienced evaporation processes.

It was found that surface water samples in the dry season had heavier isotope enrichment and lower *d*-excess values compared to those of the rainy season. For example, surface water samples in the dry season have an arithmetic mean (standard deviation) value of –5.3 (1.4) ‰ for $\delta^{18}O$, –39 (-9) ‰ for δ^2H, and 2.87 (3) ‰ for *d*-excess while those of the rainy season was -7.3 (1.3) ‰, –53 (9) ‰, and 5 (2) ‰, respectively. Moreover, the slope of the surface water regression line in the dry season (6.45) was lower than that of the LMWL (7.56) while the surface regression line in the rainy season (7.41) was closed to that of the

LMWL. This indicated that the influence of evaporation processes on changes in stable isotope compositions of surface water in the dry season was stronger than in the rainy season.

Table 6- 1: Statistical analyses of stable isotope compositions ($\delta^{18}O$, $\delta^{2}H$), *d*-excess and Cl^- concentrations of surface water and groundwater samples in Soc Trang Province.

Water Sources	Number of Samples	Parameters	Min	Average	Max	STD
Surface water in dry season	38	$\delta^{18}O$	-7.3	-5.3	-0.2	1.4
		$\delta^{2}H$	-52	-39	-8	9
		d-excess	-6	3	7	3
		Cl^-	26.28	3015.84	9354.58	2462.84
Surface water in rainy season	41	$\delta^{18}O$	-8.9	-7.3	-3.4	1.3
		$\delta^{2}H$	-64	-53	-24	9
		d-excess	1	5	8	2
		Cl^-	2.44	260.14	4642.72	767.1
Aquifers qh, qp_3	13	$\delta^{18}O$	-7.3	-5.0	-1.7	1.7
		$\delta^{2}H$	-50	-35	-9	12
		d-excess	0	5	12	3
		Cl^-	58.41	3961.28	15883.51	4740.54
Aquifer qp_{23}	163	$\delta^{18}O$	-7.9	-5.6	-3.5	1.0
		$\delta^{2}H$	-51	-41	-32	5
		d-excess	-11	4	13	4
		Cl^-	2.85	182.38	4068.56	524.30
Aquifer qp_1	54	$\delta^{18}O$	-7.9	-5.2	-2.2	1.1
		$\delta^{2}H$	-54	-39	-10	6
		d-excess	-5	2	10	4
		Cl^-	5.00	175.06	3191.94	443.26
Aquifer n_{22}	2	$\delta^{18}O$	-5.6	-5.6	-5.6	0.0
		$\delta^{2}H$	-36	-34	-32	2
		d-excess	9	11	12	2
		Cl^-	5419.83	6352.92	7286.02	933.10
Aquifer n_{13}	47	$\delta^{18}O$	-7.9	-7.1	-4.9	0.6
		$\delta^{2}H$	-52	-49	-32	4
		d-excess	1	8	12	2
		Cl^-	53.01	579.85	7286.02	1249.50

Note: $\delta^{18}O$, $\delta^{2}H$ and d-excess values in ‰ VSMOW and Cl^- chloride concentrations in mg L^{-1}

The seasonal differences in stable isotope compositions of surface water in the Mekong Delta were also observed by Nguyen et al. (K. C. Nguyen et al., 2007) and Kabeya et al. (Kabeya et al., 2008). It indicates that the seasonal changes in stable isotopes of surface water in the Mekong Delta is a common phenomenon which could be altered by seasonal variations in discharge (Anh, Hoang, Bui, & Rutschmann, 2018) and precipitation (N. Le Duy et al., 2018) in the delta. The relationship between stable isotope compositions ($\delta^{18}O$ and $\delta^{2}H$) and Cl^- concentration of surface water indicates different magnitudes of seawater mixing between the dry and rainy seasons.

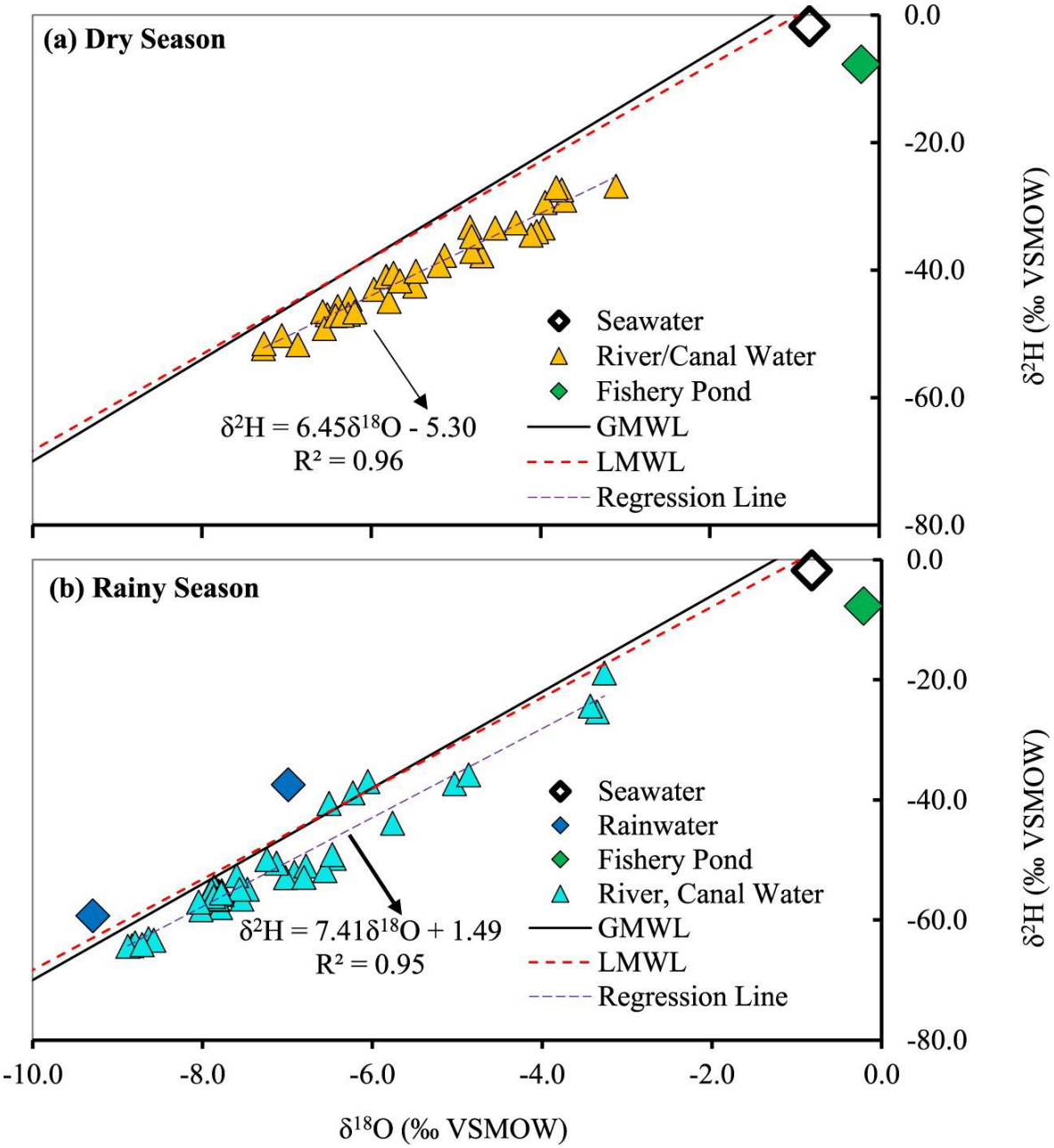

Figure 6- 4: Dual-isotope plot for surface water, fishery pond and rainfall samples in (a) the dry season and (b) the rainy season. The global meteoric water line (GMWL) and the local meteoric water line (LMWL) in the Mekong Delta shown for comparison.

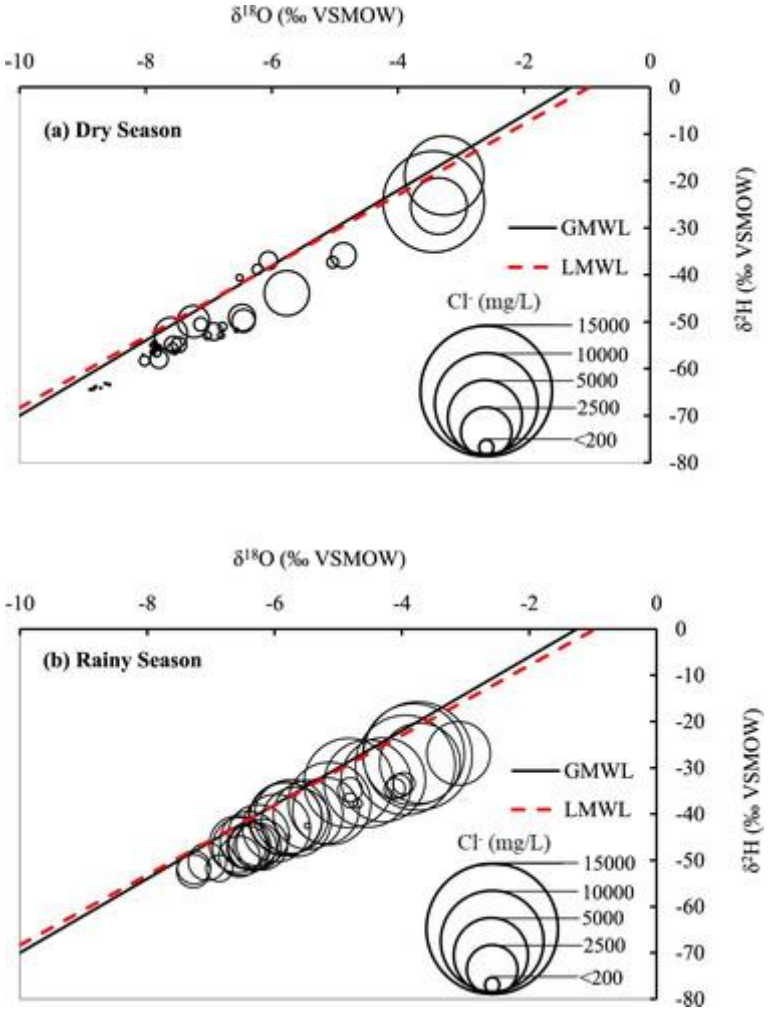

Figure 6- 5: Dual-isotope plot for surface water samples in (a) the dry season and (b) the rainy season with Cl- (mg/L) concentrations. The global meteoric water line (GMWL) and local meteoric water line (LMWL) in the Mekong Delta shown for comparison.

In the dry season, most of the surface water samples have heavy isotope enrichment ($\delta^{18}O$ > -7.0 ‰ and $\delta^{2}H$ > -50 ‰) and high Cl^- concentration (> 200 mg L^{-1}) (Figure 5a). In contrast, stable isotopes and Cl^- concentration were slightly depleted in the rainy season with $\delta^{18}O$ > -7.0 ‰, $\delta^{2}H$ < -50 ‰, and Cl^- concentration (< 200 mg L^{-1}) (Figure 5b). The similar trend was also found in some coastal areas in China (K. Yang et al., 2018; L. Zhang, Yuan, Song, & Xia, 2017). This illustrates that the effects of seasonality in discharge on the

variabilities of stable isotope compositions and Cl^- concentration in coastal surface water are a common phenomenon, especially in the dry season (Gugliotta et al., 2017).

Seasonal variation and seawater/freshwater mixing ratios in coastal surface water systems are dependent on the distance to the sea. Similarly, Cl^- concentration and stable isotope compositions of surface water in the study also changed from inland to the sea. In the dry season, for instance, the Cl^- concentration has a decreasing gradient of 150.49 mg L^{-1} km^{-1} (Figure 6-6a), and $\delta^{18}O$ values have a decreasing gradient of 0.083 ‰ km^{-1} (Figure 6-6b). In the rainy season, however, the distance from sampling locations to the sea has a low correlation with Cl^- concentration (Figure 6-6a) and the stable isotope compositions of $\delta^{18}O$ (Figure 6-6b).

Seasonal variation of upstream flows and daily tidal fluctuation define Cl^- concentration and stable isotope compositions. It was observed that some surface water samples in the dry season have slightly depleted in stable isotopes ($\delta^{18}O < -4.0$ ‰ and $\delta^{2}H < -30$ ‰) and low Cl^- concentration (< 200 mg L^{-1}) (Figure 6-6a). Meanwhile, some samples in the rainy season have heavy isotope enrichment ($\delta^{18}O > -4.0$ ‰ and $\delta^{2}H > -30$ ‰) and high Cl^- concentration (> 200 mg L^{-1}) (Figure 6-6b). These results may attribute to seasonal variabilities in rainfall and upstream discharge, causing different mixing ratios between freshwater and seawater in this coastal area (Gugliotta et al., 2017). Consequently, surface water in the rainy season was diluted by upstream freshwater and rainwater, resulting in lower Cl^- concentration and more depleted stable isotope compositions. Meanwhile, surface water in the dry season was mixed dominantly with seawater due to low upstream discharge and less rainfall, leading to higher Cl^- concentration and heavier isotope enrichment compared to that in the rainy season.

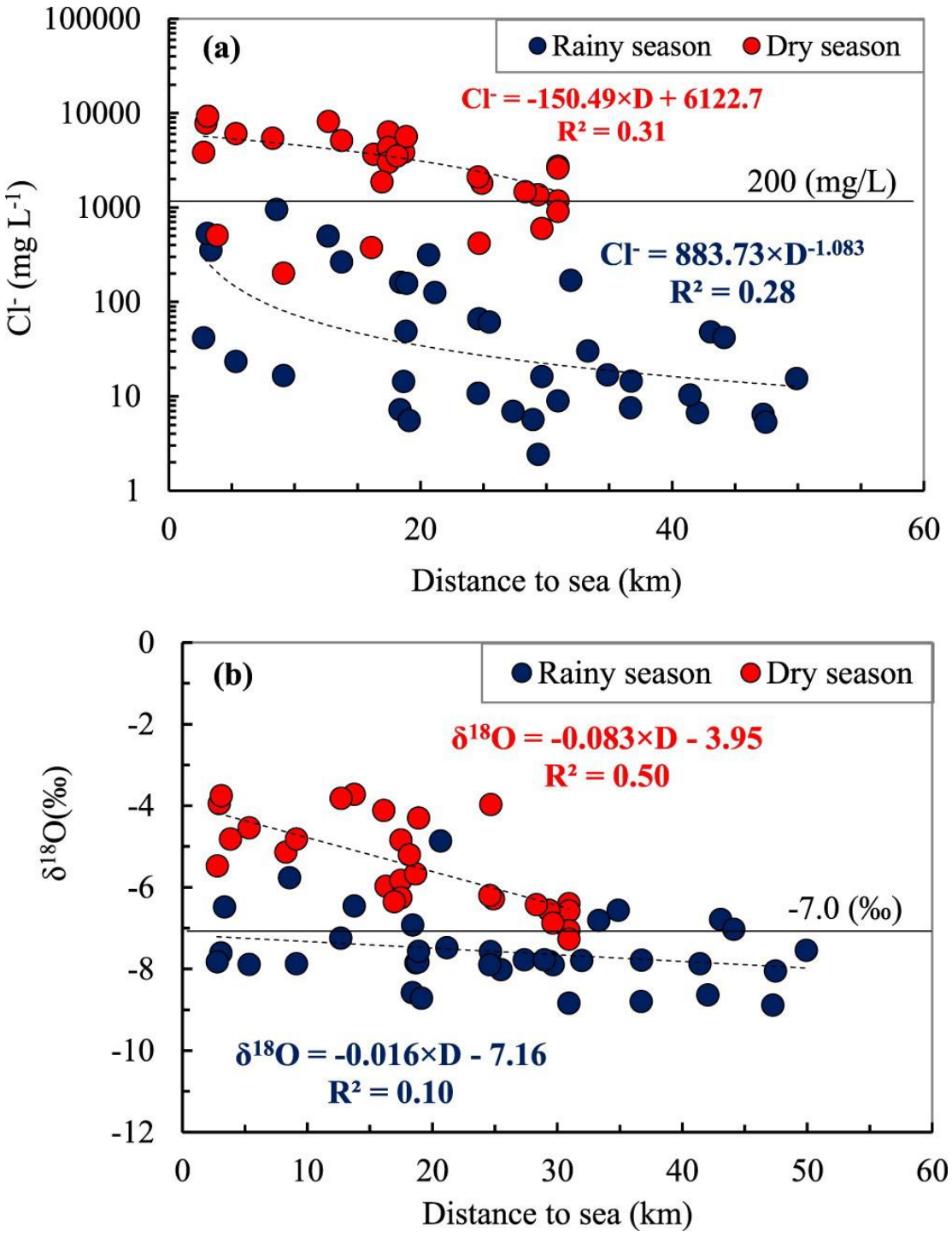

Figure 6- 6: Distribution of (a) Cl^- concentrations (mg/L) and (b) $\delta^{18}O$ (‰) compositions of surface water and the dry season and the rainy season following the distance to the sea (D) in km.

Furthermore, the changes in Cl^- concentration and stable isotopes may be driven by semi-diurnal tidal fluctuation. As shown in Figure 6-7a, Cl^- concentration increased during high tide periods in the dry season while in the rainy season, there was no clear relationship

between Cl^- concentration and tidal levels. This is because high tides increase seawater mixing with freshwater at the river mouths while in the rainy season, there is a reverse trend (Nowacki, Ogston, Nittrouer, Fricke, & Van, 2015). In contrast, tidal fluctuation does not influence on stable isotope compositions of $\delta^{18}O$ (Figure 6-7b). Even at the low tidal level, some samples are enriched in heavy isotopes ($\delta^{18}O$ > -7.0 ‰). This is because low tidal level leads to the more evaporated canal and pond water with heavy isotope enrichment mixing with light surface water at the river mouths.

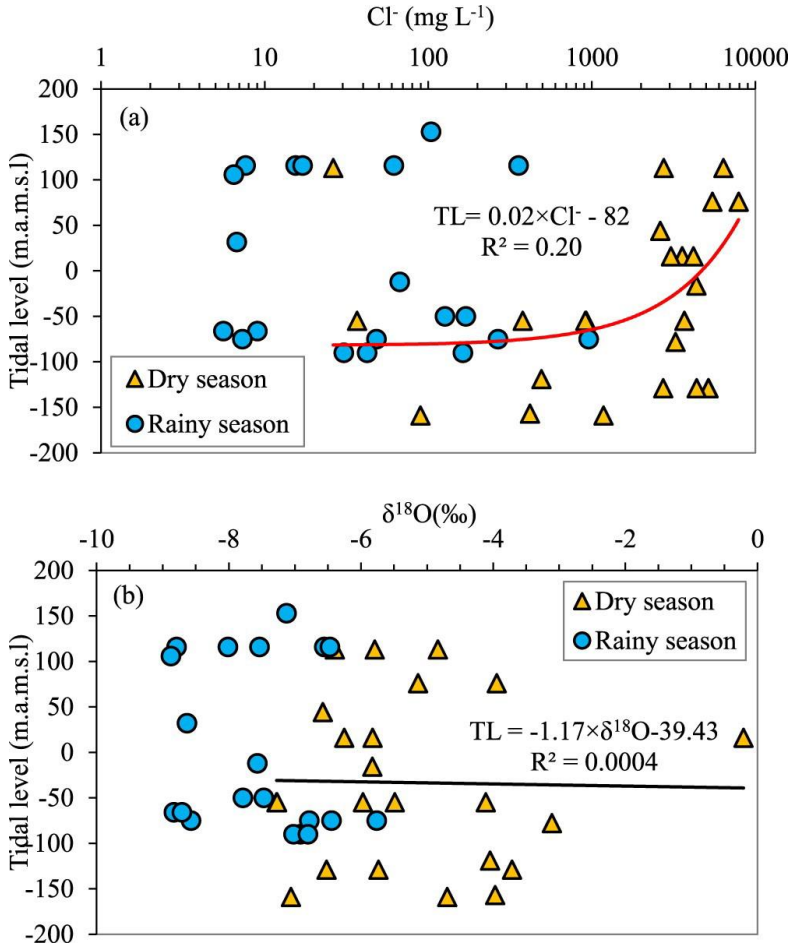

Figure 6- 7: Distribution of (a) Cl^- concentrations (mg/L) and (b) $\delta^{18}O$ (‰) compositions of surface water in the dry season and rainy seasons following tide levels.

It was noted that the distribution of Cl^- concentration and stable isotope compositions might also be influenced by vertical stratification due to the different densities between

freshwater and seawater (Gat, 1995; H.-z. Jiang, Shen, & Wang, 2009; Xu, Lin, & Wang, 2008). However, the previous studies showed that vertical stratification did not impact on the distribution of Cl^- concentration in this study area, especially in the dry season (T. V. Nguyen & Tanaka, 2007; Wolanski, Nguyen Huu, & Simon, 1998). In the rainy season, Cl^- concentration analyses showed a vertical heterogeneity due to the mixing between freshwater from upstream, rainfall and tidal flows (Nowacki et al., 2015). In this study, we focused more on temporal changes in Cl^- concentration, and further studies are needed to better understand the spatial distribution of Cl^- concentrations and stable isotopes.

6.3.2. Characteristics of stable isotopes and d-*excess of groundwater resources*

Shallow and deep aquifers in the study have different ranges and trends of stable isotopic compositions (Table 6-1, Figure 6-8). For example, the isotopic compositions of $\delta^{18}O$ and $\delta^{2}H$ in shallow groundwater (SGW) samples varied from -7.3 ‰ to -3.6 ‰ and -50 ‰ to -24 ‰, respectively. Similarly, the isotopic compositions of $\delta^{18}O$ and $\delta^{2}H$ in deep groundwater samples ranged from -7.9 ‰ to -2.4 ‰ and from -54 ‰ to -10 ‰, respectively.

Overall, all groundwater samples were distributed close to the LMWL with the slope and intercept of groundwater regression lines were smaller than those of the LMWL (Figure 6-8). The result indicates that these water samples were originated from meteoric water and experienced a certain degree of evaporation. However, groundwater samples from different aquifers showed a difference in isotopic compositions and chloride concentration (Figure 6-9). For example, some groundwater samples in the shallow aquifers are enriched in heavy isotopes ($\delta^{18}O$ > -4.0 ‰ and $\delta^{2}H$ > -30 ‰) and very high Cl^- concentration (>5,000 mg L^{-1}). Although most of the groundwater samples from deep aquifers (qp_{23}, qp_1, n_{21} and n_{13}) are enriched in heavy isotopes ($\delta^{18}O$ > -5.5 ‰ and $\delta^{2}H$ > - 40 ‰), they have relatively low Cl^- concentration (Cl^- < 1,000 mg L^{-1}). Meanwhile, some groundwater samples from these

aquifers have relatively high Cl^- concentrations (> 2,500 mg L^{-1}), but they were depleted in stable isotope compositions ($\delta^{18}O$ < -7.0 ‰ and δ^2H < - 50 ‰). These might indicate that groundwater from these aquifers had experienced significant evaporation processes, and some parts of these aquifers were also influenced by seawater intrusion.

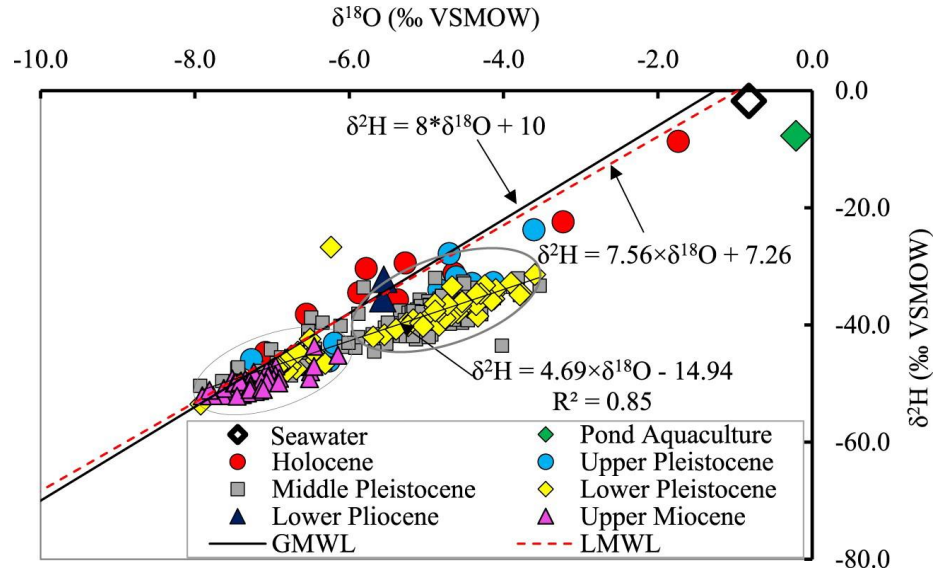

Figure 6- 8: Dual-isotope plot for groundwater, seawater and pond aquaculture samples. The global meteoric water line (GMWL) and the local meteoric water line (LMWL) in the Mekong Delta shown for comparison.

More specifically, stable isotope compositions, *d*-excess values, and Cl^- concentration of groundwater samples from the qp_{23}, qp_1 and n_{13} aquifers showed different trends (Table 6-1 and Figure 6-9). For example, groundwater in the qp_{23} and qp_1 aquifers are enriched in heavy isotopes (average $\delta^{18}O$ of -5.5‰ and average δ^2H of -40 ‰) and low *d*-excess values (average of *d*-excess values < 4.0 ‰). Meanwhile, Cl^- concentration in groundwater samples from the qp_{23} and qp_1 aquifers were relatively low with the average values < 180 mg L^{-1} (Table 6-1). These reveal that groundwater in the qp_{23} and qp_1 aquifers have experienced a significant evaporative loss and less influenced by seawater intrusion. Some groundwater samples, however, have relatively high Cl^- concentration (> 2,000 mg L^{-1}) but depleted in

$\delta^{18}O$ (< -5 ‰) and $\delta^{2}H$ (< - 40 ‰). This shows that saline sources of these groundwater samples might originate from paleo-seawater intrusion (H. T. Hoang & Bäumle, 2018; Hung Van et al., 2019). In contrast, groundwater samples in the Upper Miocene aquifer (n_{13}) depleted in $\delta^{18}O$ (< -7 ‰) and $\delta^{2}H$ (< -50 ‰) values and low Cl^- concentration (< 1,000 mg L^{-1}). In addition, these groundwater samples have high *d*-excess values (average of 7.78 ‰) which were similar to the global deuterium excess (d =10 ‰) (Dansgaard, 1964). This fact may indicate that groundwater from the Upper Miocene aquifer has been dominantly recharged by rainfall with less evaporative effects and low saltwater-freshwater mixing ratios.

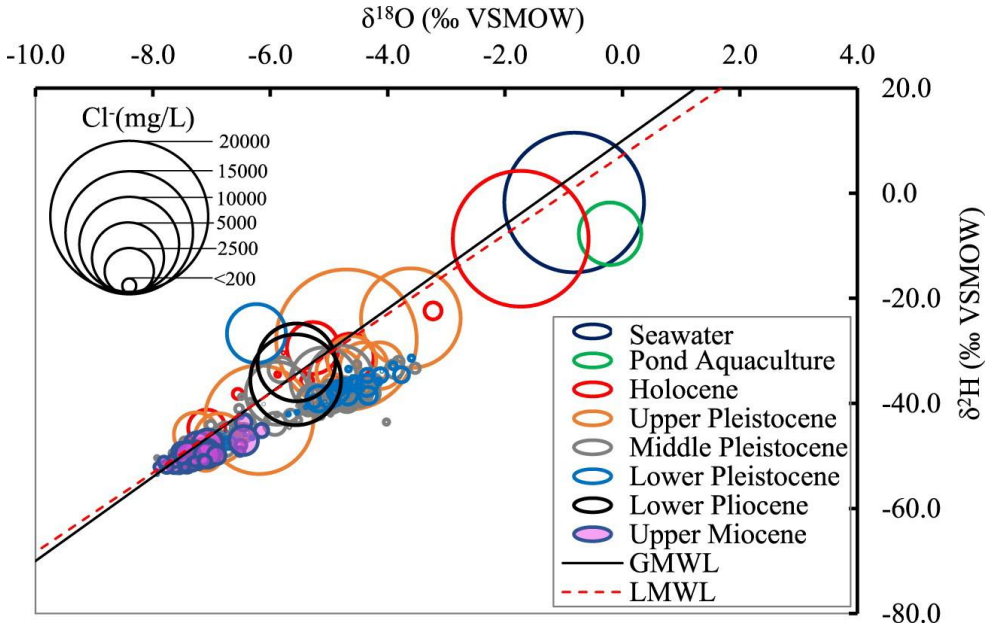

Figure 6- 9: Dual-isotope plot for surface water samples in (a) the dry season and (b) the rainy season with Cl- (mg/L) concentrations. The global meteoric water line (GMWL) and local meteoric water line (LMWL) in the Mekong Delta shown for comparison.

6.3.3. Effects of evaporation and mixing processes on characteristics of stable isotopes

In general, evaporation processes have stronger influences on changes of stable isotopes in both surface water and groundwater compared to seawater mixing (Table 6-2).

In surface water, evaporation processes have very high contribution ratios to the enrichment of $\delta^{18}O$ ($F^{18}O_{EV}$) and $\delta^{2}H$ ($F^{2}H_{EV}$). In the dry season, $F^{18}O_{EV}$ was 0.98 while that in the rainy season was 0.85. Similarly, the average value of $F^{2}H_{EV}$ was 0.98 in the dry season while that of the rainy season was 0.84. Although mixing between surface water and seawater resulted in minimal changes in stable isotopes compared to evaporation processes, the $F^{18}O_{MIX}$ and $F^{2}H_{MIX}$ values are primarily different between the dry and rainy seasons. For example, in the dry season, the contribution ratio of seawater (f_{sw}) to surface water was relatively high (f_{sw} = 0.16) causing high values of $F^{18}O_{MIX}$ (0.15) and $F^{2}H_{MIX}$ (0.16). Meanwhile, in the rainy season, the f_{sw} value was only 0.02, resulting in the very low values of $F^{18}O_{MIX}$ (0.02) and $F^{2}H_{MIX}$ (0.02) (Table 6-2).

Table 6- 2: Degree changes in stable isotope compositions ($\delta^{18}O$, $\delta^{2}H$) from sources due to evaporation processes and seawater mixing.

Parameters	Surface water		Groundwater					
	Dry season	Rainy season	Holocene	Upper Pleistocene	Middle Pleistocene	Lower Pleistocene	Lower Pliocene	Upper Miocene
$\Delta^{18}O_{EV}$	5.5	4.0	0.6	1.4	5.3	6.2	0.0	2.2
$\Delta^{18}O_{MIX}$	0.8	0.1	0.9	2.0	0.1	0.0	2.2	0.1
$\Delta^{18}O_{Total}$	6.3	4.1	1.5	3.4	5.3	6.2	2.2	2.3
$F^{18}O_{EV}$	0.85	0.98	0.40	0.41	0.98	1.00	0.00	0.94
$F^{18}O_{MIX}$	0.15	0.02	0.60	0.59	0.02	0.00	1.00	0.06
$\Delta^{2}H_{EV}$	35	26	3	9	34	39	0	14
$\Delta^{2}H_{MIX}$	6	0	7	13	0	0	13	1
$\Delta^{2}H_{Total}$	41	26	10	22	34	40	13	15
$F^{2}H_{EV}$	0.84	0.98	0.34	0.41	0.98	1.00	0.00	0.94
$F^{2}H_{MIX}$	0.16	0.02	0.66	0.59	0.02	0.00	1.00	0.06
f_{sw}	0.16	0.02	0.13	0.22	0.01	0.01	0.33	0.02

In groundwater, evaporation processes have a great influence on changes in stable isotope compositions, but different aquifers have different patterns. In the qh and qp_3 aquifers, for instance, evaporation processes and seawater mixing have a similar role in changes of stable isotope compositions from sources with an average value of 0.4 for $F^{18}O_{EV}$ and 0.6

for F^2H_{MIX}. In the qp_{23}, qp_1, and n_{13} aquifers, evaporation processes have a significant contribution to the total stable isotope enrichment from sources with an average value of $F^{18}O_{EV}$ and F^2H_{EV} higher than 0.90. This indicates that substantial isotope enrichment in these aquifers is mainly because of evaporative effects while seawater mixing plays an insignificant role.

The $\Delta^{18}O_{EV}$ and $\Delta^{18}O_{MIX}$ of surface water and groundwater in the study area showed a spatial heterogeneity (Figure 6-10a and Figure 6-10b).

In surface water, high values of $\Delta^{18}O_{EV}$ (> 9.0‰) and Δ^2H_{EV} (> 20‰) were observed in the small canal/ rivers in the central part of the study area far from the sea (> 40 km). This indicates that surface water has experienced evaporative losses because of the long retention time. High values of $\Delta^{18}O_{EV}$ and Δ^2H_{EV} were also found in most of the groundwater samples from the qp_{23} and qp_1 aquifers located in the central part and along the Hau River in the northern part of the study area. This indicated that original water sources recharging into these aquifers had experienced high evaporation processes. Groundwater samples from the qh and qp_3 aquifers have relatively low values of $\Delta^{18}O_{EV}$ (< 9.0 ‰) and high values of Δ^2H_{EV} (< 20 ‰), except for some samples in the central area. Most of the surface water and groundwater samples have low values of $\Delta^{18}O_{MIX}$ (< 3.0 ‰), and Δ^2H_{MIX} (< 20 ‰) revealed that seawater intrusion has lower influences on changes in stable isotope compositions from original sources. However, some groundwater samples of the qh and qp_3 aquifers located in the central area and along the Hau river have high seawater mixing ratios (> 0.15), resulting in relatively high values of $\Delta^{18}O_{MIX}$ (3.0 - 6.0 ‰) and Δ^2H_{MIX} (20 - 40 ‰) (Figure 6-11a and Figure 6-11b).

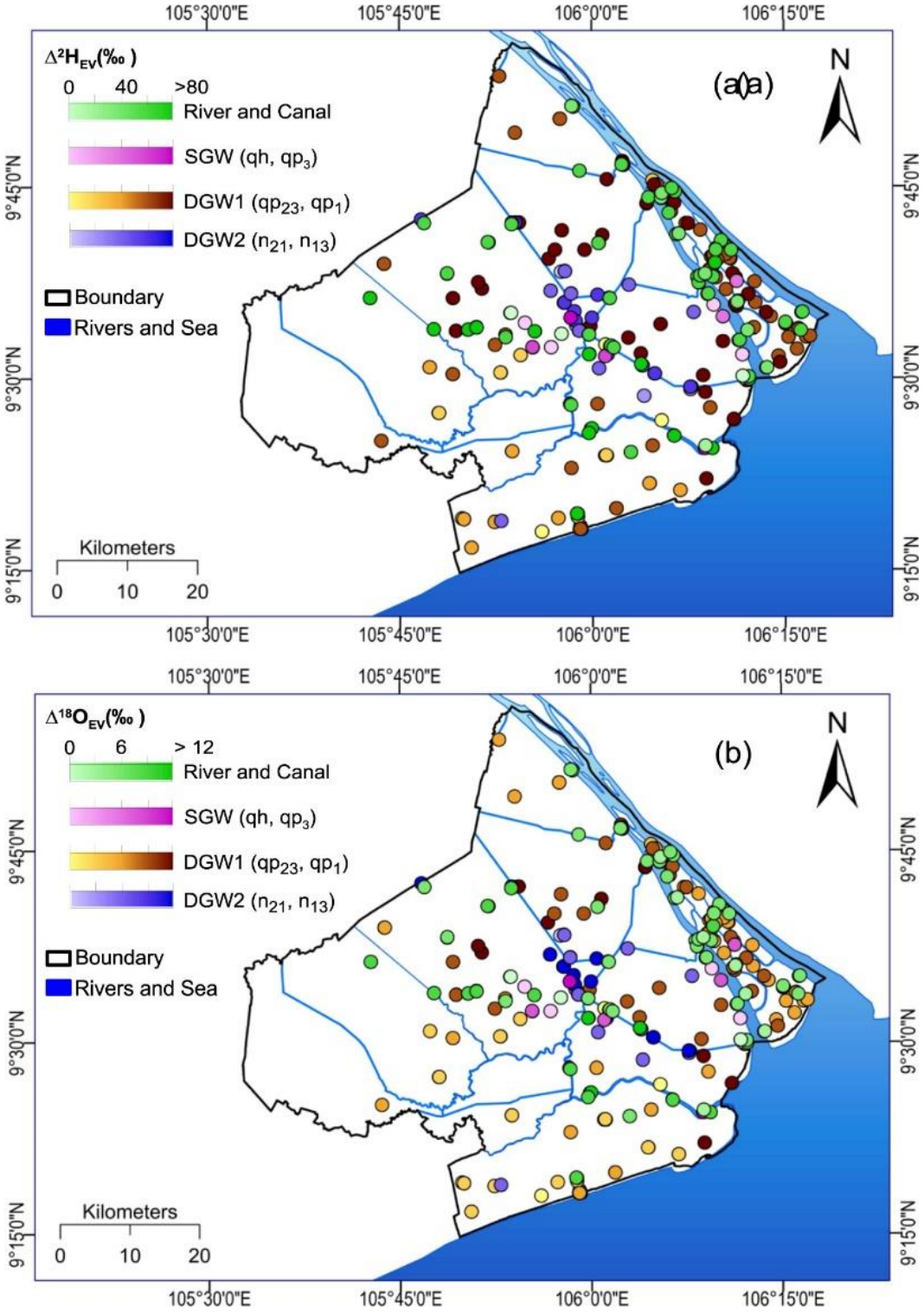

Figure 6- 10: Spatial distribution of the degree changes in stable isotopes due to evaporation processes (a) $\Delta^{18}O_{EV}$, and (b) $\Delta^{2}H_{EV}$.

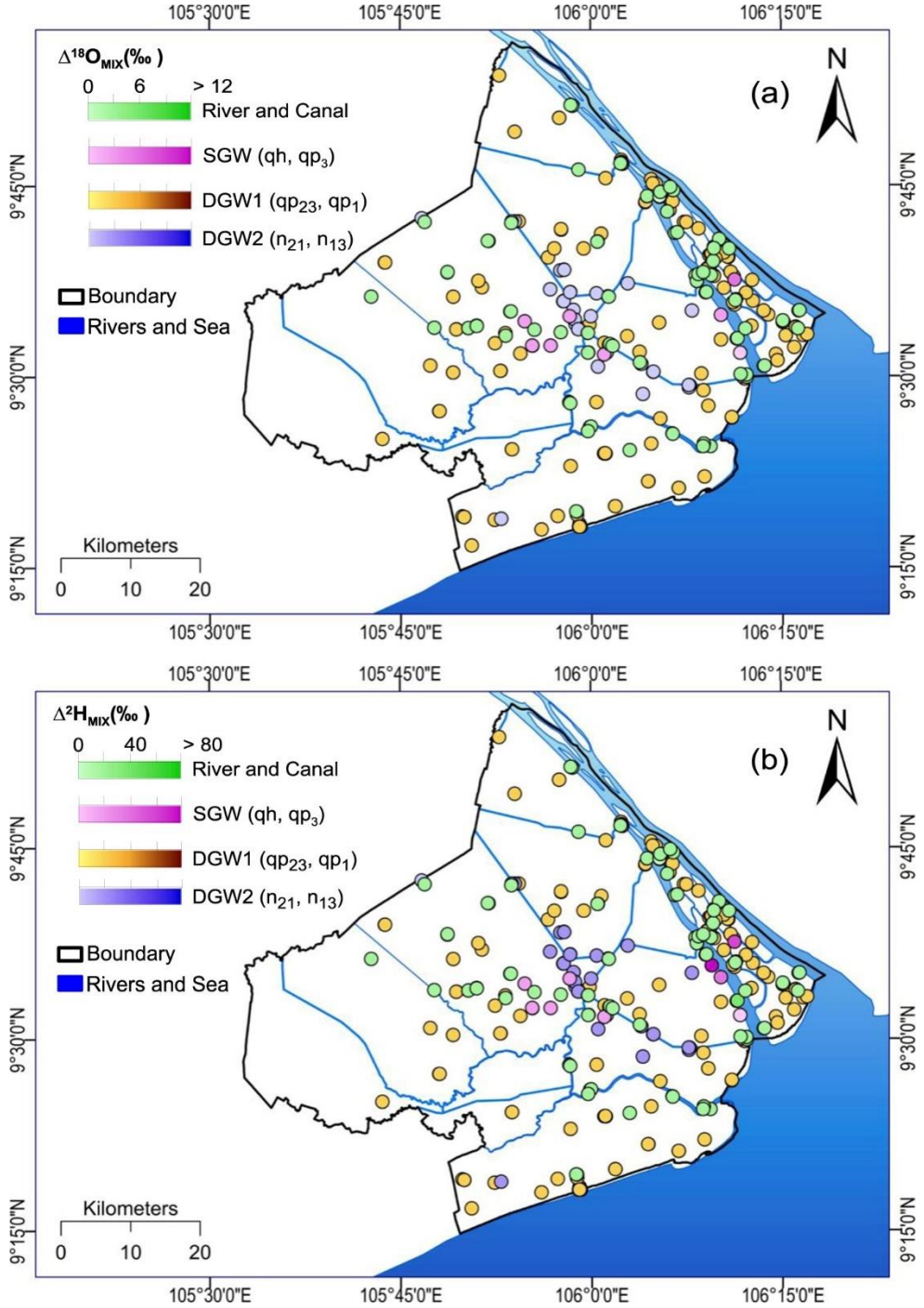

Figure 6- 11: Spatial distribution of the degree changes in stable isotopes due to mixing with seawater (a) $\Delta^{18}O_{MIX}$, and (b) $\Delta^{2}H_{MIX}$.

6.3.4. Recharge processes and mixing with seawater

Generally, rainfall and surface water are the primary sources of groundwater in tropical regions (C., M., & L., 2015; Larsen et al., 2017c; Ricardo & Christian, 2016). Rainfall may originate from different moistures and vapour sources (W. Huang, Chang, Xie,

& Zhang, 2017; Insa et al., 2017) while surface water is influenced by local and regional climate and topography (Ala-aho et al., 2018). Moreover, these potential recharge sources may also experience different stages of evaporation and mixing with seawater during geological formation periods (Groen, 2000). Therefore, evaporative enrichment (Δ^2H_{EV}) and mixing ratio with seawater (f_{sw}) of water samples could use to interpret original recharged sources of groundwater under different evaporation processes and seawater intrusion (Yamanaka et al., 2011). Groundwater samples in the study area could be classified into four groups based on the evaporative enrichment (Δ^2H_{EV}) and seawater/freshwater mixing ratio (f_{sw}). These groups could identify original recharged sources, evaporation and seawater intrusion into coastal aquifers in the study area (Figure 6-12). Groundwater samples in Group 1 (G1) have high f_{sw} values (> 0.10) and negative values of Δ^2H_{EV}; this indicates that these groundwater samples have experienced high evaporative losses and a severe seawater intrusion. The groundwater samples in Group 2 (G2) have negative values of Δ^2H_{EV} and low f_{sw} values (< 0.10), reflecting lower influences of evaporation and seawater intrusion on these locations. It was noted that most of the groundwater samples from G1 and G2 belong to the qh aquifer (Holocene) with low evaporative effects and different seawater/freshwater mixing ratios. The results indicate that groundwater in these locations could be recharged by rainfall and surface water with low evaporative losses. Also, seawater intrusion that occurred in shallow aquifers during the late Holocene age (Dung, Stattegger, Unverricht, Phach, & Thanh, 2013; Hanebuth, Proske, Saito, Nguyen, & Ta, 2012; T. M. Hoang, van Lap, Oanh, & Jiro, 2016; V. L. Nguyen, Ta, & Saito, 2010; Ta, Nguyen, Tateishi, Kobayashi, & Saito, 2001; Ta, Nguyen, Tateishi, Kobayashi, Saito, et al., 2002; Tamura et al., 2009; Tanabe, 2003). Group 3 (G3) have more positive Δ^2H_{EV} values and low f_{sw} values (< 0.10). Also, most of the groundwater samples in G3 from deep aquifers (qp_{23}, qp_1, and n_{13}) have the similar values of Δ^2H_{EV} and f_{sw} to surface water (river and canals) in the rainy season. It

reveals that groundwater in these aquifers was recharged by evaporated surface water (in lagoons, marshes, swamp and bare soil) during the last glacial age or delta formation processes. It was supported by previous studies using sediment facies (T. M. Hoang et al., 2016; V. L. Nguyen et al., 2010; Ta et al., 2001; Ta, Nguyen, Tateishi, Kobayashi, Saito, et al., 2002), groundwater age dating (Ho et al., 1991; H. T. Hoang & Bäumle, 2018), and paleo-hydrogeological modelling (Hung Van et al., 2019). Moreover, a similar phenomenon was also found in other coastal aquifers such in Thailand (Yamanaka et al., 2011), Netherland (Delsman et al., 2014a), and in the Red River Delta, Vietnam (Larsen et al., 2017c). It was noted that a small number of groundwater samples from the qp_{23}, qp_1, and n_{21} aquifers belonging to Group 4 (G4) showed more positive values of Δ^2H_{EV} and higher f_{sw} values (> 0.10). It suggests that these groundwater samples also experienced intensive seawater intrusion during the Holocene period due to rapid sea-level rise (Hung Van et al., 2019; Larsen et al., 2017c).

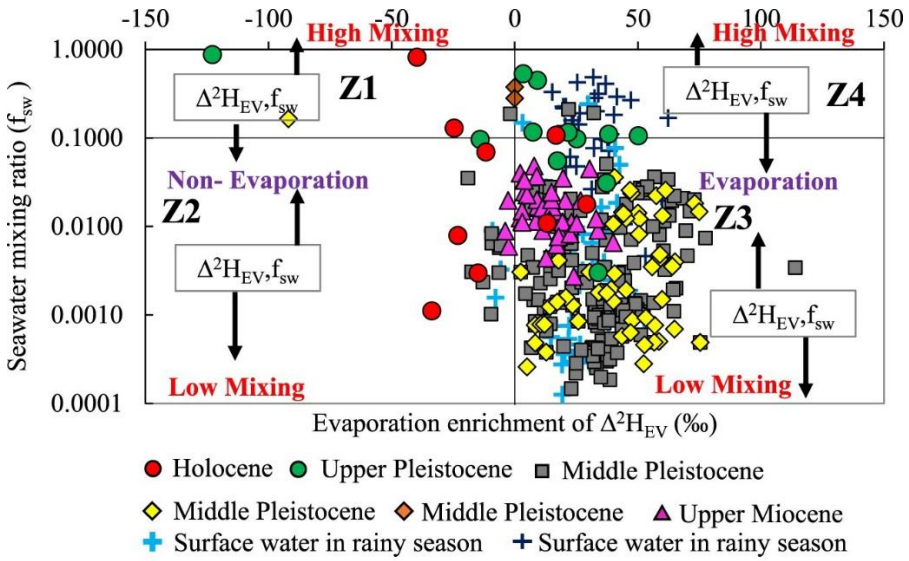

Figure 6- 12: The degree changes in stable isotope δ^2H due to evaporative effects (Δ^2H_{EV}) concerning the seawater mixing ratio (f_{sw}) showing the origin of surface water and groundwater in the study area.

6.4. Conclusion

This chapter presents the main characteristics of stable isotopes of surface and groundwater in a coastal area of the Mekong Delta, Vietnam. The main findings are as follows:

(1) Stable isotopes and Cl^- concentration of surface water have a seasonal trend with an increased substantial isotope enrichment during the dry season. Strong spatial variations of stable isotope compositions and Cl^- concentration in groundwater are found, especially with the distance to the sea and depth of screened well.

(2) Seasonality in discharge and rainfall influence both stable isotopes and Cl^- concentration while tidal fluctuation and distance to the sea control Cl^- concentration in surface water in the river mouths.

(3) Evaporation processes contribute significantly to the changes in stable isotope compositions from sources, while seawater mixing is the primary source of salinity in surface water and groundwater in the study area.

(4) Stable isotopic signatures and mixing seawater/freshwater ratios show that shallow groundwater from the qh aquifer was recharged by rainfall and surface water with less evaporation and experienced different magnitudes of seawater intrusion. Groundwater in deep (qp_3, qp_{23}, qp_1, n_{21}, and n_{13}) aquifers might be recharged by evaporated-open surface water sources (lagoon, marshes, swamp and or bare soil) during last glacial age or the delta formation processes and experienced a certain degree of seawater intrusion during late Holocene age.

CHAPTER 7 SPATIAL PREDICTION OF GROUNDWATER SALINITY IN COASTAL AQUIFERS OF THE MEKONG RIVER DELTA (VIETNAM) USING A NEW ARTIFICIAL INTELLIGENCE APPROACH BASED ON EXTREME GRADIENT BOOSTING AND GENETIC OPTIMIZATION

Groundwater salinity is considered as a severe environmental problem in many coastal areas, causing various problems to human health, agriculture, ecosystems, and infrastructure; however, saline concentrations are difficult to predict with high accuracy. In this chapter, we propose and verify a new artificial intelligence approach for predicting groundwater salinity and identifying the main factors of salinisation. In the proposed approach, Extreme Gradient Boosting (XGB) was used to build a groundwater salinity model, and Genetic Optimization (GO) was employed to optimise the model parameters. Gaussian Processes (GP) and Random Forests (RF) were also used as a benchmark for the model comparison. The results show that the proposed GO-XGB model yields high performance both on the training dataset (r = 0.999, RMSE = 18.450, MAPE = 2.070, and MAE = 4.864) and the validation dataset (r = 0.787, RMSE = 141.042, MAPE = 87.250, and MAE = 74.993). Compare with the benchmark, GP and RF; the proposed GO-XGB model performed better. There are seven factors (groundwater level, vertical hydraulic conductivity, lithology, extraction capacity, horizontal hydraulic conductivity, distance to saline sources, and well density) have a strong influence of groundwater salinization in coastal aquifers of the MD. Findings from the study are useful for policymakers in proposing remediation strategies for the problem of groundwater salinity in the context of excessive groundwater exploitation in coastal lowland regions. Since human-induced influencing factors have significantly influenced groundwater salinisation, urgent actions must be taken to sustainable groundwater management in the coastal area of the MRD.

7.1. Introduction

Groundwater is identified as the main source of water for about two billion people and accounts for 33% of the total water withdrawal worldwide (Famiglietti, 2014). In many coastal areas, groundwater is an important water supply for domestic uses, industrial development, and irrigational activities (Kagabu, Shimada, Delinom, Tsujimura, & Taniguchi, 2011; Mohanty & Rao, 2019). Groundwater in coastal areas is, however, highly vulnerable to overexploitation, seawater intrusion, climate change, and sea-level rise (Ferguson & Gleeson, 2012b). Groundwater is likely to increase in salinity due to paleo-seawater intrusion (Delsman et al., 2014b), modern seawater intrusion (Dongmei Han & Matthew J. Currell, 2018), leaking brines from oil fields and irrigation activities (Paine, 2003). Recent studies show that high salt concentrations in groundwater may also cause various environmental and health issues. For example, high salinity in irrigated water may cause physiological drought and reduce crop yield (Nishanthiny, Thushyanthy, Barathithasan, & Saravanan, 2010). High salt in drinking water increases the risk of hypertension (Vineis, Chan, & Khan, 2011), coronary heart disease (Junhyung Park & Kwock, 2015), and chronic kidney disease (Naser et al., 2017); therefore, assessing groundwater quality, especially the salinization level, is crucial to protect the environment and human health (Carretero, Rapaglia, Bokuniewicz, & Kruse, 2013; Gallardo & Marui, 2007; Guhl et al., 2006; Larsen et al., 2017b; Melloul & Goldenberg, 1997).

For last several decades, mathematical model has been used widely in prediction of groundwater dynamics and seawater intrusion into coastal aquifers (Abdelhamid, Javadi, Abd-Elaty, & Sherif, 2016; Lal & Datta, 2019; Mahmoodzadeh & Karamouz, 2019; Stein, Yechieli, Shalev, Kasher, & Sivan, 2019; Voss & Souza, 1987; Yu & Michael, 2019). However, mathematical groundwater modelling requires expert knowledge about the physical characteristics of hydrogeological system, governing process, various types of input

data (i.e., topography, soil properties, geology, initial and boundary conditions, hydrological and climate data, etc.) while the accuracy of the model simulation depends on reliable model input parameters (Lal & Datta, 2019; Sun, Wendi, Kim, & Liong, 2016). Meanwhile, machine learning is a data-driven model with little requirement about the physical process, and it could provide an accurate prediction (Sun et al., 2016; Yadav, Mathur, Ch, & Yadav, 2018). Therefore, machine learning has been considered as an alternative, i.e., Genetics algorithm (Sreekanth & Datta, 2010), artificial neural networks (Banerjee, Singh, Chatttopadhyay, Chandra, & Singh, 2011), multi-objective optimisation (Javadi, Hussain, Sherif, & Farmani, 2015), multivariate adaptive regression spline (Roy & Datta, 2017), support vector regression (Isazadeh, Biazar, & Ashrafzadeh, 2017; Lal & Datta, 2019; Nadiri, Sedghi, Khatibi, & Sadeghfam, 2018; S. K. Singh, Taylor, Rahman, & Pradhan, 2018), Kernel Extreme Learning Machine (Song et al., 2018), and Gaussian Process Regression (Kopsiaftis, Protopapadakis, Voulodimos, Doulamis, & Mantoglou, 2019; Yadav et al., 2018), and hybrid computational intelligence models (W. Chen et al., 2019; Pham, Jaafari, et al., 2019). A common conclusion from the above works is that machine learning is a highly flexible tool with the ability to handle complex non-linear relationships between groundwater salinity and influencing factors (Naghibi, Pourghasemi, & Dixon, 2015; Ransom et al., 2017; Sajedi-Hosseini et al., 2018). Nonetheless, no studies have figured out which are the most important factors influencing on groundwater salinity in coastal areas, while the rapid development in the field of computer science has introduced more superior methods.

Groundwater is a primary source for domestic, industrial and agricultural activities in the Mekong River Delta (MRD) (Ha et al., 2018). However, groundwater management in the MRD has been facing many challenges, e.g., groundwater level depletion and groundwater quality degradation due to excessive groundwater exploitation (Erban et al.,

2013; Minderhoud et al., 2017). Drought and seawater intrusion into the river system, especially in the dry season (Tran, Nguyen, & Vo, 2019; Vu, Yamada, & Ishidaira, 2018), have put high pressures on groundwater exploitation with the extraction capacity of approximately 244,000 m^3/day (An et al., 2018). These issues in combination with changes in annual recharge rates of the aquifer system (Kazama et al., 2007), impacts of climate change and sea-level rise (Shrestha et al., 2016) and inappropriate groundwater management practices (Ha et al., 2018) may result in saltier coastal aquifers of the Mekong River Delta. Therefore, understanding the controlling factors of groundwater salinization is essential to provide accurate and robust quantification of saline intrusion. Suitable solutions can be proposed for water authorities to protect and manage groundwater resources efficiently.

In this research, we propose and validate a new artificial intelligence approach, which is based on Extreme Gradient Boosting (XGB) and Genetic Optimization (GO), named as GO-XGB, for predicting groundwater salinity in the coastal aquifers of the Mekong River Delta (Vietnam). To the best of our knowledge, this is the first time that GO-XGB is considered for groundwater salinity modelling. We also compare and discuss the performance of our models and traditional models such as random forests and Gaussian processes to understand if this approach adds value to the prediction of seawater intrusion into fresh aquifers. Moreover, the role of various influencing factors in aquifer salinization is assessed.

7.2. Background of the machine learning algorithms used

In this section, we first review two traditional machine learning models which are already applied to predict groundwater salinity, namely random forests and Gaussian processes. We then introduce the idea of the combination of Extreme Gradient Boosting and

Genetic Optimization to form a new hybrid algorithm. The performance of the two traditional models is then considered as benchmarks to assess our model.

7.2.1. Gaussian processes

Gaussian processes (GP) are a type of supervised learning for both regression and classification problems (Azimi, Azhdary Moghaddam, & Hashemi Monfared, 2018; Hall, Rasmussen, & Maciejowski, 2012; Kopsiaftis et al., 2019; Rasmussen, 2004). The principal idea of Gaussian processes is that in the input space $x = [x_1, \ldots, x_n]$ T, every point is associated with a random variable, so as the joint distribution of them can be modelled as a multivariate Gaussian and a function (called f) can be modelled using an infinite multivariate Gaussian distribution (X. Ma, Xu, & Chen, 2019). Similarly, assuming that we have a salinity dataset $M = ([X_i, y_i], i = 1, 2, \ldots, m)$ with $X_i \in R_n$ is a matrix of m input variables with n observation. Whereas $y_i \in R$ is an output variable (Cl^- concentration in groundwater), the relation of the input and output variables is formulated by a GP regression model as following equation (Hoa et al., 2019; Rasmussen, 2004):

$$y\,(x) \;= \sum_{i=1}^{n} \alpha_i \, K(X_i, X) \qquad (7\text{-}1)$$

where α_i is the weight and K is the Radial Basis kernel function (RBF) (Equation 2) (J. Park & Sandberg, 1991; Scholkopf et al., 1997).

$$K(X_i, X) = \beta \times e^{-\sum_{i=1}^{m}\left[\frac{(X_i^m - X_i^m)^2}{2\sigma^2}\right]} \qquad (7\text{-}2)$$

where β is the scaling factor and σ is the kernel parameter.

The performance of the GP model is dependent on the parameters β and weights α_i, and they could be automatically turned and optimized through maximizing the marginal likelihood (Rasmussen, 2004).

7.2.2. Random forests

A random forest (RF) is a method for both classification and regression based on the ensemble of decision trees (Breiman, 2001). A decision tree is a top-down tree-like structure, in which each non-leaf node is a test, each branch is an outcome of the test, and each leaf node is a decision. Regression with a single decision tree may result in the problem of overfitting (high variance) and is dependent on the distribution of training sets. A large number of decorrelated decision trees can form a random forest which then can reduce the variance and boost model performance (Criminisi, 2011). The procedure creating RFs is as follows: (1) n random subsets (called "bootstrapped subsets") are sampled from a training dataset based on a random selection of features of the dataset. A subset may contain overlapped data in other subsets; (2) n decision trees are built using these n bootstrapped subsets (Figure 7-1). The number of trees n is decided using either cross-validation or out-of-bag (OOB) error methods. A detailed description of the statistical formulation of RF can be found in Breiman (2001).

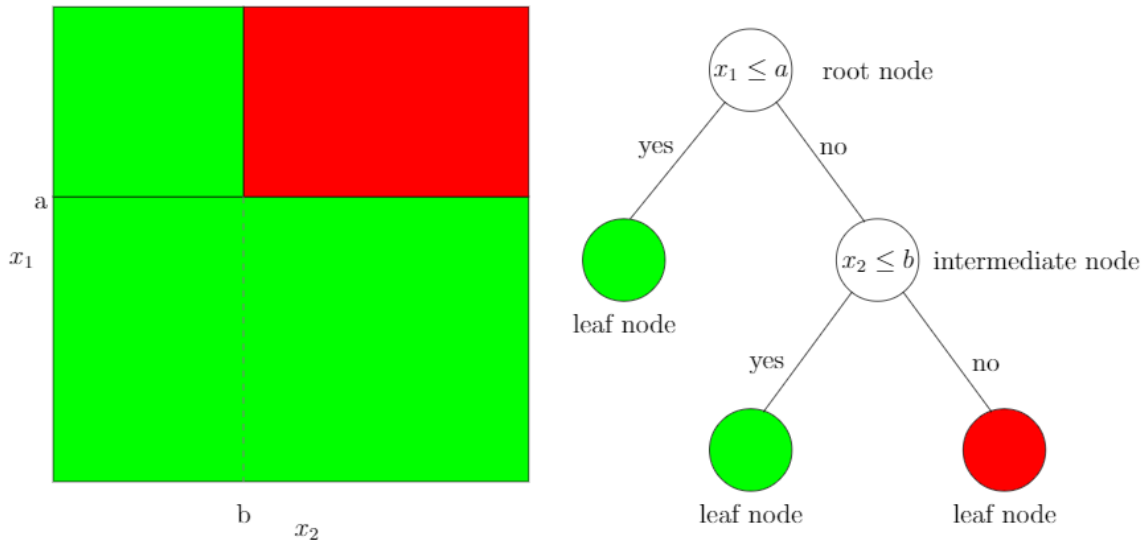

Figure 7- 1: Example of the partitions left and classification tree structure right with two classes coloured in green and red.

7.2.3. Extreme Gradient Boosting

Similar to the random forest, and Extreme Gradient Boosting (XGB) is an ensemble-machine learning algorithm that is based on decision trees (weak learners) (Friedman, 2001). However, a boosting model constructs the "forest" of decision trees sequentially, or one decision tree can be built based on learning experience inherited from previous trees (T. Chen & Guestrin, 2016; Johnson, Bonczak, & Kontokosta, 2018). The second tree focuses on the cases in which the first tree gives a poor prediction, and this learning process is repeated many times, so as the combination of these trees can better capture the relationship between predictands and predictors. Gradient Boosting is a form of boosting models in which weak prediction cases are assessed if they contribute to minimize the overall lost function (also called the prediction error) (Lim & Chi, 2019). An example can be considered as highly valuable if the adding decision tree built for this case can reduce the prediction error significantly while no change in the error implicates a no value case; thus, only useful decision trees are kept. This may give XGB models advantages in complex problems like quantifying saline concentration in groundwater since data measurement in the underground environment may contain many exceptional cases. It is also worth to notice that the learning efficiency of each machine learning algorithm is controlled by its model parameters, and in the case of the XGB model, they include three groups: tree-specific, boosting and miscellaneous parameters. Selection to these model parameters is a challenging task and depends on user experience while this process does not always return in an optimum set of parameters. Thus, we propose to use a genetic algorithm to automatically search in parameter spaces to improve the accuracy of numerical forecasts.

7.2.4. Genetic Algorithm

Genetic Algorithm takes the idea from the Darwinian theory of natural selection to evolve solutions by utilizing computer capacity to tune model parameters as an alternative to manual

efforts (Forrest, 1993). The most critical concept of GA is the chromosome which consists of model parameters to define a solution (called individual) (Jennings, Lysgaard, Hummelshøj, Vegge, & Bligaard, 2019). A certain number of individuals then forms a population. In the lower level, each chromosome consists of some genes which are often denoted as 0s or 1s ($X \equiv (x_1, x_2, \ldots, x_n)$, $x_k \in [0.0, 1.0] \; \forall \; k$). Each individual is evaluated by its fitness value, a result of a fitness function.

The basic operation performed during the training of XGB based model is as following steps: (1) A number of individuals are initialized to form a population, (2) individuals with the best fitness values are selected to generate a mating pool, (3) from the mating pool, parents are selected by either sequential or random selection methods, and (4) several operators called crossover and mutation are then applied to each pair of parents to generate their offspring. This process keeps high-quality individuals to generate more individuals, so as it evolves solutions to obtain the desired solutions.

7.3. **Study area and data**

7.3 1. Description of the study area

Soc Trang province – a coastal area of the Mekong Delta, Vietnam was selected for this study. Soc Trang province has an area of 3,312 km^2 with an elevation ranging from 0.5 to 2.5 m above the mean sea level (Figure 7-2). The region is bordered by the Hau river (one main branch of the Mekong river) to the Northwest and the Vietnamese East Sea (South China Seas) to the Southwest. Since this area has a dense river system connected to the sea, the hydrological regime in the study area is complex and strongly influenced by the flow regime of the Mekong river and tidal fluctuation (Dang et al., 2016; Nhan, 2016).

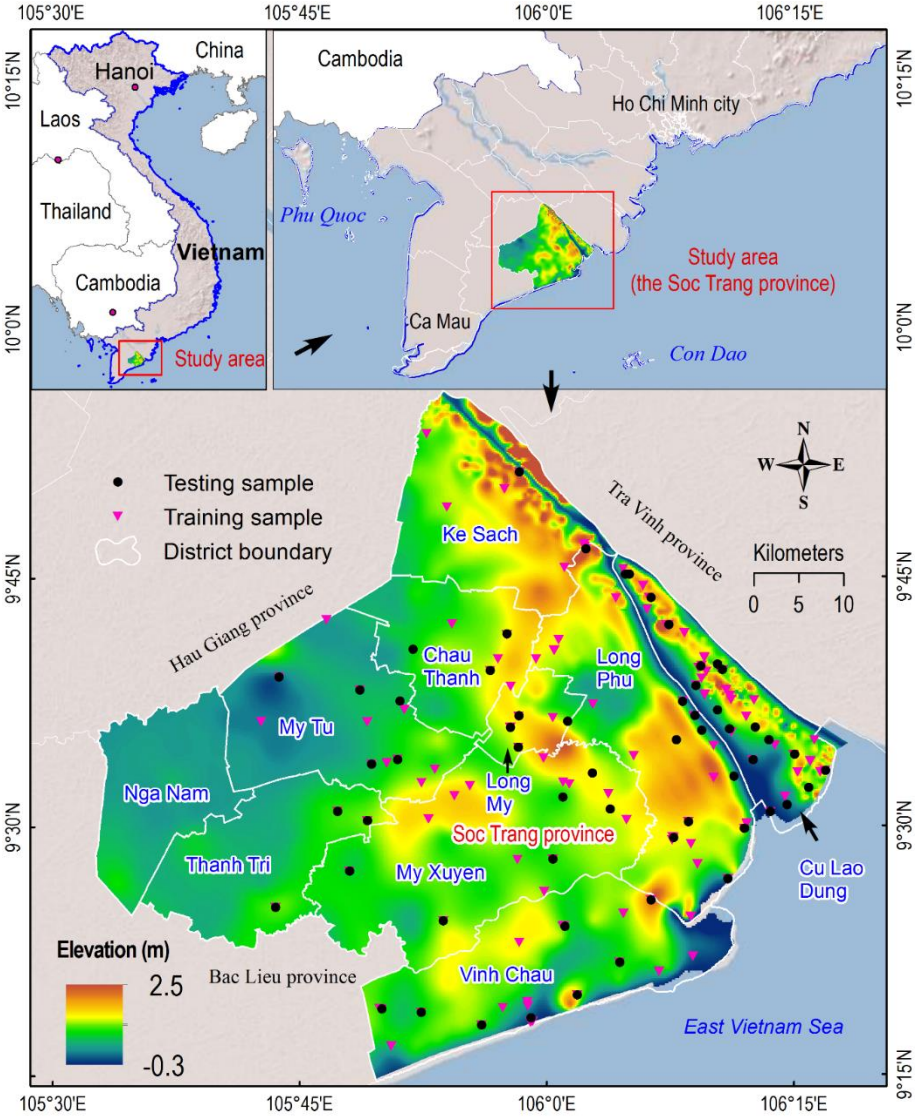

Figure 7- 2: Location of the study area (the Soc Trang province).

The climate is characterized by tropical monsoon region with two distinct seasons, the dry season from May to November and the rainy season from December to April (in the following year). The annual average rainfall is about 1,772 mm with substantial seasonal variation. About 85% of the yearly rainfall occurs during the rainy season. The study area has recognized as one of the most vulnerable regions to climate change and sea-level rise in the world (Shrestha et al., 2016; Vu et al., 2018).

The population in Soc Trang province is approximately 1.42 million people (General Statistics Office of Vietnam, 2019). Most of the community involved in agricultural

activities which contributes to 42% of the total GDP to the province (H. T. Hoang & Bäumle, 2018). Agriculture lands are dominant, accounting for 84.77% (276,690 ha of total area), which includes rice fields (52.98%), fish ponds (19.69%), orchards (15.51%), and lands of other vegetable types (6.75%), and other types of land use (Decision No.108/NQ-CP of the Government 2018).

In the study area, groundwater is used as a dominant source of water for domestic, industrial and agricultural activities, resulting in rapid groundwater level depletion in the irrigated regions (H. T. Hoang & Bäumle, 2018; Minderhoud et al., 2017). Groundwater salinization has been identified as one of the significant threats to the groundwater resource in this region (An et al., 2018). The extent of groundwater salinization in the study area has recently been increased due to the rapid increase in groundwater demand (Minderhoud et al., 2017; Nam et al., 2019).

The hydrogeological setting of the study area is characterized by a multi-layered aquifer system, formed between the Miocene and Holocene epoch (Hung Van et al., 2019; Wagner et al., 2012). Groundwater in the Pleistocene aquifers is the primary source of drinking water because these aquifers have high yields and good-quality water compared to other aquifers (An et al., 2018). In this study, we focus on assessing the vulnerability and risk of groundwater in the Pleistocene aquifers to salinity

7.3.2. Data preparation and variables selection

In this research, 225 groundwater samples from the Pleistocene aquifers were collected between 2013 and 2018. On-site measurements were conducted to obtain physical parameters such as groundwater temperature T (°C), pH, dissolved oxygen DO, and electrical conductivity EC using the HANNA portable instruments (Hanna Instruments

Inc.2015). The chloride concentration in groundwater samples was analyzed using Ion Liquid Chromatography (Shimadzu Co. Ltd., Japan) at the University of Tsukuba, Japan.

The accumulation of salinity in groundwater is a complex process because it is controlled by influencing factors (Kanagaraj et al., 2018; Mahlknecht et al., 2017a). The selection of influencing factors for groundwater sanitization prediction should base on the possibilities of saltwater migration into aquifers. In the Pleistocene aquifers, groundwater salinity is derived from (1) downward or upward leakage of paleo-saline water (Chatton et al., 2016b; Khaska et al., 2013a), (2) halite dissolution in the topsoil layer (Blasco et al., 2019; Walter et al., 2017), (3) seawater intrusion (Dongmei Han & Matthew J. Currell, 2018; Kanagaraj et al., 2018; Werner et al., 2013), and (4) irrigation return flow (Essaid & Caldwell, 2017; Lapworth, Krishan, MacDonald, & Rao, 2017; Malki, Bouchaou, Hirich, Ait Brahim, & Choukr-Allah, 2017; Tweed et al., 2018). The downward or upward leakages of paleo-saline water may relate to the formation of aquifers, which is further incorporated into the lithology influencing factor. Furthermore, the thicknesses of aquitards, distance to the hydraulic window, distance to fault, fault density, and vertical hydraulic conductivity could also affect the leaking rate (Elmahdy & Mohamed, 2013; Y. Liu, Lam, Wu, & Lam, 2018). In addition, other geographical variables such as distance from main rivers, distance to the drainage and drainage density are widely impacted on groundwater salinization (Winkel, Berg, Amini, Hug, & Annette Johnson, 2008a). The halite dissolution process is characterized by salt rock/sediment properties, soil type, and horizontal and vertical hydraulic conductivity. Variables which represent the effect human activities on groundwater salinity in the study area are the groundwater level, extraction capacity, well density, extraction density, and operation time. The severity of seawater intrusion may also depend on the distance to the sea, groundwater level, well density, extraction capacity, extraction density, and horizontal hydraulic conductivity (S. Lee, Currell, & Cendón, 2016;

Yechieli et al., 2019). The four processes interact with each other and result in a complex salinization process in the study area (An et al., 2018). Based on an analysis of the groundwater flow system in the study area, 20 influencing factors were selected for predicting the spatial distribution of salinity in groundwater (Table 7-1 and Figure 7-3).

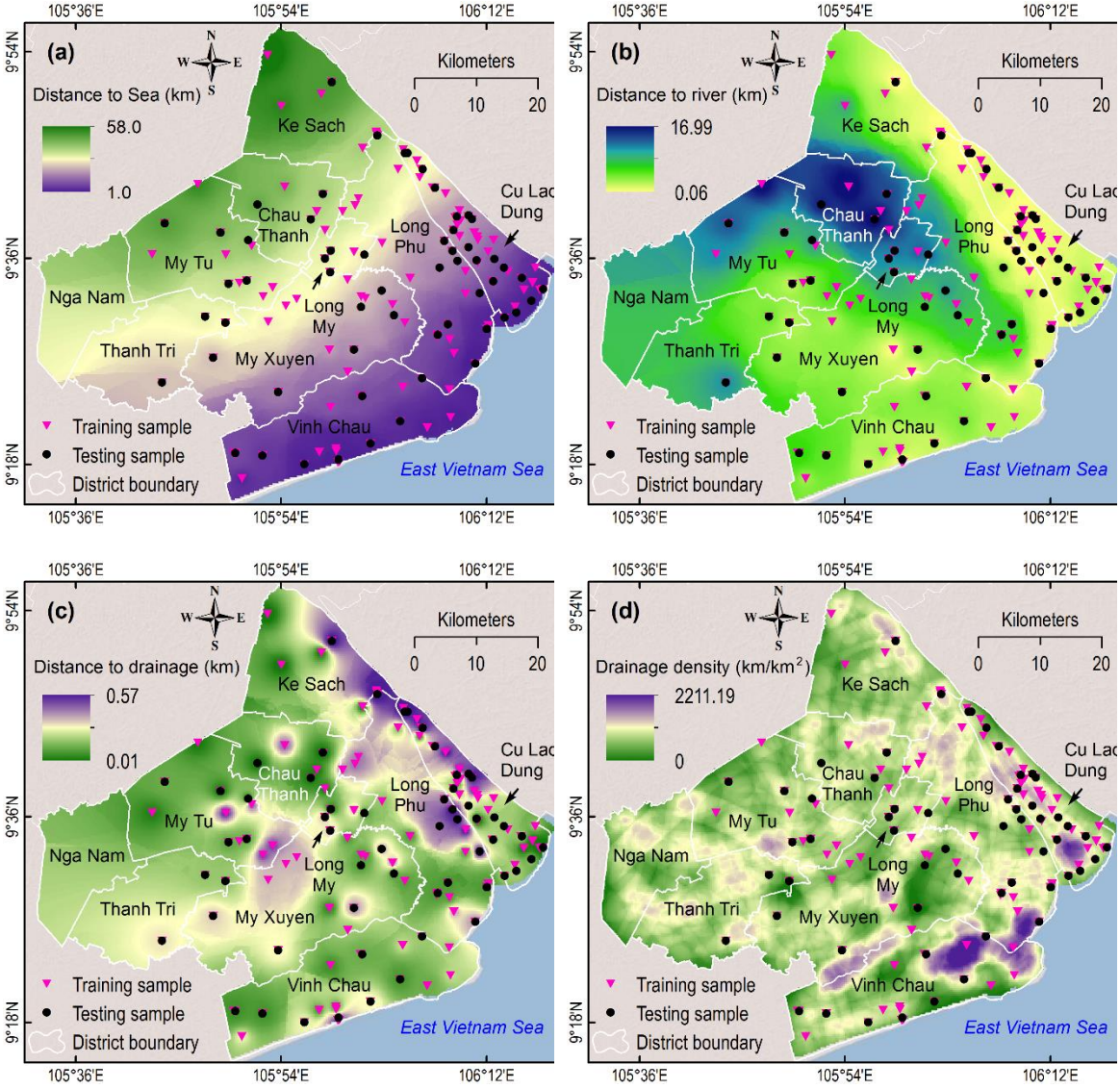

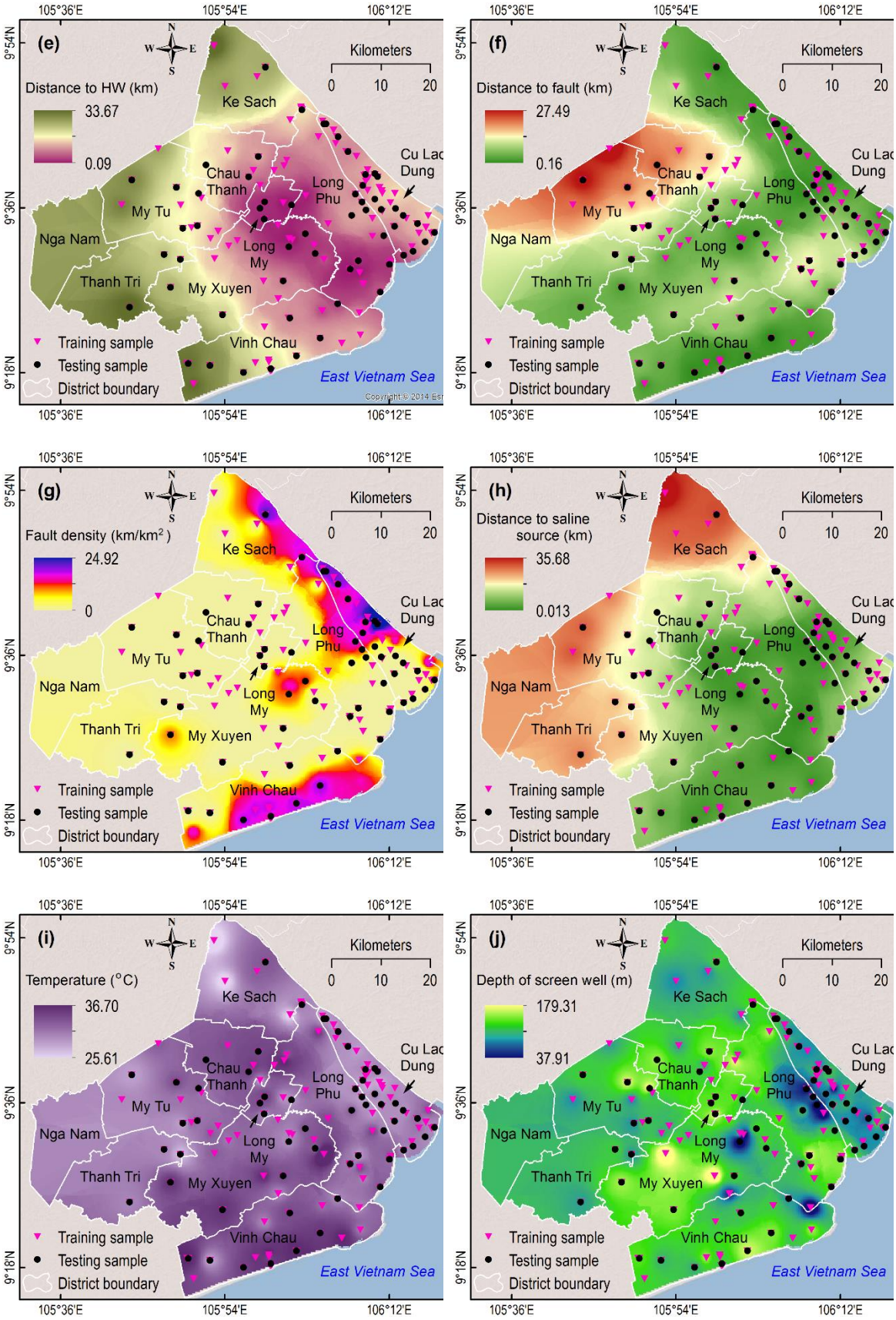
(e)
Distance to HW (km)
33.67
0.09
(f)
Distance to fault (km)
27.49
0.16
(g)
Fault density (km/km²)
24.92
0
(h)
Distance to saline source (km)
35.68
0.013
(i)
Temperature (°C)
36.70
25.61
(j)
Depth of screen well (m)
179.31
37.91
Kilometers
0 10 20
Ke Sach
Chau Thanh
Long Phu
Cu Lao Dung
My Tu
Nga Nam
Long My
Thanh Tri
My Xuyen
Vinh Chau
Training sample
Testing sample
District boundary
East Vietnam Sea
105°36'E
105°54'E
106°12'E
9°54'N
9°36'N
9°18'N

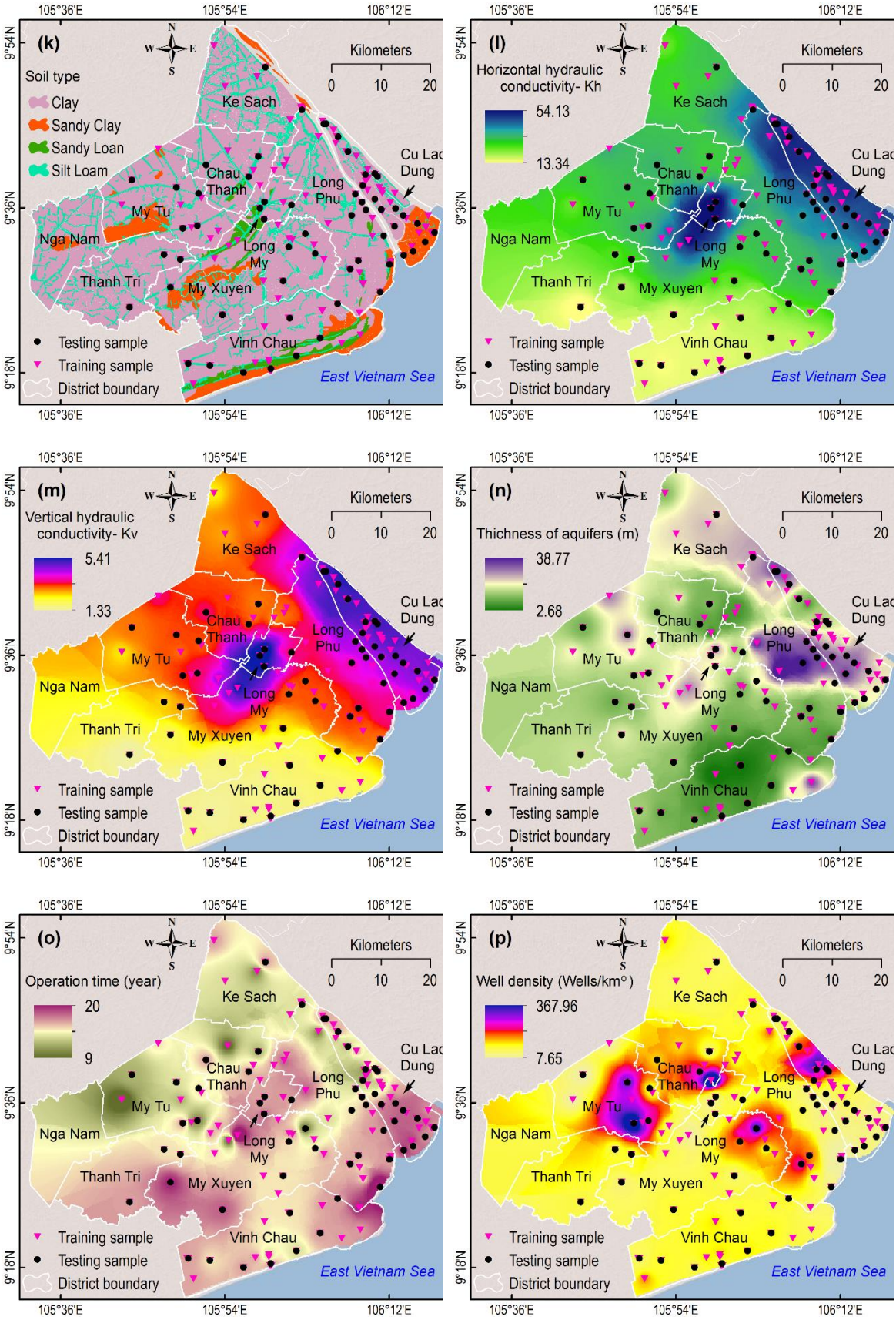
(k)
Soil type
Clay
Sandy Clay
Sandy Loan
Silt Loam
(l)
Horizontal hydraulic conductivity- Kh
54.13
13.34
(m)
Vertical hydraulic conductivity- Kv
5.41
1.33
(n)
Thichness of aquifers (m)
38.77
2.68
(o)
Operation time (year)
20
9
(p)
Well density (Wells/km°)
367.96
7.65
Kilometers
0 10 20
Ke Sach
Cu Lao Dung
Chau Thanh
Long Phu
My Tu
Nga Nam
Long My
Thanh Tri
My Xuyen
Vinh Chau
Testing sample
Training sample
District boundary
East Vietnam Sea
105°36'E
105°54'E
106°12'E
9°54'N
9°36'N
9°18'N

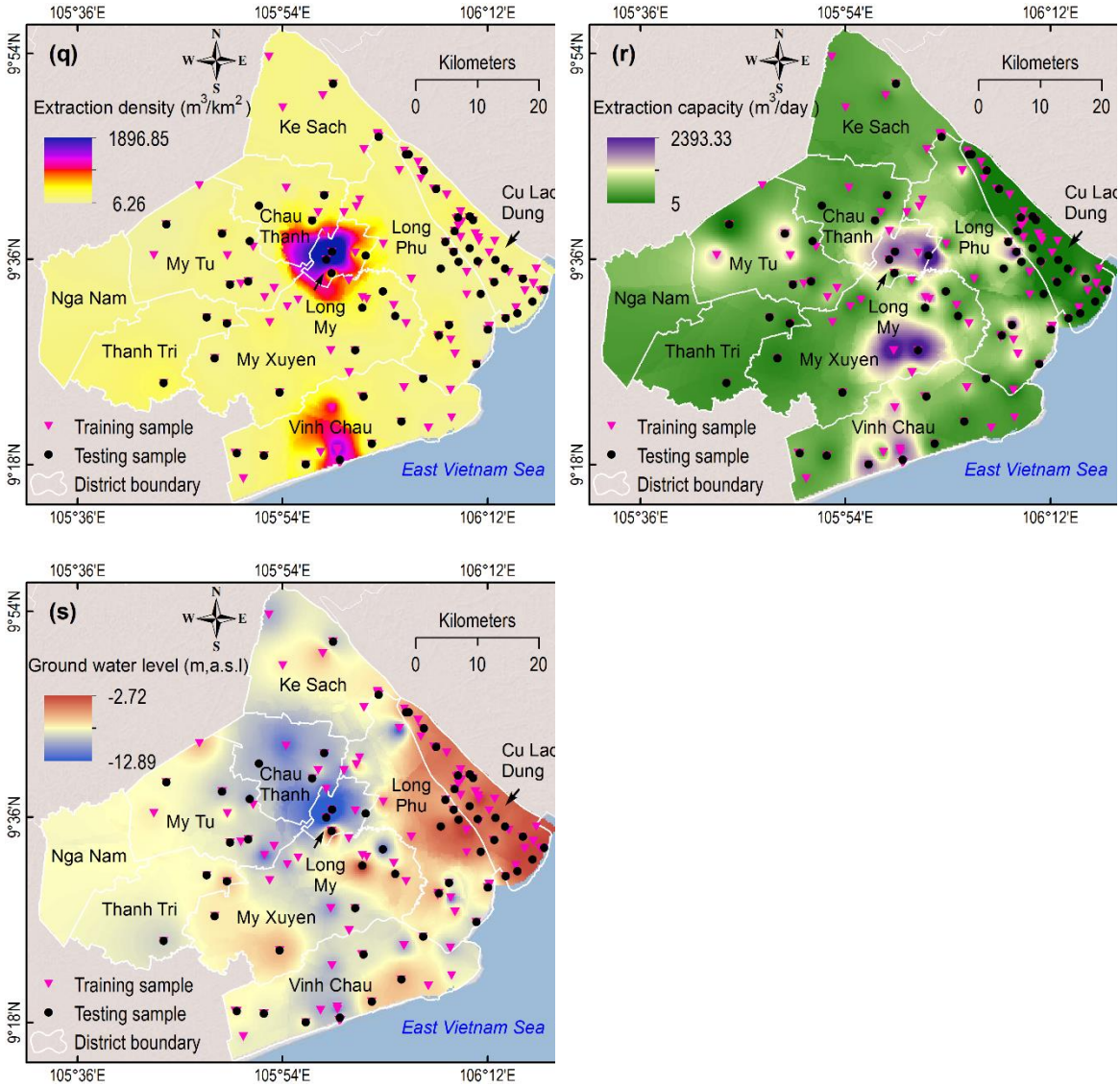

Figure 7- 3: Groundwater salinization influencing factors: (a) Distance to sea; (b) Distance to river; (c) Distance to drain; (d) Drain density; (e) Distance to hydraulic window; (f) Distance to fault; (g) Fault density; (h) Distance to saline source; (i) Temperature; (j) Depth of screen well; (k) Soil type; (l) Horizontal hydraulic conductivity- Kh; (m) Vertical hydraulic conductivity- Kv; (n) Thickness of aquitard; (i) Operation time of well;(p) Well density; (q) Extraction density; (r) Extraction capacity; (s) Groundwater level.

7.4. The proposed methodology for the prediction of groundwater salinity in coastal aquifers with artificial intelligence techniques

The modelling framework includes the following steps: (1) data pre-processing, (2) feature selection, (3) model parameters, (4) model performance and evaluation, (5) Data post-processing (Figure 7-4).

7.4.1 Data pre-processing

Before modelling, 215 groundwater samples from middle and lower Pleistocene aquifers were selected, and each sample consists of 20 variables (Table 7-1). The measured Cl^- concentration is assigned as a dependent variable, while the 20 influencing factors are assigned as independent variables. The dataset was then randomly split to training and testing datasets 80% of the dataset was used for training, and 20% of the dataset was used for testing.

Table 7- 1: Influencing factors for prediction of groundwater salinity using machine learning models.

No	Explanatory Variables	Coding	Unit	Data type
1	Distance to the sea	DTS	km	Continuous
2	Distance to main river	DTR	km	Continuous
3	Distance to drainage	DTD	km	Continuous
4	Drainage density	DD	m/km	Continuous
5	Distance to hydraulic window	DTW	km	Continuous
6	Distance to fault	DTF	km	Continuous
7	Fault density	FD	m/km	Continuous
8	Distance to saline sources	DTS	km	Continuous
9	Temperature of groundwater	T	0C	Continuous
10	Depth of screen well	DSW	m	Continuous
11	Soil properties	AT	#	Ordinal
12	Horizontal hydraulic conductivity	Kh	m/d	Continuous
13	Vertical hydraulic conductivity	Kv	m/d	Continuous
14	Thickness of aquitard	WA	m	Continuous
15	Operation time (of the well)	OTW	year	Continuous

16	Well density	WD	well/km2	Continuous
17	Discharge density	DCD	m3/km2	Continuous
18	Extraction capacity	EXC	m3/d	Continuous
19	Groundwater level	GWL	m.abmsl	Continuous
20	Lithology	LT	#	Ordinal

7.4.2 Feature selection

Because many factors control groundwater salinization processes in coastal aquifers, the choice of influencing factors is essential to reduce time and cost of computation processes and to improve the accuracy of prediction results. For several decades, numerous variable selection methods have been applied to identify significant variables before feeding machine learning algorithms to construct predictive models such as filters, wrappers and embedded techniques (Guyon & Elisseeff; Hira & Gillies, 2015; Kohavi & John, 1997). Recently, Random Forests (RF) and its improved algorithms (XGB) have been widely used not only for predicting but also for selecting essential variables as the embedded technique to predictive models (Hira & Gillies, 2015; Rodriguez-Galiano, Mendes, Garcia-Soldado, Chica-Olmo, & Ribeiro, 2014; Zhao et al., 2019; Zheng, Yuan, & Chen, 2017). In this study, the RF algorithm is employed to select input parameters for predicting chloride concentrations in the middle and lower Pleistocene aquifers of the study area. The procedure was followed below steps:

Step 1: Estimation of permutation-based mean squared error (MSE) reduction as Eq.7-2 as below:

$$MSE_{OOB}^{t} = \frac{1}{nOOB(t)} \cdot \sum_{i=1}^{nOOB} (y_i - \hat{y}_{iOOB,t}) \tag{7-2}$$

Where MSE_{OOB} is mean squared error, nOOB is the total of out-of-bag (OOB) samples, y_i is the measure Cl^- concentration in groundwater samples, and $\hat{y}_{iOOB,t}$ is the predicted Cl^- concentration of the i-th sample from a decision tree t of OOB samples.

Step 2: Estimation of MSE for permuted input variable x_i using the following equation:

$$MSE_{OOB}^{t}[x_i permuted] = \frac{1}{nOOB(t)} . \sum_{i=1}^{nOOB} (y_i - \hat{y}_{iOOB,t})[x_i permuted] \quad (7\text{-}3)$$

Step 3: Estimation of variable importance score for variable x_i using the following equation:

$$VI(x_i) = \frac{1}{T_{tree}} . \sum_{t=1}^{Ttree} (MSE_{OOB}^{t}[x_i permuted] - MSE_{OOB}^{t}) \quad (7\text{-}4)$$

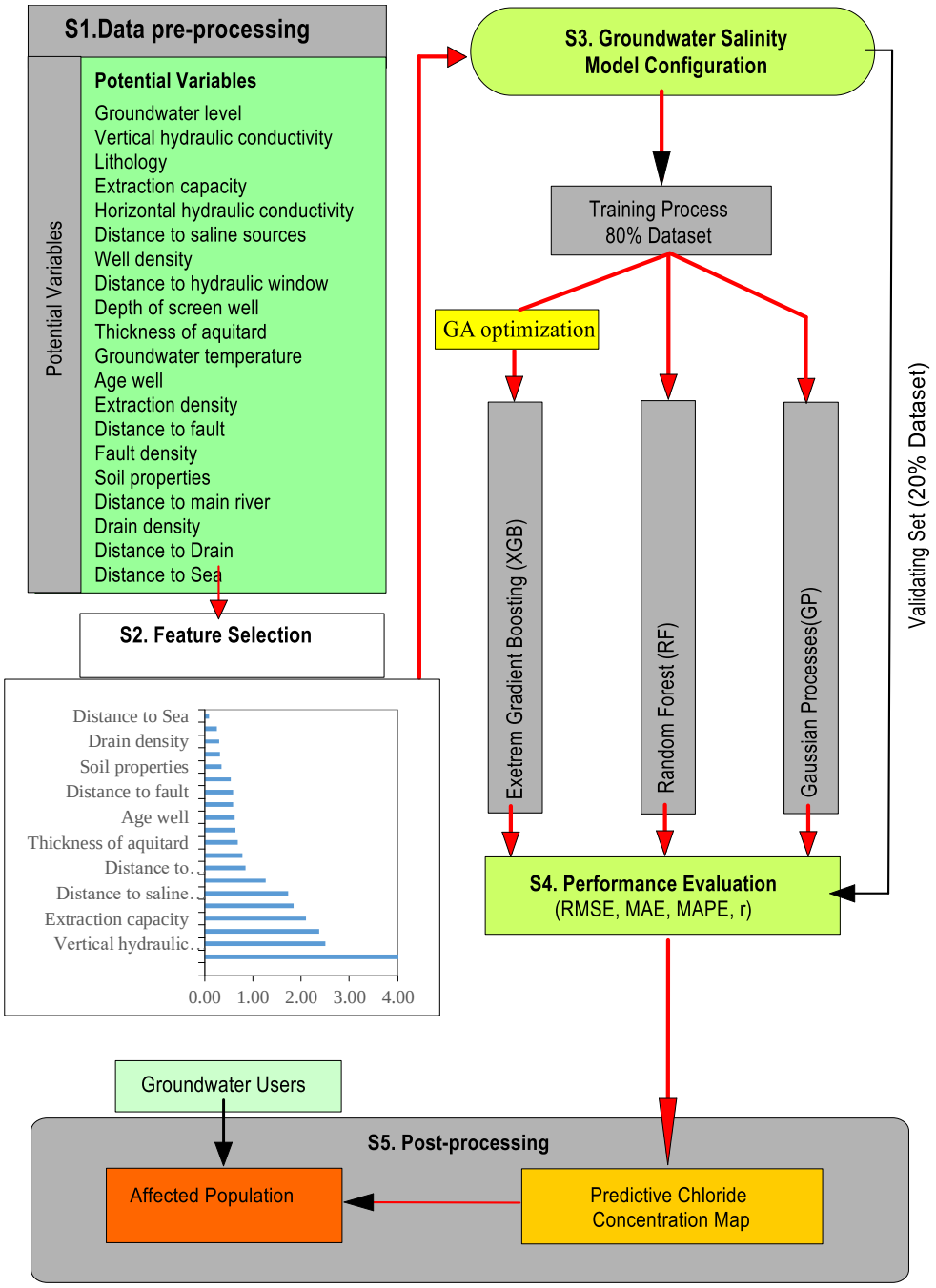

Figure 7- 4: Methodological chart of the present study.

7.4.3. Model configuration and training

The configuration and training for the three machine learning models are conducted using a training dataset (80% of measured data). For the RF model, the tree-net system is built from 1,000 trees with a maximum of 4 nodes per tree and the maximal tree depth of 17. For the GP model, the radial basis function (RBF) kernel and gamma = 0.014 are chosen to

predict chloride concentrations in groundwater. In the GO-XGB model, each XGB prediction rule is trained with 10-fold cross-validation to identify the number of trees (*ntree*) that minimizes an objective function. The prediction rule is fine-tuned by identifying the optimal combination of hyperparameters that further minimized the objective function for each area. The hyperparameters include the number of base classifiers (*n_estimators*), the maximum depth of each tree (*max_depth*), the learning rate (*eta*), the number of observations in each leaf node of the tree (*min_child_weight*), the minimum loss reduction required to further partition a leaf node on a single tree (*gamma and reg_alpha*), the proportion of observed data were used by XGB algorithm to grow each tree (subsample), and the proportion of predictor variables used at each level of tree splitting (*colsample_bytree*). The *n_estimators* is defined as the number of base classifiers, and improper setting of *n_estimators* will result in model failure. The *maximum_tree_depth* was selected appropriately to prevent model complexity. This parameter is crucial in controlling under and over-fitting issues in which too small values of *maximum_tree_depth* will cause underfitting while too large values will result in overfitting. *Learning_rate* represents the weight-reduction factor of each base classifier. *Min_child_weight* represents the weight of the minimum leaf node sample and is used to improve the generalisation of the model. The value of gamma ranges from 0 to-infinitive, which represents the minimum loss reduction required to make a further partition on a leaf node of the tree. The gamma parameter controls the drop value of the model loss function when the node splits. The subsample controls the proportion of random sampling for each tree, typically between 0.5–1. The regularisation parameter alpha (*reg_alpha*) denotes the L1 regularisation term of the weight, which is used to simplify the complexity of the model.

In this study, the XGB algorithm was used to construct the model and optimises parameters with GA. The details framework is described in Figure 4. The main parameters

of the XGB algorithm that need to be optimised are *max_depth*, *learning_rate*, *min_child_weight*, *subsample*, *alpha*, and *gamma*. After adjusting parameters by a genetic optimization function, we found the best value of these parameters *max_depth* = 15, *learning_rate* = 0.153, *min_child_weight* = 1, *subsample* = 1, *alpha* = 0.005, and *gamma* = 0.0015. In addition, *n_estimators* = s1200, *colsample_bytree* = 0.635, and *n_estimators* = 1200 were selected. The decision rule was retrained and applied to the withheld testing data to predict a new series of count observations and evaluate the accuracy of the decision rule based on the optimal values of the hyperparameters and number of trees. The variable importance of each environmental predictor variable was also obtained using the XGB algorithm.

7.4.4. Performance assessment

The performance criteria used for evaluating model performance depends on the output variables of each model, e.g., categorical or continuous variable (Tien Bui, Tuan, Klempe, Pradhan, & Revhaug, 2016). For evaluating the model with output values is continuous, performance criteria such as the root mean square error (RMSE), the mean absolute percentage error (MAPE), the mean absolute error (MAE), and Pearson's correlation coefficient (r) (Pham, Nguyen, et al., 2019) are used. Each performance criteria term indicates specific information regarding predictive performance efficiency (Li, Yang, Wan, Dai, & Zhang, 2016; Tien Bui, Hoang, & Nhu, 2018). RMSE is a quadratic scoring rule that measures the average magnitude of errors (Antti Syväjärvi, 2010). It gives a relatively high weight to large errors; hence, it is most useful when large errors are undesirable. The Mean Absolute Percentage Error (MAPE) is the average of absolute errors divided by actual observation values. MAE measures the average magnitude of errors in a set of predictions without considering their direction. It is a linear score, implying that all individual differences between predictions and corresponding observed values are weighted

equally in the average. The r is a measure of the linear correlation between observation and prediction values. RMSE, MAPE, MAE, and r are estimated by the equations (Pham, Nguyen, et al., 2019; Yoo, Yoo, Lee, Shukla, & Park, 2018):

$$RMSE = \sqrt{\frac{\sum_{t=1}^{n}(y_i^{obs} - y_i^{pr})^2}{n}} \quad (3)$$

$$MAE = \frac{1}{n}\sum_{i=1}^{n}(y_i^{obs} - y_i^{pr}) \quad (4)$$

$$MAPE = \sum_{i=1}^{n}\frac{\left|\frac{y_i^{obs} - y_i^{pr}}{y_i^{obs}}\right|}{n} \times 100 \quad (5)$$

$$r = \frac{\sum_{t=1}^{n}(y_i^{obs} - \overline{y_{obs}}) \times (y_i^{pr} - \overline{y_{pr}})}{\sqrt{\sum_{t=1}^{n}(y_i^{obs} - \overline{y_{obs}})} \times \sqrt{\sum_{t=1}^{n}(y_i^{pr} - \overline{y_{pr}})}} \quad (6)$$

where y_i^{obs} and y_i^{pr} are measured and predicted Cl^- concentration in observation i, and n is the number of observations. Higher values of rare preferred, i.e. close to 1, means better model performance and regression line fits the data well. Conversely, the lower values of RMSE, MAPE, and MAE values the better model performances.

Since the influencing factors for predicting groundwater salinization have significantly different ranges, normalization was used to convert the values of numeric columns into a scale from 0 to 1 using the following equation(Tien Bui et al., 2018):

$$X_n = \frac{X_i - X_{max}}{X_{max} - X_{min}} \quad (7)$$

Where xn and xi represent the moralised and raw training and testing data; xmax and xmin are the minimum and maximum of the training and testing data.

7.4.5. Generating groundwater salinity map

The results from the three machine learning models are then used to create chloride concentration maps. Prediction maps are constructed with four main steps as follows: (i) interpolating chloride concentrations in groundwater based on prediction results, (ii) reclassifying chloride concentrations based on the drinking water standard from WHO, (iii) estimating the salinity affected area, and (iv) estimating the number of people in each class of salinity affected area. In the first step, the predicted chloride concentrations are interpolated to create maps using the Kriging method by Spatial Analysis Tool in ArcGIS 10.3. In the second step, the interpolated results are reclassified into four main classes, including low ($Cl^- < 250$ mg/L), moderate ($250 \leq Cl^- \leq 500$ mg/L), high ($500 \leq Cl^- \leq 1000$ mg/L), and high ($Cl^- >1,000$ mg/L). In the third step, the salinity affected area for each class of the salinity concentration in groundwater was calculated using geometry functions in ArcGIS 10.3. In the final step, the numbers of people within each salinity affected area was estimated based on the salinity-affected areas and population density.

7.5. Result and Discussion

7.5.1 Feature selection for the Groundwater Salinity modelling

The results in Table 7-2 showed the variable importance selection with the permutation-based MSE decreased values ranged from 4.03 to 0.69. In the study area, the top ten most important influencing factors are groundwater level (4.03), vertical hydraulic conductivity (2.50), lithology (2.37), extraction capacity (2.10), horizontal hydraulic conductivity (1.85), distance to saline sources (1.73), well density (1.26), distance to hydraulic windows (0.85), depth of screen wells (0.79), and thickness of aquitards (0.69). The result reveals that groundwater salinization depends not only on hydrogeological features (vertical and horizontal hydraulic conductivities, lithology, paleo-saline sources, hydraulic connection, depth of screen well, and thickness of aquitard) but also groundwater

extraction practices (groundwater level, extraction capacity, well density). These factors also play an important role in transportation processes of other solutes such as arsenic, fluoride and nitrate in groundwater (Podgorski, Labhasetwar, Saha, & Berg, 2018; Ransom et al., 2017; Winkel et al., 2008b). The hydrogeological features influence on moving of saline groundwater from shallow to deeper aquifers (Hung Van et al., 2019) while groundwater exploitation activities exacerbate groundwater salinization(An et al., 2018; H. T. Hoang & Bäumle, 2018). The result may also suggest that saline groundwater leaking from upper layers to lower layers is a dominant process, resulting in an increase of chloride concentration in groundwater of the study area. Hydraulically, an increase hydraulic gradient due to groundwater depletion coupled with high vertical hydraulic conductivity, think aquitard, and high-density gradients cause an increase of vertical flow rate as shown in the following equations (Q. Ma et al., 2015).

$$q_v = -\delta \times K_v \left[\frac{h_{up} - h_{low}}{\Delta L} + \varepsilon\left(\frac{C_{up} + C_{low}}{2}\right)\right] \quad (7\text{-}8)$$

$$\delta = \frac{\mu_0}{\mu} = 1 - \xi \times \varepsilon \quad (7\text{-}9)$$

Where δ – the ratio of the dynamic viscosity of freshwater to seawater; K_v is a vertical hydraulic conductivity [m d^{-1}]; h_{up} and h_{low} denote the freshwater equivalent hydraulic heads at upper and lower layers [m], ΔL is the distance from upper to lower layers [m]; μ_0 and μ denote the dynamic viscosity [kg m^{-1} d^{-1}]; ξ is a constant; C_{up} is average observed salinity of pore water in upper aquifers [kg/m^3]; C_{low} is observed salinity of pore water in lower aquifers [kg/m^3]; and ε is a constant. The similar findings were also observed in other coastal aquifers in the world (Cary et al., 2015; Chatton et al., 2016a; Delsman et al., 2014a; Larsen et al.,

2017c), which indicated strong influences of over groundwater exploitation on seawater intrusion in coastal aquifers (Han et al., 2015; Yechieli et al., 2019; Yu & Michael, 2019).

Table 7- 2: Variable importance (permutation-based MSE decreased)

No	Variable	Permutation-based MSE decreased	Number of nodes used	Ranking
1	Groundwater level	4.03	636	1
2	Vertical hydraulic conductivity	2.50	35	2
3	Lithology	2.37	50	3
4	Extraction capacity	2.10	281	4
5	Horizontal hydraulic conductivity	1.85	260	5
6	Distance to saline sources	1.73	379	6
7	Well density	1.26	242	7
8	Distance to hydraulic window	0.85	529	8
9	Depth of screen well	0.79	518	9
10	Thickness of aquitard	0.69	376	10
11	Groundwater temperature	0.64	354	11
12	Age well	0.62	135	12
13	Extraction density	0.59	208	13
14	Distance to fault	0.59	400	14
15	Fault density	0.54	158	15
16	Soil properties	0.35	83	16
17	Distance to main river	0.32	863	17
18	Drain density	0.30	686	18
19	Distance to Drain	0.25	628	19
20	Distance to Sea	0.10	2199	20

The other critical influencing factors have permutation-based MSE values from 0.64 for groundwater temperature to 0.10 for distance to the sea. It was noted that the distance to

the sea had a little score value of 0.10, indicating less contribution to groundwater salinization processes. This result may suggest that direct seawater intrusion from the sea to coastal aquifers of the study is not dominant in the study area.

7.5.2 Model performance evaluation and comparison

In this study, the predictive models for groundwater salinization are built using the training and the testing datasets, drawing upon a total of 215 observation wells and 20 variables. The results of the goodness-of-fit assessment of the three machine learning algorithms-based models including the GO-XGB model, RF model and the GP model for both training and testing steps are shown in Figure 7-5, Tables 7-3 and Table 7-4, respectively.

The training model performance (Table 7-3) shows that the GO-XGB model has the lowest value RMSE = 141.042 mg/L, followed by the RF (RMSE=176.179 mg/L) and GP (RMSE=176.179 mg/L) models. The similar trend is also observed in MAE and MAPE for the GO-XGB (MAE=4.864, MAPE=2.070), RF (MAE=58.286 mg/L, MAPE=29.410 mg/L) and GP (MAE=71.802 mg/L, MAPE=61.42 mg/L). In contrast, the GO-XGB model has the highest r value of 0.999 compared to that of RF (r= 0.786) and Gaussian Processes (r=0.882).

In the testing step, the results of the predictive models are validated by using the testing dataset consisted of 20% random samples from the original dataset. The testing results show that the GO-XGB model has the highest performance compared to the RF and GP models (Table 7-4). For example, GO-XGB has the best result of r = 0.787, followed by the RF model (r =0.99) and the GP model (r=0.214). Similarly, the GO-XGB model shows the lowest values of RMSE=141.042 mg/L, MAE=74.993 mg/L, and MAPE=87.250 mg/L, followed by the RF (RMSE =176.179 mg/L, MAE=84.708 mg/L, MAPE=95780 mg/L) and GP (RMSE =305.782 mg/L, MAE=127.355 mg/L, MAPE=130.840 mg/L) models.

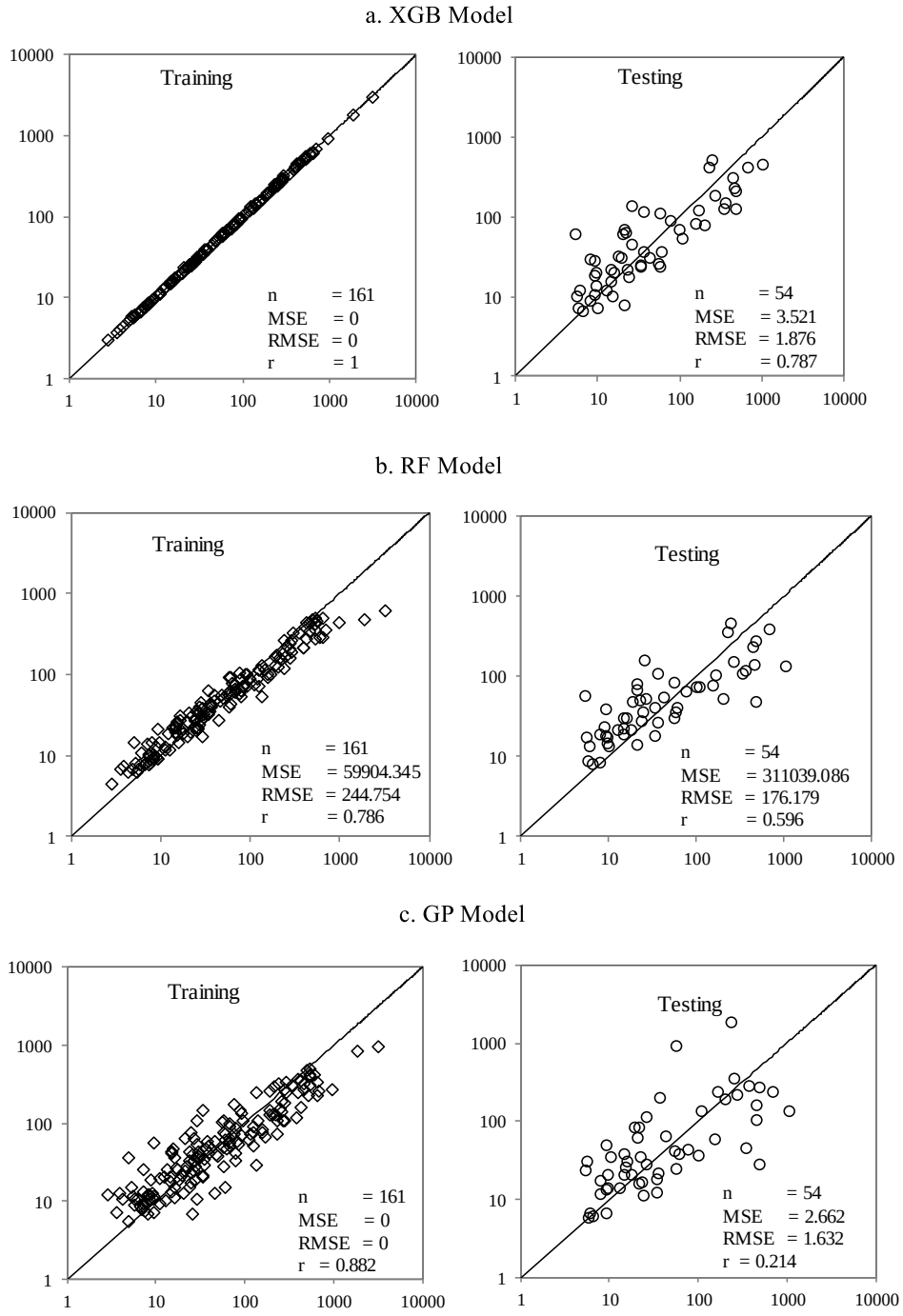

Figure 7- 5: Observed vs predicted chloride concentration for training and test data for XGB, RF and GP model.

Table 7- 3: Goodness-of-fit of the groundwater salinity models on the training dataset.

Statistical metrics	GO-XGB	RF	Gaussian Processes

RMSE	18.450	244.754	219.329
MAE	4.864	58.286	71.802
MAPE	2.070	29.410	61.42
r	0.999	0.786	0.882

Table 7- 4: Prediction performance of the groundwater salinity models using the validation dataset.

Statistical metrics	GO-XGB	RF	Gaussian Processes
RMSE	141.042	176.179	305.782
MAE	74.993	84.708	127.355
MAPE	87.250	95.780	130.840
r	0.787	0.596	0.214

Overall, the GO-XGB model produces an excellent predictive performance with the highest value of r = 0.99 and r= 0.787 for training and validation steps among three predictive models. Likewise, this model also has the lowest values of RMSE, MAE, and MAPE compared to the RF and GP models in both training and validation steps.

Although we have considered various influencing factors to provide the accurate prediction of groundwater salinity in a coastal area of the Mekong River Delta, however, the processes of seawater intrusion into fresh aquifers depend not only human activities but also natural variations. Therefore, for broader applicability, these models would be required to include additional influencing factors such as the regional groundwater flow system, tidal fluctuation and sea-level rise. Also, the performance of prediction models compares to numerical models and other stochastic models.

7.5.3 Mapping salt-groundwater-affected area

In general, the average results obtained from the three machine learning models, including the GO-XGB, RF, and the GP models, shows the salinity-affected region, extending from the My Thanh River to the Central of Soc Trang City (Figure 7-6). The prediction results strongly agree with salinity observation in this study(Figure 7-6a) and previous studies (An et al., 2018).

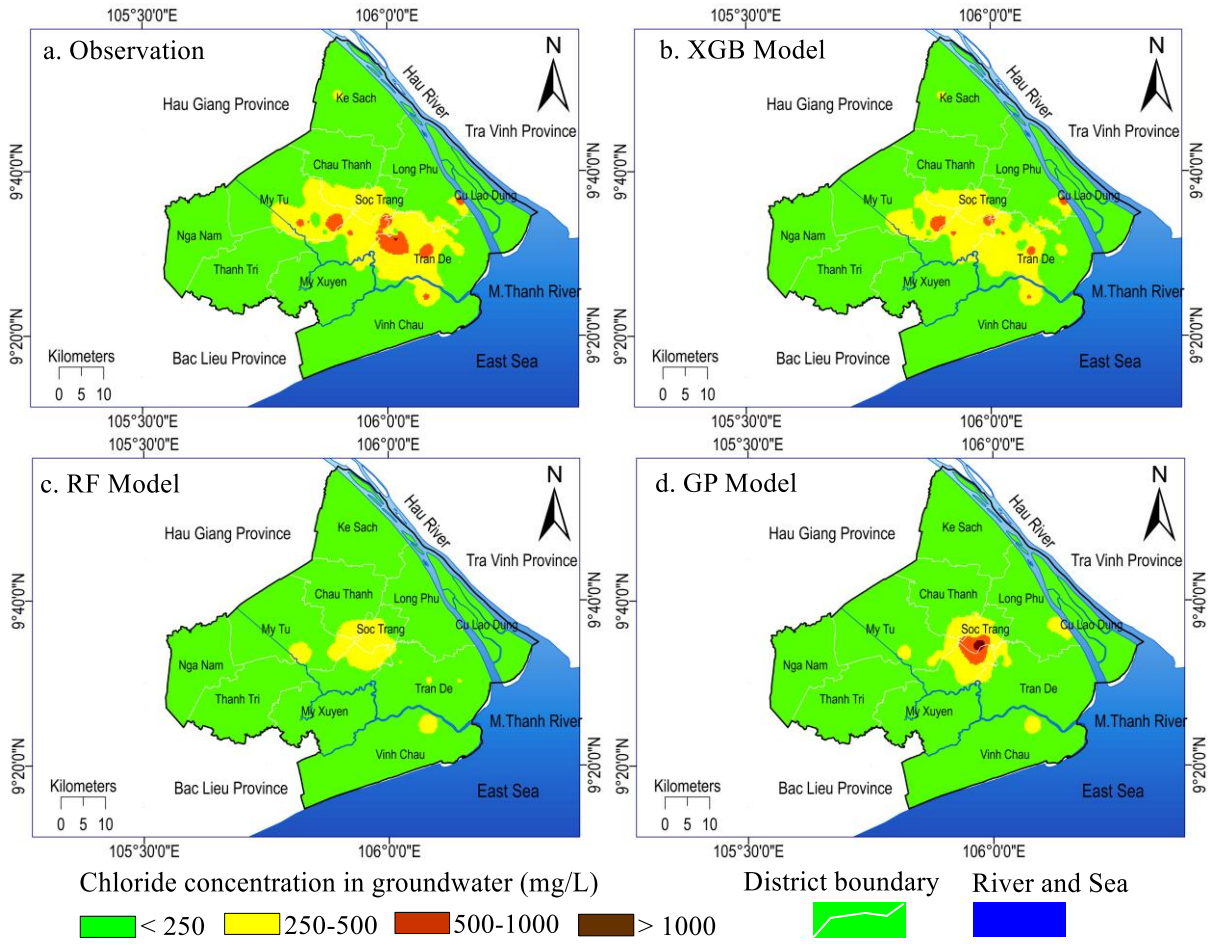

Figure 6. Chloride concentration in groundwater of the study area (a) observation data, (b) XGB model, (b) RF model, and GP model (d).

Accordingly, high chloride concentrations which exceed the limited standard for drinking water Cl^- >250 mg/L is predicted in the areas with to paleo-saline sources, high extraction rates, and significant groundwater level depletion. The severely affected areas are the Tran De estuary, the My Thanh river and the central region including Soc Trang city and

My Xuyen district where chloride concentrations in wells elevate to 2,000 mg/L. Surprisingly, low chloride concentrations (Cl^- <250 mg/L) in groundwater is predicted in coastal areas even if in the production wells located just around 2 km from the sea and at -10.5 meters below the mean sea level (m.a.m.sl)). Meanwhile, Soc Trang city, which locates far from the sea approximately 40 km, is predicted to have high chloride concentrations in groundwater. This reveals that processes of salinity accumulation in aquifers are very complex, depending not only on influencing factors but also anthropogenic activities.

The spatial distributions of affected areas with moderate and high chloride concentration are relative differences among models. For example, in the GO-XGB model, the affected area is predicted to extend from the coastal line to the central area of the study (Figure 7). Also, the profoundly affected area is observed in the dense groundwater extraction locations. These locations are located close to the paleo-saline groundwater sources coupled, and these areas also have high groundwater extraction rates and significant groundwater level depletion. This indicates that these influencing factors play an essential role in increasing chloride concentrations in groundwater. The similar finding is also in-line with recent studies (Hoang et at., 2018, An et al., 2018 and Nam et al., 2019). Conversely, the results from the RF (Figure 7-6c) and the GP models (Figure 7-6d) show that the moderately affected areas are the central area of the study region.

The three models provide different predictions in the affected area (Table 7-5). The RF model predicted the largest affected area (3,118.50 km^2) followed by the GP model (3,055.35 km^2) and GO-XGB (2,879.0 km^2) with low chloride concentration (Cl^- <250 mg/L). Meanwhile, the largest affected-areas with moderate-high chloride concentration (Cl^- =250 – 500 mg/L) are observed by the GO-XGB model (433 km^2), the GP model (256.65 km^2), and the RF model (193.50 km^2). Both the GO-XGB model and the GP models predicted the large affected-areas with high (Cl=500-1000 mg/L) and very chloride

concentration (> 1000 mg/L) while RF model predicted non-affected areas of high and very high chloride concentration.

Table 7- 5: Predictive results of affected areas (in km^2) following four classes of chloride concentration in groundwater.

Statistical metrics	Low (Cl< 250 mg/L)	Moderate (250 ≤ Cl^- ≤ 500 mg/L)	High (500 < Cl^- ≤ 1000 mg/L)	Very high (Cl^- > 100 mg/L)	% affected area
GO-XGB	2,879.00	433.00	42.40	0.88	14.0
RF	3,118.50	193.50	0	0	6.0
Gaussian Processes	3,055.35	256.65	34.46	4.86	9.0
Average	3,017.62	294.38	25.62	1.91	10.0

Table 7- 6: Estimation of the number of the affected population following four classes of chloride concentration in groundwater.

Models	Low (Cl< 250 mg/L)	Moderate (250 ≤ Cl^- ≤ 500 mg/L)	High (500 < Cl^- ≤ 1000 mg/L)	Very high (Cl^- > 100 mg/L)	% affected population
GO-XGB	719,750	502,170	84,800	5,280	45
RF	935,550	376,450	-	-	29
Gaussian Processes	916,605	297,315	68,920	29,160	30
Average	857,302	391,978	51,240	11,480	35

7.5.4 Mapping salt-groundwater-affected population

Table 7-6 shows the approximate number of people in the study may have to use groundwater with exceeding the chloride concentration standard (250 mg/L) obtained from the GO-XGB, RF and GP models. It was based on the 2017 population statistics in Soc Trang province. Accordingly, the mean number of affected people from the three different models were 454,698 people, accounting for nearly 35% of the total population of Soc Trang province. Each predictive model shows a different prediction result. The GO-XGB model estimates the highest number of 592,250 people, approximately 45% of the total population

followed by 395,395 (30% of the total population) and 376,450 (29% of the total population) obtained from the GP and the RF models (Table 7-6). These results suggest that groundwater resources in the study area are highly vulnerable due to seawater intrusion. When the delta is susceptible to sea-level rise, and a large number of people may have to face freshwater shortages shortly.

7.6. Concluding remarks

In this study, three advanced machine learning models, including GO-XGB, RF, and GP, were employed to predict chloride concentration in groundwater and assess impacts of salinity on water users in a coastal area of the Mekong River Delta, Vietnam. Twenty influencing factors were evaluated using the RF model based on score estimation. The most influenced factors to groundwater salinization are related to both groundwater exploitation (groundwater level depletion, extraction capacity, and well density) and hydrogeological features (vertical hydraulic conductivity lithology, horizontal hydraulic conductivity, distance to the saline source, distance to the hydraulic window, depth of screen well, and thickness of aquitard). This finding confirms previous studies in which groundwater exploitation is one of the most important influencing factors to seawater intrusion in coastal lowland regions.

All three models perform well in predicting the probability of groundwater salinity. However, the GO-XGB model provides the highest accuracy prediction with RMSE =18.450, MAE=4.864, MAPE =2.070, and r =0.999 compared to the GP model (RMSE =219.329, MAE=71.329, MAPE =61.42, and r =0.882) and the RF model (RMSE =244.754, MAE=58.286, MAPE =29.410, and r =0.786). It indicated that GO-XGB model could be a useful tool to predict groundwater salinization in the coastal aquifers.

All three models predicted that approximately 35% of the total population might have to use groundwater with chloride concentration exceeding the WHO drinking water standard (Cl^- > 250 mg/L). More seriously, urban areas are close to paleo-saline sources. While the thicknesses of aquitards are thin and groundwater levels deplete quickly, leaking paleo-saline becomes more server and cause groundwater salinization. It is stimulated by the hydraulic connection between aquifers and over groundwater exploitation. Given the rapid increase of water demand, significant groundwater depletion and unpredictable impacts of climate change and sea-level rise, immediate actions must be taken by the water authorities to find a suitable solution to this environmental crisis.

CHAPTER 8 INFLUENCES OF GROUNDWATER EXPLOITATION ON GROUNDWATER FLOW SYSTEM IN A COASTAL REGION

Chapter 8 presents the development of the groundwater model to investigate the influences of pumping activities and regional groundwater levels on groundwater flow dynamics in the coastal area of the Mekong Delta, Vietnam. Groundwater model was constructed and calibrated to reproduce historical groundwater flow dynamics between 2000-2016 under influences of groundwater exploitation. Based on the calibrated model, the projection of future changes in groundwater levels in the study area was predicted based on different scenarios of future pumping activities and changes in regional groundwater levels.

8.1. Introduction

The freshwater shortage is becoming the most challenge for satisfying domestic, industrial and agricultural water demands in many countries around the world in the 21st century (J. Liu, Liu, & Yang, 2016; Wichelns, 2017). As groundwater is a largely invisible resource, its dynamic change of quantity and quality is difficult to grasp even for experts (Aeschbach-Hertig & Gleeson, 2012). Understanding the groundwater quality and its controlling factors, therefore, is the critical task for groundwater planning and management, ensuring the sustainability of safe water use for national and global socio-economic development (Alaya, Saidi, Zemni, & Zargouni, 2014).

In natural conditions, groundwater moves slowly through the aquifer system under regulating of complex factors such as climatic variation and hydro-geological characteristics (Rosenthal, Zilberbrand, & Livshitz, 2007; C. K. Singh et al., 2017; Wen, Diao, Wang, & Gao, 2012; R. Zhang, Hu, Zhang, & Yu, 2007). However, anthropogenic activities may alter groundwater flow system causing substantial changes in groundwater quantity and quality (Hosono et al., 2009; Khalaj, Kholghi, Saghafian, & Bazrafshan, 2019; Lamichhane & Shakya, 2019). For example, excessive groundwater exploitation extraction has resulted in significant groundwater depletion causing arsenic contamination (Bui Huy, Tuyet-Hanh, Johnston, & Nguyen-Viet, 2014; J.-Q. Jiang, Ashekuzzaman, Jiang, Sharifuzzaman, & Chowdhury, 2013; Kaltreider, Davis, Lariviere, & Hamilton, 2001; Mandal & Suzuki, 2002; Shankar, Shanker, & Shikha, 2014), heavy metals and nitrate contamination (Almasri, 2007; B. Singh & Sekhon, 1976; Vithanage, Mikunthan, Pathmarajah, Arasalingam, & Manthrithilake, 2014; Zhai et al., 2017; Q. Zhang et al., 2015; W. L. Zhang, Tian, Zhang, &

Li, 1996) and seawater intrusion into coastal aquifers worldwide (Abd-Elhamid & Javadi, 2011; De Filippis et al., 2016; Mahlknecht, Merchán, Rosner, Meixner, & Ledesma-Ruiz, 2017b; H.-Y. Park, Jang, Ju, & Yeo, 2012; Vengosh, 2003; Werner et al., 2013). Additionally, the unpredictable impacts of climate change and sea-level rise in the coastal regions might potentially accelerate seawater intrusion putting groundwater resources be a likely high crisis (Aeschbach-Hertig & Gleeson, 2012; Ferguson & Gleeson, 2012a; Russo & Lall, 2017). This fact, thus, poses the most prominent issue to sustainable water management in coastal regions around the world in this century (Ferguson & Gleeson, 2012a; Gleeson, Wada, Bierkens, & van Beek, 2012).

Over the last several decades, groundwater modelling has been widely applied to understand hydrological processes and solute transportation within porous media such as groundwater contamination (Sathe & Mahanta, 2019) and seawater intrusion (Simmons, Fenstemaker, & Sharp, 2001). Recently, many studies (Arfib & Charlier, 2016; Boschetti, González-Hernández, Hernández-Díaz, Naclerio, & Celico, 2015; Lu, Xin, Li, & Luo, 2015; Mehdizadeh, Karamalipour, & Asoodeh, 2017; Werner et al., 2013) has been proven that the deterioration of groundwater quality in many coastal regions is a result of excessive groundwater extraction and significant land-use changes coupled with unpredictable impacts of climate change, and sea-level rise. As the intensive human development and natural dynamics may alter groundwater flow system (sources, flow paths, resident time and quality), the future prediction to changes of groundwater quantity and quality is crucial for sustainable groundwater management, especially in coastal low-lying deltas where groundwater resources play an essential role for socio-economic development (Hornero, Manzano, Ortega, & Custodio, 2016).

In the Vietnamese Mekong Delta (VMD), groundwater is a primary source for domestic, industrial and agricultural water supply system (Ha et al., 2018). However, long-term exploitation and inappropriate management of groundwater have resulted in severe arsenic contamination (Benner et al., 2008; Merola et al., 2015; Stuckey et al., 2016) and land subsidence (Minderhoud et al., 2017). Additionally, some previous studies such as Ho et al. (Ho et al., 1991), Khoi et al. (Le Van Khoi, 2002) and An et al. (An et al., 2014b) stated that groundwater resources in the coastal aquifers of the Mekong Delta is highly vulnerable to seawater intrusion. Yet the influences of groundwater exploitation activities to groundwater flow system and groundwater quality in the coastal area of the Mekong Delta has remained unknown. Meanwhile, towards the sustainability of groundwater use and

management in the context of rapid socio-economic development and natural variation requires an in-depth understanding not only groundwater characteristics but also the main driver.

To better our future groundwater management in coastal lowland regions, insights into influences of groundwater pumping practices on groundwater flow and saltwater expanding in the deep aquifers under different groundwater extraction scenarios are needed. In this study, MODFLOW and SEAWAT packages in Aquaveo GMS 10.4 model was built to predict groundwater levels and saltwater transportation within the deep aquifers based on observed groundwater levels and hydro-geological parameters. Based on the socio-economic planning between 2017-2030, different future groundwater abstraction scenarios were constructed. The groundwater model could predict groundwater flow and chloride transportation in the coastal aquifer system accurately.

8.2. Study site

Locating in the lowest part of the Mekong River Basin, Soc Trang province has approximately 3,312 km^2 and accounts for around 0.7% and 5.9 % areas of Vietnam and Mekong Delta, respectively, with an average population of 1,310,700 people (General Statistics Office of Vietnam 2015). The study area is located in an active tropical monsoon region with two distinguish seasons, the dry and rainy seasons. In the rainy season, climate condition is strongly affected by the Southwest Monsoon, which brings more than 85% amount of annual rainfall, having a high temperature and humidity. Meanwhile, the Northeast Monsoon dominates in the dry season from November until April, contributing to 15% of the annual rainfall with a relatively low temperature and humidity. The average annual air temperature is 26.8°C with over 36°C in the warmest months (April and May), and the lowest mean monthly temperature in January is around 24°C; average annual relative humidity of 84%; and annual precipitation of 1,772 mm with low rainfall from January to April. As relatively lowland region (0.5 - 2.5 m above mean sea level) and reaching directly with East Sea, the hydrological regime in the MD, therefore, is regulated by upstream discharge, local rainfall and river-marine dynamic interactions. These factors remarkably affect the water quality of both surface water and groundwater sources in this region.

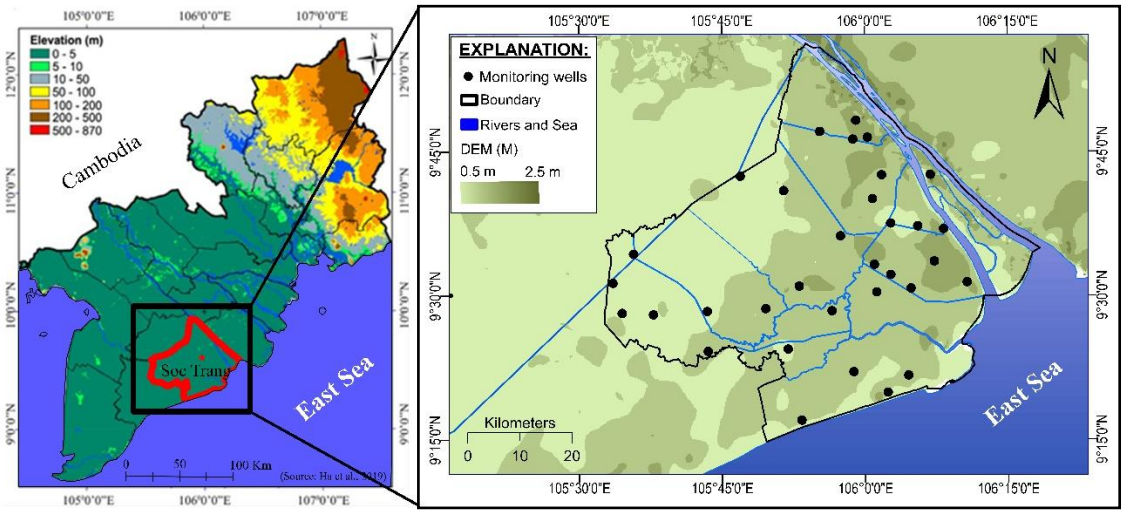

Figure 8- 1: Map of Soc Trang Province, Vietnam

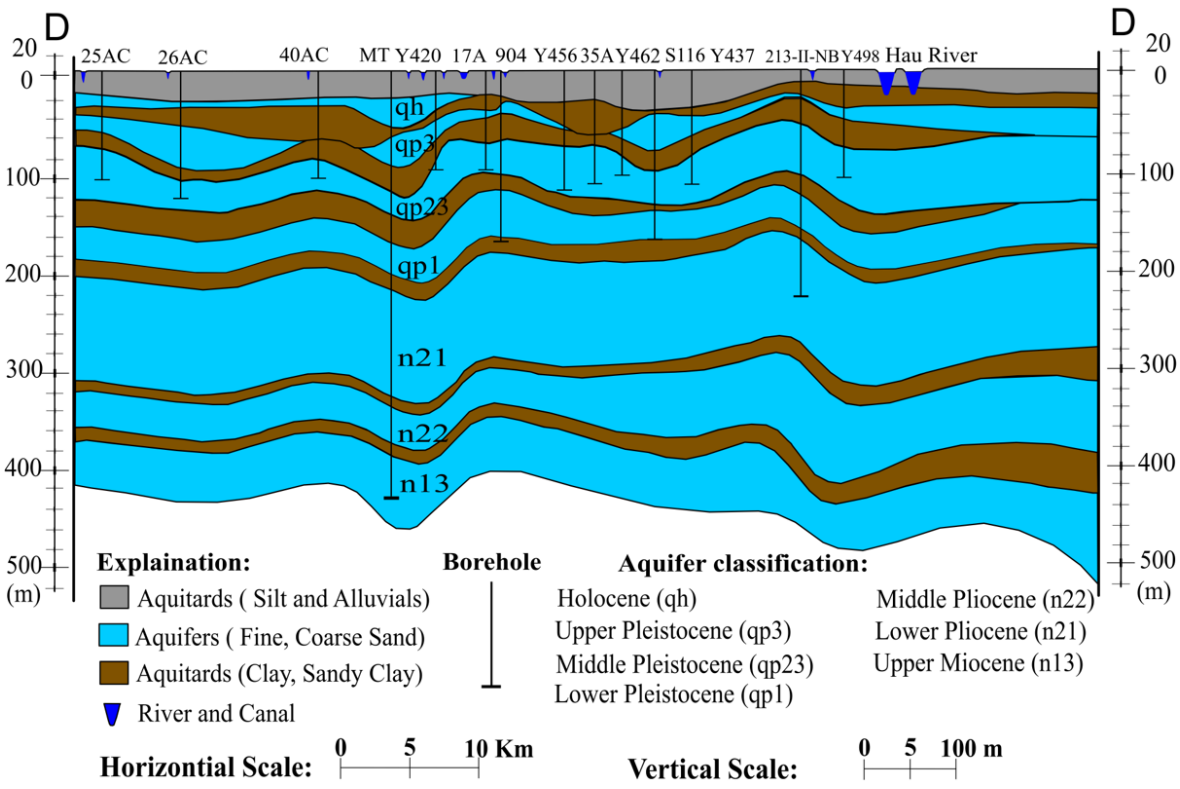

Figure 8- 2: Hydrogeological cross-section D-D' from SW to NE of the study area.

(Source: DONRE, Soc Trang province, 2013)

The geology and geomorphology of Soc Trang province were formed by the glacial-eustatic sea-level change and the ongoing tectonic subsidence of the Mekong River Basin, therefore, its hydrogeology is somewhat complicated (Frank Wagner, Vuong Bui Tran, & Renaud, 2010). In general, hydrogeology consists of seven distinct aquifers namely,

Holocene (qh), Upper Pleistocene (qp_3), Upper-Middle Pleistocene (qp_{23}), Lower Pleistocene (qp1), Middle Pliocene (n_{22}), Lower Pliocene (n_{21}), Upper Miocene (n_{13}) aquifer layers. Generally, the lithology of each aquifer consists of fine to coarse sand, gravel, and pebbles (Fig.2).

The Holocene layer (qh) was formed from the coarse-grained rocks sedimentary rocks originating from mainly three types of sediments, including: Lower to Middle Holocene sediments (qh1-2) of alluvial and marine origin composed dominantly of clayey silt and fine sand and are fatty organic compositions. Alluvial, marine and eolian sediments (qh_{2-3}) include 1.0 -12.0 m below ground level (m.b.g.l) thick remnants of sand dunes from paleo-sea shores which can be found in Long Phu, Vinh Chau, Soc Trang and My Tu districts. These sand dunes are often shaped arc extends parallel with the coast of the northeast-southwest or northwest-southeast, extending from 3.0 to 4.0 km along the coast and distributing around 200-300 m from the shoreline to inland. Upper Holocene sediments (qh_3), accumulated in the river valleys and flood plains, consists of clayey silt, silt-mud, and fine sand. Slug tests results of wells in this area point out that groundwater flow rate (Q) ranges approximately 0.20 - 0.50 L/s (Avg. 0.30 L/), drawdown (S) is 0.30 - 0.70 m (Avg. 0.53 m).

The Upper Pleistocene unit (qp_3) is widely distributed over the whole Soc Trang province, mainly overlaying by Holocene sediments. This aquifer was formed by coarse-grained sedimentary rock formations of Long My (mQ_{13}^{lm}), composed mainly of fine sand, fine gravel and medium and small grey-green shells, grey and white sand with thickness changing 3.0 -50.9 m (Avg. 20.50 m). Hydro-geologically, qp3 strata could be divided into two parts: The Lower part of the high permeable aquifer is covered by an upper part of low permeable aquitards, generally consisting of silt to a clay-size fraction. The top of qp_3 aquifer distributes heterogeneously with a depth of 24.0 m - 95.0 m.b.g.l (Avg. 50.39 m.b.g.l) and its bottom ranges around 30.0 - 125.0 m.b.g.l (Avg. 70.74 m.b.g.l). There is the limited slug test result of the qp_3 aquifer, however, based on analyzing the thickness and grain size suggest that groundwater flow rate of this aquifer is 0.185 L/s - 0.195 L/s.

Middle Pleistocene aquifer (qp_{23}) was overplayed by Upper Pleistocene (qp_3). The lithology is dominantly composed of alluvial sediments, marine alluvial and marine origins from Long Toan formations system. The aquifer covers and distributes widely throughout the province. This aquifer is also divided into a low permeable part, composing silt and clay, which can be encountered in depth from 54.0 m.b.g.l to 137.0 m.b.g.l (Avg. 83.63 m.b.g.l).

A confined aquifer represents the low part, consisting of well stored and high permeable fine to coarse sand mixing with gravel-sand and thin lenses of clay powder in the depth of 92.0-175.0 m.b.g.l (Avg. 131.47 m.b.g. l). The thickness of this part ranges from 7.0 m to 81.0 m (Avg. 49.75 m). The composition is mainly coarse sand in various sizes containing water. The result of pumping test showed that water absorption is very high in aquifers with groundwater flow rate from 9.05 to 19.10 L/s (Avg. 14.57l L/s), drawdown (S) is 2.51 -18.81 m (Avg. 10.31 m).

Lower Pleistocene aquifer (qp_1) is generally formed from the coarse-grained rock under the bottom part of the Binh Minh formation system (m, amQ_{11}^{bm}). Lithology consists of dominate fine to coarse sand and less gravel. The qp_1 aquifer distributed widely over the whole Soc Trang province. The depth of the top part of the qp_1 aquifer varies from 110.50 m.b.g.l to 192.0 m.b.g.l (average of 145.29 m.b.g.l) while that of bottom part ranges from 146.00 m to 250.0 m (average of 187.40 m). The thickness of the aquifer varies from 6.0 m to 79.50 m (Avg. 40.29 m depth). The static groundwater level of this aquifer varies from -0.50m to -8.78 m above sea level (m.a.m.s.l) with an average. of -1.78 m.a.m.s.l. The slug test result shows that this aquifer has very high groundwater flow rate (Q) distributing from 12.26 to 33.90 L/s (average of 17.92 L/s), drawdown (S) ranges 2.571- 13.55 m (average of. 8.48 m).

For last several decades, the Middle Pleistocene (qp_{23}) and Lower Pleistocene (qp_1) aquifers have become the most attractive aquifer for groundwater pumping practices because of high yield and good quality compared to remaining aquifers (An, Tsujimura, Le Phu, Kawachi, & Ha, 2014a). Recently, however, groundwater degradation has occurred in many parts of these aquifers due to intensive groundwater withdrawal with approximately 200 wells/km2. Consequently, the residents have to access groundwater at deeper aquifers (n_{21}, n_{22} and n_{13} aquifers). This fact, coupled with the changes of recharge pattern into the aquifer system, seawater intrusion poses a significant challenge to the sustainable use and effective management practices of water resources in the study area.

8.3. Groundwater model construction

8.3.1. Groundwater modelling equations

In this study, variable-density groundwater flow equation is employed to simulate the seawater intrusion processes. The SEAWAT package in Aquaveo GMS 4.6 which considers the effect of density on the groundwater flow system was used to predict influences of

excessive groundwater exploitation on groundwater salinisation in the study area (Graf & Therrien, 2005; Simmons et al., 2001). The variable density groundwater flow can be expressed as the following equations (Guo, Huang, Zhou, & Wang, 2019):

$$\frac{\partial}{\partial x}\left(K_{fx}\frac{\partial h_f}{\partial x}+\frac{\rho-\rho_f}{\rho_f}\frac{\partial Z}{\partial x}\right)+\frac{\partial}{\partial y}\left(K_{fy}\frac{\partial h_f}{\partial y}+\frac{\rho-\rho_f}{\rho_f}\frac{\partial Z}{\partial y}\right)+\frac{\partial}{\partial z}\left(K_{fz}\frac{\partial h_f}{\partial z}+\frac{\rho-\rho_f}{\rho_f}\frac{\partial Z}{\partial z}\right)=$$

$$\rho S_s\frac{\partial h_f}{\partial t}+\theta\frac{\partial \rho}{\partial C}\frac{\partial C}{\partial t}-\rho_s q_s \quad (8\text{-}1)$$

where *x*, *y*, *z* is the flow direction in the Cartesian coordinate axes spatial dimensions; K_{fx}, K_{fy}, K_{fz} are the hydraulic conductivities in different directions (LT^{-1}); S_s is the specific storage of porous media in terms of freshwater head (L^{-1}); h_f is the freshwater hydraulic head (L); θ is the effective porosity of porous media; ρ is the density of saline groundwater (ML^{-3}); ρ_f is the density of freshwater (kg/m^3); ρ_s is density of water entering from a source or leaving through a sink (ML^{-3}); q_s is the volumetric flow rate of sources or sinks per unit volume of aquifer (MT^{-1}); C is the solute concentration (ML^{-3}); and t is the time of simulation (T) (Guo et al., 2019).

Seawater intrusion is the processes of moving saltwater into fresh aquifers throughout advection, dispersion, and diffusion mechanisms. As illustrated in the equation (1), any change of concentration will affect to groundwater flow in aquifers. Therefore, seawater intrusion model needs to solve both the groundwater flow equation and the solute transport equation. The solute transport processes consist of groundwater convection term, hydrodynamic dispersion term, source-sink term, and reaction term are expressed following equation 8.2 below(Guo et al., 2019):

$$\frac{\partial(\theta C)}{\partial t}=\nabla(\theta D\nabla C)-\nabla(\theta VC)+q_sC_s+R_n \qquad (8\text{-}2)$$

Where D is the hydrodynamic dispersion coefficient tensor (L^2T^{-1}), C_s is the solute concentration of water entering from sources or sinks (ML^{-3}), ∇ is nabla operator; V is the average linear velocity (LT^{-1}), and R_n is the reaction term of chemical substance.

8.3.2. Groundwater conceptualization

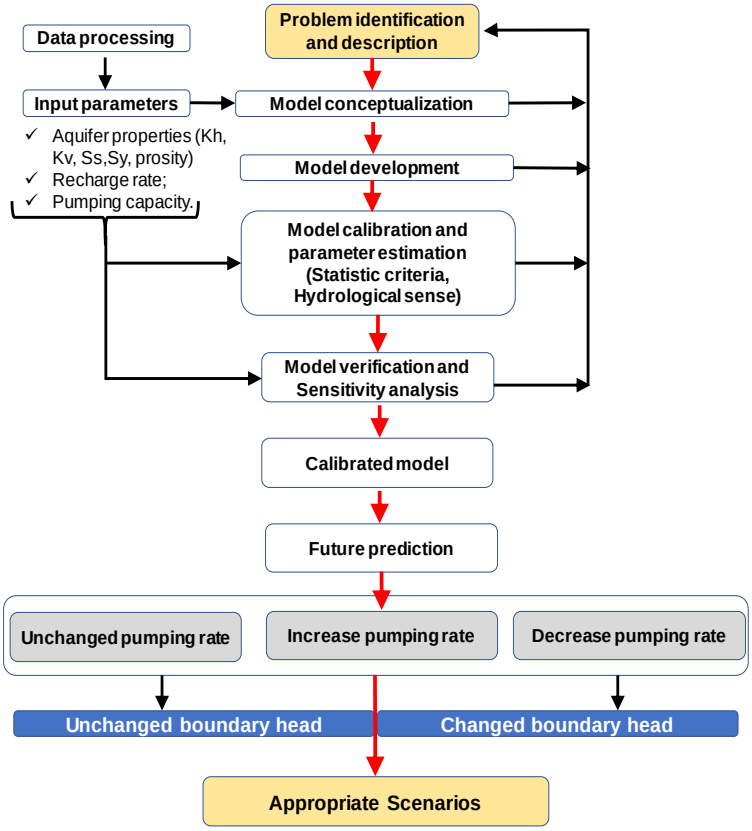

Figure 8- 3: Flowchart of groundwater modelling

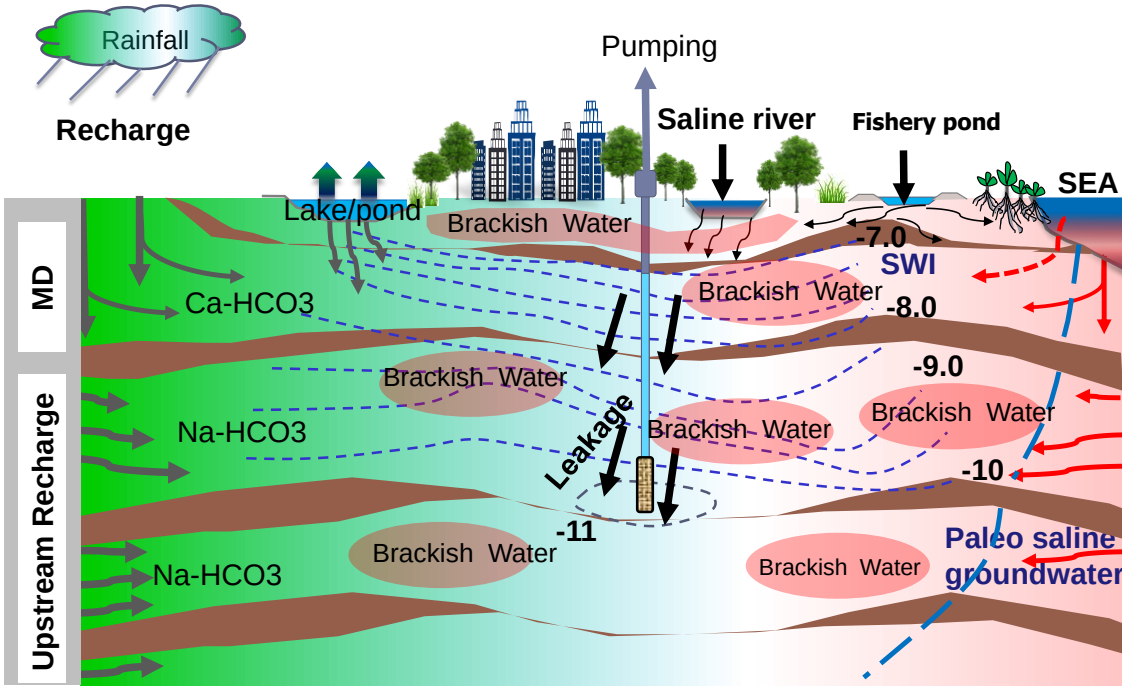

Figure 8- 4: Simplified conceptual groundwater flow system in the study area.

Figure 8-3 presents the processes of groundwater modelling in the study area. In groundwater modelling, building the conceptual model of the groundwater flow system is the first important step which shows how the hydrological system works could reproduce the physical characteristics of the study area hydrological system and processes (Figure 8-4). The conceptual model is developed based on the GIS tools in the map module in the Aquaveo GMS 10.4.6 model. The hydrogeological borehole data were used to create 3D hydrogeological profiles (Figure 8-5). The groundwater conceptual model includes the model boundaries, canals and rivers, recharge areas, hydraulic conductivity, wells, observation points and all other data necessary for the simulation. Figure 8-5 shows the soil stratigraphy data from available drilling boreholes.

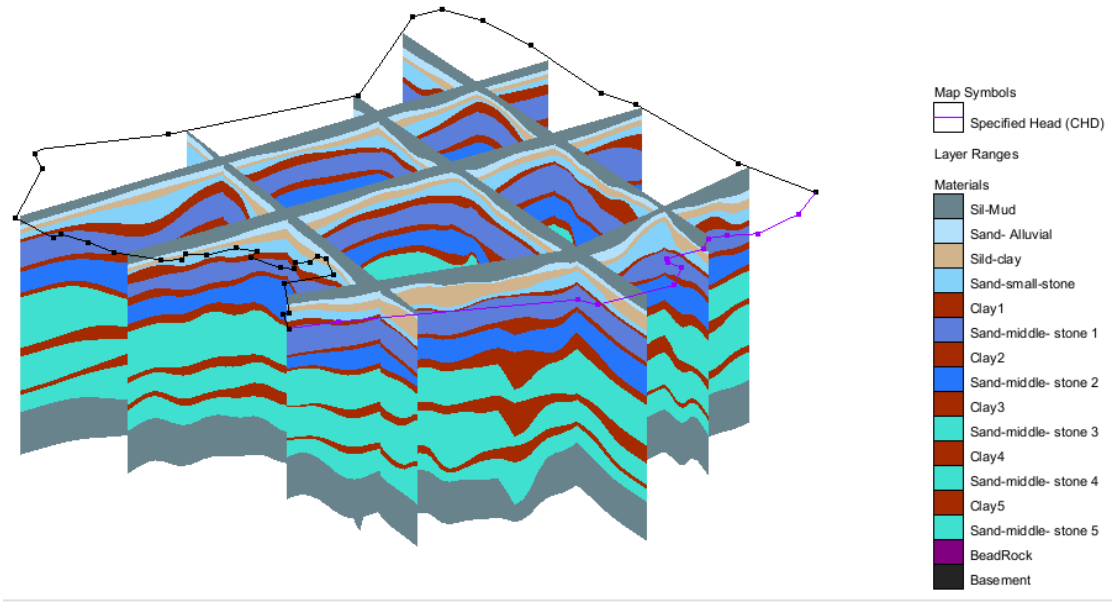

Figure 8- 5: Soil stratigraphy model based on hydrogeological boreholes.

We used hydrogeological boreholes data to create a solid model interpolating the elevation data (bottom/top) of each layer for the numerical model. In this area, most of the extraction wells were located in the upper, middle and lower Pleistocene aquifers which the depth of well ranging from 40- 160m (DONREs, 2012). Besides, some of the production wells from the upper Miocene aquifer. Groundwater flow and solute transport were simulated for major aquifers to understand the influences of pumping activity on groundwater flow system,

8.3.3. Model Domain and Discretization

The groundwater model consists of a grid size of 200 × 200 cells with 15 layers, as shown in Figure 8-4. Because the input layers to build a conceptual model were in different grid sizes and different coordinate systems, the Arc GIS 10.3 was used to reprocess the data. Then, the GIS tool package in Aquaveo GMS 10.4 version was used to input ArcGIS files into the model. In this study, the simulation of groundwater flow and solute transportation based on the monthly interval input datasets such as groundwater level, rainfall, recharge and pumping capacity.

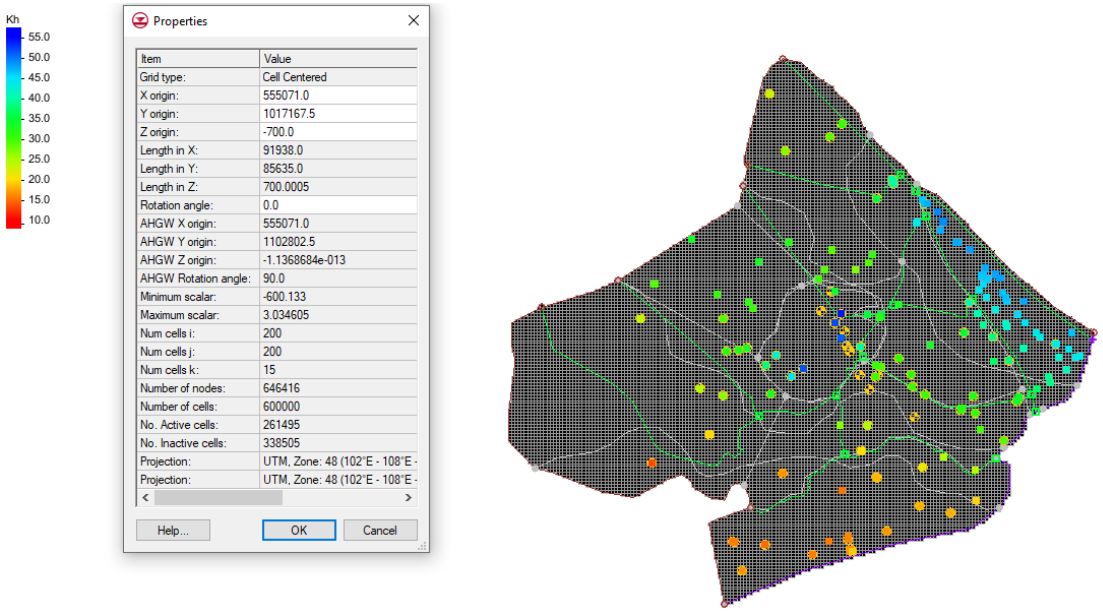

Figure 8- 6: The grid information of groundwater model in the study area.

8.3.4. Initial Conditions

Identifying initial conditions is one of the essential steps for groundwater modelling. Based on the literature review and historical data, the groundwater monitoring began in January 1994. However, between 1994 to 2000, the groundwater level at monitoring well has not changed significantly because the groundwater extraction rate was still low. In addition to this, the available pumping capacity has been measured since the 2000s which could use to simulate the influences of pumping on groundwater flow in the study area. Hence, in this study, all subsequent simulations were started from January 2000 as the initial condition.

8.3.5. Boundary Conditions

In groundwater modelling, boundary conditions in the simulated area must be given. The boundary conditions in this model are defined as specified heads and head-dependent flux for the model domain, while the sea area is defined as constant head equal to the average sea level of 0.0 m (Figure 8-5). The previous studies showed that river and canal system in the Mekong Delta connects to the shallow aquifer (Holocene) while deep aquifers may not have a direct connection to the surface water system(H. T. Hoang & Bäumle, 2019). For Holocene aquifer, therefore, river and canal system was assigned as head-dependent flux. The cross-section of the rivers and canals in the study area was provided by the Department of Science and International Collaboration, Thuyloi University, 2nd Base Ho Chi Minh City. The Cauchy's equation was used in the Aquaveo GMS model to estimate flux into the aquifer,

8.3.6. Hydrogeological data

Hydraulic parameters for each aquifer were selected based on the hydrogeological test from several boreholes in the Soc Trang province from DWRPIS and synthesized data from previous studies (Boehmer, 2000; Hung Van et al., 2019; Nam, Goto, & Osawa, 2017; Shrestha et al., 2016). The assigned hydrogeological parameters for each aquifer in the study area was shown in Table 8-1 as below.

Table 8- 1: The input hydrogeological parameters for each aquifer in the study area.

Aquifers		Kh (m/d)	Kv (m/d)	Ss (1/m)	Sy	Porosity	ΔH	Recharge rate (m/d)
2nd	qp_3	25	2.5	0.0004	1.82E-03	0.3	0.52	2.59E-06
3rd	qp_{23}	18.6	1.9	0.0007	1.76E-03	0.3	0.47	2.27E-06
4th	qp_1	25	2.5	1E-05	1.29E-03	0.3	0.47	1.66E-06
7th	n_{13}	9.4	0.9	0.0001	1.83E-03	0.3	0.33	1.65E-06

8.3.7. Groundwater extraction data

Groundwater level observation data showed that over the last two decades groundwater level in the study has significantly depleted mainly because of intensive pumping activities. According to a report by DWRPIS (2010), Soc Trang province has over 85,000 of extraction wells including small well owned by households and production well from Center for Rural Water Supply and Sanitation of Soc Trang

(CRWSSST) and Soc Trang Water Supply Company (STRAWACO). Most of production well (> 200 m3/d) locates in the small town and cities where use the majority groundwater exploitation for drinking and industrial development. Also, groundwater is used for irrigation system, especially along the coastal area. The groundwater extraction capacity for domestic and industrial consumption was collected from CRWSSST, STRAWACO and households. Meanwhile, groundwater extraction for agricultural purposes was based on the area of plants, fishery and cultivation calendar. The total groundwater consumption in the study area was approximately 165,000 m3/d in 2017.

8.3.8. Recharge rate

Recharge rate is vital for groundwater modelling. However, estimation of this parameter requires the various type of data related to hydraulic properties of topsoil layers, surface water system, rainfall, surface temperature, and land use. The estimation of recharge in the Mekong aquifer system ranges from 0.01 mm/d to 1 mm/d (Boehmer, 2000; Shrestha et al., 2016). Due to the data sparsity in this study, the recharge rate was estimated using water table fluctuation (WTF) method (Hung Vu & Merkel, 2019; Varni, Comas, Weinzettel, & Dietrich, 2013; L. Yang et al., 2018). The WTF method is based on the assumption that rises in groundwater level are due to recharge water arriving at the water table (Figure 8-7).

Although this method has some limitations, it has been widely used to estimate recharge rate into aquifers. In the study area, the primary recharge source into the Holocene aquifer could be rainfall and surface water while deep aquifers may be recharged by vertical flow rate from upper layers or rainfall from high elevation areas. Annual average rainfall in Soc Trang province is around 1,800 mm (DONREs, 2012). The rainfall and groundwater level data between 2000 and 2016 were used to estimate recharge rate into the aquifer system following the equation as below:

$$R_{gw} = \frac{S_y \times \Delta H}{\Delta t} \qquad (8\text{-}2)$$

Where R_{gw} is recharge rate to the aquifer, Sy is a specific yield, ΔH is the change in groundwater table height over the time interval, Δt (month). The estimation of average recharge in each aquifer was shown in table 8-1.

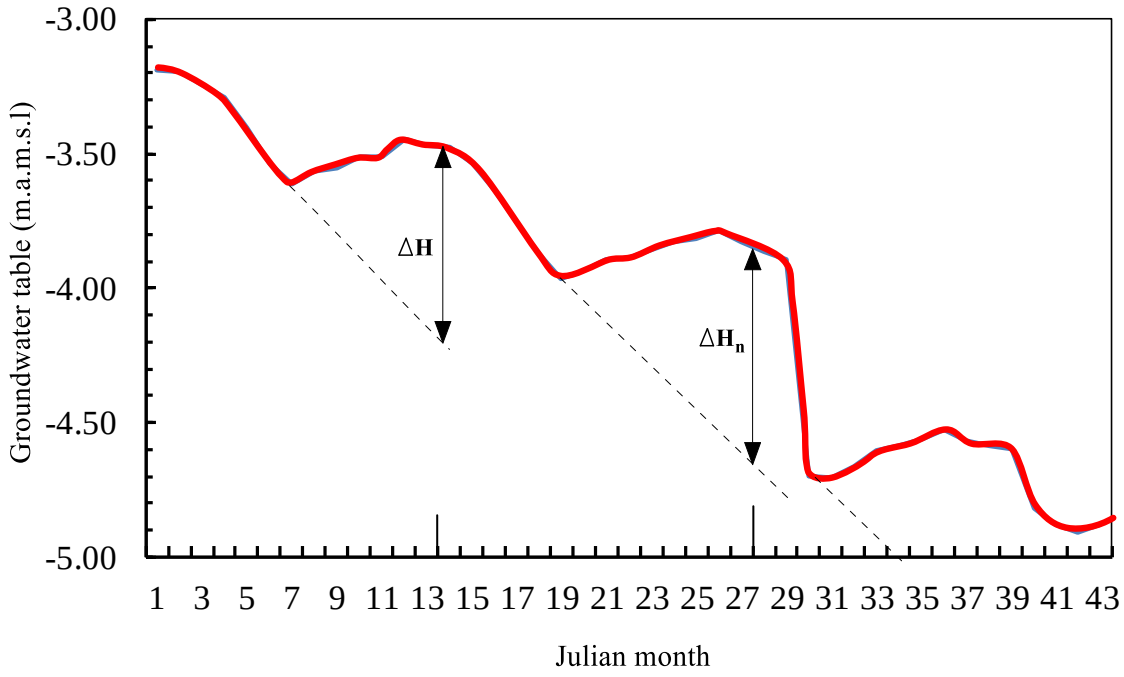

Figure 8- 7: Hypothetical groundwater hydrograph showing groundwater level rise in observation wells response to rainfall recharge for shallow aquifers and infiltration for deep aquifers. ΔHis equal to the difference between the peak of the rise and low point of the extrapolated antecedent recession curve (dashed line) at the time of the peak (adopted based on (Healy & Cook, 2002)).

8.3.3. Evaporation rate

The evaporation in the model is estimated for shallow aquifer based on the assumption that shallow aquifer may occur evaporation processes under a given climatic condition while deep aquifers are not influenced by evaporation processes. To estimate evaporation rate from a shallow aquifer, the average open pan evaporation (ETO) and the depth to the GW level were input into the Aquaveo GMS 4.6 model.

8.4. Model Calibration and Validation Process

8.4.1. Calibration procedures

Model calibration is an essential step in groundwater modelling, during calibration the input parameters were adjusted, so that computed groundwater levels get a good agreement with observation data and hydrological sense of groundwater flow system in the study. The groundwater level was collected and synthesized from different monitoring system including Department of Natural Resources and Environment of Soc Trang province, National monitoring system (DWRIPS, 2017), and on-site measured groundwater levels between 2013 and 2018. The steady condition was calibrated using groundwater levels measured in dry season March 2017 at the study area while the transient simulation was calibrated and validated using monthly groundwater levels between 2000-2016. The general calibration procedure was presented in Figure 8-8 as below.

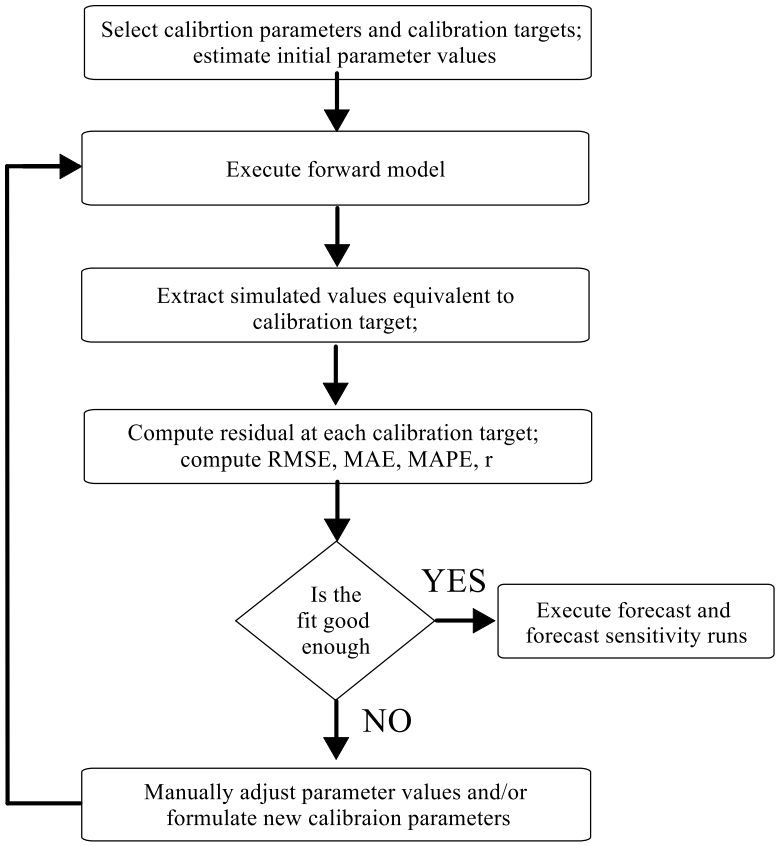

Figure 8- 8: Flowchart showing the manual trial and error calibration procedure (M. P. Anderson, Woessner, & Hunt, 2015)

The calibrated model was obtained when the difference between measured and computed groundwater levels was minimized. In this study, calibration for steady transient state condition was conducted through a trial and error process, in which the initial estimates hydraulic conductivities and storage coefficients of the aquifer system were iteratively adjusted over reasonable ranges to improve the match between simulated and observed GW levels (Figure 8-8). Calibration was carried out for the long-term observation wells for the period from 2000 to 2012 while validation was tested between 2013-2016. The model was calibrated by adjusting pumping rates of abstraction wells and recharge rates in wet and dry periods.

8.4.2. Evaluation of model forecasting

To construct an accuracy groundwater model for future projection, we estimate the monthly hydraulic head values for both steady and unsteady conditions. The stable simulation was conducted for Pleistocene (Upper, Middle and Lower) and Miocene (Upper) aquifers for in dry season March 2017 while the unsteady condition was performed only for middle Pleistocene aquifer which is the most crucial groundwater extraction aquifer for Soc Trang province. The computed hydraulic heads are compared with the measured groundwater levels from 136 wells for steady simulation and ones in 36 piezometric wells for the transient condition. The results of groundwater model simulation is assessed using root mean square error (RMSE), index of agreement (d), and the Nash-Sutcliffe (NSE) which are commonly used in many previous studies (Karimi, Motagh, & Entezam, 2019; Matiatos, Varouchakis, & Papadopoulou, 2019; Mustafa et al., 2019; Willmott, Robeson, & Matsuura, 2012).

$$RMSE = \sqrt{\frac{\sum_{t=1}^{n}(H_i^{obs} - H_i^{pr})^2}{n}} \quad (3)$$

$$NSE = 1 - \left[\frac{\sum_{i=1}^{n}(H_i^{obs} - H_i^{pr})^2}{\sum_{i=1}^{n}(H_i^{obs} - H_{mean}^{obs})^2}\right] \quad (4)$$

$$d = 1 - \left[\frac{\sum_{i=1}^{n}(H_i^{obs} - H_i^{pr})^2}{\sum_{i=1}^{n}(|H_i^{obs} - H_{mean}^{obs}| + |H_i^{obs} - H_i^{pr}|)^2}\right] \quad (5)$$

where H_i^{obs} and H_i^{pr} are measured and predicted hydraulic head in observation i, and n is the number of observations. The RMSE is always non-negative, and a value closer to zero indicates a more accurate model. NSE ranges from minus infinity to 1.0, with higher values indicating that the proposed model gets more accuracy. The index of agreement varies from 0.0 to 1.0 with a value closer to 1.0, indicating the better model performances (Mustafa et al., 2019).

8.4.3. Scenario setting for model application

In the study area, deep groundwater aquifers (Pleistocene and Upper Miocene aquifers) have very long resident time which means that the recharge into these aquifers may not strongly influence on groundwater flow in short period compared to their age. Meanwhile, based on groundwater level monitoring, groundwater exploitation has strongly affected on groundwater flow system. Therefore, we consider pumping activities and regional groundwater levels are two main factors affecting the groundwater flow dynamics in the deep aquifers. In the study area, over 80% amount of total pumping capacity derives from the Middle Pleistocene aquifer (qp_{23}). During the last two decades, a large number of GW abstraction wells have been installed in this aquifer (DONREs, 2012). For sustainable GW management planning, the future scenarios are needed to find out the most appropriate solutions by considering both local and regional influencing factors. To obtain these objectives, different scenarios were established by considering influencing by local and regional groundwater exploitation between 2017 and 2030. As an essential aquifer for groundwater supply in the study area, Middle Pleistocene aquifer (qp_{23}) was selected to project influences of future groundwater consumption and changes in regional groundwater levels. For this purpose, seven different scenarios were created and simulated, as shown in

Table 8-2 in which scenario 3 (SN3) is an extreme scenario which presents to the maximum increase of pumping capacity in this study area. SN1, SN2 and SN3 will be used to assess influences of groundwater level depletion on groundwater salinization.

Table 8- 2: Groundwater extraction scenarios (SN) for future pumping capacity and regional groundwater levels in 2030.

3rd Aquifer	Pumping Capacity (Q m3/d)	Regional GWL (m.a.m.s.l)	Note
SN1	+1%Q/year	-12.5	
SN2	+5%Q/year	-12.5	
SN3	+20%Q/year	-12.5	Extreme Scenario
SN4	+1%Q/year	-7.5	
SN5	+5%Q/year	-7.5	
SN6	-1%Q/year	-7.5	
SN7	-5%Q/year	-7.5	

8.5. Result and Discussion

8.5.1 Groundwater levels variation

The results of the model calibration for steady and transient simulation were shown in Tables 8-2, Figure 8-9 and Figure 8-11. For steady condition, calibration model performance (Table 8-2) for four main aquifers shows a good reproduction of groundwater levels in the dry season in March 2017. Accordingly, aquifer n_{13} has the best simulation with the lowest value RMSE = 0.42 m, followed by the qp_3, qp_{23} (RMSE=0.53m) and qp_1 (RMSE=0.56 m). The similar trend is also observed in NSE and d for aquifer n_{13} (NSE=0.67, d=0.87), qp_{23} (NSE=0.87, d= 0.91), qp_3 (NSE=0.25, d=0.77) and qp_1 (NSE=0.72, d=0.86). These results indicated that the constructed model for qp_{23} and qp_1 are good for future projection. The calibration results for aquifer qp_3 obtained the lowest value of NSE =0.25 may be due to the lack of observation groundwater levels in the study area. The groundwater in dry season for

four main aquifers showed that groundwater levels have significant depletion in the large groundwater exploitation areas such as in the central and coastal parts of the study area (Figure 8-10).

Table 8- 3: The result of model evaluation for the prefer aquifers in the study area at the steady condition.

Parameter	Aquifer qp_3	Aquifer qp_{23}	Aquifer qp_1	Aquifer n_{13}
RMSE	0.53	0.53	0.56	0.42
NSE	0.25	0.87	0.72	0.67
d	0.77	0.91	0.86	0.84
N- samples	4	73	39	20

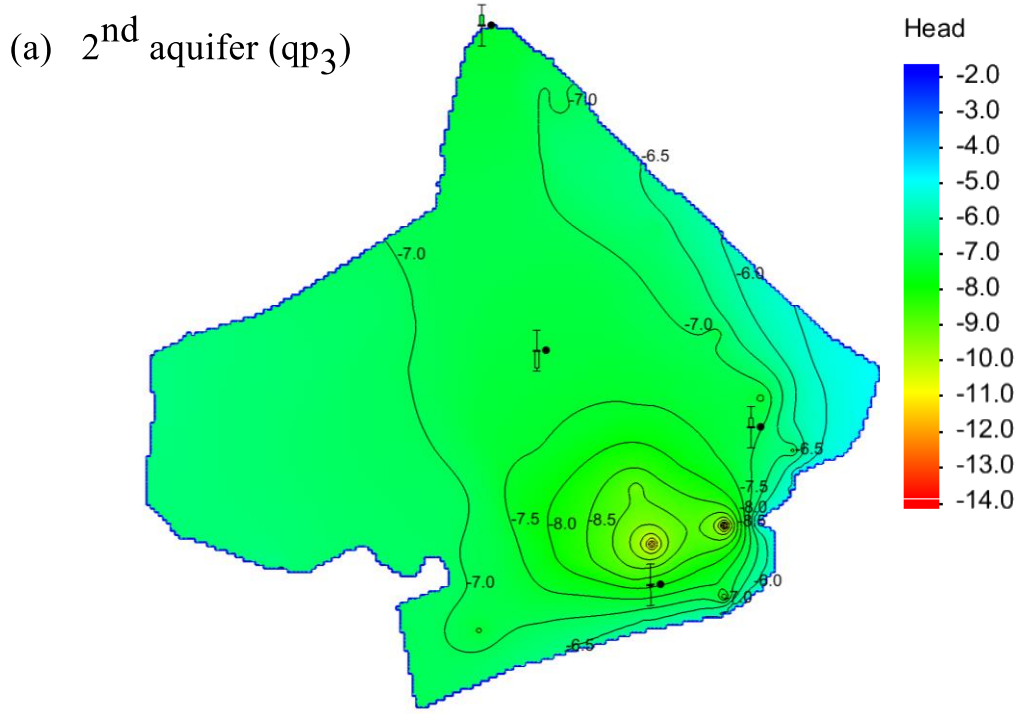

(b) 3rd aquifer (qp_{23})

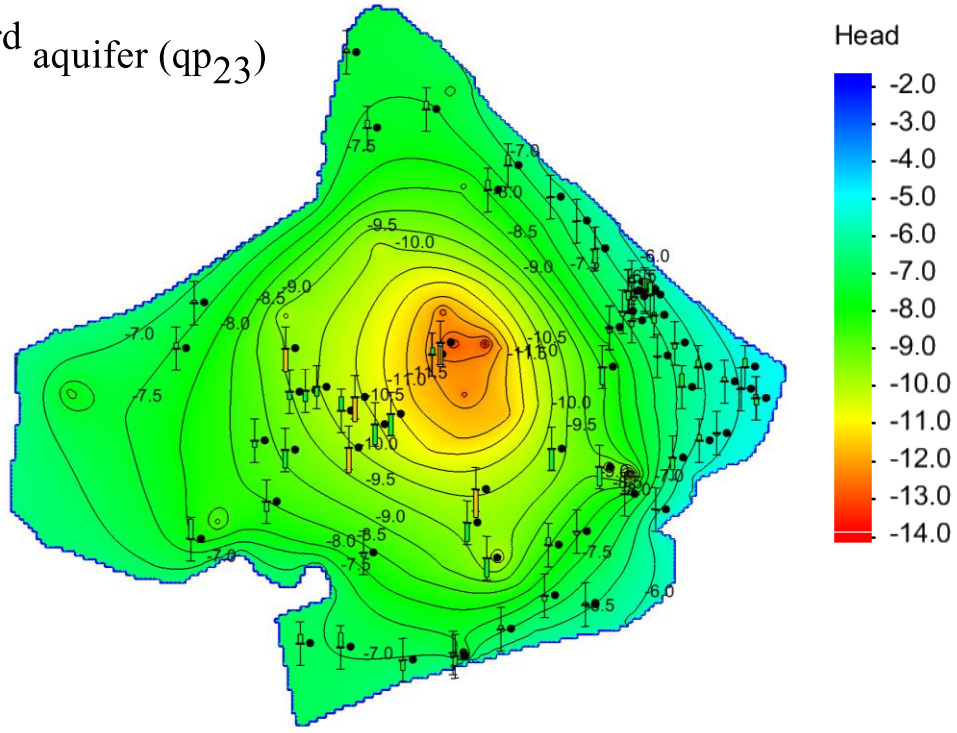

(c) 4th aquifer (qp_1)

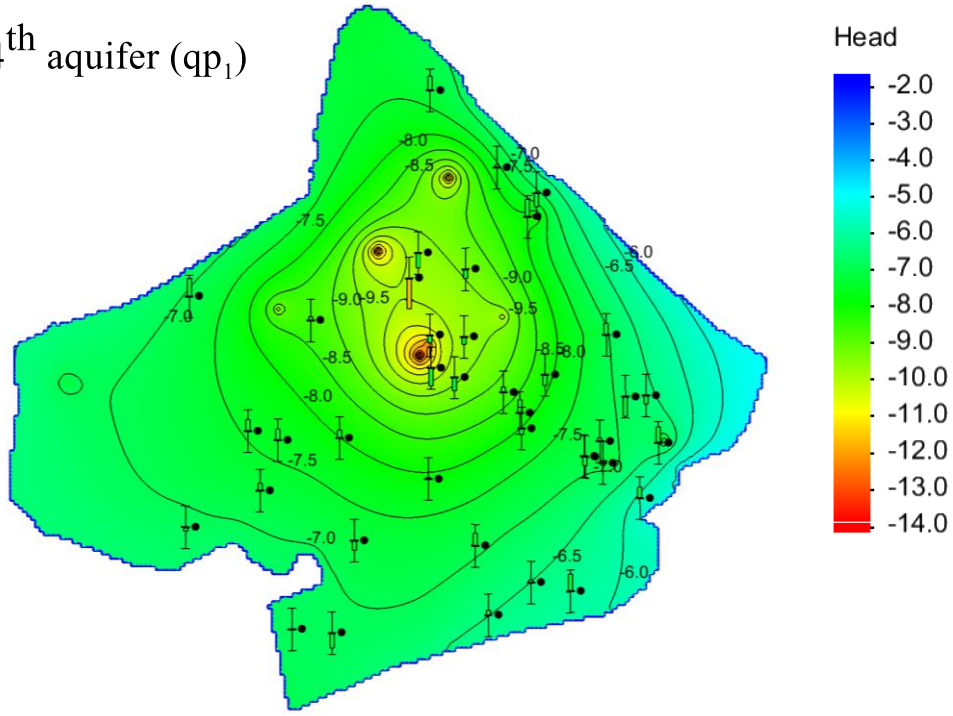

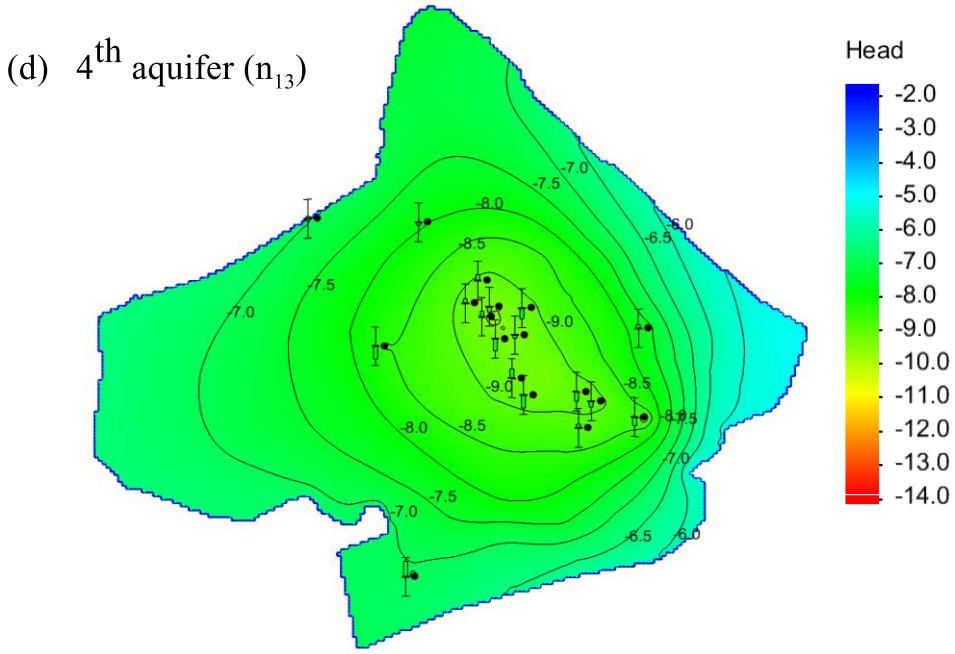

Figure 8- 9: Calibration result for the steady condition at **a.** Upper Pleistocene aquifer (qp_3), **b.** Middle Pleistocene aquifer(qp_{23}), **c.** Lower Pleistocene aquifer(qp_1), and **d.** Upper Miocene aquifer(n_{13}).

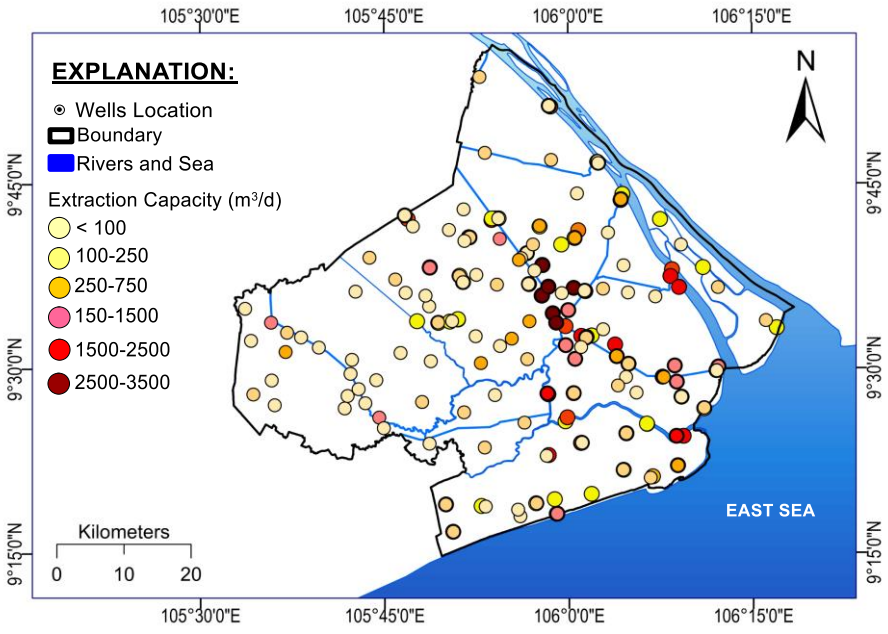

Figure 8- 10: Spatial distribution of pumping capacity in the study area in the dry season, March 2017.

For transient calibration between 2000-2016, we focused on the Middle Pleistocene aquifer (qp_{23}), which is the most important in the study area. The calibration results were presented in Figure 8-10.

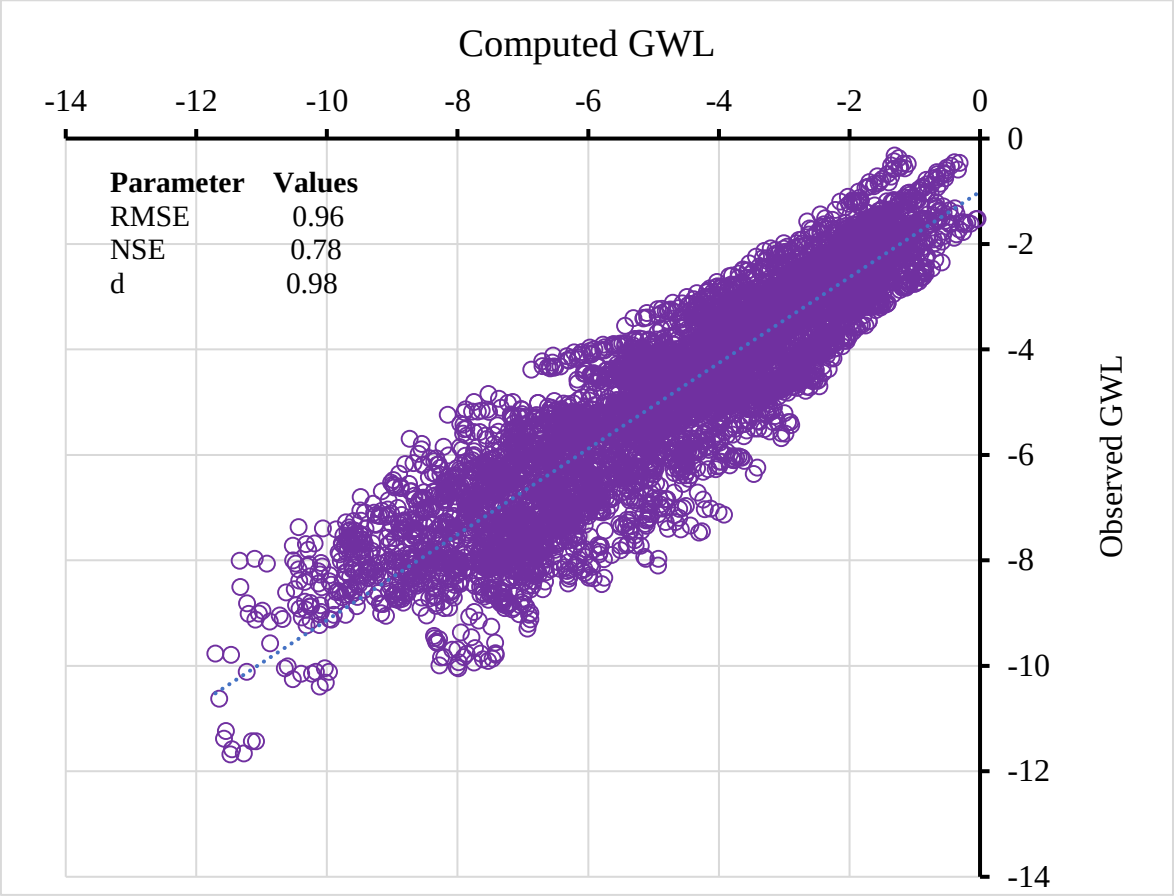

Figure 8- 11: Calibration result for the transient condition at Pleistocene aquifer (qp_{23}) between 2000-2016.

The results of model performance showed that RMSE has a very high value (0.98). It indicated the computed and observed monthly groundwater between 2000-2016 have a good agreement with the index of agreement (d) was at 0.98 and Nash-Sutcliffe coefficient of efficiency (NSE=0.78).

8.5.2. Influences of groundwater pumping on groundwater levels

The results showed that in the condition of increase 1%Q/year, the groundwater levels in the study area reach a maximum of -18.0 m.a.m.s.l (Figure 8-12a). The highest depression areas located in the central and coastal cities where have high pumping capacity. Similarly, an increase of 5%Q/year until 2030 may cause significant groundwater level depletion with the maximum of -25.0 m.a.m.s.l in the central area and approximately -20 m.a.m.s.l in coastal towns such as Tran De and Vinh Chau (Figure 8-12b). However, in case of reducing groundwater pumping capacity of 1% and 5%Q/year until 2030 groundwater levels in the study area will recovery remarkably even regional groundwater level in the Mekong Delta continues to decrease and reach the maximum of -12.5 in 2030.

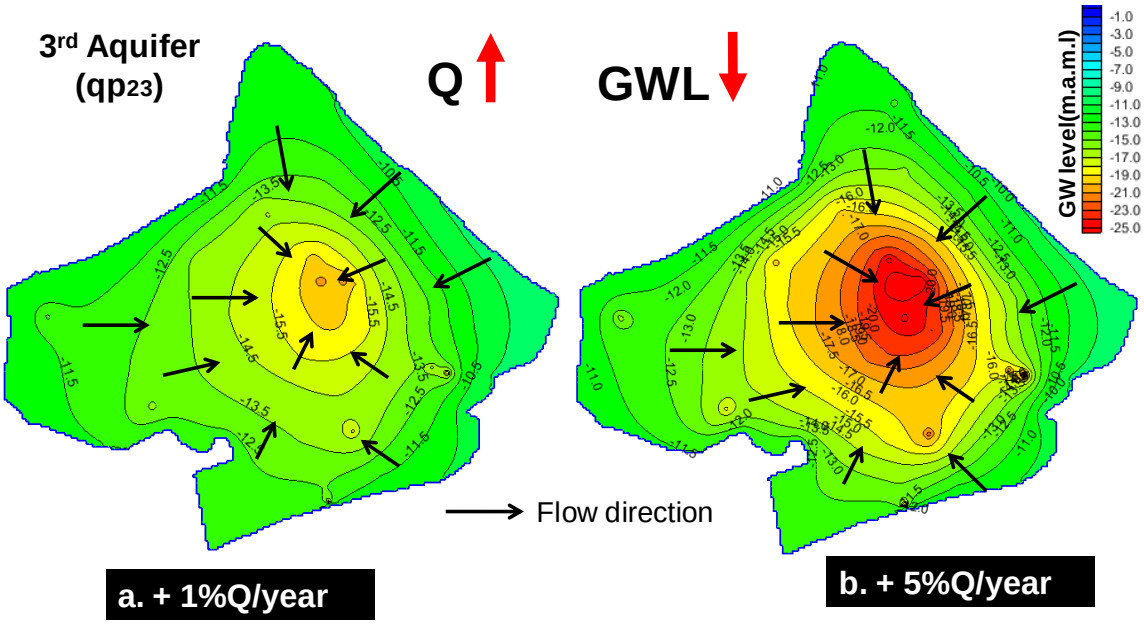

Figure 8- 12: Prediction of groundwater levels in 2030, **a.** SN1 (increase 1% Q) and **b.** SN2 (an increase of 5% Q annually) with continuing groundwater levels depletion (-12.5) in the boundary.

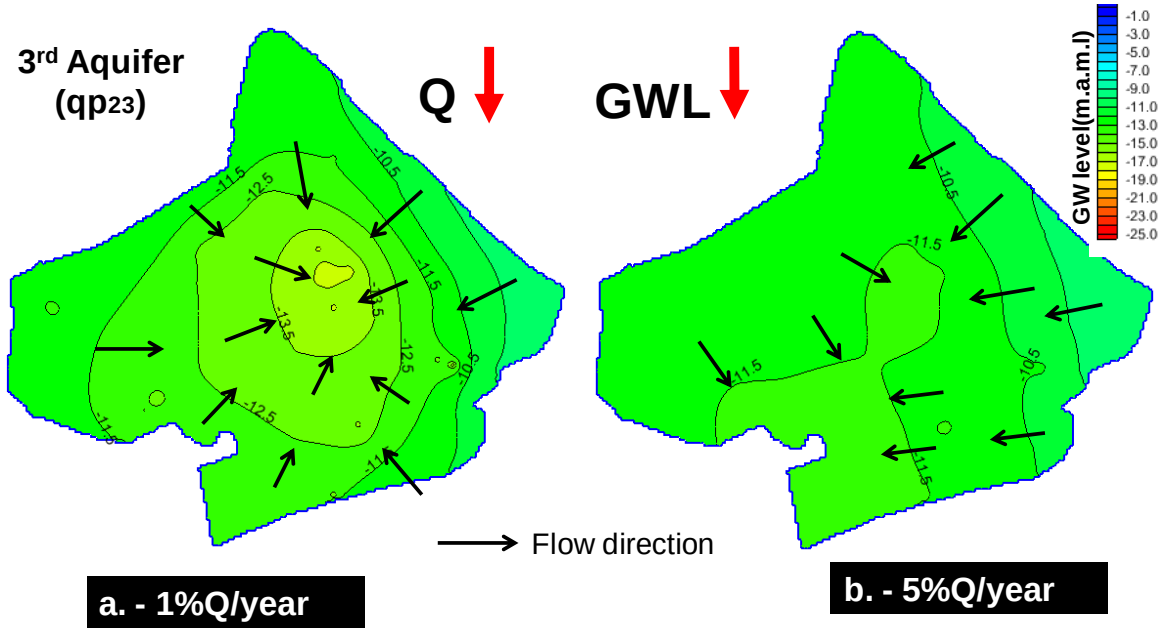

Figure 8- 13: Prediction of groundwater levels in 2030, **a.** SN4 (reduce 1% Q/year) and **b.** SN5 (reduce 5% Q/year) with keeping stable groundwater level at -7.5 m.a.m.s.l in the boundary.

As shown in the Figure 8-13, the groundwater level may decrease slowly and reach to maximum depletion of -16.0 m.a.m.s.l and -11.5 m.a.m.s.l in case of decreasing 1% and 5% Q/year. Interestingly, the depression area might disappear from the central area where pumping capacity will be decreased significantly until 2030. Also, groundwater levels in the study area are not only influenced by local pumping activities but also regional groundwater flow dynamics. To understand how local pumping activities and regional groundwater flow effect on groundwater flow dynamics in the coastal area, the scenario of reducing local pumping rate and stabilisation of head boundary was setup. The results showed that local pumping reduction combined with keeping stable groundwater levels in the surrounding area would result in significant groundwater level recovery in the study area. The maximum depletion of groundwater levels in the study area reach to -9.5 ma.m.s.l for reducing 1%Q/year (Figure 8-14a) and -6.5 ma.m.s.l for reducing 5%Q/year (Figure 8-14b). Surprisingly, the depression area will be disappeared in 2030 if we could reduce 5%Q/year

together with keeping groundwater levels in the surrounding at the level of March 2017 (-7.5 m.a.m.s.l).

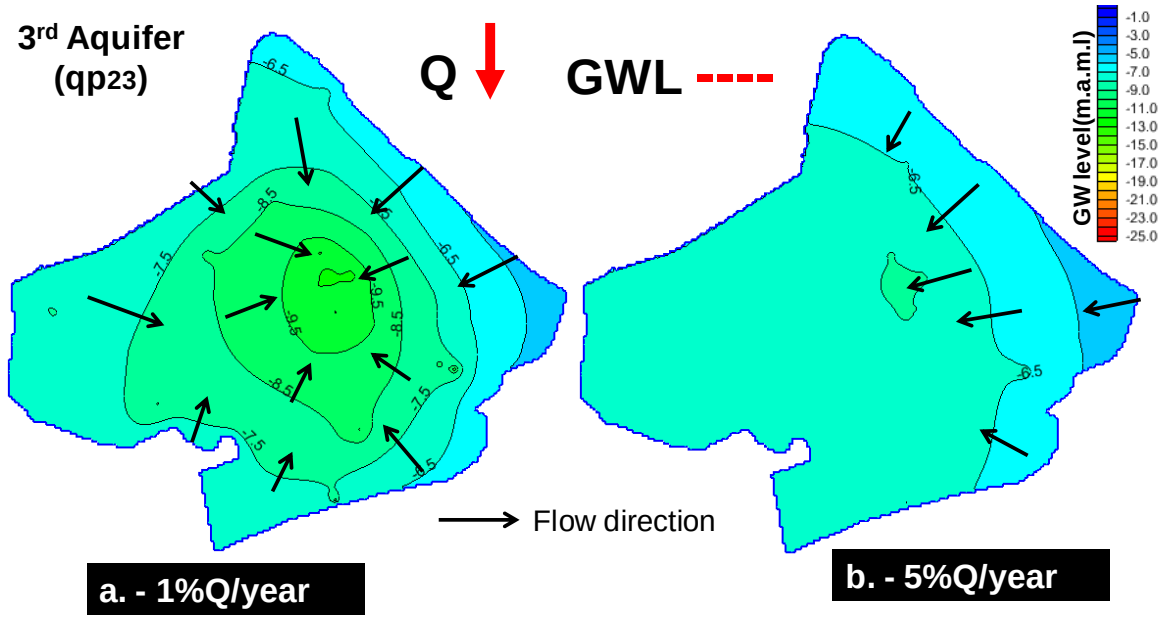

Figure 8- 14: Prediction of groundwater levels in 2030, **a.** SN6 (reduce 1% Q/year) and **b.** SN7 (reduce 5% Q/year) with keeping stable groundwater level at -7.5 m.a.m.s.l in the boundary.

These results may indicate that pumping activities have a strong influence on groundwater level depletion in coastal lowland aquifers where groundwater flow dynamics are strongly controlled by groundwater exploitation.

8.5.3. Influences of groundwater pumping on groundwater salinization

Many previous showed processes of seawater intrusion into coastal aquifers are very complex and depending on many influencing factors (Werner et al., 2013). In coastal lowland regions, significant groundwater level depletion in one of the most influencing factors controlling processes of saltwater immigrating in fresh aquifers (Sherif, Sefelnasr, & Javadi, 2012). The Mekong Delta is a flat and lowland region with elevation ranging from +0.5 to maximum +3.0 above mean sea level and the aquifer system consists of multi-mixed and discontinuous layers. These characteristics of the MD coupled with rapid sea-level rise started in the last maximum glacial resulted in a heterogeneous distribution of saltwater in different layers in the MD, especially high salinity in Holocene and Upper Pleistocene aquifers(Hung Van et al., 2019). Due to significant groundwater level depletion in deeper

aquifers, mainly in Middle and Lower Pleistocene aquifers, vertical movement of saltwater from shallow to deeper aquifer has been occurring faster than natural processes. The vertical salinity movement is due to solute differences between the upper and lower aquifers. Additionally, significant groundwater drawdown will increase the hydraulic gradient among layers contributing to more saline sources moving down. Figure 8-15 presented the simulation of salinity transportation caused by different scenarios of groundwater exploitation. Accordingly, if groundwater pumping capacity increases around 1% per year (SN1) will cause groundwater drawdown at -15.5 m.a.m.s.l but will not strongly influence to vertical saline groundwater moving deeper. However, if pumping capacity increase 5% (SN2) and 20% per year (SN3) will cause reaching to -24.5 and -35.0 m.a.m.s.l, respectively. As a result, saline groundwater will expand vertically until 100 (SN2) to 150m (SN3) downward with the highest concentration around 2000 mg/L.

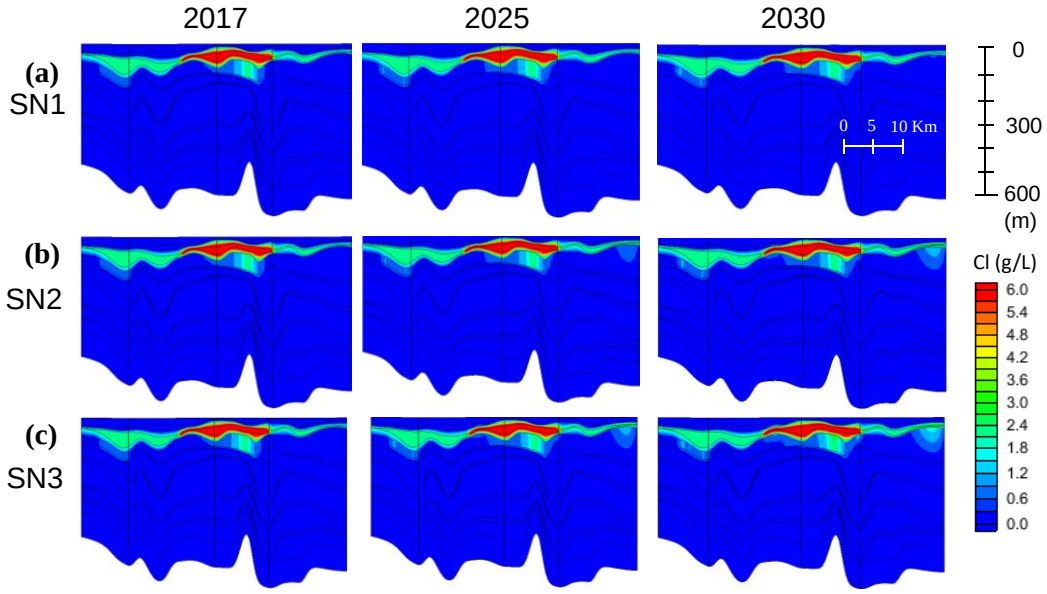

Figure 8- 15: Prediction of chloride concentration in 3rd and 4th aquifers from 2017 to 2030, **a.** SN1 (increase 1% Q/year), **b.** SN2 (increase 5% Q/year), and c**.** SN3 (increase 20% Q/year).

Therefore, if the authorities do not take any action to reduce groundwater pumping, the aquifers in this region will be at high risk of salinizarion.

8.6. Conclusion

Groundwater overexploitation has been occurred in many regions in Vietnam and continuing pumping out groundwater from aquifers will eventually cause water crisis, especially in coastal lowland areas. In this study, mudflow and seawater packages in the Aquaveo GMS 10.4.6 model were successfully built to examine influences of pumping activities and regional flow on groundwater flow dynamics in coastal aquifers of the MD, Vietnam. Groundwater levels in the study area were reproduced by simulating groundwater levels variation between 2000 and 2016 for transient condition and groundwater levels in March 2017 for the steady condition. The results showed good agreement between observed and computed groundwater levels with RMSE values ranging from 0.42 to 0.56 m and NSE values were over 0.70 for both steady and transient simulations. The influences of pumping activities on groundwater flow dynamics and salinization processes summarized as follows:

- Groundwater model could help to produce a reliable groundwater flow dynamics in the coastal area of the Mekong Delta under influences of pumping activities.
- Increasing groundwater pumping capacity less than 1% per year (SN1) will not cause significant groundwater level depletion and vertical saline groundwater movement. Conversely, increasing pumping capacity up to 20%Q/year (SN3) will create a remarkable groundwater level drawdown (-35.0 m.a.m.s.l) and severely vertical saline groundwater movement until 150 m in deeper aquifers.
- The simulation also illustrates that cutting of 1% (SN1) and 5%Q/year (SN2) will reduce groundwater level depletion with the maximum groundwater levels in the central area at -11.5 and -16 m.a.m.s.l, respectively.

Therefore, to prevent groundwater level depletion and groundwater salinization it is better to keep an increase of groundwater pumping capacity per lower than 1% per year until to 2030 coupled with stabilizing of regional groundwater level at -7.5 m.a.s.l.

CHAPTER 9 GENERAL DISCUSSION

9.1. Hydrogeochemical evolution

Hydrogeochemical data of groundwater samples in the study area showed unclearly seasonal variation but having different water facies ranging from freshwater Ca-HCO3, mixed water types (Na-Mg-Ca-HCO3, Na-Mg-Ca-HCO3-SO4 and Na-HCO3-Cl), Na–HCO3 and Na-Cl (Figure 9-1).

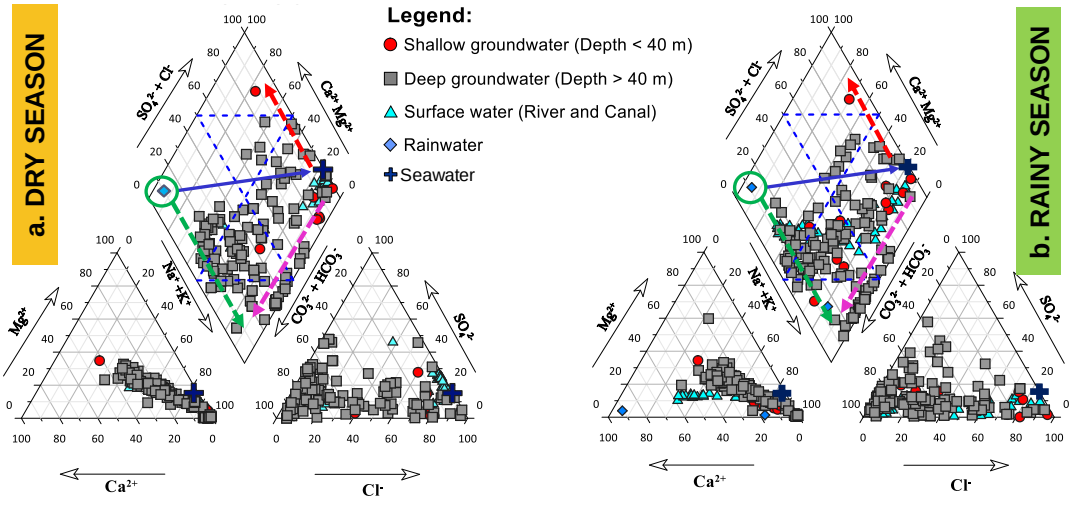

Figure 9- 1: Piper diagrams show the water facies classification and geochemical evolution in coastal aquifers of the Mekong Delta **a.** dry season, **b.** rainy season.

High salinity in central parts of the study area may indicate influences of mixing with saltwater maybe because of seawater intrusion directly from the sea and leaching paleo-seawater trapped in sediment, and especially leaking saline from upper to lower layers. In contrast, low salinity in groundwater may originate from rainfall/freshwater with fewer influences of mixing with seawater (Figure 9-2). This fact indicated that groundwater in this study area experienced different processes of recharge, mixing with seawater and mineral dissolution which also found elsewhere (Beaudry, Lefebvre, Rivard, & Cloutier, 2018; Mohanty & Rao, 2019).

Firstly, most of the groundwater samples from shallow aquifers (Holocene and Upper Pleistocene) classified mainly into Na-Cl water type. Additionally, groundwater samples from these aquifers have the heterogeneous distribution of chloride and stable isotopes indicating mixing with seawater through different pathways. Moreover, seawater intrusion into freshwater aquifers has caused transferring Ca-HCO3 to Na-Cl face. Notably, some groundwater samples along the coast have extraordinarily high salinity (> 10,000 mg/L) and

more enrichment of $\delta^{18}O$ (> -2.0‰) that may attribute to mixing directly with seawater during global sea-level rise starting from Late Glacial Maximum Period (Khaska et al., 2013a; Larsen et al., 2017c; Ya Wang & Jiao, 2012)(Figure 9-3.

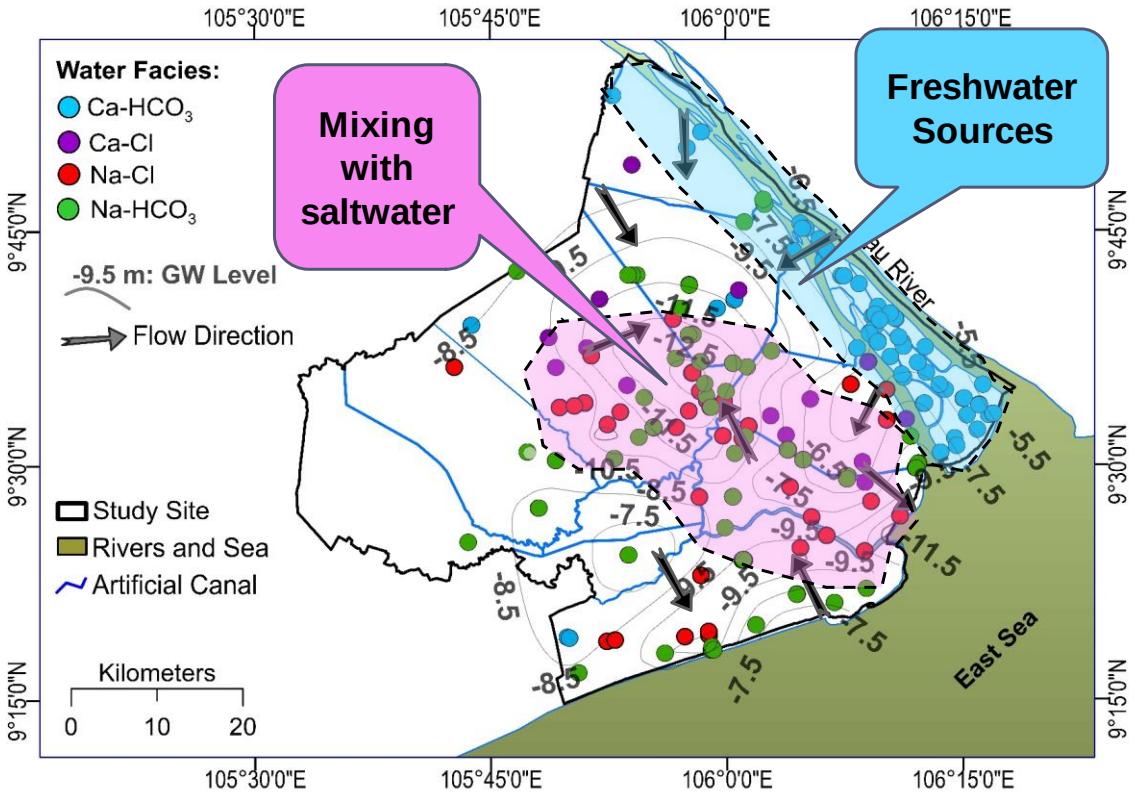

Figure 9- 2: Spatial distribution of groundwater types in coastal aquifers of the Mekong Delta, Vietnam.

Secondly, groundwater samples from deep aquifers have relatively high salinity (> 1000 mg/L) but do not enrich in $\delta^{18}O$ (<-6.0‰) indicates that leaching seawater trapped in the sediment layers may contribute to increasing salinity in these samples (Figure 9-4). Heterogeneous distribution of chloride and $\delta^{18}O$ may also reflect the spatial-temporal variation of seawater intrusion, recharge/infiltration rate, and leaching saline from clay/sediment layers. Likewise, previous studies demonstrated influences of coastal progradation and seawater intrusion into coastal aquifers of during the MD during the Holocene period (Hung Van et al., 2019; Ta et al., 2001). However, the leaching seawater trapped in sediments in coastal aquifers of the MD may have somewhat differences compared to other coastal aquifers in the world because of different climatic conditions, recharge rates and geological conditions, especially in arid and semi-arid regions. For example, Han et al., 2015 concluded that an increase of salinity in groundwater samples do

not accompany with heavier stable isotopes may reflect influences of evaporation processes (Han et al., 2015).

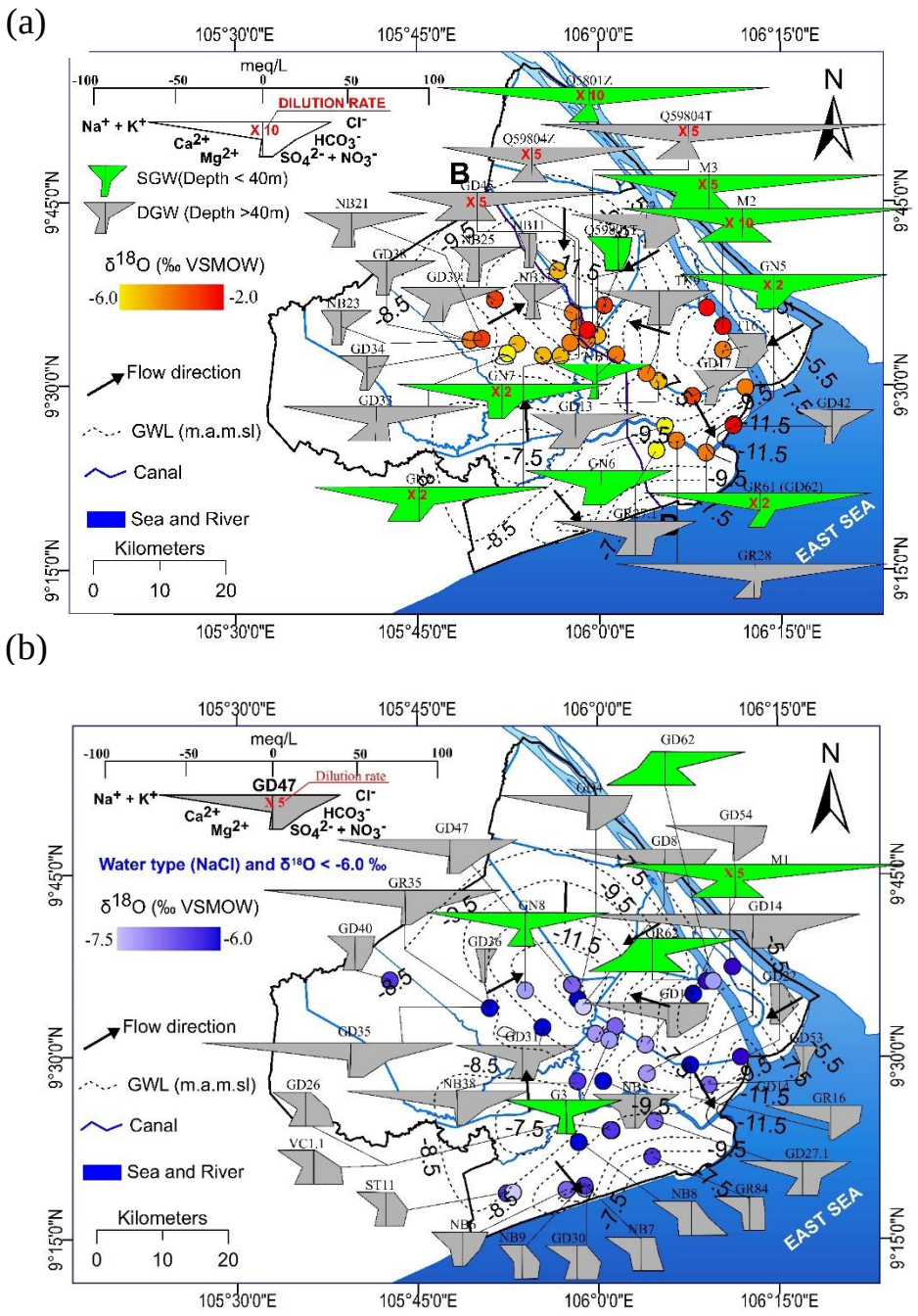

Figure 9- 3: Spatial distribution of Hexa diagram and $\delta^{18}O$ of groundwater samples in coastal aquifers of the Mekong Delta, Vietnam **a.** high salinity and heavy $\delta^{18}O$, **b.** high salinity and low $\delta^{18}O$.

Thirdly, the vertical flow system from upper to lower layers might occur due to increase chemical and hydraulic gradient between upper and lower aquifers. As shown in Figure 9-4, high salinity (> 10,000 mg/L) in shallow aquifers could move down through a

thin clay layer. This process was intensified by significant groundwater level depletion in the deep aquifers, especially in central parts of the study area.

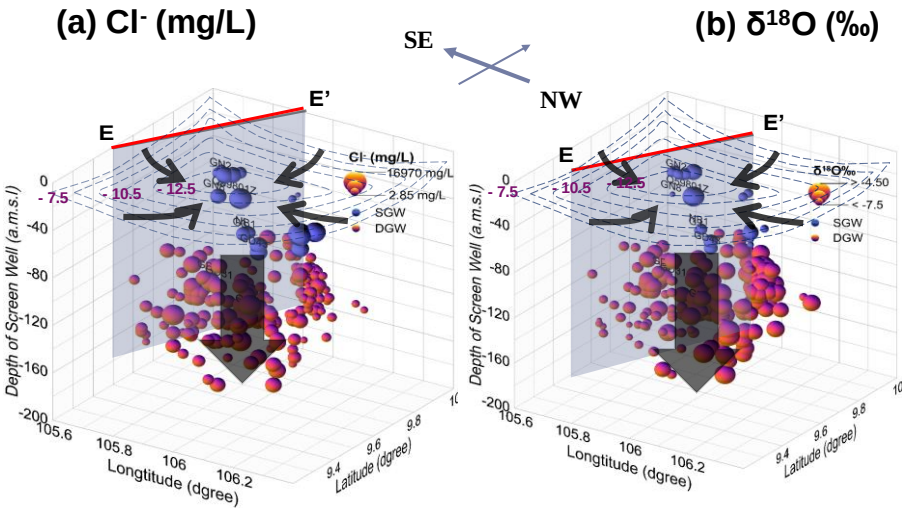

Figure 9- 4: 3D distribution of **a.** chloride and **b.** $\delta^{18}O$ of groundwater in coastal aquifers of the Mekong Delta, Vietnam.

Furthermore, a similar chemical and $\delta^{18}O$ data from two deep aquifers (qp_{23} and qp_1) showed that aquifer connection might occur in some locations where have discontinuous layers and significant groundwater level depletion (Figure 9-5).

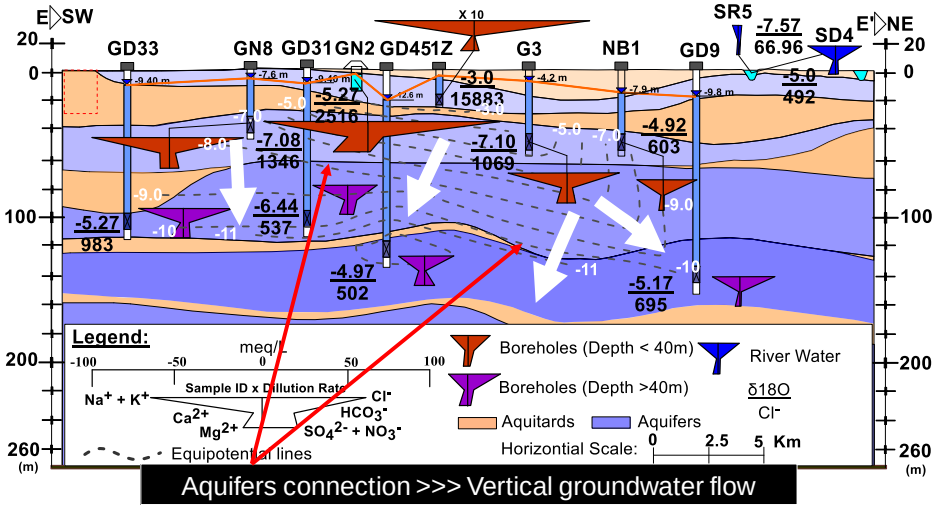

Figure 9- 5: Hydrogeological profile showing the spatial distribution of groundwater quality

In addition to seawater intrusion, mineral dissolution/precipitation and freshening aquifers are also main processes which control the geochemical evolution in coastal aquifers

worldwide (Argamasilla et al., 2017). In the coastal aquifers of the MD, saturation indexes of mineral phases such as aragonite, calcite, dolomite, and chalcedony showed nearly saturated to neutral in groundwater indicating different magnitudes of mineral dissolution and precipitation. An increase of Ca^{2+}, Mg^{2+}, HCO_3, and SiO_2 concentrations indicates influences of ion exchanges and silicate weathering, which formed mixed water types (Na-Mg-Ca-HCO3, Na-Mg-Ca-HCO3-SO4 and Na-HCO3-Cl) in most of the deep aquifers which are similar to other coastal low-lying regions in the world (D. Han & M. J. Currell, 2018; Kanagaraj et al., 2018; Sappa, Iacurto, Ferranti, & De Filippi, 2019). It is because groundwater travelled a very long distance from headwater to coastal regions which different processes of mineral dissolution and precipitation.

Moreover, the Na-Cl changes through Na-SO4-HCO3 to Na-HCO3, indicating freshening aquifers occurred in deep aquifers. This process occurred naturally in coastal regions when more freshwater from headwater was recharged and move to deeper aquifers. The freshwater replaces saltwater in saline aquifers resulting in more freshwater in these aquifers. Depending on the magnitudes of freshening and resident time, groundwater in these aquifers may form as Na-HCO3-Cl to Na-HCO3 or even mixed freshwater Na-Ca-Mg-HCO3. However, the primary process of freshening aquifer could be explained as the following equation.

$$Na^{+} + \frac{1}{2}Ca - X_2 \rightarrow Na - X + \frac{1}{2}Ca^{2+} \quad (9-1)$$

9.2. Origin of groundwater

The stable isotopes ($\delta^{18}O$ and $\delta^{2}H$) values of groundwater from coastal aquifers of the MD varied from -8.5‰ to -2.0‰ and from -60‰ to -9.0‰ showing the relationship between $\delta^{18}O$ and $\delta^{2}H$ of groundwater samples in comparison to Global and Local Meteoric Water Line (GMWL and LMWL) (Figure 9-6). The isotopes data of groundwater samples deviate at lower slope compared to the LMWL which indicates that groundwater from the study area organed from rainfall and then it was either affected by seawater or experienced evaporation before recharging into aquifers. On the one hand, deep groundwater samples have lower stable isotopes ($\delta^{18}O$ < -6.0 ‰ and $\delta^{2}H$ < -40.0 ‰) indicates that either they were recharged by high rainfall intensity which has a lower enrichment of stable isotopes within the Mekong Delta or high recharged elevation from upstream of the Mekong River Basin. However, stable isotopes data of rainfall from the Mekong Delta (N. Le Duy et al., 2018) and Ho Chi

Minh City (Munksgaard et al., 2019) show an unclear relationship to rainfall amount (Figure 9-7). It means that these deep groundwater samples might originate from a high elevation area. On the other hand, some groundwater samples distributed along fresh seawater mixing line indicating they mixed with seawater (Figure 9-6). As shown in Figure 9-9, most of the groundwater in the study area have d-excess values are lower than global d-excess (-10‰) indicating that evaporation might have a strong influence on original recharged sources of groundwater in the study area. Influences of evaporation and mixing with seawater are also common processes which have been observed in many coastal aquifers (Chandrajith et al., 2016; Vallejos, Sola, Yechieli, & Pulido-Bosch, 2018).

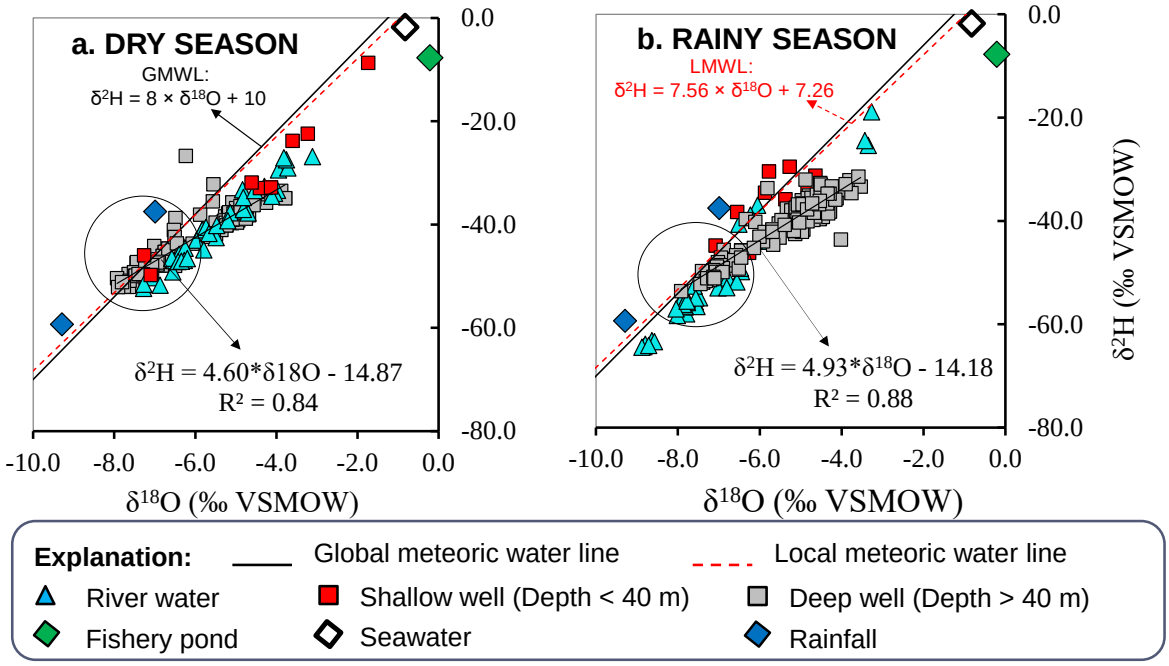

Figure 9- 6: Delta diagram showing hydrological characteristics of groundwater and surface water concerning recharge sources.

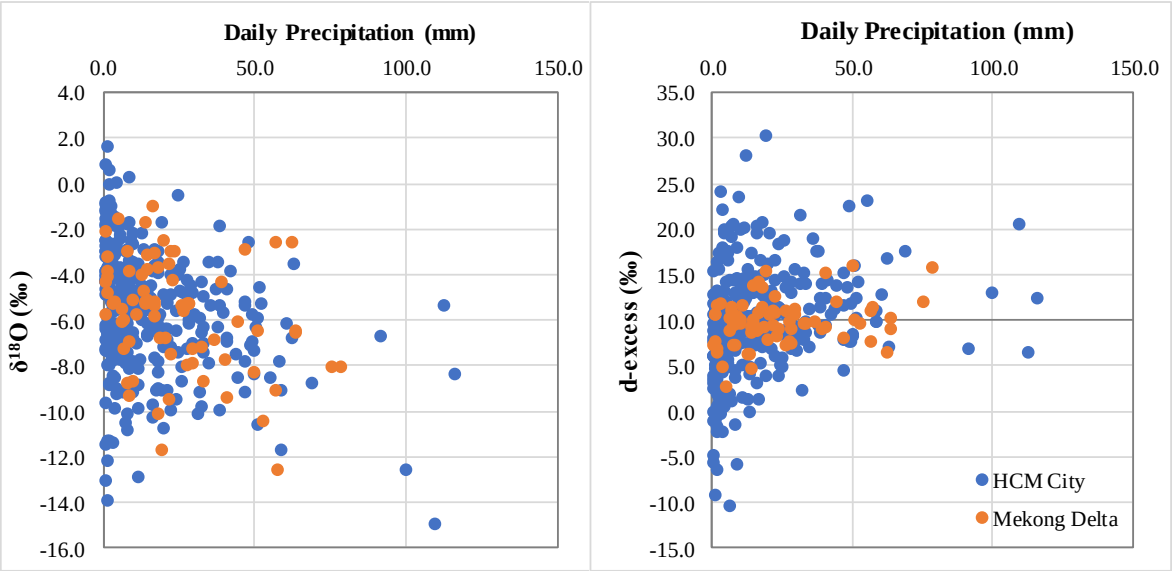

Figure 9- 7: Delta diagram showing hydrological characteristics of groundwater and surface water concerning recharge sources.

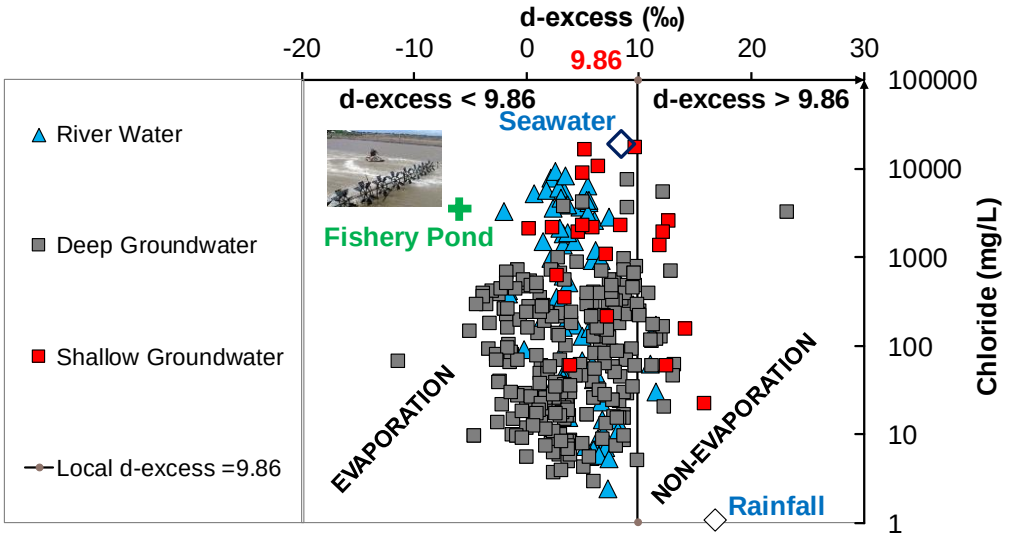

Figure 9- 8: Scattered graph of d-excess vs chloride showing effects of evaporation.

However, the spatially heterogenous variation of salinity and evaporation in the coastal aquifers of the Mekong Delta reflects the complex processes of evaporation, recharge and or infiltration, and mixing with seawater occurring in the study area. Shallow groundwater (SGW) along the coast have extraordinarily high salinity accompanies more enriched isotopes, and high d-excess suggests that SGW originated from rainfall and mixed with seawater. In contrast, high salinity but relatively light values of stable isotopes in the central area indicates that SGW was recharged by rainfall and mixing with paleo-seawater trapped in sediment during the Holocene period.

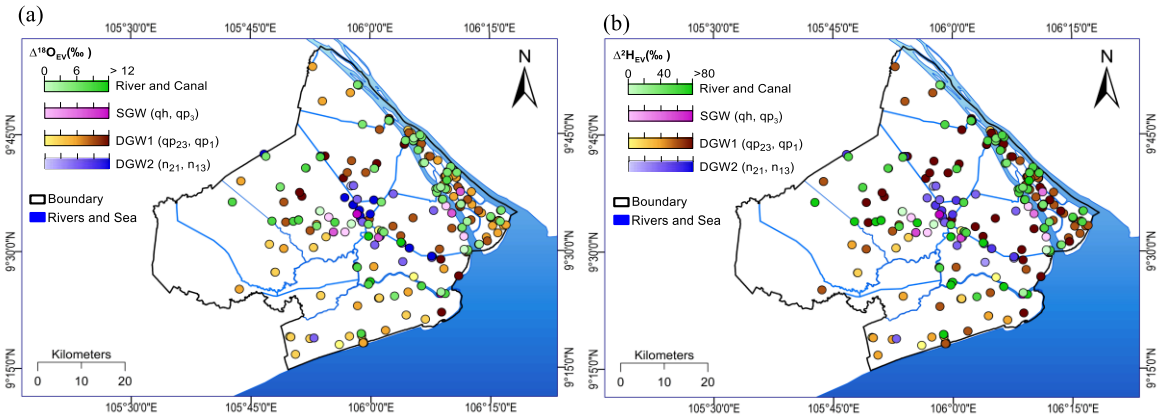

Figure 9- 9: 3D distribution of chloride and $\delta^{18}O$ of groundwater in coastal aquifers of the Mekong Delta, Vietnam.

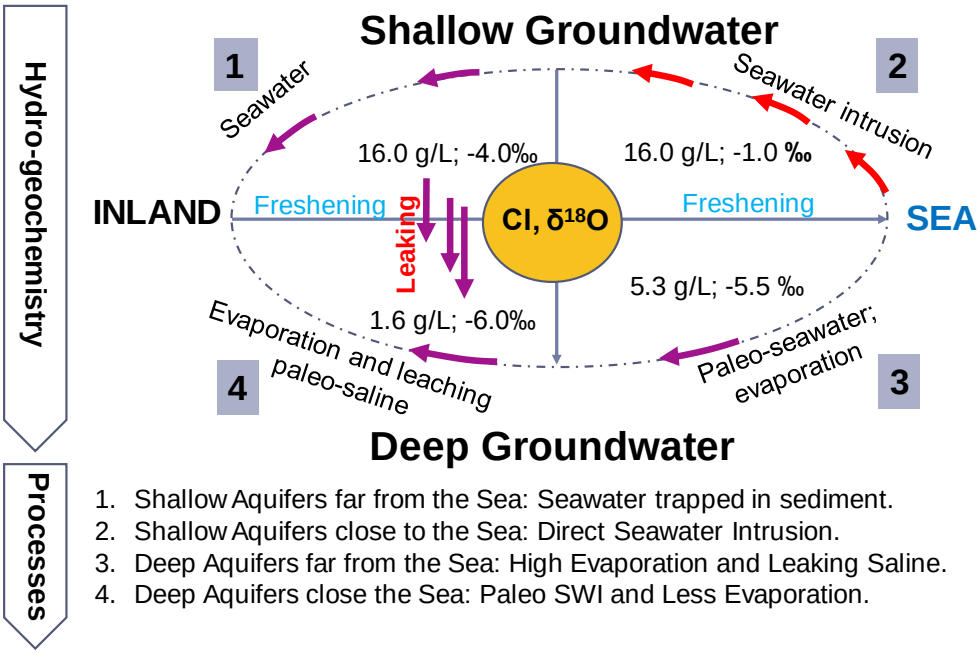

Figure 9- 10: Summary the spatial distribution of chloride and $\delta^{18}O$ of groundwater in coastal aquifers of the Mekong Delta, Vietnam.

Regards deep aquifers, most of the groundwater samples in these aquifers have relatively low chloride concentration (< 500 mg/L) and more depleted in stable isotopes (< -6.0‰) indicating rainfall origin during the Last Glacial Maximum and mixing. However, some deep groundwater (DGW) samples have a high chloride concentration (>1500 mg/L), and enriched isotopes values (> -6.0‰) may reflect influences of leaching paleo-seawater from sediment and evaporation before infiltrating into these aquifers (Figure 9-10).

9.3. Mixing processes

Hydrogeochemical and stable isotopes showed that groundwater resources in the coastal aquifers of the MD originated from different sources including rainfall, evaporated-open surface water and seawater. This research used the end-member analysis (EMMA) model to quantify the contribution ratios of each potential to groundwater resource. However, determining potential water sources contributing to groundwater in the study area is high uncertainty depending on groundwater flow paths and hydro-geochemical processes.

The main flow paths of groundwater in the coastal aquifers of the MD is the regional flow starting from high elevation region, probably upstream area of the Mekong River Basin to the coastline (E. Lee, Jayakumar, Shrestha, & Han, 2018). Moreover, vertical flow paths may also occur as a result of an increase of chemical and hydraulic gradient caused by paleo seawater intrusion (Hung Van et al., 2019) and significant groundwater level depletion (Minderhoud et al., 2017). Also, high variation in solute and isotopic concentration revealed that groundwater in coastal aquifers of the Mekong Delta might experience different processes of evaporation, mineral dissolution and mixing with seawater. Therefore, selected indicators need to be representative and differentiated meaning that the values of variables are different for each end member and have no relationship each other to avoid the superposition of information (Duan et al., 2019). Table 9-1 and Table 9-2 showed results of correlation test for shallow and deep groundwater, respectively. Chloride (Cl^-) and d-excess have no linear relationship with r = -0.254 and 0.159, which may be considered as signatures of mixing processes. It is highly recognized that chloride is the most dominative element of seawater, and it is a conservative ion which is not absorbed by plant, bacteria, has high solubility and non-evaporation. Meanwhile, d-excess is a tracer concerning to climate variation and hydrological processes, especially influences of evaporation on the water sources. Therefore, Cl^- and d-excess are good indicators for water end members in the mixing model. For selecting water end-member sources, stable isotopes data showed that groundwater distributed along local meteoric water line indicating the origin of groundwater from local rainfall. Also, most of the groundwater samples in the study area has lower d-excess (<-10‰) indicating influenced or recharged by open-evaporated freshwater. Moreover, groundwater in the study area has a wide variation in chloride concentration ranging from below 5.0 mg/L to 16,883 mg/L, indicating affected by mixing with brackish water. However, the origin of brackish water in shallow and deep aquifers are very different. It may originate from seawater intrusion directly from the sea or seawater trapped in

sediment and rocks during the transgression processes in the last glacial period. Previous studies illustrated that most of the coastal shallow aquifers in the Mekong Delta experienced seawater intrusion during a rapid sea-level rise in the Holocene period(Ta, Nguyen, Tateishi, Kobayashi, Tanabe, et al., 2002; Tjallingii, Stattegger, Wetzel, & Van Phach, 2010). characterizing by high salinity and heavy isotopes. Conversely, deep groundwater might experience leaching paleo-seawater trapped in rocks/sediment having high salinity but relatively low isotopes. Moreover, geochemical characteristics of shallow and deep groundwater are similar in some extends indicating the vertical saline movement from upper to lower layers because of the high density of brackish water in upper layers. This process has been intensified due to significant groundwater level depletion in the deep aquifers. Therefore, three potential end-members would be rainfall, evaporated freshwater and brackish water (Figure 9-10).

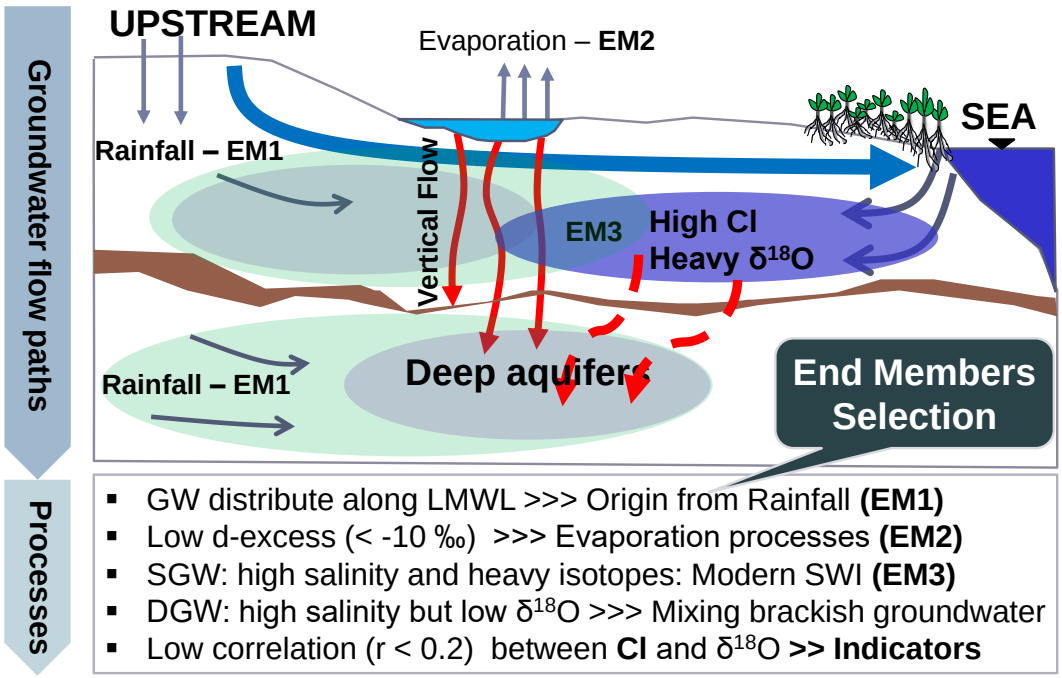

Figure 9-11: Mixing conceptual model showing groundwater flow paths and hydrogeological processes occurring in coastal aquifers of the Mekong Delta, Vietnam.

Table 9- 1: Correlation matrix of variables in shallow groundwater

Variables	EC	Na^+	K^+	Ca^{2+}	Mg^{2+}	Cl^-	NO_3^-	$S0_4^{2-}$	HCO_3^-	$\delta_{18}O$	δ^2H	d-excess
EC	**1**											
Na^+	**0.883**	**1**										
K^+	**0.756**	**0.821**	**1**									
Ca^{2+}	0.404	0.202	-0.012	**1**								
Mg^{2+}	**0.790**	**0.663**	**0.484**	**0.821**	**1**							
Cl^-	**0.908**	**0.983**	**0.791**	0.363	**0.785**	**1**						
N O_3^-	**0.839**	**0.961**	**0.821**	0.285	**0.732**	**0.971**	**1**					
$S0_4^{2-}$	**0.694**	**0.570**	0.411	**0.841**	**0.936**	**0.694**	**0.677**	**1**				
HCO_3^-	0.047	-0.053	-0.051	0.142	-0.011	-0.074	-0.154	-0.077	**1**			
$\delta^{18}O$	**0.607**	**0.679**	**0.574**	0.066	0.324	**0.631**	**0.577**	0.227	0.375	**1**		
δ^2H	**0.568**	**0.703**	**0.595**	0.076	0.350	**0.661**	**0.638**	0.244	0.307	**0.934**	**1**	
d-excess	-0.390	-0.291	-0.244	-0.011	-0.108	-0.254	-0.160	-0.080	-0.334	**-0.646**	-0.330	**1**

Note: Values in bold are different from 0 with a significance level alpha=0.05

Table 9- 2: Correlation matrix of variables in deep groundwater

Variables	EC	Na^+	K^+	Ca^{2+}	Mg^{2+}	Cl^-	NO_3^-	$S0_4^{2-}$	HCO_3^-	$\delta_{18}O$	δ^2H	d-excess
EC	**1**											
Na^+	**0.852**	**1**										
K^+	**0.607**	**0.633**	**1**									
Ca^{2+}	**0.465**	**0.306**	**0.158**	**1**								
Mg^{2+}	**0.665**	**0.622**	**0.392**	**0.899**	**1**							
Cl^-	**0.807**	**0.950**	**0.625**	**0.468**	**0.770**	**1**						
N O_3^-	**0.547**	**0.681**	**0.496**	**0.265**	**0.550**	**0.734**	**1**					
$S0_4^{2-}$	**0.610**	**0.441**	**0.217**	**0.873**	**0.830**	**0.487**	**0.317**	**1**				
HCO_3^-	0.084	0.108	-0.089	**-0.231**	**-0.257**	**-0.154**	**-0.136**	0.016	**1**			
$\delta^{18}O$	**-0.164**	**-0.180**	-0.048	0.122	0.125	0.019	0.008	**-0.141**	**-0.650**	**1**		
δ^2H	-0.055	-0.049	-0.025	**0.208**	**0.251**	**0.149**	**0.151**	-0.044	**-0.592**	**0.935**	**1**	
d-excess	**0.277**	**0.319**	0.069	0.017	0.070	**0.159**	**0.185**	**0.242**	**0.593**	**-0.881**	**-0.655**	**1**

Note: Values in bold are different from 0 with a significance level alpha=0.05

Figure 9-11 showed all shallow groundwater was inside the triangle boundary of three water end-member sources, including rainfall (EM1), evaporated freshwater (EM2) and brackish water (EM3). Similarly, all deep groundwater samples were bounded by triangle zone that was created by three water end-member sources including rainfall (EM1), evaporated freshwater (EM2) and brackish water (EM3) (Figure 9-12).

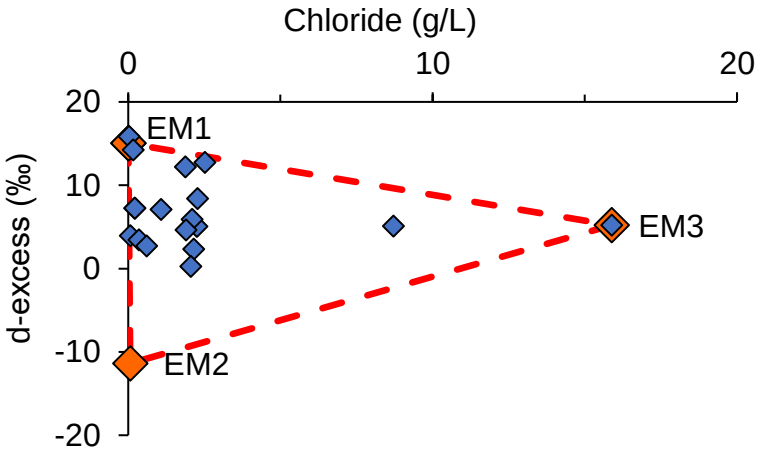

Figure 9- 12: Endmember mixing analysis for shallow groundwater

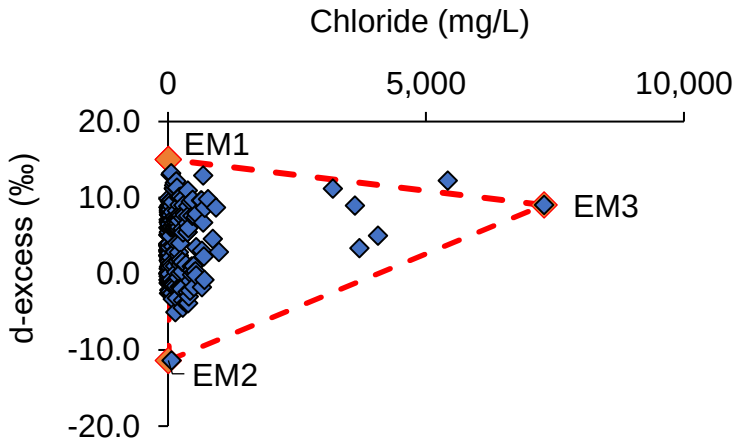

Figure 9- 13: Endmember mixing analysis for deep groundwater

The estimation of mixing ratio showed that both of shallow and deep groundwater were dominantly recharged by rainfall with an average contribution ratio of 59% for shallow (Table 9-3) and 56% for deep aquifers (Table 9-4). Evaporated-open surface water contributed tremendous proportion for deep aquifers (41%) compared to that of shallow aquifers (25%) while mixing ratio with seawater was very high in shallow aquifers (average of 15%) compared to only 5% in deep aquifers. More interesting, deep groundwater in the north and southwestern parts of the study area may experience substantial evaporation processes with an average ratio of 52% compared to the rest of the study area (Figure 9-14). Also, mixing with saltwater occurred predominantly in the river mouth extending to central parts of study area indicating seawater has intruded in these locations in both shallows (Figure 9-13) and deep groundwater (Figure 9-14).

Table 9- 3: Mixing ratio of three water end-member sources contribution to shallow aquifers

Ratio	EM1 (Rain)	EM2 (Evaporation)	EM3 (Brackish water)
Min	0.00	0.00	0.00
Aver	0.59	0.25	0.15
Max	1.00	0.51	1.00
STD	0.23	0.17	0.24

Table 9- 4: Mixing ratio of three water end-member sources contribution to deep aquifers

Ratio	EM1 (Rain)	EM2 (Evaporation)	EM3 (Brackish water)
Min	0.00	0.00	0.00
Aver	0.56	0.41	0.05
Max	0.93	1.00	1.00
STD	0.17	0.17	0.11

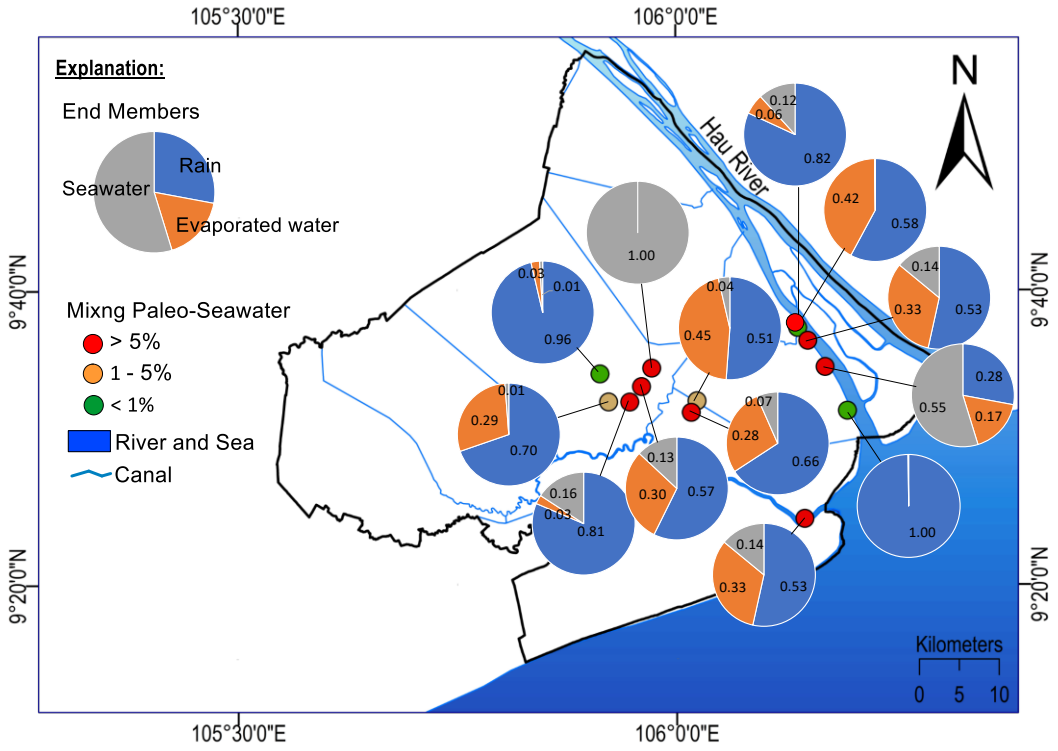

Figure 9- 14: Contribution ratio of three water end-member sources for shallow groundwater

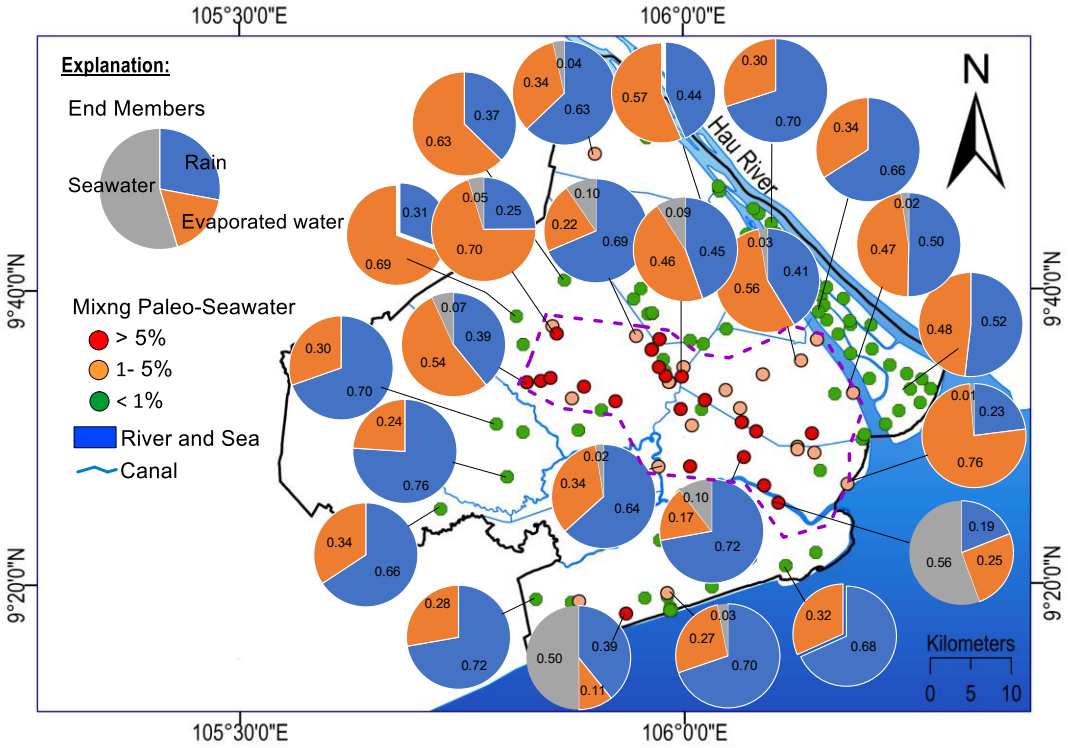

Figure 9- 15: Contribution ratio of three water end-member sources for shallow groundwater

9.4. Groundwater salinization and its controlling factors

Previous studies show that anthropogenic activities and geological characteristics have very different effects on groundwater flow dynamics and salinization processes in the coastal aquifers (Hosono et al., 2009; Khalaj et al., 2019; Lamichhane & Shakya, 2019). In Soc Trang province, one of the most influencing factors on groundwater flow direction is over-groundwater exploitation occurring since the 1990s (Minderhoud et al., 2017) which is also demonstrated by groundwater levels and pumping capacity and confirmed by stochastic and hydrological models in this study. It is because a rapid increase in groundwater exploitation capacity caused significant groundwater level depletion resulting in groundwater flow towards the depletion areas. Additionally, the study area is a flat and lowland area with a low groundwater velocity, especially in the deep aquifers (H. T. Hoang & Bäumle, 2018). Therefore, groundwater flow occurs in two directions: (i) horizontal flow direction from low to high groundwater extraction rates and (ii) the vertical movement of groundwater from upper layers to lower layers via thin and discontinuous impermeable layers due to significant groundwater depletion in the deeper aquifers. Besides, vertical paleo-saline infiltration occurs in coastal aquifers of the Mekong Delta because of different solute concentration between upper and lower parts caused by paleo-seawater intrusion (Hung Van et al., 2019; Larsen et al., 2017c; Meyer, Engesgaard, & Sonnenborg, 2019). An increase hydraulic gradient in deeper aquifers due to groundwater level depletion is also a driving force behind saline dissolution and leakage from salt soil and salt sediment in groundwater. Hydrogeochemical and isotopic data showed that current seawater does not directly influence on coastal aquifers of the study area. However, leaking paleo-saline sources from shallow aquifers to deeper aquifers has been occurring and become a most severe problem threating sustainable groundwater in the coastal aquifers of the Mekong Delta. Results from groundwater modelling showed that high chloride concentration (> 2,000 mg/L) would be expanded horizontally and vertically in fresh aquifers of the Mekong Delta if pumping capacity (Q) continues to increase at 5% and 20% per year until 2030 (Figure 8-15). The predictive results reveal that continuing excessive groundwater exploitation and rapid groundwater level depletion will eventually put groundwater resources in the coastal aquifers are at high risk of salinization.

Notably, there is unclear evidence of infiltrating river water to groundwater due to limited data available. However, infiltrating saline river water to shallow aquifers is a severe problem causing the freshwater scarcity in many coastal aquifers around the world

(Mastrocicco, Busico, Colombani, Vigliotti, & Ruberti, 2019; I. R. Santos et al., 2017; Zhu et al., 2019), and it is needed to pay more attendant in the Mekong Delta as well (Nguyen Le Duy et al., 2019).

9.5. Groundwater flow system

Groundwater resource in the low-lying coastal delta is the mixer of different water components including rainfall, infiltrated water from the surface water system and mixing with saltwater as a result of seawater intrusion, leaching paleo-seawater trapped in the sediment and soil layers. Figure 9-10 showed a conceptual groundwater flow system model based on the results of hydrogeochemistry, stable isotopes and hydraulic head. The model explains the origin of groundwater in coastal aquifers of the Mekong Delta and hydrological and geochemical processes during groundwater formation processes. Firstly, shallow groundwater is recharged directly by local rainfall and infiltrated surface water while deep groundwater is recharged by rainwater and open evaporated surface water. Secondly, shallow and deep groundwater experience different magnitudes of mineral dissolution and precipitation which forms solute concentration in groundwater, especially groundwater has increased sodium, calcium, magnesium, and bicarbonate concentration when they have long resident time. Eventually, a part of fresh groundwater has been mixing with saltwater throughout different processes such as seawater intrusion directly from seawater, leaching saline from sediment and saline leaking because of increase chemical and hydraulic gradient.

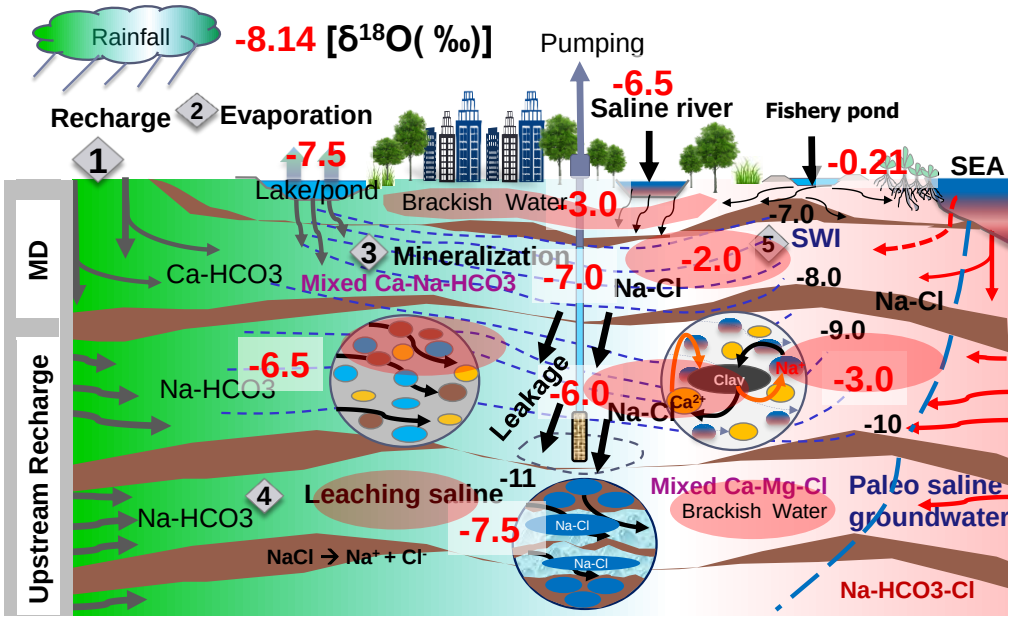

Figure 9- 16: Conceptual model of the groundwater flow system in coastal aquifers of the Mekong Delta.

CHAPTER 10 CONCLUSIONS AND PERSPECTIVES

10.1 Conclusions

(ii) Groundwater flow dynamics

In the coastal lowland area of the Mekong Delta, shallow groundwater flow (water level and flow direction) shows highly seasonal variation while that of deep groundwater changes sensitively under impacts of groundwater exploitation with significant groundwater level depletion (0.85 m/year) in dense pumping locations and in coastal areas. It was noted that vertical groundwater flow also occurs intensively in depression areas leading to an increase of salinity movement from upper to lower layers.

(iii) Hydrogeochemical characteristics and origin of groundwater

Groundwater in coastal aquifers of the MD mainly consists of Na-Cl, Na-Mg-Ca-HCO3, Na-Mg-Ca-HCO3-SO4 and Na-HCO3-Cl water types. Groundwater samples have a spatial heterogeneity in stable isotopes and salinity reflecting different recharge sources and hydrogeochemical processes, especially mixing with seawater intrusion. Groundwater from the Holocene aquifer could be directly recharged by rainfall/or surface water with less evaporative losses, and it experienced different magnitudes of seawater intrusion due to the rapid sea-level rise during the late Holocene age. Evaporated surface water sources might recharge groundwater from deep aquifers in the last glacial period with fewer impacts of seawater intrusion on these aquifers.

(iv) Hydrogeochemical processes

The main hydro-geochemical processes influencing on groundwater quality in the Mekong Delta are included: (i) seawater intrusion in shallow aquifers and freshening process in deep aquifers, (ii) carbonate-silicate weathering and minerals dissolution have occurred in both shallow and deep aquifers (iii) leaking saline from upper layers to lower layers may occur in some locations resulted in elevated salinity concentration production wells due to the structure of discontinuous impermeable layers and significant groundwater level depletion.

(v) Groundwater salinization processes in coastal aquifers

The results of groundwater flow dynamics, hydro-geochemistry and stable isotopes showed that groundwater salinization in a coastal area of the MD was caused by various

processes, including paleo-saline water trapped in sediment/rock, halite dissolution, and leaking saline from upper layers to lower layers. However, the problem of groundwater salinization is further exacerbated in recent years due to excessive groundwater exploitation with an increase of hydraulic connection between saline and fresh aquifers.

End member mixing analysis shows that both groundwaters shallow and deep groundwater were recharged dominantly by rainfall with an average ratio of 59% and 56%, respectively. Evaporation has a strong influence on deep groundwater, which contributed to 41% of deep groundwater. In contrast, brackish water has a substantial impact on the shallow aquifer, providing to 15% for shallow groundwater compared to only 5% for deep groundwater.

The prediction results of groundwater salinization based on three state-of-art machine learning models showed that high salinity affected-areas extends from coast to the central city with a length of 40 km and width of 20 km. The highest affected-areas occurs in the areas close to the massive groundwater exploitation, the hydraulic connection between upper and lower layers, and paleo-saline sources. In practice, therefore, the groundwater exploitation in the areas close to paleo-saline sources with substantial extraction rate and significant groundwater level depletion need to be limited.

The projection of groundwater exploitation and regional groundwater levels fluctuation in different scenarios indicates that continuing increase of pumping capacity together with decreasing groundwater levels in surrounding areas may cause significant groundwater level depletion in the near future, especially in central and coastal cities. Meanwhile, reducing groundwater pumping capacity in combination with stopping regional groundwater level depletion will help groundwater levels in the study area recovery remarkably.

These findings could provide insights into the groundwater flow system, hydrogeochemical characteristics and seawater intrusion processes in coastal aquifers of the Mekong Delta. It may also help water authorities and policymakers in Vietnam and other countries to propose appropriate policies and regulations on sustainable water resources use and management under pressure of human activities and unpredictable impacts of climate change and sea-level rise in coastal lowland regions around the world.

10.2. Perspectives

Continuing overexploitation of groundwater together with the changing hydrological system may cause much threat to fresh coastal aquifers, while seawater intrusion affects strongly surface water system and it intends to expand widely into the inland of the Mekong Delta, Vietnam. These issues will eventually lead to severe water scarcity or even water crisis on a large scale, threatening to the large population in many coastal lowland regions only in Vietnam but also other countries in the world. Therefore, to sustainably manage groundwater sources in this province, appropriate solutions should be considered as follows:

(i) Effective management groundwater extraction

In groundwater management practices, understanding groundwater extraction status is critical. Therefore, it is needed to control groundwater extraction capacity from households, industries and irrigation users. Registration new wells and extraction licensing measures must be realized consequently and transparently.

(ii) (2) Reducing extraction

Because groundwater resources in the coastal lowland areas are highly vulnerable to natural variation and anthropogenic activities, therefore, it should be used efficiently and safely. On the one hand, the extraction capacity should be prioritized to drinking water purpose while groundwater providing to other objects should be reduced dramatically. On the other hand, the integrated use of surface water, rainwater, and groundwater should consider appropriate to reduce the pressure of groundwater exploitation.

(iii) Recharge mechanism

Along with reducing pumping capacity, identifying recharge solutions into coastal aquifers of Soc Trang province is needed to recovery groundwater levels and to mitigate groundwater contamination, especially seawater intrusion along the coast and expanding saline boundary in central areas.

(iv) Preventing and mitigating seawater intrusion

Some parts in Soc Trang province seem to be affected by saline diffusion and are high vulnerability to seawater intrusion through river-groundwater connection, which threatens

to sustainable groundwater use in coastal areas. Therefore, solutions to prevent and mitigate seawater intrusion, such as reducing groundwater exploitation in combination with other water resources, are needed.

(v) Groundwater monitoring practices

Monitoring groundwater quality and quantity play a significant role to understand groundwater flow dynamics and geochemical characteristics. Thereby, the environment monitoring system should establish and operate effectively to assess surface water and groundwater environment, both quality and quantity.

REFERENCES

Abboud, I. A. (2018). Geochemistry and quality of groundwater of the Yarmouk basin aquifer, north Jordan. *Environmental Geochemistry and Health, 40*(4), 1405-1435. doi:10.1007/s10653-017-0064-x

Abd-Elhamid, H. F., & Javadi, A. A. (2011). Impact of sea level rise and over-pumping on seawater intrusion in coastal aquifers. *Journal of Water and Climate Change, 2*(1), 19-28. doi:10.2166/wcc.2011.053

Abdelhamid, H., Javadi, A., Abd-Elaty, I., & Sherif, M. (2016). *Simulation of seawater intrusion in the Nile Delta aquifer under the conditions of climate change* (Vol. 47).

Abu-alnaeem, M. F., Yusoff, I., Ng, T. F., Alias, Y., & Raksmey, M. (2018). Assessment of groundwater salinity and quality in Gaza coastal aquifer, Gaza Strip, Palestine: An integrated statistical, geostatistical and hydrogeochemical approaches study. *Science of The Total Environment, 615*, 972-989. doi:https://doi.org/10.1016/j.scitotenv.2017.09.320

Abu Al Naeem, M. F., Yusoff, I., Ng, T. F., Maity, J. P., Alias, Y., May, R., & Alborsh, H. (2019). A study on the impact of anthropogenic and geogenic factors on groundwater salinization and seawater intrusion in Gaza coastal aquifer, Palestine: An integrated multi-techniques approach. *Journal of African Earth Sciences, 156*, 75-93. doi:https://doi.org/10.1016/j.jafrearsci.2019.05.006

Aeschbach-Hertig, W., & Gleeson, T. (2012). Regional strategies for the accelerating global problem of groundwater depletion. *Nature Geosci, 5*(12), 853-861.

Ala-aho, P., Soulsby, C., Pokrovsky, O. S., Kirpotin, S. N., Karlsson, J., Serikova, S., . . . Tetzlaff, D. (2018). Using stable isotopes to assess surface water source dynamics and hydrological connectivity in a high-latitude wetland and permafrost influenced landscape. *Journal of Hydrology, 556*, 279-293. doi:https://doi.org/10.1016/j.jhydrol.2017.11.024

Alaya, M. B., Saidi, S., Zemni, T., & Zargouni, F. (2014). Suitability assessment of deep groundwater for drinking and irrigation use in the Djeffara aquifers (Northern Gabes, south-eastern Tunisia). *Environmental Earth Sciences, 71*(8), 3387-3421. doi:10.1007/s12665-013-2729-9

Alfarrah, N., & Walraevens, K. (2018). Groundwater Overexploitation and Seawater Intrusion in Coastal Areas of Arid and Semi-Arid Regions. *Water, 10*(2), 143.

Almasri, M. N. (2007). Nitrate contamination of groundwater: A conceptual management framework. *Environmental Impact Assessment Review, 27*(3), 220-242. doi:http://dx.doi.org/10.1016/j.eiar.2006.11.002

Ameur, M., Hamzaoui–Azaza, F., & Gueddari, M. (2016). Nitrate contamination of Sminja aquifer groundwater in Zaghouan, northeast Tunisia: WQI and GIS assessments. *Desalination and Water Treatment, 57*(50), 23698-23708. doi:10.1080/19443994.2015.1137495

Amiri, V., Nakhaei, M., Lak, R., & Kholghi, M. (2016). Investigating the salinization and freshening processes of coastal groundwater resources in Urmia aquifer, NW Iran. *Environ Monit Assess, 188*(4), 233. doi:10.1007/s10661-016-5231-5

An, T. D., Tsujimura, M., Le Phu, V., Kawachi, A., & Ha, D. T. (2014a). Chemical Characteristics of Surface Water and Groundwater in Coastal Watershed, Mekong Delta, Vietnam. *Procedia Environmental Sciences, 20*(0), 712-721. doi:http://dx.doi.org/10.1016/j.proenv.2014.03.085

An, T. D., Tsujimura, M., Le Phu, V., Kawachi, A., & Ha, D. T. (2014b). Chemical Characteristics of Surface Water and Groundwater in Coastal Watershed, Mekong Delta, Vietnam. *Procedia Environmental Sciences, 20*, 712-721. doi:http://dx.doi.org/10.1016/j.proenv.2014.03.085

An, T. D., Tsujimura, M., Phu, V. L., Ha, D. T., & Hai, N. V. (2018). Isotopic and Hydrogeochemical Signatures in Evaluating Groundwater Quality in the Coastal Area of the Mekong Delta, Vietnam. In D. Tien Bui, A. Ngoc Do, H.-B. Bui, & N.-D. Hoang (Eds.), *Advances and Applications in Geospatial Technology and Earth Resources: Proceedings of the International Conference on Geo-Spatial Technologies and Earth Resources 2017* (pp. 293-314). Cham: Springer International Publishing.

Anderson, H. R. (1978). *Hydrogeologic reconnaissance of the Mekong Delta in South Vietnam and Cambodia*. Retrieved from

Anderson, M. P., Woessner, W. W., & Hunt, R. J. (2015). Chapter 9 - Model Calibration: Assessing Performance. In M. P. Anderson, W. W. Woessner, & R. J. Hunt (Eds.), *Applied Groundwater Modeling (Second Edition)* (pp. 375-441). San Diego: Academic Press.

Anh, D. T., Hoang, L. P., Bui, M. D., & Rutschmann, P. (2018). Modelling seasonal flows alteration in the Vietnamese Mekong Delta under upstream discharge changes, rainfall changes and sea level rise. *International Journal of River Basin Management*, 1-15. doi:10.1080/15715124.2018.1505735

Antti Syväjärvi, J. S. (2010). *Data Mining in Public and Private Sectors: Organizational and Government Perspectives* (K. Klinger Ed.). United States of America: Information Science Reference (an imprint of IGI Global).

Appelo, C., Postma, D. (2005). *Geochemistry, Groundwater and Pollution* (Second Edition ed.). London: CRC Press.

Appelo, C. A. J. (1994). Cation and proton exchange, pH variations, and carbonate reactions in a freshening aquifer. *Water Resources Research, 30*(10), 2793-2805. doi:doi:10.1029/94WR01048

Appelo, C. a. P., D. . (2005). *Geochemistry, Groundwater and Pollution. 2nd Edition, Balkema, Rotterdam*.

Arfib, B., & Charlier, J.-B. (2016). Insights into saline intrusion and freshwater resources in coastal karstic aquifers using a lumped Rainfall–Discharge–Salinity model (the Port-Miou brackish spring, SE France). *Journal of Hydrology, 540*, 148-161. doi:http://dx.doi.org/10.1016/j.jhydrol.2016.06.010

Argamasilla, M., Barberá, J. A., & Andreo, B. (2017). Factors controlling groundwater salinization and hydrogeochemical processes in coastal aquifers from southern Spain. *Science of The Total Environment, 580*, 50-68. doi:https://doi.org/10.1016/j.scitotenv.2016.11.173

Arnell, N. W. (2004). Climate change and global water resources: SRES emissions and socio-economic scenarios. *Global Environmental Change, 14*(1), 31-52. doi:https://doi.org/10.1016/j.gloenvcha.2003.10.006

Arslan, H., & Demir, Y. (2013). Impacts of seawater intrusion on soil salinity and alkalinity in Bafra Plain, Turkey. *Environ Monit Assess, 185*(2), 1027-1040. doi:10.1007/s10661-012-2611-3

Ayed, B., Jmal, I., Sahal, S., Saidi, S., & Bouri, S. (2018, 2018//). *Assessment of Seawater Intrusion in the Maritime Djeffara Coastal Aquifer (Southeastern Tunisia).* Paper presented at the Recent Advances in Environmental Science from the Euro-Mediterranean and Surrounding Regions, Cham.

Azimi, S., Azhdary Moghaddam, M., & Hashemi Monfared, S. A. (2018). Large-scale association analysis of climate drought and decline in groundwater quantity using Gaussian process classification (case study: 609 study area of Iran). *Journal of Environmental Health Science and Engineering, 16*(2), 129-145. doi:10.1007/s40201-018-0301-y

Bădăluță, C.-A., Perșoiu, A., Ionita, M., Nagavciuc, V., & Bistricean, P.-I. (2019). Stable H and O isotope-based investigation of moisture sources and their role in river and groundwater recharge in the NE Carpathian Mountains, East-Central Europe. *Isotopes Environ Health Stud*, 1-18. doi:10.1080/10256016.2019.1588895

Badaruddin, S., Werner, A. D., & Morgan, L. K. (2017). Characteristics of active seawater intrusion. *Journal of Hydrology, 551*(Supplement C), 632-647. doi:https://doi.org/10.1016/j.jhydrol.2017.04.031

Banerjee, P., Singh, V., Chatttopadhyay, K., Chandra, P., & Singh, B. (2011). Artificial neural network model as a potential alternative for groundwater salinity forecasting. *Journal of Hydrology, 398*(3-4), 212-220.

Bank, W. (2010). *Deep Wells and Prudence: Towards Pragmatic Action for Addressing Ground water Overexploitation in India*. Retrieved from http://siteresources.worldbank.org/INDIAEXTN/Resources/295583-1268190137195/DeepWellsGroundWaterMarch2010.pdf.

Barlow, P. M., & Reichard, E. G. (2010). Saltwater intrusion in coastal regions of North America. *Hydrogeology Journal, 18*(1), 247-260. doi:10.1007/s10040-009-0514-3

Barragán, J. M., & de Andrés, M. (2015). Analysis and trends of the world's coastal cities and agglomerations. *Ocean & Coastal Management, 114*, 11-20. doi:https://doi.org/10.1016/j.ocecoaman.2015.06.004

Barthold, F. K., Tyralla, C., Schneider, K., Vaché, K. B., Frede, H.-G., & Breuer, L. (2011). How many tracers do we need for end member mixing analysis (EMMA)? A sensitivity analysis. *Water Resources Research, 47*(8), n/a-n/a. doi:10.1029/2011WR010604

Batsaikhan, N., Lee, J. M., Nemer, B., & Woo, N. C. (2018). Water Resources Sustainability of Ulaanbaatar City, Mongolia. *Water, 10*(6), 750.

Beaudry, C., Lefebvre, R., Rivard, C., & Cloutier, V. (2018). Conceptual model of regional groundwater flow based on hydrogeochemistry (Montérégie Est, Québec, Canada). *Canadian Water Resources Journal / Revue canadienne des ressources hydriques, 43*(2), 152-172. doi:10.1080/07011784.2018.1461579

Befus, K. M., Darhower, S., Liefert, D. T., & Shuman, B. N. (2019). Reconstructing the groundwater recharge history for the Plymouth-Carver Aquifer Massachusetts, USA. *Quaternary International*. doi:https://doi.org/10.1016/j.quaint.2019.06.026

Benner, S. G., Polizzotto, M. L., Kocar, B. D., Ganguly, S., Phan, K., Ouch, K., . . . Fendorf, S. (2008). Groundwater flow in an arsenic-contaminated aquifer, Mekong Delta, Cambodia. *Applied Geochemistry, 23*(11), 3072-3087. doi:https://doi.org/10.1016/j.apgeochem.2008.06.013

Berg, M., Stengel, C., Trang, P. T. K., Hung Viet, P., Sampson, M. L., Leng, M., . . . Fredericks, D. (2007). Magnitude of arsenic pollution in the Mekong and Red River Deltas — Cambodia and Vietnam. *Science of The Total Environment, 372*(2), 413-425. doi:https://doi.org/10.1016/j.scitotenv.2006.09.010

Blasco, M., Auqué, L. F., & Gimeno, M. J. (2019). Geochemical evolution of thermal waters in carbonate – evaporitic systems: The triggering effect of halite dissolution in the dedolomitisation and albitisation processes. *Journal of Hydrology, 570*, 623-636. doi:https://doi.org/10.1016/j.jhydrol.2019.01.013

Bodrud-Doza, M., Bhuiyan, M. A. H., Islam, S. M. D.-U., Quraishi, S. B., Muhib, M. I., Rakib, M. A., & Rahman, M. S. (2019). Delineation of trace metals contamination in groundwater using geostatistical techniques: A study on Dhaka City of Bangladesh. *Groundwater for Sustainable Development, 9*, 100212. doi:https://doi.org/10.1016/j.gsd.2019.03.006

Boehmer, W. (2000). *Ground Water Study Mekong Delta, Modelling*. Retrieved from

Boschetti, T., González-Hernández, P., Hernández-Díaz, R., Naclerio, G., & Celico, F. (2015). Seawater intrusion in the Guanahacabibes Peninsula (Pinar del Rio Province, western Cuba): effects on karst development and water isotope composition. *Environmental Earth Sciences, 73*(9), 5703-5719. doi:10.1007/s12665-014-3825-1

Breiman, L. (2001). Random Forests. *Machine Learning, 45*(1), 5-32. doi:10.1023/A:1010933404324

Bui Huy, T., Tuyet-Hanh, T. T., Johnston, R., & Nguyen-Viet, H. (2014). Assessing Health Risk due to Exposure to Arsenic in Drinking Water in Hanam Province, Vietnam. *International Journal of Environmental Research and Public Health, 11*(8), 7575-7591. doi:10.3390/ijerph110807575

Bui Tran Vuong, D. T. L., Le Thi Mai Van. (2016). *Groundwater Issues and Hydrogeological Survey of the Mekong River Basin in Vietnam*. Retrieved from

C., W. S., M., H. G., & L., G. S. (2015). Source, transport, and evolution of saline groundwater in a shallow Holocene aquifer on the tidal deltaplain of southwest Bangladesh. *Water Resources Research, 51*(7), 5791-5805. doi:doi:10.1002/2014WR016262

Carretero, S., Rapaglia, J., Bokuniewicz, H., & Kruse, E. (2013). Impact of sea-level rise on saltwater intrusion length into the coastal aquifer, Partido de La Costa, Argentina. *Continental Shelf Research, 61–62*, 62-70. doi:http://dx.doi.org/10.1016/j.csr.2013.04.029

Cary, L., Petelet-Giraud, E., Bertrand, G., Kloppmann, W., Aquilina, L., Martins, V., . . . Pierre, D. (2015). Origins and processes of groundwater salinization in the urban coastal aquifers of Recife (Pernambuco, Brazil): A multi-isotope approach. *Science of The Total Environment, 530-531*, 411-429. doi:https://doi.org/10.1016/j.scitotenv.2015.05.015

Chandrajith, R., Diyabalanage, S., Premathilake, K. M., Hanke, C., van Geldern, R., & Barth, J. A. C. (2016). Controls of evaporative irrigation return flows in comparison to seawater intrusion in coastal karstic aquifers in northern Sri Lanka: Evidence from solutes and stable isotopes. *Science of The Total Environment, 548-549*, 421-428. doi:https://doi.org/10.1016/j.scitotenv.2016.01.050

Chatton, E., Aquilina, L., Pételet-Giraud, E., Cary, L., Bertrand, G., Labasque, T., . . . Pauwels. (2016a). Glacial recharge, salinisation and anthropogenic contamination in the coastal aquifers of Recife (Brazil). *Science of The Total Environment, 569–570*, 1114-1125. doi:https://doi.org/10.1016/j.scitotenv.2016.06.180

Chatton, E., Aquilina, L., Pételet-Giraud, E., Cary, L., Bertrand, G., Labasque, T., . . . Pauwels. (2016b). Glacial recharge, salinisation and anthropogenic contamination in the coastal aquifers of Recife (Brazil). *Science of The Total Environment, 569-570*, 1114-1125. doi:10.1016/j.scitotenv.2016.06.180

Chau, N. D. G., Sebesvari, Z., Amelung, W., & Renaud, F. G. (2015). Pesticide pollution of multiple drinking water sources in the Mekong Delta, Vietnam: evidence from two provinces. *Environmental Science and Pollution Research, 22*(12), 9042-9058. doi:10.1007/s11356-014-4034-x

Chau Tran Vinh, Tran Hong Thai, Doan Van Canh, Dang Duc Nhan, Nguyen Cao Huan, Nguyen Van Nghia, . . . Van, T. T. T. (2017). Genesis and Quality of Groundwater in the Southeastern Region of Southern Vietnam. *Journal of Environmental Science and Engineering, A*(6), 277-292.

Chea, R., Grenouillet, G., & Lek, S. (2016). Evidence of Water Quality Degradation in Lower Mekong Basin Revealed by Self-Organizing Map. *PLOS ONE, 11*(1), e0145527. doi:10.1371/journal.pone.0145527

Chekirbane, A., Tsujimura, M., Kawachi, A., Isoda, H., Tarhouni, J., & Benalaya, A. (2013). Hydrogeochemistry and groundwater salinization in an ephemeral coastal flood plain: Cap Bon, Tunisia. *Hydrological Sciences Journal, 58*(5), 1097-1110. doi:10.1080/02626667.2013.800202

Chen, T., & Guestrin, C. (2016). *XGBoost: A Scalable Tree Boosting System*. Paper presented at the Proceedings of the 22nd ACM SIGKDD International Conference on Knowledge Discovery and Data Mining, San Francisco, California, USA.

Chen, W., Panahi, M., Tsangaratos, P., Shahabi, H., Ilia, I., Panahi, S., . . . Ahmad, B. B. (2019). Applying population-based evolutionary algorithms and a neuro-fuzzy system for modeling landslide susceptibility. *CATENA, 172*, 212-231. doi:https://doi.org/10.1016/j.catena.2018.08.025

Clauss, K., Ottinger, M., Leinenkugel, P., & Kuenzer, C. (2018). Estimating rice production in the Mekong Delta, Vietnam, utilizing time series of Sentinel-1 SAR data. *International Journal of Applied Earth Observation and Geoinformation, 73*, 574-585. doi:https://doi.org/10.1016/j.jag.2018.07.022

Cloquet, C., Carignan, J., Libourel, G., Sterckeman, T., & Perdrix, E. (2006). Tracing Source Pollution in Soils Using Cadmium and Lead Isotopes. *Environmental Science & Technology, 40*(8), 2525-2530. doi:10.1021/es052232+

Conroy, J. L., Thompson, D. M., Cobb, K. M., Noone, D., Rea, S., & Legrande, A. N. (2017). Spatiotemporal variability in the δ18O-salinity relationship of seawater across the tropical Pacific Ocean. *Paleoceanography, 32*(5), 484-497. doi:10.1002/2016PA003073

Creel, L. (2003). Ripple Effects: Population and Coastal Regions. *Population Reference Bureau*.

Criminisi, A. (2011). Decision Forests: A Unified Framework for Classification, Regression, Density Estimation, Manifold Learning and Semi-Supervised Learning. *Foundations and Trends® in Computer Graphics and Vision, 7*(2-3), 81-227. doi:10.1561/0600000035

Cui, J., Tian, L., Biggs, T. W., & Wen, R. (2017). Deuterium-excess determination of evaporation to inflow ratios of an alpine lake: Implications for water balance and modeling. *HYDROLOGICAL PROCESSES, 31*(5), 1034-1046. doi:10.1002/hyp.11085

Cuthbert, M. O., Gleeson, T., Moosdorf, N., Befus, K. M., Schneider, A., Hartmann, J., & Lehner, B. (2019). Global patterns and dynamics of climate–groundwater interactions. *Nature Climate Change, 9*(2), 137-141. doi:10.1038/s41558-018-0386-4

D'Alessandro, W., Bellomo, S., Brusca, L., Kyriakopoulos, K., Calabrese, S., & Daskalopoulou, K. (2017). The impact of natural and anthropogenic factors on groundwater quality in an active volcanic/geothermal system under semi-arid climatic conditions: The case study of Methana peninsula (Greece). *Journal of Geochemical Exploration, 175*, 110-119. doi:http://dx.doi.org/10.1016/j.gexplo.2017.01.003

Dalin, C., Wada, Y., Kastner, T., & Puma, M. J. (2017a). Groundwater depletion embedded in international food trade. *Nature, 543*, 700. doi:10.1038/nature21403

https://www.nature.com/articles/nature21403#supplementary-information

Dalin, C., Wada, Y., Kastner, T., & Puma, M. J. (2017b). Groundwater depletion embedded in international food trade. *Nature, 543*(7647), 700-704. doi:10.1038/nature21403

http://www.nature.com/nature/journal/v543/n7647/abs/nature21403.html#supplementary-information

Dang, T. D., Cochrane, T. A., Arias, M. E., Van, P. D. T., & de Vries, T. T. (2016). Hydrological alterations from water infrastructure development in the Mekong floodplains. *HYDROLOGICAL PROCESSES, 30*(21), 3824-3838. doi:10.1002/hyp.10894

Dansgaard, W. (1964). Stable isotopes in precipitation. *Tellus, 16*(4), 436-468. doi:10.1111/j.2153-3490.1964.tb00181.x

Datta, B., Vennalakanti, H., & Dhar, A. (2009). Modeling and control of saltwater intrusion in a coastal aquifer of Andhra Pradesh, India. *Journal of Hydro-environment Research, 3*(3), 148-159. doi:https://doi.org/10.1016/j.jher.2009.09.002

De Filippis, G., Foglia, L., Giudici, M., Mehl, S., Margiotta, S., & Negri, S. L. (2016). Seawater intrusion in karstic, coastal aquifers: Current challenges and future scenarios in the Taranto area (southern Italy). *Science of The Total Environment, 573*, 1340-1351. doi:https://doi.org/10.1016/j.scitotenv.2016.07.005

de Graaf, I. E. M., van Beek, R. L. P. H., Gleeson, T., Moosdorf, N., Schmitz, O., Sutanudjaja, E. H., & Bierkens, M. F. P. (2017). A global-scale two-layer transient groundwater model: Development and application to groundwater depletion. *Advances in Water Resources, 102*, 53-67. doi:https://doi.org/10.1016/j.advwatres.2017.01.011

Delsman, J. R., Hu-a-ng, K. R. M., Vos, P. C., de Louw, P. G. B., Oude Essink, G. H. P., Stuyfzand, P. J., & Bierkens, M. F. P. (2014a). Paleo-modeling of coastal saltwater intrusion during the Holocene: an application to the Netherlands. *Hydrol. Earth Syst. Sci., 18*(10), 3891-3905. doi:10.5194/hess-18-3891-2014

Delsman, J. R., Hu-a-ng, K. R. M., Vos, P. C., de Louw, P. G. B., Oude Essink, G. H. P., Stuyfzand, P. J., & Bierkens, M. F. P. (2014b). Paleo-modeling of coastal saltwater intrusion during the Holocene: an application to the Netherlands. *Hydrology and Earth System Sciences, 18*(10), 3891-3905. doi:10.5194/hess-18-3891-2014

Duan, X., Ma, F., Zhao, H., Guo, J., Gu, H., Lu, R., & Liu, G. (2019). Determining mine water sources and mixing ratios affected by mining in a coastal gold mine, in China. *Environmental Earth Sciences, 78*(10), 299. doi:10.1007/s12665-019-8310-4

Dublyansky, Y. V., Klimchouk, A. B., Tokarev, S. V., Amelichev, G. N., & Spötl, C. (2019). Groundwater of the Crimean peninsula: a first systematic study using stable isotopes. *Isotopes Environ Health Stud*, 1-19. doi:10.1080/10256016.2019.1650743

Ducci, D., Della Morte, R., Mottola, A., Onorati, G., & Pugliano, G. (2019). Nitrate trends in groundwater of the Campania region (southern Italy). *Environmental Science and Pollution Research, 26*(3), 2120-2131. doi:10.1007/s11356-017-0978-y

Dung, B. V., Stattegger, K., Unverricht, D., Phach, P. V., & Thanh, N. T. (2013). Late Pleistocene–Holocene seismic stratigraphy of the Southeast Vietnam Shelf. *Global and Planetary Change, 110*, 156-169. doi:http://dx.doi.org/10.1016/j.gloplacha.2013.09.010

Duy, N. L., Dung, N. V., Heidbüchel, I., Meyer, H., Weiler, M., Merz, B., & Apel, H. (2019). Identification of groundwater mean transit times of precipitation and riverbank infiltration by two-component lumped parameter models. *HYDROLOGICAL PROCESSES, 0*(ja). doi:10.1002/hyp.13549

Elmahdy, S. I., & Mohamed, M. M. (2013). Influence of geological structures on groundwater accumulation and groundwater salinity in Musandam Peninsula, UAE and Oman. *Geocarto International, 28*(5), 453-472. doi:10.1080/10106049.2012.724455

Erban, L. E., Gorelick, S. M., Zebker, H. A., & Fendorf, S. (2013). Release of arsenic to deep groundwater in the Mekong Delta, Vietnam, linked to pumping-induced land subsidence. *Proc Natl Acad Sci U S A, 110*(34), 13751-13756. doi:10.1073/pnas.1300503110

Eslami, S., Hoekstra, P., Kernkamp, H., Nguyen Trung, N., Do Duc, D., Tran Quang, T., . . . van der Vegt, M. (2019). Flow Division Dynamics in the Mekong Delta: Application of a 1D-2D Coupled Model. *Water, 11*(4). doi:10.3390/w11040837

Essaid, H. I., & Caldwell, R. R. (2017). Evaluating the impact of irrigation on surface water – groundwater interaction and stream temperature in an agricultural watershed. *Science of The Total Environment, 599-600*, 581-596. doi:10.1016/j.scitotenv.2017.04.205

Evaristo, J., & McDonnell, J. J. (2017). Prevalence and magnitude of groundwater use by vegetation: a global stable isotope meta-analysis. *Sci Rep, 7*, 44110-44110. doi:10.1038/srep44110

Famiglietti, J. S. (2014). The global groundwater crisis. *Nature Climate Change, 4*(11), 945-948. doi:10.1038/nclimate2425

Ferguson, G., & Gleeson, T. (2012a). Vulnerability of coastal aquifers to groundwater use and climate change. *Nature Clim. Change, 2*(5), 342-345. doi:http://www.nature.com/nclimate/journal/v2/n5/abs/nclimate1413.html#supplementary-information

Ferguson, G., & Gleeson, T. (2012b). Vulnerability of coastal aquifers to groundwater use and climate change. *Nature Climate Change, 2*(5), 342-345. doi:10.1038/nclimate1413

Fleckenstein, J. H., Krause, S., Hannah, D. M., & Boano, F. (2010). Groundwater-surface water interactions: New methods and models to improve understanding of processes and dynamics. *Advances in Water Resources, 33*(11), 1291-1295. doi:https://doi.org/10.1016/j.advwatres.2010.09.011

Forrest, S. (1993). Genetic algorithms: principles of natural selection applied to computation. *Science, 261*(5123), 872-878. doi:10.1126/science.8346439

Frank Wagner, Vuong Bui Tran, & Renaud, F. G. (2010). Chapter 7: Groundwater Resources in the Mekong Delta: Availability, Utilization and Risks. In F. G. R. a. C. Kuenze (Ed.), *The Mekong Delta system: Interdisciplinary Analyses of a River Delta*. Dordrecht Heidelberg New York London: Springer

Friedman, J. H. (2001). Greedy Function Approximation: A Gradient Boosting Machine. *The Annals of Statistics, 29*(5), 1189-1232.

Gallardo, A. H., & Marui, A. (2007). Modeling the dynamics of the freshwater-saltwater interface in response to construction activities at a coastal site. *International Journal of Environmental Science & Technology, 4*(3), 285-294. doi:10.1007/bf03326286

Gasda, S. E., Bachu, S., & Celia, M. A. (2004). Spatial characterization of the location of potentially leaky wells penetrating a deep saline aquifer in a mature sedimentary basin. *Environmental Geology, 46*(6), 707-720. doi:10.1007/s00254-004-1073-5

Gat, J. R. (1995). Stable Isotopes of Fresh and Saline Lakes. In A. Lerman, D. M. Imboden, & J. R. Gat (Eds.), *Physics and Chemistry of Lakes* (pp. 139-165). Berlin, Heidelberg: Springer Berlin Heidelberg.

Gat, J. R., & Tzur, Y. (1967). *Modification of the isotopic composition of rainwater by processes which occur before groundwater recharge*. International Atomic Energy Agency (IAEA): IAEA.

Gemitzi, A., Stefanopoulos, K., Schmidt, M., & Richnow, H. H. (2014). Seawater intrusion into groundwater aquifer through a coastal lake - complex interaction characterised by water isotopes 2H and 18O. *Isotopes Environ Health Stud, 50*(1), 74-87. doi:10.1080/10256016.2013.823960

Giordano, M. (2009). Global Groundwater? Issues and Solutions. *Annual Review of Environment and Resources, 34*(1), 153-178. doi:10.1146/annurev.environ.030308.100251

Gleeson, T., Befus, K. M., Jasechko, S., Luijendijk, E., & Cardenas, M. B. (2016). The global volume and distribution of modern groundwater. *Nature Geosci, 9*(2), 161-167. doi:10.1038/ngeo2590

http://www.nature.com/ngeo/journal/v9/n2/abs/ngeo2590.html#supplementary-information

Gleeson, T., Wada, Y., Bierkens, M. F. P., & van Beek, L. P. H. (2012). Water balance of global aquifers revealed by groundwater footprint. *Nature, 488*(7410), 197-200. doi:http://www.nature.com/nature/journal/v488/n7410/abs/nature11295.html#supplementary-information

González-Trinidad, J., Pacheco-Guerrero, A., Júnez-Ferreira, H., Bautista-Capetillo, C., & Hernández-Antonio, A. (2017). Identifying Groundwater Recharge Sites through Environmental Stable Isotopes in an Alluvial Aquifer. *Water, 9*(8), 569.

Gopinath, S., Srinivasamoorthy, K., Saravanan, K., & Prakash, R. (2019). Tracing groundwater salinization using geochemical and isotopic signature in Southeastern coastal Tamilnadu, India. *Chemosphere, 236*, 124305. doi:https://doi.org/10.1016/j.chemosphere.2019.07.036

Gracz, M. B., Moffett, M. F., Siegel, D. I., & Glaser, P. H. (2015). Analyzing peatland discharge to streams in an Alaskan watershed: An integration of end-member mixing analysis and a water balance approach. *Journal of Hydrology, 530*, 667-676. doi:https://doi.org/10.1016/j.jhydrol.2015.09.072

Graf, T., & Therrien, R. (2005). Variable-density groundwater flow and solute transport in porous media containing nonuniform discrete fractures. *Advances in Water Resources, 28*(12), 1351-1367. doi:https://doi.org/10.1016/j.advwatres.2005.04.011

Groen, H. K. a. J. (2000). Modes of seawater intrusion during transgressions. *Water Resources Research, 36*(12), 3581-3589. doi:doi:10.1029/2000WR900243

Gugliotta, M., Saito, Y., Nguyen, V. L., Ta, T. K. O., Nakashima, R., Tamura, T., . . . Yamamoto, S. (2017). Process regime, salinity, morphological, and sedimentary trends along the fluvial to marine transition zone of the mixed-energy Mekong River delta, Vietnam. *Continental Shelf Research, 147*, 7-26. doi:https://doi.org/10.1016/j.csr.2017.03.001

Guhl, F., Pulido-Bosch, A., Pulido-Leboeuf, P., Gisbert, J., Sanchez-Martos, F., & Vallejos, A. (2006). Geometry and dynamics of the freshwater—seawater interface in a coastal aquifer in southeastern Spain. *Hydrological Sciences Journal, 51*(3), 543-555. doi:10.1623/hysj.51.3.543

Guo, Q., Huang, J., Zhou, Z., & Wang, J. (2019). Experiment and Numerical Simulation of Seawater Intrusion under the Influences of Tidal Fluctuation and Groundwater

Exploitation in Coastal Multilayered Aquifers. *Geofluids, 2019*, 17. doi:10.1155/2019/2316271

Guyon, I., & Elisseeff, A. An Introduction to Feature Extraction *Feature Extraction* (pp. 1-25): Springer Berlin Heidelberg.

Ha, T. P., Dieperink, C., Dang Tri, V. P., Otter, H. S., & Hoekstra, P. (2018). Governance conditions for adaptive freshwater management in the Vietnamese Mekong Delta. *Journal of Hydrology*, *557*, 116-127. doi:https://doi.org/10.1016/j.jhydrol.2017.12.024

Haase, C., Ebert, M., & Dethlefsen, F. (2016). Uncertainties of geochemical codes and thermodynamic databases for predicting the impact of carbon dioxide on geologic formations. *Applied Geochemistry, 67*, 81-92. doi:https://doi.org/10.1016/j.apgeochem.2016.01.008

Haddout, S., Igouzal, M., & Maslouhi, A. (2017). Seawater Intrusion in Semi-Closed Convergent Estuaries (Case Study of Moroccan Atlantic Estuaries): Application of Salinity Analytical Models. *Marine Geodesy*, *40*(5), 275-296. doi:10.1080/01490419.2017.1319446

Hall, J., Rasmussen, C., & Maciejowski, J. (2012, 10-13 Dec. 2012). *Modelling and control of nonlinear systems using Gaussian processes with partial model information.* Paper presented at the 2012 IEEE 51st IEEE Conference on Decision and Control (CDC).

Han, D., & Currell, M. J. (2018). Delineating multiple salinization processes in a coastal plain aquifer, northern China: hydrochemical and isotopic evidence. *Hydrology and Earth System Sciences, 22*(6), 3473-3491. doi:10.5194/hess-22-3473-2018

Han, D., & Currell, M. J. (2018). Delineating multiple salinization processes in a coastal plain aquifer, northern China: hydrochemical and isotopic evidence. *Hydrol. Earth Syst. Sci., 22*(6), 3473-3491. doi:10.5194/hess-22-3473-2018

Han, D., Post, V. E. A., & Song, X. (2015). Groundwater salinization processes and reversibility of seawater intrusion in coastal carbonate aquifers. *Journal of Hydrology, 531*, 1067-1080. doi:https://doi.org/10.1016/j.jhydrol.2015.11.013

Hanebuth, T. J. J., Proske, U., Saito, Y., Nguyen, V. L., & Ta, T. K. O. (2012). Early growth stage of a large delta — Transformation from estuarine-platform to deltaic-progradational conditions (the northeastern Mekong River Delta, Vietnam). *Sedimentary Geology*, *261*, 108-119. doi:http://dx.doi.org/10.1016/j.sedgeo.2012.03.014

Healy, R. W., & Cook, P. G. (2002). Using groundwater levels to estimate recharge. *Hydrogeology Journal*, *10*(1), 91-109. doi:10.1007/s10040-001-0178-0

Hecht, J. S., Lacombe, G., Arias, M. E., Dang, T. D., & Piman, T. (2019). Hydropower dams of the Mekong River basin: A review of their hydrological impacts. *Journal of Hydrology, 568*, 285-300. doi:https://doi.org/10.1016/j.jhydrol.2018.10.045

Herrera, C., Gamboa, C., Custodio, E., Jordan, T., Godfrey, L., Jódar, J., . . . Sáez, A. (2018). Groundwater origin and recharge in the hyperarid Cordillera de la Costa, Atacama Desert, northern Chile. *Science of The Total Environment, 624*, 114-132. doi:https://doi.org/10.1016/j.scitotenv.2017.12.134

Hillel, N., Wine, M. L., Laronne, J. B., Licha, T., Be'eri-Shlevin, Y., & Siebert, C. (2019). Identifying spatiotemporal variations in groundwater-surface water interactions using shallow pore water chemistry in the lower Jordan river. *Advances in Water Resources, 131*, 103388. doi:https://doi.org/10.1016/j.advwatres.2019.103388

Himi, M., Tapias, J., Benabdelouahab, S., Salhi, A., Rivero, L., Elgettafi, M., . . . Casas, A. (2017). Geophysical characterization of saltwater intrusion in a coastal aquifer: The

case of Martil-Alila plain (North Morocco). *Journal of African Earth Sciences, 126*, 136-147. doi:https://doi.org/10.1016/j.jafrearsci.2016.11.011

Hira, Z. M., & Gillies, D. F. (2015). A Review of Feature Selection and Feature Extraction Methods Applied on Microarray Data. *Advances in Bioinformatics, 2015*, 1-13. doi:10.1155/2015/198363

Ho, H. D., Aramyossy, J. F., Louvat, D., Huu, M. Q., Nguyen, T. V., & Nguyen, K. C. (1991). *Environmental isotopes study related to the origin, salinization and movement of groundwater in the Mekong Delta (Vietnam)*. Retrieved from VIENNA:

Hoa, P. V., Giang, N. V., Binh, N. A., Hai, L. V. H., Pham, T.-D., Hasanlou, M., & Tien Bui, D. (2019). Soil Salinity Mapping Using SAR Sentinel-1 Data and Advanced Machine Learning Algorithms: A Case Study at Ben Tre Province of the Mekong River Delta (Vietnam). *Remote Sensing, 11*(2), 128.

Hoang, H. T., & Bäumle, R. (2018). Complex hydrochemical characteristics of the Middle–Upper Pleistocene aquifer in Soc Trang Province, Southern Vietnam. *Environmental Geochemistry and Health*. doi:10.1007/s10653-018-0167-z

Hoang, H. T., & Bäumle, R. (2019). Complex hydrochemical characteristics of the Middle–Upper Pleistocene aquifer in Soc Trang Province, Southern Vietnam. *Environmental Geochemistry and Health, 41*(1), 325-341. doi:10.1007/s10653-018-0167-z

Hoang, T. M., van Lap, N., Oanh, T. T. K., & Jiro, T. (2016). The influence of delta formation mechanism on geotechnical property sequence of the late Pleistocene–Holocene sediments in the Mekong River Delta. *Heliyon, 2*(11), e00165. doi:https://doi.org/10.1016/j.heliyon.2016.e00165

Hoogewerff, J., Kemp, H. F., Leng, M. J., & Meier-Augenstein, W. (2019). Spatial variability of 2H and 18O composition of meteoric freshwater lakes in Scotland. *Isotopes Environ Health Stud, 55*(3), 237-253. doi:10.1080/10256016.2019.1609958

Hooper, R. P., Christophersen, N., & Peters, N. E. (1990). Modelling streamwater chemistry as a mixture of soilwater end-members — An application to the Panola Mountain catchment, Georgia, U.S.A. *Journal of Hydrology, 116*(1), 321-343. doi:https://doi.org/10.1016/0022-1694(90)90131-G

Hornero, J., Manzano, M., Ortega, L., & Custodio, E. (2016). Integrating soil water and tracer balances, numerical modelling and GIS tools to estimate regional groundwater recharge: Application to the Alcadozo Aquifer System (SE Spain). *Science of The Total Environment, 568*, 415-432. doi:http://dx.doi.org/10.1016/j.scitotenv.2016.06.011

Hosono, T., Ikawa, R., Shimada, J., Nakano, T., Saito, M., Onodera, S.-i., . . . Taniguchi, M. (2009). Human impacts on groundwater flow and contamination deduced by multiple isotopes in Seoul City, South Korea. *Science of The Total Environment, 407*(9), 3189-3197. doi:https://doi.org/10.1016/j.scitotenv.2008.04.014

Howcroft, W., Cartwright, I., Fifield, L. K., & Cendón, D. I. (2017). Differences in groundwater and chloride residence times in saline groundwater: The Barwon River Catchment of Southeast Australia. *Chemical Geology, 451*, 154-168. doi:https://doi.org/10.1016/j.chemgeo.2017.01.015

Huang, P., & Wang, X. (2017). Applying Environmental Isotope Theory to Groundwater Recharge in the Jiaozuo Mining Area, China. *Geofluids, 2017*, 11. doi:10.1155/2017/9568349

Huang, W., Chang, S.-Q., Xie, C.-L., & Zhang, Z.-P. (2017). Moisture sources of extreme summer precipitation events in North Xinjiang and their relationship with

atmospheric circulation. *Advances in Climate Change Research, 8*(1), 12-17. doi:https://doi.org/10.1016/j.accre.2017.02.001

Huang, Y., Miyauchi, K., Endo, G., Don, L. D., Manh, N. C., & Inoue, C. (2016). Arsenic contamination of groundwater and agricultural soil irrigated with the groundwater in Mekong Delta, Vietnam. *Environmental Earth Sciences, 75*(9), 757. doi:10.1007/s12665-016-5535-3

Huizer, S., Radermacher, M., de Vries, S., Oude Essink, G. H. P., & Bierkens, M. F. P. (2018). Impact of coastal forcing and groundwater recharge on the growth of a fresh groundwater lens in a mega-scale beach nourishment. *Hydrol. Earth Syst. Sci., 22*(2), 1065-1080. doi:10.5194/hess-22-1065-2018

Hung Van, P., Van Geer, F. C., Bui Tran, V., Dubelaar, W., & Oude Essink, G. H. P. (2019). Paleo-hydrogeological reconstruction of the fresh-saline groundwater distribution in the Vietnamese Mekong Delta since the late Pleistocene. *Journal of Hydrology: Regional Studies, 23*, 100594. doi:https://doi.org/10.1016/j.ejrh.2019.100594

Hung Vu, V., & Merkel, B. J. (2019). Estimating groundwater recharge for Hanoi, Vietnam. *Science of The Total Environment, 651*, 1047-1057. doi:https://doi.org/10.1016/j.scitotenv.2018.09.225

Huyen, D. T., Tabelin, C. B., Thuan, H. M., Dang, D. H., Truong, P. T., Vongphuthone, B., . . . Igarashi, T. (2019). The solid-phase partitioning of arsenic in unconsolidated sediments of the Mekong Delta, Vietnam and its modes of release under various conditions. *Chemosphere, 233*, 512-523. doi:https://doi.org/10.1016/j.chemosphere.2019.05.235

Idris, A. N., Aris, A. Z., Praveena, S. M., Suratman, S., Tawnie, I., Samsuddin, M. K. N., & Sefei, A. (2016). Hydrogeochemistry Characteristics in Kampong Salang, Tioman Island, Pahang, Malaysia. *IOP Conference Series: Materials Science and Engineering, 136*, 012065. doi:10.1088/1757-899x/136/1/012065

Insa, O., Florian, D., Adrian, G., Martha, S., Ralf, K., Tim, A., & Thomas, N. (2017). Seasonality of stable isotope composition of atmospheric water input at the southern slopes of Mt. Kilimanjaro, Tanzania. *HYDROLOGICAL PROCESSES, 31*(22), 3932-3947. doi:doi:10.1002/hyp.11311

IPCC. (2007). *Climate Change 2007: Impacts, Adaptation and Vulnerability*. Retrieved from Cambridge, UK. (IPCC: Intergovernmental Panel on Climate Change):

Isa, N. M., Aris, A. Z., & Sulaiman, W. N. A. W. (2012). Extent and severity of groundwater contamination based on hydrochemistry mechanism of sandy tropical coastal aquifer. *Science of The Total Environment, 438*, 414-425. doi:https://doi.org/10.1016/j.scitotenv.2012.08.069

Isazadeh, M., Biazar, S. M., & Ashrafzadeh, A. (2017). Support vector machines and feed-forward neural networks for spatial modeling of groundwater qualitative parameters. *Environmental Earth Sciences, 76*(17), 610. doi:10.1007/s12665-017-6938-5

Iwamori, H., Yoshida, K., Nakamura, H., Kuwatani, T., Hamada, M., Haraguchi, S., & Ueki, K. (2017). Classification of geochemical data based on multivariate statistical analyses: Complementary roles of cluster, principal component, and independent component analyses. *Geochemistry, Geophysics, Geosystems, 18*(3), 994-1012. doi:10.1002/2016GC006663

James, A. L., & Roulet, N. T. (2006). Investigating the applicability of end-member mixing analysis (EMMA) across scale: A study of eight small, nested catchments in a temperate forested watershed. *Water Resources Research, 42*(8), n/a-n/a. doi:10.1029/2005WR004419

Jankowski, J., & Acworth, R. I. (1997). Impact of Debris-Flow Deposits on Hydrogeochemical Processes and the Developement of Dryland Salinity in the Yass River Catchment, New South Wales, Australia. *Hydrogeology Journal, 5*(4), 71-88.

Javadi, A., Hussain, M., Sherif, M., & Farmani, R. (2015). Multi-objective optimization of different management scenarios to control seawater intrusion in coastal aquifers. *Water Resources Management, 29*(6), 1843-1857.

Jennings, P. C., Lysgaard, S., Hummelshøj, J. S., Vegge, T., & Bligaard, T. (2019). Genetic algorithms for computational materials discovery accelerated by machine learning. *npj Computational Materials, 5*(1), 46. doi:10.1038/s41524-019-0181-4

Jia, X., O'Connor, D., Hou, D., Jin, Y., Li, G., Zheng, C., . . . Luo, J. (2019). Groundwater depletion and contamination: Spatial distribution of groundwater resources sustainability in China. *Science of The Total Environment, 672*, 551-562. doi:https://doi.org/10.1016/j.scitotenv.2019.03.457

Jiang, H.-z., Shen, Y.-m., & Wang, S.-d. (2009). Numerical study on salinity stratification in the Oujiang River Estuary. *Journal of Hydrodynamics, Ser. B, 21*(6), 835-842. doi:https://doi.org/10.1016/S1001-6058(08)60220-6

Jiang, J.-Q., Ashekuzzaman, S. M., Jiang, A., Sharifuzzaman, S. M., & Chowdhury, S. R. (2013). Arsenic Contaminated Groundwater and Its Treatment Options in Bangladesh. *International Journal of Environmental Research and Public Health, 10*(1), 18-46. doi:10.3390/ijerph10010018

Johnson, N. E., Bonczak, B., & Kontokosta, C. E. (2018). Using a gradient boosting model to improve the performance of low-cost aerosol monitors in a dense, heterogeneous urban environment. *Atmospheric Environment, 184*, 9-16. doi:https://doi.org/10.1016/j.atmosenv.2018.04.019

Kabeya, N., Kubota, T., Shimizu, A., Nobuhiro, T., Tsuboyama, Y., Chann, S., & Tith, N. (2008). Isotopic investigation of river water mixing around the confluence of the Tonle Sap and Mekong rivers. *Hydrological Processes, 22*(9), 1351-1358. doi:10.1002/hyp.6944

Kagabu, M., Shimada, J., Delinom, R., Tsujimura, M., & Taniguchi, M. (2011). Groundwater flow system under a rapidly urbanizing coastal city as determined by hydrogeochemistry. *Journal of Asian Earth Sciences, 40*(1), 226-239. doi:https://doi.org/10.1016/j.jseaes.2010.07.012

Kaiser, H. F. (1974). An index of factorial simplicity. *Psychometrika, 39*(1), 31-36. doi:10.1007/BF02291575

Kaltreider, R. C., Davis, A. M., Lariviere, J. P., & Hamilton, J. W. (2001). Arsenic alters the function of the glucocorticoid receptor as a transcription factor. *Environ Health Perspect, 109*(3), 245-251.

Kanagaraj, G., Elango, L., Sridhar, S. G. D., & Gowrisankar, G. (2018). Hydrogeochemical processes and influence of seawater intrusion in coastal aquifers south of Chennai, Tamil Nadu, India. *Environmental Science and Pollution Research, 25*(9), 8989-9011. doi:10.1007/s11356-017-0910-5

Karimi, L., Motagh, M., & Entezam, I. (2019). Modeling groundwater level fluctuations in Tehran aquifer: Results from a 3D unconfined aquifer model. *Groundwater for Sustainable Development, 8*, 439-449. doi:https://doi.org/10.1016/j.gsd.2019.01.003

Kazama, S., Hagiwara, T., Ranjan, P., & Sawamoto, M. (2007). Evaluation of groundwater resources in wide inundation areas of the Mekong River basin. *Journal of Hydrology, 340*(3), 233-243. doi:https://doi.org/10.1016/j.jhydrol.2007.04.017

Khalaj, M., Kholghi, M., Saghafian, B., & Bazrafshan, J. (2019). Impact of climate variation and human activities on groundwater quality in northwest of Iran. *Journal of Water Supply: Research and Technology-Aqua, 68*(2), 121-135. doi:10.2166/aqua.2019.064

Khan, A., Ireson, A., & Kovats, S. (2011). Drinking water salinity and maternal health in coastal Bangladesh: implications of climate change. *Environ Health Perspect, 119*. doi:10.1289/ehp.1002804

Khan, A. E., Scheelbeek, P. F. D., Shilpi, A. B., Chan, Q., Mojumder, S. K., Rahman, A., . . . Vineis, P. (2014). Salinity in Drinking Water and the Risk of (Pre)Eclampsia and Gestational Hypertension in Coastal Bangladesh: A Case-Control Study. *PLOS ONE, 9*(9), e108715. doi:10.1371/journal.pone.0108715

Khan, M. M. A., & Umar, R. (2010). Significance of silica analysis in groundwater in parts of Central Ganga Plain, Uttar Pradesh, India. *Current Science, 98*(9), 1237-1240.

Khaska, M., Le Gal La Salle, C., Lancelot, J., team, A., Mohamad, A., Verdoux, P., . . . Simler, R. (2013a). Origin of groundwater salinity (current seawater vs. saline deep water) in a coastal karst aquifer based on Sr and Cl isotopes. Case study of the La Clape massif (southern France). *Applied Geochemistry, 37*, 212-227. doi:10.1016/j.apgeochem.2013.07.006

Khaska, M., Le Gal La Salle, C., Lancelot, J., team, A., Mohamad, A., Verdoux, P., . . . Simler, R. (2013b). Origin of groundwater salinity (current seawater vs. saline deep water) in a coastal karst aquifer based on Sr and Cl isotopes. Case study of the La Clape massif (southern France). *Applied Geochemistry, 37*(Supplement C), 212-227. doi:https://doi.org/10.1016/j.apgeochem.2013.07.006

Kim, J.-H., Kim, K.-H., Thao, N. T., Batsaikhan, B., & Yun, S.-T. (2017). Hydrochemical assessment of freshening saline groundwater using multiple end-members mixing modeling: A study of Red River delta aquifer, Vietnam. *Journal of Hydrology, 549*, 703-714. doi:https://doi.org/10.1016/j.jhydrol.2017.04.040

Kim, R.-H., Kim, J.-H., Ryu, J.-S., & Koh, D.-C. (2018). Hydrogeochemical characteristics of groundwater influenced by reclamation, seawater intrusion, and land use in the coastal area of Yeonggwang, Korea. *Geosciences Journal*. doi:10.1007/s12303-018-0065-5

Kohavi, R., & John, G. H. (1997). Wrappers for feature subset selection. *Artificial Intelligence, 97*(1), 273-324. doi:https://doi.org/10.1016/S0004-3702(97)00043-X

Konikow, L. F., & Reilly, T. E. (1999). Seawater Intrusion in the United States. In J. Bear, A. H. D. Cheng, S. Sorek, D. Ouazar, & I. Herrera (Eds.), *Seawater Intrusion in Coastal Aquifers — Concepts, Methods and Practices* (pp. 463-506). Dordrecht: Springer Netherlands.

Kopsiaftis, G., Protopapadakis, E., Voulodimos, A., Doulamis, N., & Mantoglou, A. (2019). Gaussian Process Regression Tuned by Bayesian Optimization for Seawater Intrusion Prediction. *Computational Intelligence and Neuroscience, 2019*, 12. doi:10.1155/2019/2859429

Kumar, M., Jain, V., Yamanaka, T., Li, Y., & Bhattacharya, P. (2018). Contaminant Transport and Fate in Freshwater Systems – Integrating the fields of geochemistry, geomorphology and nanotechnology. *Groundwater for Sustainable Development*. doi:https://doi.org/10.1016/j.gsd.2018.09.001

Lal, A., & Datta, B. (2019). Multi-objective groundwater management strategy under uncertainties for sustainable control of saltwater intrusion: Solution for an island country in the South Pacific. *Journal of Environmental Management, 234*, 115-130. doi:https://doi.org/10.1016/j.jenvman.2018.12.054

Lamichhane, S., & Shakya, N. M. (2019). Alteration of groundwater recharge areas due to land use/cover change in Kathmandu Valley, Nepal. *Journal of Hydrology: Regional Studies, 26*, 100635. doi:https://doi.org/10.1016/j.ejrh.2019.100635

Lapworth, D. J., Krishan, G., MacDonald, A. M., & Rao, M. S. (2017). Groundwater quality in the alluvial aquifer system of northwest India: New evidence of the extent of anthropogenic and geogenic contamination. *Science of The Total Environment, 599-600*, 1433-1444. doi:https://doi.org/10.1016/j.scitotenv.2017.04.223

Larsen, F., Tran, L. V., Van Hoang, H., Tran, L. T., Christiansen, A. V., & Pham, N. Q. (2017a). Groundwater salinity influenced by Holocene seawater trapped in incised valleys in the Red River delta plain. *Nature Geosci, 10*(5), 376-381. doi:10.1038/ngeo2938

http://www.nature.com/ngeo/journal/v10/n5/abs/ngeo2938.html#supplementary-information

Larsen, F., Tran, L. V., Van Hoang, H., Tran, L. T., Christiansen, A. V., & Pham, N. Q. (2017b). Groundwater salinity influenced by Holocene seawater trapped in incised valleys in the Red River delta plain. *Nature Geoscience, 10*(5), 376-381. doi:10.1038/ngeo2938

Larsen, F., Tran, L. V., Van Hoang, H., Tran, L. T., Christiansen, A. V., & Pham, N. Q. (2017c). Groundwater salinity influenced by Holocene seawater trapped in incised valleys in the Red River delta plain. *Nat Geosci, 10*, 376. doi:10.1038/ngeo2938

https://www.nature.com/articles/ngeo2938#supplementary-information

Le Duy, N., Dung, N. V., Heidbüchel, I., Meyer, H., Weiler, M., Merz, B., & Apel, H. (2019). Identification of groundwater mean transit times of precipitation and riverbank infiltration by two-component lumped parameter models. *Hydrological Processes, 33*(24), 3098-3118. doi:10.1002/hyp.13549

Le Duy, N., Heidbüchel, I., Meyer, H., Merz, B., & Apel, H. (2018). What controls the stable isotope composition of precipitation in the Mekong Delta? A model-based statistical approach. *Hydrol. Earth Syst. Sci., 22*(2), 1239-1262. doi:10.5194/hess-22-1239-2018

Le Van Khoi, N. K. C., Do Tien Hung. (2002). Groundwater salinity study in the Mekong Delta using isotope techniques. *Communications in Physics, 1*(1), 30-35.

Lee, E., Jayakumar, R., Shrestha, S., & Han, Z. (2018). Assessment of transboundary aquifer resources in Asia: Status and progress towards sustainable groundwater management. *Journal of Hydrology: Regional Studies, 20*, 103-115. doi:https://doi.org/10.1016/j.ejrh.2018.01.004

Lee, S., Currell, M., & Cendón, D. I. (2016). Marine water from mid-Holocene sea level highstand trapped in a coastal aquifer: Evidence from groundwater isotopes, and environmental significance. *Science of The Total Environment, 544*, 995-1007. doi:10.1016/j.scitotenv.2015.12.014

Lever, J., Krzywinski, M., & Altman, N. (2017). Principal component analysis. *Nature Methods, 14*, 641. doi:10.1038/nmeth.4346

Li, B., Yang, G., Wan, R., Dai, X., & Zhang, Y. (2016). Comparison of random forests and other statistical methods for the prediction of lake water level: a case study of the Poyang Lake in China. *Hydrology Research*. doi:10.2166/nh.2016.264

Lim, S., & Chi, S. (2019). Xgboost application on bridge management systems for proactive damage estimation. *Advanced Engineering Informatics, 41*, 100922. doi:https://doi.org/10.1016/j.aei.2019.100922

Liu, J., Liu, Q., & Yang, H. (2016). Assessing water scarcity by simultaneously considering environmental flow requirements, water quantity, and water quality. *Ecological Indicators, 60*, 434-441. doi:http://dx.doi.org/10.1016/j.ecolind.2015.07.019

Liu, Y., Lam, K.-F., Wu, J. T., & Lam, T. T.-Y. (2018). Geographically weighted temporally correlated logistic regression model. *Scientific Reports, 8*(1). doi:10.1038/s41598-018-19772-6

Llamas, R., Custodio, E., Coleto, C., Huerga, A., & Cortina, L. M. (2001). *Intensive Use of Groundwater: Challenges and Opportunities*. LISSE /ABINGDON/EXTON (PA) /TOKYO: A.A.BALKEMAPUBLISHERS.

Loáiciga, H. A., Pingel, T. J., & Garcia, E. S. (2012). Sea Water Intrusion by Sea-Level Rise: Scenarios for the 21st Century. *Groundwater, 50*(1), 37-47. doi:10.1111/j.1745-6584.2011.00800.x

Lu, C., Xin, P., Li, L., & Luo, J. (2015). Seawater intrusion in response to sea-level rise in a coastal aquifer with a general-head inland boundary. *Journal of Hydrology, 522*, 135-140. doi:http://dx.doi.org/10.1016/j.jhydrol.2014.12.053

Lucía, S., Romina, S., Eleonora, C., Esteban, V., & Héctor, P. (2019). Using H, O, Rn isotopes and hydrometric parameters to assess the surface water-groundwater interaction in coastal wetlands associated to the marginal forest of the Río de la Plata. *Continental Shelf Research, 186*, 104-110. doi:https://doi.org/10.1016/j.csr.2019.08.002

Ma, Q., Li, H., Wang, X., Wang, C., Wan, L., Wang, X., & Jiang, X. (2015). Estimation of seawater–groundwater exchange rate: case study in a tidal flat with a large-scale seepage face (Laizhou Bay, China). *Hydrogeology Journal, 23*(2), 265-275. doi:10.1007/s10040-014-1196-z

Ma, X., Xu, F., & Chen, B. (2019). Interpolation of wind pressures using Gaussian process regression. *Journal of Wind Engineering and Industrial Aerodynamics, 188*, 30-42. doi:https://doi.org/10.1016/j.jweia.2019.02.002

Machel, H. G. (1999). Effects of groundwater flow on mineral diagenesis, with emphasis on carbonate aquifers. *Hydrogeology Journal, 7*(1), 94-107. doi:10.1007/s100400050182

Mahlknecht, J., Merchán, D., Rosner, M., Meixner, A., & Ledesma-Ruiz, R. (2017a). Assessing seawater intrusion in an arid coastal aquifer under high anthropogenic influence using major constituents, Sr and B isotopes in groundwater. *Science of The Total Environment, 587-588*, 282-295. doi:https://doi.org/10.1016/j.scitotenv.2017.02.137

Mahlknecht, J., Merchán, D., Rosner, M., Meixner, A., & Ledesma-Ruiz, R. (2017b). Assessing seawater intrusion in an arid coastal aquifer under high anthropogenic influence using major constituents, Sr and B isotopes in groundwater. *Science of The Total Environment, 587–588*, 282-295. doi:https://doi.org/10.1016/j.scitotenv.2017.02.137

Mahmoodzadeh, D., & Karamouz, M. (2019). Seawater intrusion in heterogeneous coastal aquifers under flooding events. *Journal of Hydrology, 568*, 1118-1130. doi:https://doi.org/10.1016/j.jhydrol.2018.11.012

Malki, M., Bouchaou, L., Hirich, A., Ait Brahim, Y., & Choukr-Allah, R. (2017). Impact of agricultural practices on groundwater quality in intensive irrigated area of Chtouka-Massa, Morocco. *Science of The Total Environment, 574*, 760-770. doi:https://doi.org/10.1016/j.scitotenv.2016.09.145

Mandal, B. K., & Suzuki, K. T. (2002). Arsenic round the world: a review. *Talanta, 58*(1), 201-235. doi:https://doi.org/10.1016/S0039-9140(02)00268-0

Manh, N. V., Dung, N. V., Hung, N. N., Kummu, M., Merz, B., & Apel, H. (2015). Future sediment dynamics in the Mekong Delta floodplains: Impacts of hydropower development, climate change and sea level rise. *Global and Planetary Change, 127*, 22-33. doi:http://dx.doi.org/10.1016/j.gloplacha.2015.01.001

Mas-Pla, J., & Menció, A. (2019). Groundwater nitrate pollution and climate change: learnings from a water balance-based analysis of several aquifers in a western Mediterranean region (Catalonia). *Environ Sci Pollut Res Int, 26*(3), 2184-2202. doi:10.1007/s11356-018-1859-8

Masciopinto, C., & Liso, I. S. (2016). Assessment of the impact of sea-level rise due to climate change on coastal groundwater discharge. *Science of The Total Environment, 569-570*, 672-680. doi:https://doi.org/10.1016/j.scitotenv.2016.06.183

Mastrocicco, M., Busico, G., Colombani, N., Vigliotti, M., & Ruberti, D. (2019). Modelling Actual and Future Seawater Intrusion in the Variconi Coastal Wetland (Italy) Due to Climate and Landscape Changes. *Water, 11*(7). doi:10.3390/w11071502

Matiatos, I., Varouchakis, E. A., & Papadopoulou, M. P. (2019). Performance Evaluation of Multiple Groundwater Flow and Nitrate Mass Transport Numerical Models. *Environmental Modeling & Assessment, 24*(6), 659-675. doi:10.1007/s10666-019-9653-7

Maupin, M. A., Kenny, J.F., Hutson, S.S., Lovelace, J.K., Barber, N.L., and Linsey, K.S. (2014). *Estimated use of water in the United States in 2010*. Retrieved from

Mehdizadeh, S. S., Karamalipour, S. E., & Asoodeh, R. (2017). Sea level rise effect on seawater intrusion into layered coastal aquifers (simulation using dispersive and sharp-interface approaches). *Ocean & Coastal Management, 138*, 11-18. doi:http://dx.doi.org/10.1016/j.ocecoaman.2017.01.001

Melloul, A. J., & Goldenberg, L. C. (1997). Monitoring of Seawater Intrusion in Coastal Aquifers: Basics and Local Concerns. *Journal of Environmental Management, 51*(1), 73-86. doi:10.1006/jema.1997.0136

Merola, R. B., Hien, T. T., Quyen, D. T. T., & Vengosh, A. (2015). Arsenic exposure to drinking water in the Mekong Delta. *Science of The Total Environment, 511*, 544-552. doi:http://dx.doi.org/10.1016/j.scitotenv.2014.12.091

Meyer, R., Engesgaard, P., & Sonnenborg, T. O. (2019). Origin and Dynamics of Saltwater Intrusion in a Regional Aquifer: Combining 3-D Saltwater Modeling With Geophysical and Geochemical Data. *Water Resources Research, 55*(3), 1792-1813. doi:10.1029/2018WR023624

Michael, E. D. (1971). Use of Ground Water in Developing the Mekong Delta, Republic of Viet Nam. *Groundwater, 9*(1), 20-24. doi:doi:10.1111/j.1745-6584.1971.tb03527.x

Minderhoud, P. S. J., Erkens, G., Pham, V. H., Bui, V. T., Erban, L., Kooi, H., & Stouthamer, E. (2017). Impacts of 25 years of groundwater extraction on subsidence in the Mekong delta, Vietnam. *Environmental Research Letters, 12*(6), 064006.

Minh, N. H., Minh, T. B., Kajiwara, N., Kunisue, T., Iwata, H., Viet, P. H., . . . Tanabe, S. (2007). Pollution sources and occurrences of selected persistent organic pollutants (POPs) in sediments of the Mekong River delta, South Vietnam. *Chemosphere, 67*(9), 1794-1801. doi:http://dx.doi.org/10.1016/j.chemosphere.2006.05.144

Mohanty, A. K., & Rao, V. V. S. G. (2019). Hydrogeochemical, seawater intrusion and oxygen isotope studies on a coastal region in the Puri District of Odisha, India. *CATENA, 172*, 558-571. doi:https://doi.org/10.1016/j.catena.2018.09.010

Mondal, N. C., Singh, V. P., Singh, V. S., & Saxena, V. K. (2010). Determining the interaction between groundwater and saline water through groundwater major ions chemistry. *Journal of Hydrology, 388*(1), 100-111. doi:https://doi.org/10.1016/j.jhydrol.2010.04.032

Munksgaard, N. C., Kurita, N., Sánchez-Murillo, R., Ahmed, N., Araguas, L., Balachew, D. L., . . . Zwart, C. (2019). Data Descriptor: Daily observations of stable isotope ratios of rainfall in the tropics. *Scientific Reports, 9*(1), 14419. doi:10.1038/s41598-019-50973-9

Mustafa, S. M. T., Hasan, M. M., Saha, A. K., Rannu, R. P., Van Uytven, E., Willems, P., & Huysmans, M. (2019). Multi-model approach to quantify groundwater-level prediction uncertainty using an ensemble of global climate models and multiple abstraction scenarios. *Hydrol. Earth Syst. Sci., 23*(5), 2279-2303. doi:10.5194/hess-23-2279-2019

Nadiri, A. A., Sedghi, Z., Khatibi, R., & Sadeghfam, S. (2018). Mapping specific vulnerability of multiple confined and unconfined aquifers by using artificial intelligence to learn from multiple DRASTIC frameworks. *Journal of Environmental Management, 227*, 415-428. doi:https://doi.org/10.1016/j.jenvman.2018.08.019

Naghibi, S. A., Pourghasemi, H. R., & Dixon, B. (2015). GIS-based groundwater potential mapping using boosted regression tree, classification and regression tree, and random forest machine learning models in Iran. *Environmental Monitoring and Assessment, 188*(1). doi:10.1007/s10661-015-5049-6

Nam, N. D. G., Akira, G., Kazutoshi, O., Trung, N. H., & Ngan, N. V. C. (2019). Assessment of Groundwater Quality and Its Suitability for Domestic and Irrigation Use in the Coastal Zone of the Mekong Delta, Vietnam. In M. A. Stewart & P. A. Coclanis (Eds.), *Water and Power: Environmental Governance and Strategies for Sustainability in the Lower Mekong Basin* (pp. 173-185). Cham: Springer International Publishing.

Nam, N. D. G., Goto, A., & Osawa, K. (2017). Groundwater Modeling for Groundwater Management in the Coastal Area of Mekong Delta, Vietnam. *農業農村工学会論文集, 85*(1), I_93-I_103. doi:10.11408/jsidre.85.I_93

Naser, A. M., Rahman, M., Unicomb, L., Doza, S., Ahmed, K. M., Uddin, M. N., . . . Luby, S. P. (2017). Drinking water salinity and kidney health in southwest coastal Bangladesh: baseline findings of a community-based stepped-wedge randomised trial. *The Lancet, 389*, S15. doi:10.1016/s0140-6736(17)31127-3

Nejatijahromi, Z., Nassery, H. R., Hosono, T., Nakhaei, M., Alijani, F., & Okumura, A. (2019). Groundwater nitrate contamination in an area using urban wastewaters for agricultural irrigation under arid climate condition, southeast of Tehran, Iran. *Agricultural Water Management, 221*, 397-414. doi:https://doi.org/10.1016/j.agwat.2019.04.015

Nguyen, A. D., & Savenije, H. H. (2006). Salt intrusion in multi-channel estuaries: a case study in the Mekong Delta, Vietnam. *Hydrol. Earth Syst. Sci., 10*(5), 743-754. doi:10.5194/hess-10-743-2006

Nguyen, A. D., Savenije, H. H. G., Pham, D. N., & Tang, D. T. (2008). Using salt intrusion measurements to determine the freshwater discharge distribution over the branches of a multi-channel estuary: The Mekong Delta case. *Estuarine, Coastal and Shelf Science, 77*(3), 433-445. doi:http://dx.doi.org/10.1016/j.ecss.2007.10.010

Nguyen, K. C., Huynh, L., Le, D. C., Nguyen, V. N., & Tran, B. L. (2007). *Isotope compositions of Mekong river flow water in the south of Vietnam*. International Atomic Energy Agency (IAEA): IAEA.

Nguyen, T. V., & Tanaka, H. (2007). Study on the Effect of Morphology Change on Salinity Distribution in the Dinh An Estuary, Lower Mekong River of Vietnam. *Journal of Coastal Research*, 268-272.

Nguyen, V. L., Ta, T. K. O., & Saito, Y. (2010). Early Holocene initiation of the Mekong River delta, Vietnam, and the response to Holocene sea-level changes detected from DT1 core analyses. *Sedimentary Geology, 230*(3), 146-155. doi:http://dx.doi.org/10.1016/j.sedgeo.2010.07.006

Nguyen, V. L., Ta, T. K. O., & Tateishi, M. (1998). Late Holocene depositional environments and coastal evolution of the Mekong River Delta, Southern Vietnam. *Journal of Asian Earth Sciences*(18), 427- 439.

Nhan, N. H. (2016). Tidal regime deformation by sea level rise along the coast of the Mekong Delta. *Estuarine, Coastal and Shelf Science, 183*, 382-391. doi:http://dx.doi.org/10.1016/j.ecss.2016.07.004

Nishanthiny, S. C., Thushyanthy, M., Barathithasan, T., & Saravanan, S. (2010). Irrigation water quality based on hydro chemical analysis, Jaffna, Sri Lanka. *Am Eurasian J Agric Environ Sci, 7*(1), 100-102.

Nofal, E. R., Amer, M. A., El-Didy, S. M., & Fekry, A. M. (2015). Delineation and modeling of seawater intrusion into the Nile Delta Aquifer: A new perspective. *Water Science, 29*(2), 156-166. doi:https://doi.org/10.1016/j.wsj.2015.11.003

Nogueira, G., Stigter, T. Y., Zhou, Y., Mussa, F., & Juizo, D. (2019). Understanding groundwater salinization mechanisms to secure freshwater resources in the water-scarce city of Maputo, Mozambique. *Science of The Total Environment, 661*, 723-736. doi:https://doi.org/10.1016/j.scitotenv.2018.12.343

Norrman, J., Sparrenbom, C. J., Berg, M., Dang, D. N., Jacks, G., Harms-Ringdahl, P., . . . Rosqvist, H. (2015). Tracing sources of ammonium in reducing groundwater in a well field in Hanoi (Vietnam) by means of stable nitrogen isotope (δ15N) values. *Applied Geochemistry, 61*(Supplement C), 248-258. doi:https://doi.org/10.1016/j.apgeochem.2015.06.009

Nowacki, D. J., Ogston, A. S., Nittrouer, C. A., Fricke, A. T., & Van, P. D. T. (2015). Sediment dynamics in the lower Mekong River: Transition from tidal river to estuary. *Journal of Geophysical Research: Oceans, 120*(9), 6363-6383. doi:10.1002/2015JC010754

Okakita, N., Iwatake, K., Hirata, H., & Ueda, A. (2019). Contribution of precipitation to groundwater flow systems in three major alluvial fans in Toyama Prefecture, Japan: stable-isotope characterization and application to the use of groundwater for urban heat exchangers. *Hydrogeology Journal, 27*(1), 345-362. doi:10.1007/s10040-018-1850-y

Paine, J. G. (2003). Determining salinization extent, identifying salinity sources, and estimating chloride mass using surface, borehole, and airborne electromagnetic induction methods. *Water Resources Research, 39*(3). doi:10.1029/2001WR000710

Parizi, E., Hosseini, S. M., Ataie-Ashtiani, B., & Simmons, C. T. (2019). Vulnerability mapping of coastal aquifers to seawater intrusion: Review, development and application. *Journal of Hydrology, 570*, 555-573. doi:https://doi.org/10.1016/j.jhydrol.2018.12.021

Park, H.-Y., Jang, K., Ju, J. W., & Yeo, I. W. (2012). Hydrogeological characterization of seawater intrusion in tidally-forced coastal fractured bedrock aquifer. *Journal of Hydrology, 446–447*, 77-89. doi:http://dx.doi.org/10.1016/j.jhydrol.2012.04.033

Park, J., & Kwock, C. K. (2015). Sodium intake and prevalence of hypertension, coronary heart disease, and stroke in Korean adults. *Journal of Ethnic Foods, 2*(3), 92-96. doi:https://doi.org/10.1016/j.jef.2015.08.007

Park, J., & Sandberg, I. W. (1991). Universal Approximation Using Radial-Basis-Function Networks. *Neural Computation, 3*(2), 246-257. doi:10.1162/neco.1991.3.2.246

Parra Suárez, S., Peiffer, S., & Gebauer, G. (2019). Origin and fate of nitrate runoff in an agricultural catchment: Haean, South Korea – Comparison of two extremely different monsoon seasons. *Science of The Total Environment, 648*, 66-79. doi:https://doi.org/10.1016/j.scitotenv.2018.08.115

Pelizardi, F., Bea, S. A., Carrera, J., & Vives, L. (2017). Identifying geochemical processes using End Member Mixing Analysis to decouple chemical components for mixing ratio calculations. *Journal of Hydrology, 550*, 144-156. doi:https://doi.org/10.1016/j.jhydrol.2017.04.010

Peng, C., He, J.-T., Wang, M.-l., Zhang, Z.-g., & Wang, L. (2018). Identifying and assessing human activity impacts on groundwater quality through hydrogeochemical anomalies and NO3−, NH4+, and COD contamination: a case study of the Liujiang River Basin, Hebei Province, P.R. China. *Environmental Science and Pollution Research, 25*(4), 3539-3556. doi:10.1007/s11356-017-0497-x

Pham, B. T., Jaafari, A., Prakash, I., Singh, S. K., Quoc, N. K., & Bui, D. T. (2019). Hybrid computational intelligence models for groundwater potential mapping. *CATENA, 182*, 104101. doi:https://doi.org/10.1016/j.catena.2019.104101

Pham, B. T., Nguyen, M. D., Bui, K.-T. T., Prakash, I., Chapi, K., & Bui, D. T. (2019). A novel artificial intelligence approach based on Multi-layer Perceptron Neural Network and Biogeography-based Optimization for predicting coefficient of consolidation of soil. *CATENA, 173*, 302-311. doi:https://doi.org/10.1016/j.catena.2018.10.004

Phillips, F. M., Peeters, L. A., Tansey, M. K., & Davis, S. N. (1986). Paleoclimatic inferences from an isotopic investigation of groundwater in the central San Juan Basin, New Mexico. *Quaternary Research, 26*(2), 179-193. doi:https://doi.org/10.1016/0033-5894(86)90103-1

Piña, A., Donado, L. D., Blake, S., & Cramer, T. (2018). Compositional multivariate statistical analysis of the hydrogeochemical processes in a fractured massif: La Línea tunnel project, Colombia. *Applied Geochemistry, 95*, 1-18. doi:https://doi.org/10.1016/j.apgeochem.2018.05.012

Piper, A. M. (1944). A graphic procedure in the geochemical interpretation of water-analyses. *Eos, Transactions American Geophysical Union, 25*(6), 914-928. doi:10.1029/TR025i006p00914

Pistocchi, C., Tamburini, F., Gruau, G., Ferhi, A., Trevisan, D., & Dorioz, J.-M. (2017). Tracing the sources and cycling of phosphorus in river sediments using oxygen isotopes: Methodological adaptations and first results from a case study in France. *Water Research, 111*(Supplement C), 346-356. doi:https://doi.org/10.1016/j.watres.2016.12.038

Podgorski, J., Labhasetwar, P., Saha, D., & Berg, M. (2018). Prediction modeling and mapping of groundwater fluoride contamination throughout India. *Environmental Science & Technology*. doi:10.1021/acs.est.8b01679

Pokhrel, Y., Burbano, M., Roush, J., Kang, H., Sridhar, V., & Hyndman, W. D. (2018). A Review of the Integrated Effects of Changing Climate, Land Use, and Dams on Mekong River Hydrology. *Water, 10*(3). doi:10.3390/w10030266

Praveena, S. M., & Aris, A. Z. (2010). Groundwater resources assessment using numerical model: A case study in low-lying coastal area. *International Journal of Environmental Science & Technology, 7*(1), 135-146. doi:10.1007/BF03326125

R., D. J., Oude, E. G. H. P., J., B. K., & J., S. P. (2013). Uncertainty estimation of end-member mixing using generalized likelihood uncertainty estimation (GLUE), applied in a lowland catchment. *Water Resources Research, 49*(8), 4792-4806. doi:doi:10.1002/wrcr.20341

R., H. E., Paul, B., J., B. A., C., N. S., B., F. R., Marcelo, A., . . . Peter, G. (2015). A global perspective on wetland salinization: ecological consequences of a growing threat to freshwater wetlands. *Ecosphere, 6*(10), art206. doi:doi:10.1890/ES14-00534.1

Ransom, K. M., Nolan, B. T., A. Traum, J., Faunt, C. C., Bell, A. M., Gronberg, J. A. M., . . . Harter, T. (2017). A hybrid machine learning model to predict and visualize nitrate concentration throughout the Central Valley aquifer, California, USA. *Science of The Total Environment, 601-602*, 1160-1172. doi:https://doi.org/10.1016/j.scitotenv.2017.05.192

Rao, N. S., Vidyasagar, G., Surya Rao, P., & Bhanumurthy, P. (2017). Chemistry and quality of groundwater in a coastal region of Andhra Pradesh, India. *Applied Water Science, 7*(1), 285-294. doi:10.1007/s13201-014-0244-0

Rasmussen, C. E. (2004). Gaussian Processes in Machine Learning. In O. Bousquet, U. von Luxburg, & G. Rätsch (Eds.), *Advanced Lectures on Machine Learning: ML Summer Schools 2003, Canberra, Australia, February 2 - 14, 2003, Tübingen, Germany, August 4 - 16, 2003, Revised Lectures* (pp. 63-71). Berlin, Heidelberg: Springer Berlin Heidelberg.

Reilly, T. E., & Goodman, A. S. (1987). Analysis of saltwater upconing beneath a pumping well. *Journal of Hydrology, 89*(3), 169-204. doi:https://doi.org/10.1016/0022-1694(87)90179-X

Ricardo, S. M., & Christian, B. (2016). Groundwater recharge mechanisms inferred from isoscapes in a complex tropical mountainous region. *Geophys Res Lett, 43*(10), 5060-5069. doi:doi:10.1002/2016GL068888

Richards, L. A., Magnone, D., Boyce, A. J., Casanueva-Marenco, M. J., van Dongen, B. E., Ballentine, C. J., & Polya, D. A. (2018). Delineating sources of groundwater recharge in an arsenic-affected Holocene aquifer in Cambodia using stable isotope-based mixing models. *Journal of Hydrology, 557*, 321-334. doi:https://doi.org/10.1016/j.jhydrol.2017.12.012

Rodriguez-Galiano, V., Mendes, M. P., Garcia-Soldado, M. J., Chica-Olmo, M., & Ribeiro, L. (2014). Predictive modeling of groundwater nitrate pollution using Random Forest and multisource variables related to intrinsic and specific vulnerability: A case study in an agricultural setting (Southern Spain). *Science of The Total Environment, 476-477*, 189-206. doi:10.1016/j.scitotenv.2014.01.001

Rosenthal, E., Zilberbrand, M., & Livshitz, Y. (2007). The hydrochemical evolution of brackish groundwater in central and northern Sinai (Egypt) and in the western Negev (Israel). *Journal of Hydrology, 337*(3–4), 294-314. doi:https://doi.org/10.1016/j.jhydrol.2007.01.042

Roy, D. K., & Datta, B. (2017). Multivariate adaptive regression spline ensembles for management of multilayered coastal aquifers. *Journal of Hydrologic Engineering, 22*(9), 04017031.

Russak, A., & Sivan, O. (2010). Hydrogeochemical Tool to Identify Salinization or Freshening of Coastal Aquifers Determined from Combined Field Work, Experiments, and Modeling. *Environmental Science & Technology, 44*(11), 4096-4102. doi:10.1021/es1003439

Russak, A., Yechieli, Y., Herut, B., Lazar, B., & Sivan, O. (2015). The effect of salinization and freshening events in coastal aquifers on nutrient characteristics as deduced from field data. *Journal of Hydrology, 529*, 1293-1301. doi:https://doi.org/10.1016/j.jhydrol.2015.07.022

Russo, T. A., & Lall, U. (2017). Depletion and response of deep groundwater to climate-induced pumping variability. *Nature Geosci, 10*(2), 105-108. doi:10.1038/ngeo2883

http://www.nature.com/ngeo/journal/v10/n2/abs/ngeo2883.html#supplementary-information

Sadeg, S., & Karahanoðlu, N. (2001). Numerical assessment of seawater intrusion in the Tripoli region, Libya. *Environmental Geology, 40*(9), 1151-1168. doi:10.1007/s002540100317

Sajedi-Hosseini, F., Malekian, A., Choubin, B., Rahmati, O., Cipullo, S., Coulon, F., & Pradhan, B. (2018). A novel machine learning-based approach for the risk assessment of nitrate groundwater contamination. *Science of The Total Environment, 644*, 954-962. doi:10.1016/j.scitotenv.2018.07.054

Sakakibara, K., Tsujimura, M., Song, X., & Zhang, J. (2017). Spatiotemporal variation of the surface water effect on the groundwater recharge in a low-precipitation region: Application of the multi-tracer approach to the Taihang Mountains, North China. *Journal of Hydrology, 545*, 132-144. doi:http://dx.doi.org/10.1016/j.jhydrol.2016.12.030

Samantara, M. K., Padhi, R. K., Sowmya, M., Kumaran, P., & Satpathy, K. K. (2017). Heavy metal contamination, major ion chemistry and appraisal of the groundwater status in coastal aquifer, Kalpakkam, Tamil Nadu, India. *Groundwater for Sustainable Development, 5*, 49-58. doi:https://doi.org/10.1016/j.gsd.2017.04.001

Sánchez-Murillo, R., & Birkel, C. (2016). Groundwater recharge mechanisms inferred from isoscapes in a complex tropical mountainous region. *Geophys Res Lett, 43*(10), 5060-5069. doi:10.1002/2016GL068888

Santos, I. R., Zhang, C., Maher, D. T., Atkins, M. L., Holland, R., Morgenstern, U., & Li, L. (2017). Assessing the recharge of a coastal aquifer using physical observations, tritium, groundwater chemistry and modelling. *Science of The Total Environment, 580*, 367-379. doi:https://doi.org/10.1016/j.scitotenv.2016.11.181

Santos, K. C. P., & Barrios, E. B. (2017). Improving predictive accuracy of logistic regression model using ranked set samples. *Communications in Statistics - Simulation and Computation, 46*(1), 78-90. doi:10.1080/03610918.2014.955113

Sappa, G., Iacurto, S., Ferranti, F., & De Filippi, F. M. (2019). Groundwater Quality Assessment in a Karst Coastal Region of the West Aurunci Mountains (Central Italy). *Geofluids, 2019*, 14. doi:10.1155/2019/3261713

Sathe, S. S., & Mahanta, C. (2019). Groundwater flow and arsenic contamination transport modeling for a multi aquifer terrain: Assessment and mitigation strategies. *Journal of Environmental Management, 231*, 166-181. doi:https://doi.org/10.1016/j.jenvman.2018.08.057

Scholkopf, B., Kah-Kay, S., Burges, C. J. C., Girosi, F., Niyogi, P., Poggio, T., & Vapnik, V. (1997). Comparing support vector machines with Gaussian kernels to radial basis function classifiers. *IEEE Transactions on Signal Processing, 45*(11), 2758-2765. doi:10.1109/78.650102

Schott, J., Bénézeth, P., Gautier, Q., & Stefánsson, A. (2013). Mineral Solubility and Aqueous Speciation Under Hydrothermal Conditions to 300 °C – The Carbonate

System as an Example. *Reviews in Mineralogy and Geochemistry, 76*(1), 81-133. doi:10.2138/rmg.2013.76.4

Seddique, A. A., Masuda, H., Anma, R., Bhattacharya, P., Yokoo, Y., & Shimizu, Y. (2019). Hydrogeochemical and isotopic signatures for the identification of seawater intrusion in the paleobeach aquifer of Cox's Bazar city and its surrounding area, south-east Bangladesh. *Groundwater for Sustainable Development, 9*, 100215. doi:https://doi.org/10.1016/j.gsd.2019.100215

Sefie, A., Aris, A. Z., Ramli, M. F., Narany, T. S., Shamsuddin, M. K. N., Saadudin, S. B., & Zali, M. A. (2018). Hydrogeochemistry and groundwater quality assessment of the multilayered aquifer in Lower Kelantan Basin, Kelantan, Malaysia. *Environmental Earth Sciences, 77*(10), 397. doi:10.1007/s12665-018-7561-9

Selvakumar, S., Chandrasekar, N., & Kumar, G. (2017). Hydrogeochemical characteristics and groundwater contamination in the rapid urban development areas of Coimbatore, India. *Water Resources and Industry, 17*(Supplement C), 26-33. doi:https://doi.org/10.1016/j.wri.2017.02.002

Shankar, S., Shanker, U., & Shikha. (2014). Arsenic Contamination of Groundwater: A Review of Sources, Prevalence, Health Risks, and Strategies for Mitigation. *The Scientific World Journal, 2014*, 18. doi:10.1155/2014/304524

Sheikhy Narany, T., Sefie, A., & Aris, A. Z. (2018). The long-term impacts of anthropogenic and natural processes on groundwater deterioration in a multilayered aquifer. *Science of The Total Environment, 630*, 931-942. doi:https://doi.org/10.1016/j.scitotenv.2018.02.190

Sherif, M., Sefelnasr, A., & Javadi, A. (2012). Incorporating the concept of equivalent freshwater head in successive horizontal simulations of seawater intrusion in the Nile Delta aquifer, Egypt. *Journal of Hydrology, 464-465*, 186-198. doi:https://doi.org/10.1016/j.jhydrol.2012.07.007

Shi, L., & Jiao, J. J. (2014). Seawater intrusion and coastal aquifer management in China: a review. *Environmental Earth Sciences, 72*(8), 2811-2819. doi:10.1007/s12665-014-3186-9

Shi, W., Lu, C., Ye, Y., Wu, J., Li, L., & Luo, J. (2018). Assessment of the impact of sea-level rise on steady-state seawater intrusion in a layered coastal aquifer. *Journal of Hydrology, 563*, 851-862. doi:https://doi.org/10.1016/j.jhydrol.2018.06.046

Shinkai, Y., Truc, D. V., Sumi, D., Canh, D., & Kumagai, Y. (2007). Arsenic and Other Metal Contamination of Groundwater in the Mekong River Delta, Vietnam. *Journal of Health Science, 53*(3), 344-346. doi:10.1248/jhs.53.344

Shrestha, S., Bach, T. V., & Pandey, V. P. (2016). Climate change impacts on groundwater resources in Mekong Delta under representative concentration pathways (RCPs) scenarios. *Environmental Science & Policy, 61*, 1-13. doi:http://dx.doi.org/10.1016/j.envsci.2016.03.010

Siebert, S., Burke, J., Faures, J. M., Frenken, K., Hoogeveen, J., Döll, P., & Portmann, F. T. (2010). Groundwater use for irrigation – a global inventory. *Hydrol. Earth Syst. Sci., 14*(10), 1863-1880. doi:10.5194/hess-14-1863-2010

Simmons, C. T., Fenstemaker, T. R., & Sharp, J. M. (2001). Variable-density groundwater flow and solute transport in heterogeneous porous media: approaches, resolutions and future challenges. *Journal of Contaminant Hydrology, 52*(1), 245-275. doi:https://doi.org/10.1016/S0169-7722(01)00160-7

Singh, B., & Sekhon, G. S. (1976). Nitrate pollution of groundwater from nitrogen fertilizers and animal wastes in the Punjab, India. *Agriculture and Environment, 3*(1), 57-67. doi:http://dx.doi.org/10.1016/0304-1131(76)90007-2

Singh, C. K., Kumar, A., Shashtri, S., Kumar, A., Kumar, P., & Mallick, J. (2017). Multivariate statistical analysis and geochemical modeling for geochemical assessment of groundwater of Delhi, India. *Journal of Geochemical Exploration, 175*, 59-71. doi:http://dx.doi.org/10.1016/j.gexplo.2017.01.001

Singh, S. K., Taylor, R. W., Rahman, M. M., & Pradhan, B. (2018). Developing robust arsenic awareness prediction models using machine learning algorithms. *Journal of Environmental Management, 211*, 125-137. doi:https://doi.org/10.1016/j.jenvman.2018.01.044

Skrzypek, G., Mydłowski, A., Dogramaci, S., Hedley, P., Gibson, J. J., & Grierson, P. F. (2015). Estimation of evaporative loss based on the stable isotope composition of water using Hydrocalculator. *Journal of Hydrology, 523*, 781-789. doi:http://dx.doi.org/10.1016/j.jhydrol.2015.02.010

Smajgl, A., Toan, T. Q., Nhan, D. K., Ward, J., Trung, N. H., Tri, L. Q., . . . Vu, P. T. (2015). Responding to rising sea levels in the Mekong Delta. *Nature Clim. Change, 5*(2), 167-174. doi:10.1038/nclimate2469

Song, J., Yang, Y., Wu, J., Wu, J., Sun, X., & Lin, J. (2018). Adaptive surrogate model based multiobjective optimization for coastal aquifer management. *Journal of Hydrology, 561*, 98-111. doi:https://doi.org/10.1016/j.jhydrol.2018.03.063

Sprenger, M., Leistert, H., Gimbel, K., & Weiler, M. (2016). Illuminating hydrological processes at the soil-vegetation-atmosphere interface with water stable isotopes. *Reviews of Geophysics, 54*(3), 674-704. doi:10.1002/2015RG000515

Sprenger, M., Tetzlaff, D., Tunaley, C., Dick, J., & Soulsby, C. (2017). Evaporation fractionation in a peatland drainage network affects stream water isotope composition. *Water Resources Research, 53*(1), 851-866. doi:10.1002/2016WR019258

Sracek, O., Geršl, M., Faimon, J., & Bábek, O. (2019). The geochemistry and origin of fluids in the carbonate structure of the Hranice Karst with the world's deepest flooded cave of the Hranicka Abyss, Czech Republic. *Applied Geochemistry, 100*, 203-212. doi:https://doi.org/10.1016/j.apgeochem.2018.11.013

Sreekanth, J., & Datta, B. (2010). Multi-objective management of saltwater intrusion in coastal aquifers using genetic programming and modular neural network based surrogate models. *Journal of Hydrology, 393*(3-4), 245-256.

Stein, S., Yechieli, Y., Shalev, E., Kasher, R., & Sivan, O. (2019). The effect of pumping saline groundwater for desalination on the fresh–saline water interface dynamics. *Water Research, 156*, 46-57. doi:https://doi.org/10.1016/j.watres.2019.03.003

Steyl, G., & Dennis, I. (2010). Review of coastal-area aquifers in Africa. *Hydrogeology Journal, 18*(1), 217-225. doi:10.1007/s10040-009-0545-9

Stiff, H. A., Jr. (1951). The Interpretation of Chemical Water Analysis by Means of Patterns. doi:10.2118/951376-G

Stuckey, J. W., Schaefer, M. V., Kocar, B. D., Benner, S. G., & Fendorf, S. (2016). Arsenic release metabolically limited to permanently water-saturated soil in Mekong Delta. *Nature Geosci, 9*(1), 70-76. doi:10.1038/ngeo2589

http://www.nature.com/ngeo/journal/v9/n1/abs/ngeo2589.html#supplementary-information

Sun, Y., Wendi, D., Kim, D. E., & Liong, S. Y. (2016). Technical note: Application of artificial neural networks in groundwater table forecasting – a case study in a Singapore swamp forest. *Hydrol. Earth Syst. Sci., 20*(4), 1405-1412. doi:10.5194/hess-20-1405-2016

Ta, T. K. O., Nguyen, V. L., Tateishi, M., Kobayashi, I., & Saito, Y. (2001). Sedimentary facies, diatom and foraminifer assemblages in a late Pleistocene–Holocene incised-

valley sequence from the Mekong River Delta, Bentre Province, Southern Vietnam: the BT2 core. *Journal of Asian Earth Sciences, 20*(1), 83-94. doi:https://doi.org/10.1016/S1367-9120(01)00028-1

Ta, T. K. O., Nguyen, V. L., Tateishi, M., Kobayashi, I., Saito, Y., & Nakamura, T. (2002). Sediment facies and Late Holocene progradation of the Mekong River Delta in Bentre Province, southern Vietnam: an example of evolution from a tide-dominated to a tide- and wave-dominated delta. *Sedimentary Geology, 152*(3), 313-325. doi:http://dx.doi.org/10.1016/S0037-0738(02)00098-2

Ta, T. K. O., Nguyen, V. L., Tateishi, M., Kobayashi, I., Tanabe, S., & Saito, Y. (2002). Holocene delta evolution and sediment discharge of the Mekong River, southern Vietnam. *Quaternary Science Reviews, 21*(16), 1807-1819. doi:https://doi.org/10.1016/S0277-3791(02)00007-0

Takagi, H., Anh, L. T., & Danh Thao, N. (2017). 1997 Typhoon Linda Storm Surge and People's Awareness 20 Years Later: Uninvestigated Worst Storm Event in the Mekong Delta. *Nat. Hazards Earth Syst. Sci. Discuss., 2017*, 1-19. doi:10.5194/nhess-2017-365

Takizawa, S. (2008). Groundwater Management in Asian Cities :Technology and Policy for Sustainability. *Book*.

Talukder, M. R. R., Rutherford, S., Huang, C., Phung, D., Islam, M. Z., & Chu, C. (2017). Drinking water salinity and risk of hypertension: A systematic review and meta-analysis. *Archives of Environmental & Occupational Health, 72*(3), 126-138. doi:10.1080/19338244.2016.1175413

Tamura, T., Saito, Y., Sieng, S., Ben, B., Kong, M., Sim, I., . . . Akiba, F. (2009). Initiation of the Mekong River delta at 8 ka: evidence from the sedimentary succession in the Cambodian lowland. *Quaternary Science Reviews, 28*(3), 327-344. doi:http://dx.doi.org/10.1016/j.quascirev.2008.10.010

Tanabe, S. (2003). Delta evolution model inferred from the Holocene Mekong Delta, southern Vietnam. *SEPM Special Publication, 76*, 175-188.

Tarki, M., Dassi, L., & Jedoui, Y. (2012). Groundwater composition and recharge origin in the shallow aquifer of the Djerid oases, southern Tunisia: implications of return flow. *Hydrological Sciences Journal, 57*(4), 790-804. doi:10.1080/02626667.2012.681783

Taufiq, A., Effendi, A. J., Iskandar, I., Hosono, T., & Hutasoit, L. M. (2019). Controlling factors and driving mechanisms of nitrate contamination in groundwater system of Bandung Basin, Indonesia, deduced by combined use of stable isotope ratios, CFC age dating, and socioeconomic parameters. *Water Research, 148*, 292-305. doi:https://doi.org/10.1016/j.watres.2018.10.049

Taweesin, K., Seeboonruang, U., & Saraphirom, P. (2018). The Influence of Climate Variability Effects on Groundwater Time Series in the Lower Central Plains of Thailand. *Water, 10*(3). doi:10.3390/w10030290

Thom, J. G. M., Dipple, G. M., Power, I. M., & Harrison, A. L. (2013). Chrysotile dissolution rates: Implications for carbon sequestration. *Applied Geochemistry, 35*, 244-254. doi:https://doi.org/10.1016/j.apgeochem.2013.04.016

Tian, C., Wang, L., Kaseke, K. F., & Bird, B. W. (2018). Stable isotope compositions (δ(2)H, δ(18)O and δ(17)O) of rainfall and snowfall in the central United States. *Sci Rep, 8*(1), 6712-6712. doi:10.1038/s41598-018-25102-7

Tien Bui, D., Hoang, N.-D., & Nhu, V.-H. (2018). A swarm intelligence-based machine learning approach for predicting soil shear strength for road construction: a case study at Trung Luong National Expressway Project (Vietnam). *Engineering with Computers*. doi:10.1007/s00366-018-0643-1

Tien Bui, D., Tuan, T. A., Klempe, H., Pradhan, B., & Revhaug, I. (2016). Spatial prediction models for shallow landslide hazards: a comparative assessment of the efficacy of support vector machines, artificial neural networks, kernel logistic regression, and logistic model tree. *Landslides, 13*(2), 361-378. doi:10.1007/s10346-015-0557-6

Timms, W. A., Young, R. R., & Huth, N. (2012). Implications of deep drainage through saline clay for groundwater recharge and sustainable cropping in a semi-arid catchment, Australia. *Hydrol. Earth Syst. Sci., 16*(4), 1203-1219. doi:10.5194/hess-16-1203-2012

Tiwari, A. K., Pisciotta, A., & De Maio, M. (2019a). Evaluation of groundwater salinization and pollution level on Favignana Island, Italy. *Environmental Pollution*. doi:https://doi.org/10.1016/j.envpol.2019.03.016

Tiwari, A. K., Pisciotta, A., & De Maio, M. (2019b). Evaluation of groundwater salinization and pollution level on Favignana Island, Italy. *Environmental Pollution, 249*, 969-981. doi:https://doi.org/10.1016/j.envpol.2019.03.016

Tjallingii, R., Stattegger, K., Wetzel, A., & Van Phach, P. (2010). Infilling and flooding of the Mekong River incised valley during deglacial sea-level rise. *Quaternary Science Reviews, 29*(11), 1432-1444. doi:https://doi.org/10.1016/j.quascirev.2010.02.022

Todd, D. K. (1960). *Salt water intrusion of coastal aquifers in the United States*. Retrieved from

Trabelsi, N., Triki, I., Hentati, I., & Zairi, M. (2016). Aquifer vulnerability and seawater intrusion risk using GALDIT, GQISWI and GIS: case of a coastal aquifer in Tunisia. *Environmental Earth Sciences, 75*(8), 669. doi:10.1007/s12665-016-5459-y

Trabelsi, R., & Zouari, K. (2019). Coupled geochemical modeling and multivariate statistical analysis approach for the assessment of groundwater quality in irrigated areas: A study from North Eastern of Tunisia. *Groundwater for Sustainable Development, 8*, 413-427. doi:https://doi.org/10.1016/j.gsd.2019.01.006

Tran, D. A., Tsujimura, M., Vo, L. P., Nguyen, V. T., Kambuku, D., & Dang, T. D. (2019). Hydrogeochemical characteristics of a multi-layered coastal aquifer system in the Mekong Delta, Vietnam. *Environmental Geochemistry and Health*. doi:10.1007/s10653-019-00400-9

Tran, T. A., Nguyen, T. H., & Vo, T. T. (2019). Adaptation to flood and salinity environments in the Vietnamese Mekong Delta: Empirical analysis of farmer-led innovations. *Agricultural Water Management, 216*, 89-97. doi:https://doi.org/10.1016/j.agwat.2019.01.020

Trenberth, K. E., Smith, L., Qian, T., Dai, A., & Fasullo, J. (2007). Estimates of the Global Water Budget and Its Annual Cycle Using Observational and Model Data. *Journal of Hydrometeorology, 8*(4), 758-769. doi:10.1175/JHM600.1

Trung, N. H., & Tri, V. P. D. (2014). 10 - Possible Impacts of Seawater Intrusion and Strategies for Water Management in Coastal Areas in the Vietnamese Mekong Delta in the Context of Climate Change A2 - Thao, Nguyen Danh. In H. Takagi & M. Esteban (Eds.), *Coastal Disasters and Climate Change in Vietnam* (pp. 219-232). Oxford: Elsevier.

Truong, M. H., Nguyen, V. L., Ta, T. K. O., & Takemura, J. (2011). Changes in late Pleistocene–Holocene sedimentary facies of the Mekong River Delta and the influence of sedimentary environment on geotechnical engineering properties. *Engineering Geology, 122*(3), 146-159. doi:https://doi.org/10.1016/j.enggeo.2011.05.012

Tsutomu, Y., Jun, S., Maki, T., Oranuj, L., Makoto, M., Atsushi, H., & Shinichi, O. (2011). Tracing a confined groundwater flow system under the pressure of excessive groundwater use in the lower central plain, Thailand. *HYDROLOGICAL PROCESSES, 25*(17), 2654-2664. doi:doi:10.1002/hyp.8007

Tweed, S., Celle-Jeanton, H., Cabot, L., Huneau, F., De Montety, V., Nicolau, N., . . . Leblanc, M. (2018). Impact of irrigated agriculture on groundwater resources in a temperate humid region. *Science of The Total Environment, 613-614*, 1302-1316. doi:https://doi.org/10.1016/j.scitotenv.2017.09.156

Udimal, T. B., Jincai, Z., Ayamba, E. C., & Mensah Owusu, S. (2017). China's water situation; the supply of water and the pattern of its usage. *International Journal of Sustainable Built Environment, 6*(2), 491-500. doi:https://doi.org/10.1016/j.ijsbe.2017.10.001

UN-Water. (2010a). Water in a chaging World (pp. 349). Netherland, : UNESCO

UN-Water. (2010b). *Water in changing world*. Retrieved from 7, place de Fontenoy, 75007 Paris, France, and Earthscan, Dunstan House, 14a St Cross Street, London EC1N 8XA, United Kingdom.:

Vallejos, A., Sola, F., Yechieli, Y., & Pulido-Bosch, A. (2018). Influence of the paleogeographic evolution on the groundwater salinity in a coastal aquifer. Cabo de Gata aquifer, SE Spain. *Journal of Hydrology, 557*, 55-66. doi:https://doi.org/10.1016/j.jhydrol.2017.12.027

Varni, M., Comas, R., Weinzettel, P., & Dietrich, S. (2013). Application of the water table fluctuation method to characterize groundwater recharge in the Pampa plain, Argentina. *Hydrological Sciences Journal, 58*(7), 1445-1455. doi:10.1080/02626667.2013.833663

Velis, M., Conti, K. I., & Biermann, F. (2017). Groundwater and human development: synergies and trade-offs within the context of the sustainable development goals. *Sustainability Science, 12*(6), 1007-1017. doi:10.1007/s11625-017-0490-9

Vengadesan, M., & Lakshmanan, E. (2019). Chapter 17 - Management of Coastal Groundwater Resources. In R. R. Krishnamurthy, M. P. Jonathan, S. Srinivasalu, & B. Glaeser (Eds.), *Coastal Management* (pp. 383-397): Academic Press.

Vengosh, A. (2003). 9.09 - Salinization and Saline Environments A2 - Holland, Heinrich D. In K. K. Turekian (Ed.), *Treatise on Geochemistry* (pp. 1-35). Oxford: Pergamon.

Vincent, A., & Violette, S. (2017). Why seawater intrusion has not yet occurred in the Kaluvelli-Pondicherry basin, Tamil Nadu, India. *Hydrogeology Journal, 25*(6), 1893-1907. doi:10.1007/s10040-017-1558-4

Vineis, P., Chan, Q., & Khan, A. (2011). Climate change impacts on water salinity and health. *Journal of Epidemiology and Global Health, 1*(1), 5-10. doi:10.1016/j.jegh.2011.09.001

Vithanage, M., Mikunthan, T., Pathmarajah, S., Arasalingam, S., & Manthrithilake, H. (2014). Assessment of nitrate-N contamination in the Chunnakam aquifer system, Jaffna Peninsula, Sri Lanka. *Springerplus, 3*, 271. doi:10.1186/2193-1801-3-271

Vörösmarty, C. J., Green, P., Salisbury, J., & Lammers, R. B. (2000). Global Water Resources: Vulnerability from Climate Change and Population Growth. *Science, 289*(5477), 284. doi:10.1126/science.289.5477.284

Voss, C. I., & Souza, W. R. (1987). Variable density flow and solute transport simulation of regional aquifers containing a narrow freshwater-saltwater transition zone. *Water Resources Research, 23*(10), 1851-1866. doi:10.1029/WR023i010p01851

Vu, D. T., Yamada, T., & Ishidaira, H. (2018). Assessing the impact of sea level rise due to climate change on seawater intrusion in Mekong Delta, Vietnam. *Water Science and Technology, 77*(6), 1632-1639. doi:10.2166/wst.2018.038

Wagner, F., Tran, V. B., & Renaud, F. G. (2010). Chapter 7: Groundwater Resources in the Mekong Delta: Availability, Utilization and Risks. In F. G. R. a. C. Kuenze (Ed.), *The Mekong Delta system: Interdisciplinary Analyses of a River Delta*. Dordrecht Heidelberg New York London: Springer

Wagner, F., Tran, V. B., & Renaud, F. G. (2012). Groundwater Resources in the Mekong Delta: Availability, Utilization and Risks. In F. G. Renaud & C. Kuenzer (Eds.), *The Mekong Delta System: Interdisciplinary Analyses of a River Delta* (pp. 201-220). Dordrecht: Springer Netherlands.

Walter, J., Chesnaux, R., Cloutier, V., & Gaboury, D. (2017). The influence of water/rock − water/clay interactions and mixing in the salinization processes of groundwater. *Journal of Hydrology: Regional Studies, 13*, 168-188. doi:10.1016/j.ejrh.2017.07.004

Wang, Y., & Jiao, J. J. (2012). Origin of groundwater salinity and hydrogeochemical processes in the confined Quaternary aquifer of the Pearl River Delta, China. *Journal of Hydrology, 438-439*, 112-124. doi:https://doi.org/10.1016/j.jhydrol.2012.03.008

Wang, Y., Le Pape, P., Morin, G., Asta, M. P., King, G., Bártová, B., . . . Bernier-Latmani, R. (2018). Arsenic Speciation in Mekong Delta Sediments Depends on Their Depositional Environment. *Environmental Science & Technology, 52*(6), 3431-3439. doi:10.1021/acs.est.7b05177

Ward, M. H., Jones, R. R., Brender, J. D., de Kok, T. M., Weyer, P. J., Nolan, B. T., . . . van Breda, S. G. (2018). Drinking Water Nitrate and Human Health: An Updated Review. *International Journal of Environmental Research and Public Health, 15*(7), 1557. doi:10.3390/ijerph15071557

Wen, X., Diao, M., Wang, D., & Gao, M. (2012). Hydrochemical characteristics and salinization processes of groundwater in the shallow aquifer of Eastern Laizhou Bay, China. *HYDROLOGICAL PROCESSES, 26*(15), 2322-2332. doi:10.1002/hyp.8362

Werner, A. D., Bakker, M., Post, V. E. A., Vandenbohede, A., Lu, C., Ataie-Ashtiani, B., . . . Barry, D. A. (2013). Seawater intrusion processes, investigation and management: Recent advances and future challenges. *Advances in Water Resources, 51*, 3-26. doi:https://doi.org/10.1016/j.advwatres.2012.03.004

Whitehead, P. G., Jin, L., Bussi, G., Voepel, H. E., Darby, S. E., Vasilopoulos, G., . . . Hung, N. N. (2019). Water quality modelling of the Mekong River basin: Climate change and socioeconomics drive flow and nutrient flux changes to the Mekong Delta. *Science of The Total Environment, 673*, 218-229. doi:https://doi.org/10.1016/j.scitotenv.2019.03.315

Wichelns, D. (2017). Volumetric water footprints, applied in a global context, do not provide insight regarding water scarcity or water quality degradation. *Ecological Indicators, 74*, 420-426. doi:http://dx.doi.org/10.1016/j.ecolind.2016.12.008

Williams, V. J. (2009). *The Ecological Effects of Salt Water Intrusion on the Agriculture Industry After Hurricane Katrina*, New York, NY.

Willmott, C. J., Robeson, S. M., & Matsuura, K. (2012). A refined index of model performance. *International Journal of Climatology, 32*(13), 2088-2094. doi:10.1002/joc.2419

Winkel, L., Berg, M., Amini, M., Hug, S. J., & Annette Johnson, C. (2008a). Predicting groundwater arsenic contamination in Southeast Asia from surface parameters. *Nature Geoscience, 1*(8), 536-542. doi:10.1038/ngeo254

Winkel, L., Berg, M., Amini, M., Hug, S. J., & Annette Johnson, C. (2008b). Predicting groundwater arsenic contamination in Southeast Asia from surface parameters. *Nat Geosci, 1*, 536. doi:10.1038/ngeo254

https://www.nature.com/articles/ngeo254#supplementary-information

Wolanski, E., Nguyen Huu, N., & Simon, S. (1998). Sediment Dynamics during Low Flow Conditions in the Mekong River Estuary, Vietnam. *Journal of Coastal Research, 14*(2), 472-482.

Wood, C., & Harrington, G. A. (2015). Influence of Seasonal Variations in Sea Level on the Salinity Regime of a Coastal Groundwater–Fed Wetland. *Groundwater, 53*(1), 90-98. doi:10.1111/gwat.12168

Xiao, J., Wang, L., Deng, L., & Jin, Z. (2019). Characteristics, sources, water quality and health risk assessment of trace elements in river water and well water in the Chinese Loess Plateau. *Science of The Total Environment, 650*, 2004-2012. doi:https://doi.org/10.1016/j.scitotenv.2018.09.322

Xu, H., Lin, J., & Wang, D. (2008). Numerical study on salinity stratification in the Pamlico River Estuary. *Estuarine, Coastal and Shelf Science, 80*(1), 74-84. doi:https://doi.org/10.1016/j.ecss.2008.07.014

Yadav, B., Mathur, S., Ch, S., & Yadav, B. K. (2018). Data-based modelling approach for variable density flow and solute transport simulation in a coastal aquifer. *Hydrological Sciences Journal, 63*(2), 210-226. doi:10.1080/02626667.2017.1413491

Yamanaka, T., Mikita, M., Lorphensri, O., Shimada, J., Kagabu, M., Ikawa, R., . . . Tsujimura, M. (2011). Anthropogenic changes in a confined groundwater flow system in the Bangkok Basin, Thailand, part II: how much water has been renewed? *Hydrological Processes, 25*(17), 2734-2741. doi:10.1002/hyp.8014

Yang, K., Han, G., Liu, M., Li, X., Liu, J., & Zhang, Q. (2018). Spatial and Seasonal Variation of O and H Isotopes in the Jiulong River, Southeast China. *Water, 10*(11). doi:10.3390/w10111677

Yang, L., Qi, Y., Zheng, C., Andrews, B. C., Yue, S., Lin, S., . . . Li, H. (2018). A Modified Water-Table Fluctuation Method to Characterize Regional Groundwater Discharge. *Water, 10*(4). doi:10.3390/w10040503

Yechieli, Y., Yokochi, R., Zilberbrand, M., Lu, Z.-T., Purtschert, R., Sueltenfuss, J., . . . Burg, A. (2019). Recent seawater intrusion into deep aquifer determined by the radioactive noble-gas isotopes 81Kr and 39Ar. *Earth and Planetary Science Letters, 507*, 21-29. doi:https://doi.org/10.1016/j.epsl.2018.11.028

Yeh, H.-F., Lin, H.-I., Lee, C.-H., Hsu, K.-C., & Wu, C.-S. (2014). Identifying Seasonal Groundwater Recharge Using Environmental Stable Isotopes. *Water, 6*(10), 2849.

Yoo, K., Yoo, H., Lee, J. M., Shukla, S. K., & Park, J. (2018). Classification and Regression Tree Approach for Prediction of Potential Hazards of Urban Airborne Bacteria during Asian Dust Events. *Sci Rep, 8*(1), 11823. doi:10.1038/s41598-018-29796-7

Yu, X., & Michael, H. A. (2019). Mechanisms, configuration typology, and vulnerability of pumping-induced seawater intrusion in heterogeneous aquifers. *Advances in Water Resources, 128*, 117-128. doi:https://doi.org/10.1016/j.advwatres.2019.04.013

Zanetti, F., Zegada-Lizarazu, W., Lambertini, C., & Monti, A. (2019). Salinity effects on germination, seedlings and full-grown plants of upland and lowland switchgrass cultivars. *Biomass and Bioenergy, 120*, 273-280. doi:https://doi.org/10.1016/j.biombioe.2018.11.031

Zeidan, B. A. (2017). Groundwater Degradation and Remediation in the Nile Delta Aquifer. In A. M. Negm (Ed.), *The Nile Delta* (pp. 159-232). Cham: Springer International Publishing.

Zghibi, A., Tarhouni, J., & Zouhri, L. (2013). Assessment of seawater intrusion and nitrate contamination on the groundwater quality in the Korba coastal plain of Cap-Bon (North-east of Tunisia). *Journal of African Earth Sciences, 87*, 1-12. doi:https://doi.org/10.1016/j.jafrearsci.2013.07.009

Zhai, Y., Zhao, X., Teng, Y., Li, X., Zhang, J., Wu, J., & Zuo, R. (2017). Groundwater nitrate pollution and human health risk assessment by using HHRA model in an agricultural area, NE China. *Ecotoxicol Environ Saf, 137*, 130-142. doi:http://dx.doi.org/10.1016/j.ecoenv.2016.11.010

Zhang, G., Lu, P., Wei, X., & Zhu, C. (2016). Impacts of Mineral Reaction Kinetics and Regional Groundwater Flow on Long-Term CO2 Fate at Sleipner. *Energy & Fuels, 30*(5), 4159-4180. doi:10.1021/acs.energyfuels.5b02556

Zhang, L., Yuan, R., Song, X., & Xia, J. (2017). Spatial variation of stable isotopic composition in surface waters of the Huai River basin, China and the regional hydrological implication. *Hydrology Research, 49*(5), 1452-1466. doi:10.2166/nh.2017.027

Zhang, Q., Sun, J., Liu, J., Huang, G., Lu, C., & Zhang, Y. (2015). Driving mechanism and sources of groundwater nitrate contamination in the rapidly urbanized region of south China. *Journal of Contaminant Hydrology, 182*, 221-230. doi:http://dx.doi.org/10.1016/j.jconhyd.2015.09.009

Zhang, R., Hu, S., Zhang, X., & Yu, W. (2007). Dissolution Kinetics of Dolomite in Water at Elevated Temperatures. *Aquatic Geochemistry, 13*(4), 309-338. doi:10.1007/s10498-007-9022-z

Zhang, W. L., Tian, Z. X., Zhang, N., & Li, X. Q. (1996). Nitrate pollution of groundwater in northern China. *Agriculture, Ecosystems & Environment, 59*(3), 223-231. doi:http://dx.doi.org/10.1016/0167-8809(96)01052-3

Zhao, X., Zhang, Y., Ning, Q., Zhang, H., Ji, J., & Yin, M. (2019). Identifying N6-methyladenosine sites using extreme gradient boosting system optimized by particle swarm optimizer. *J Theor Biol, 467*, 39-47. doi:https://doi.org/10.1016/j.jtbi.2019.01.035

Zheng, H., Yuan, J., & Chen, L. (2017). Short-Term Load Forecasting Using EMD-LSTM Neural Networks with a Xgboost Algorithm for Feature Importance Evaluation. *Energies, 10*(8). doi:10.3390/en10081168

Zhu, Y., Zhai, Y., Teng, Y., Wang, G., Du, Q., Wang, J., & Yang, G. (2019). Water supply safety of riverbank filtration wells under the impact of surface water-groundwater interaction: evidence from long-term field pumping tests. *Science of The Total Environment*, 135141. doi:https://doi.org/10.1016/j.scitotenv.2019.135141

Ziadi, A., Hariga, N. T., & Tarhouni, J. (2019). Mineralization and pollution sources in the coastal aquifer of Lebna, Cap Bon, Tunisia. *Journal of African Earth Sciences, 151*, 391-402. doi:https://doi.org/10.1016/j.jafrearsci.2019.01.004

Ziani, D., Boudoukha, A., Boumazbeur, A., Benaabidate, L., & Fehdi, C. (2016). Investigation of groundwater hydrochemical characteristics using the multivariate statistical analysis in Ain Djacer area, Eastern Algeria. *Desalination and Water Treatment, 57*(56), 26993-27002. doi:10.1080/19443994.2016.1180474

Zuo, R., Liu, X., Yang, J., Zhang, H., Li, J., Teng, Y., . . . Wang, J. (2019). Distribution, origin and key influencing factors of fluoride groundwater in the coastal area, NE China. *Human and Ecological Risk Assessment: An International Journal*, 1-16. doi:10.1080/10807039.2019.1576027